INTEGRATED PHOTOVOLTAIC-FUEL CELL GENERATION METHODOLOGIES: DESIGN, DEVELOPMENT AND OPTIMISATION FOR DISTRIBUTED APPLICATIONS

A thesis submitted to the University of Manchester for the degree of

Doctor of Philosophy

in the Faculty of Science and Engineering

2021

CHUKWUMA OGBONNAYA

SCHOOL OF ENGINEERING,

DEPARTMENT OF MECHANICAL, AEROSPACE AND CIVIL ENGINEERING

Table of Contents

List of Tables

List of Figures

Abbreviations and Nomenclature

A	ideality factor
A_{anode}	activation constant at the anode
$A_{cathode}$	activation constant at the cathode
A_{cell}	active area of a solar cell
B_{anode}	anode empirical constant
BB	block-based
BBM	block-based modelling
$B_{cathode}$	cathode empirical constant
CB	code-based
C_{batt}	capacity sizing of the battery (Ah)
CBM	code-based modelling/model
CCA	comparative cost analysis
CEC	cost-efficiency-complexity
CET	clean energy technologies
COC	cost of component (£)
COE	cost of energy (£ kWh^{-1})
COS	cost of system (£)
C_p	specific heat capacity of hydrogen (14320 J kg^{-1} K^{-1})
D_{energy}	total energy demanded/required
DOD	depth of discharge
E^4A	energy and exergy efficiencies enhancement analysis approach
E_g	bandgap energy
E^o	standard potential at equilibrium
E_{rev}	reversible potential of the reaction
$\dot{E}x$	exergy flow (kW)
ExCD	exergy-centred design
F	Faraday constant
g	gravitational constant (m s^{-2})
G	solar radiation (W m^{-2})
$(\overline{g_f})_{H_2}$	specific Gibbs free energy of hydrogen
$(\overline{g_f})_{H_2O}$	specific Gibbs free energy of water
$(\overline{g_f})_{O_2}$	specific Gibbs free energy of oxygen
GHG	greenhouse gases
H	pump head
HHV_{H_2}	higher heating value of hydrogen
$\dot{H}_{rad}$	radiative heat flux (W cm^{-2})
H_{ref}	reference radiative heat flux (1000 W m^{-2})
i	current density (A m^{-2})
I_{EL}	current density of the electrolyser (A m^{-2})
IES	integrated energy system
I_{FC}	current density of the fuel cell (A m^{-2})
$i_{l_{anode}}$	anodic electrode limiting current density (A m^{-2})
I_{mpp}	current at maximum power point (A)
I_o	output current of PV module
I_{ph}	photocurrent (A)
IPVFC	integrated photovoltaic-fuel cell system
I_s	saturation current
I_{sc}	short circuit current (A)
k	Boltzmann's constant (1.38 x 10^{-23} J K^{-1})
$\dot{m}$	mass flow rate (kg s^{-1})
$\dot{m}_c$	mass flow rate in the compressor (kg s^{-1})
$\dot{m}_{H_2}$	mass flow rate of hydrogen (kg s^{-1})
MPP	maximum power point
MPPT	maximum power point tracker
n	number of electrons
n	refractive index of a dielectric medium
N_{aut}	number of days of autonomy of a system
N_p	number of PV modules in parallel
N_s	number of solar cells in series

P_{EL}	power input into the electrolyser (W)
P_{FC}	power output from the fuel cell (W)
P_{H_2}	partial pressure of hydrogen (atm)
PEME	proton exchange membrane electrolyser
PEMFC	proton exchange membrane fuel cell
P_{H_2O}	partial pressure of water (atm)
P_{in}	inlet pressure of hydrogen from compressor (atm)
P_{load}	load power (kWh)
PMCS	power management and control system
P_o	output power from a PV module
P_{O_2}	partial pressure of oxygen (atm)
P_{out}	outlet pressure of hydrogen from a compressor (atm)
P_{pv}	output power from a PV module/array (W)
PV	photovoltaic
PVMSIC	photovoltaic modelling and simulation codes
PV/T	photovoltaic-thermal system
$\dot{P}_{elect}$	power density output (W cm^{-2})
q	electron charge (1.602 x 10^{-19} C)
Q	maximum capacity of a battery
$\dot{Q}_{losses}$	thermal losses from a TPV system (W cm^{-2})
Q_w	volumetric flow rate of water (m^3 s^{-1})
R	gas constant (J k^{-1} $mole^{-1}$ K^{-1})
R_{CR}	specific constant resistant (Ohm m^{-2})
R_{elect}	electrical resistance (Ohm)
RET	renewable energy technology
R_{ion}	resistance to ions in proton exchange membrane (Ohm)
S_{gen}	entropy generation
STC	standard test conditions (25 ^oC, 1000 W m^{-2}, AM 1.5)
T	temperature (K)
T_1	inlet temperature of hydrogen into the compressor (K)
T_{cell}	temperature of the PV cells (K)
t_{load}	duration of the load power (h)
T_{pv}	temperature of the PV cells
TPV	thermophotovoltaic
T_{Rad}	temperature of the radiator (K)
T_{ref}	reference temperature (298.15 K)
T_{sun}	temperature of the sun (approximately 6000 K)
UAV	unmanned aerial vehicle
V_{act}	activation overpotential (V)
V_{batt}	battery voltage (V)
V_{conc}	concentration overpotential (V)
V_{EL}	net voltage of the electrolyser (V)
V_{FC}	net voltage of the fuel cell (V)
V_{H_2}	volume of hydrogen in the tank (m^3)
V_m	molar volume of hydrogen (m^3)
V_{mpp}	voltage at maximum power point (V)
V_o	output voltage of the PV module (V)
V_{oc}	open circuit voltage (V)
V_{Ohm}	Ohm overpotential (V)
V_{pv}	output voltage from the PV (V)
$\dot{W}$	electrical energy flow (W)
$\dot{W}_c$	power consumed by the compressor (W)
z	compressibility factor
Greek letters	
α	charge transfer coefficient assumed to be 0.5
$\Delta\overline{g_{f,EL}}$	average change in specific Gibbs free energy in electrolyser.
$\Delta\overline{g_{f,FC}}$	average change in specific Gibbs free energy in a fuel cell
ε	emissivity
Φ	fraction of energy losses recovered
ρ	density of water (kg m^{-3})
η	energy efficiency

η_{ex}	exergy efficiency
η_{batt}	battery efficiency
η_{c}	mechanical efficiency of the compressor
η_{EL}	electrical efficiency of electrolyser
η_{FC}	electrical efficiency of fuel cell
η_{pump}	efficiency of the pump
σ	Stefan-Boltzmann's constant (5.67×10^{-12} W cm^{-2} K^{-4})
Θ_1	solar cell material constant 1
Θ_2	solar cell material constant 2
τ_{glass}	transmissivity of the glass top of the PV

Subscripts

1,2,3,4	integrated energy systems 1, 2, 3 and 4
a	ambient
cell	solar cell/fuel cell/electrolyser cell
dest	exergy destroyed
EL	electrolyser
elect	electrical
FC	fuel cell
in	inflow
loss	exergy losses
mpp	at maximum power point
out	outflow
ph	photon
pv	photovoltaic
ref	reference
rad	radiative
sun	of the sun
syst	integrated energy system
therm	thermal
k	ratio of specific heat
pv	photovoltaic

Abstract

Renewable energy technologies based on solar, wind, biomass, tidal, hydro, geothermal sources have shown the potential to significantly substitute fossil fuels in the emerging energy infrastructures. There are ongoing investigations into the applications of integrated photovoltaic-fuel cell (IPVFC) systems for grid and off-grid applications in the upcoming hydrogen economy. Consequently, this study focuses on how the overall effectiveness of IPVFC systems can be improved using a model-based systems engineering approach. Firstly, an energy and exergy efficiencies enhancement analysis (E^4A) methodology was proposed to investigate the interrelationships between cost, efficiency and complexity as usage and conversion losses are targeted for recovery in photovoltaic (PV)-led integrated energy systems (IESs). Findings showed that improving the PV, electrolyser and fuel cell components could improve the overall efficiency of IPVFC systems. Thus, a code-based modelling (CBM) approach was developed to facilitate the design, modelling, and simulation of photovoltaics. This approach enabled a creation of a photovoltaic-thermal model. Investigations with the proposed model showed that the overall improvement in exergy of a PV module could be up to 51% if the waste heat generated was utilised for useful thermal work as in photovoltaic-thermal (PV/T) systems. However, the open circuit voltage degraded with an increase in the temperature of the PV module. The CBM approach was also applied to create a thermophotovoltaic (TPV) model. TPV is another application of photovoltaics for power generation. A parametric study with the proposed TPV model indicated that a silicon-based PV module can produce a power density output, thermal losses, and maximum voltage of 115.68 W cm^{-2}, 18.14 W cm^{-2} and 30.87 V, at a radiator and PV cells temperatures of 1800 K and 300 K, respectively. Alike the solar photovoltaic generation, the open circuit voltage degraded when the temperature of the TPV cells increased. For an 80 W PV module, there was a potential for improving the power generation capacity by 45% if the radiator and PV cells of the TPV system were operated at a temperature of 1800 K and 300 K, respectively. Indeed, the intermittency of meteorological variable affects PV-based technologies such as an IPVFC system. Thus, a thermodynamic-based procedure was developed to determine an optimal location among multiple locations for installing a large-scale photovoltaic power generation to achieve economic, performance and environmental objectives. To achieve an improved efficiency, reduced cost, and lesser complexity of IPVFC systems, a Unitized Regenerative Proton Exchange Membrane Fuel Cell (URPEMFC) system was considered to replace electrolyser and fuel cell components. This is because an IPVFC system with a lower complexity would be beneficial during the manufacturing and operation stages of the system. Although the theoretical thermodynamic efficiency of a URPEMFC system was about 68.86%, the study predicted an efficiency of 44% for a stack of 10 cells at a current density of 0.5 A cm^{-2}. This performance level of a URPEMFC component was better than using a PEME and a PEMFC for electrolytic and galvanic functions, respectively. Still, to advance the performance of the URPEMFC component, the inherent power hysteresis effect needs to be addressed by reducing the overpotentials and irreversibilities in the component. Lastly, a systematic and systemic analysis of possible thermodynamic pathways to realise an IPVFC system with the optimal cost-efficiency-complexity benefits was performed. The finding indicated that a PV/T-Battery-URPEMFC system with unitized converter-inverter appeared to offer an optimal configuration to generate power, heat and hydrogen and it is therefore recommended for further investigation for various distributed applications. Overall, improving the effectiveness of IPVFC systems depended on the thermodynamic characteristics of the composition and achieving optimal design configuration of components within the design space to realise the least cumulative exergy destruction, whilst reducing the cost and complexity of the system.

Declaration

No portion of the work referred to in the thesis has been submitted in support of an application for another degree or qualification of this or any other university or other institute of learning.

Copyright Statements

Dedication

To my wife Mary Ogbonneya Chukwuma, and my children - Sophia Chikamsoaga Chukwuma, Michael Chijindum Chukwuma, Emmanuel Chizitaram Chukwuma and David Chinedum Chukwuma.

Acknowledgements

I want to thank the Petroleum Technology Development Fund (PTDF) Nigeria for funding my research through the Overseas Scholarship Scheme (OSS). Indeed, the support was fundamental in helping me to pursue this PhD research and it is sincerely appreciated.

I am blessed to have had Professor Ali Turan, Dr. Chamil Abeykoon and Dr Adel Nasser as my PhD supervisors, although Professor Ali Turan left the University after two and half years into my research. Yet, he continued to provide valuable advice and feedbacks on the direction of the research. The supervisory team gave me opportunities to take informed risks, learn, train, and aspire to the highest academic, research and professional standards. I also thank Professor Timothy Stellard, the Head of Department of Mechanical, Aerospace and Civil Engineering, for the support during the reconstitution of my supervisory team. Dr. Katherine Smith, the Head of Space Research Group, is appreciated particularly in supporting me to purchase a TRNSYS software and to attend conferences. I also acknowledge the support of my PhD advisor, Dr. Mark Quinn as well as the valued guidance of my first-year internal assessor – Dr. Imran Afgan. I am also grateful for the administrative support from Beverley Knight, Olivia Marsh and Alan Pease.

I am profoundly grateful to my External examiner, Professor Gehan Amaratunga of Cambridge University, United Kingdom; my internal examiner, Dr Jaise Kuriakose; and the Independent Chair of my PhD examination, Dr Sergey Utyuzhnikov. The PhD Viva gave me a valuable opportunity to learn and receive pertinent feedback that significantly improved all aspects of my PhD thesis.

I want to specifically acknowledge the editors and anonymous reviewers of the following Journals for their valuable feedbacks that enhanced the quality of my research process and outcomes: Solar Energy, Journal of Energy Storage, Thermal Science and Engineering Progress, Energies, Cleaner Engineering and Technology, Journal of Cleaner Production, Cleaner Environmental Systems, Applied Energy, Renewable and Sustainable Energy Reviews, International Journal of Hydrogen Energy, and others.

I want to thank the Nigerian Meteorological Agency Abuja for providing raw solar radiation and temperature data used for the simulations.

I acknowledge the enabling environment created by my wife and our children – Sophia, Michael, Emmanuel and David. Without their understanding and sacrifices, continuing the study at home when the COVID-19 pandemic caused the closure of the University would have been more difficult. I thank my mother, Josephine Ogbonnaya, and indeed my siblings and extended family for their love, prayers and supports. I thank The Brilliant Club for providing me with the opportunity to develop a public engagement handbook based on my PhD research. The handbook titled “Combating Climate Change through Renewable Energy” was used to teach over 120 KS4 pupils across Greater Manchester and the programme helped me to provide evidence for my Fellowship certification in the Advanced Higher Education Academy (FHEA). I also acknowledge the individual supports and encouragements of Engr. Dr. C. S. Ume, Dr. David Igwe, Dr Beryl Aaron, Dr. Eni Oko, Pastor Wale Hamzat, Sarah Cobain and Lekan Onasanya. May I also thank all other persons or organisations that may have contributed in one way or the other to make my overall experience during the PhD programme rewarding, bearable and transformational.

Finally, I thank God for the strength, provisions, and inspirations over the years of my PhD research.

List of publications/Conference papers

Research Articles

C. Ogbonnaya, C. Abeykoon, A. Nasser, A. Turan; C.S. Ume. Prospects of Integrated Photovoltaic-Fuel Cell Systems in a Hydrogen Economy: A Comprehensive Review. Energies 2021, 14, 6827.

C. Ogbonnaya, C. Abeykoon, A. Nasser, A. Turan, *Unitized Regenerative Proton Exchange Membrane Fuel Cell System for Renewable Power and Hydrogen Generation: Modelling, Simulation, and Case Study*, Cleaner Engineering and Technology, 4, (2021) 100241.

C. Ogbonnaya, C. Abeykoon, A. Nasser, A. Turan; C.S. Ume; U.M. Damo; Turan, A. *Engineering risk assessment of photovoltaic-thermal-fuel cell system using classical failure modes, effects, and criticality analyses.* Clean. Environ. Syst. 2021, *2*, 100021, doi:10.1016/j.cesys.2021.100021.

C. Ogbonnaya, C. Abeykoon, A. Nasser, A. Turan. *A Computational Approach to Solve a System of Transcendental Equations with Multi-Functions and Multi-Variables.* Mathematics 2021;9:920. https://doi.org/10.3390/math9090920.

C. Ogbonnaya, A. Turan, C. Abeykoon, *Robust code-based modeling approach for advanced photovoltaics of the future*, Sol. Energy. 199 (2020) 521–529. https://doi.org/10.1016/j.solener.2020.02.043.

C. Ogbonnaya, C. Abeykoon, A. Nasser, A. Turan, *Radiation-Thermodynamic Modelling and Simulating the Core of a Thermophotovoltaic System*, Energies, 13(22) 2020, https://doi.org/10.3390/en13226157.

C. Ogbonnaya, A. Turan, C. Abeykoon, *Numerical integration of solar, electrical and thermal exergies of photovoltaic module: A novel thermophotovoltaic model*, Sol. Energy. 185 (2019) 298–306. https://doi.org/10.1016/j.solener.2019.04.058.

C. Ogbonnaya, C. Abeykoon, U.M. Damo, A. Turan, *The current and emerging renewable energy technologies for power generation in Nigeria: A review*, Therm. Sci. Eng. Prog. 13 (2019). https://doi.org/10.1016/j.tsep.2019.100390.

C. Ogbonnaya, A. Turan, C. Abeykoon, *Novel thermodynamic efficiency indices for choosing an optimal location for large-scale photovoltaic power generation*, J. Clean. Prod. (2019) 119405. https://doi.org/10.1016/j.jclepro.2019.119405.

C. Ogbonnaya, A. Turan, C. Abeykoon, *Energy and exergy efficiencies enhancement analysis of integrated photovoltaic-based energy systems*, J. Energy Storage. 26 (2019). https://doi.org/10.1016/j.est.2019.101029.

Conference papers/Seminars

C. Ogbonnaya, *Exergy-Centred Design: Implications for Cost-Efficiency-Complexity Interrelationships for Integrated Clean Energy Systems*, Aerospace And Thermofluids Research Group Seminar Series, University of Manchester, United Kingdom, 24 November 2021.

C. Ogbonnaya, C. Abeykoon, A. Nasser, *Advanced theromodynamic modelling and simulation of photovoltaic and thermophotovoltaic systems*, MACE PGR Seminar Series, 29 April, 2021.

C. Ogbonnaya, C. Abeykoon, A. Nasser, *Ending Energy Poverty in Africa using Renewable Energy*, 2021 Africans in STEM Symposium, 23 – 24th April, 2021.

C. Ogbonnaya, A. Turan, C. Abeykoon, *Novel Code-Based Modeling approach for photovoltaic power generation*, in: Proc. 2019 MACE PGR Conf., 2019: pp. 24–26.

C. Ogbonnaya, A. Turan, C. Abeykoon, Modularization of integrated photovoltaic-fuel cell system for remote distributed power systems. In *Industry 4.0–Shaping The Future of The Digital World: Proceedings of the 2nd International Conference on Sustainable Smart Manufacturing (S2M 2019), 9–11 April 2019, Manchester, UK* (p. 303). CRC Press.

Awards/Recognitions

- Teaching Excellence Award 2021, FSE GTA LEAP Team
- Doctoral Researcher Award (DRA) 2020 (5th Position – Engineering Sciences)
- Fellow, Higher Education Academy (FHEA)
- Member, The Institution of Engineering and Technology (MIET).
- The University of Manchester Library Opencon2018 Award.

Chapter 1: Introduction

Renewable energy technologies (RETs) are actively researched to mitigate the current global energy crises, climate change impacts and energy poverty particularly in developing countries [1–3]. Indeed, there is a need to improve the competitiveness of RETs over the conventional energy systems given that renewable energy resources are sustainable because they are inexhaustible in nature [3,4]. However, for RETs to replace most of the existing conventional (or fossil-fuel-based) energy systems, components for harvesting, storing, transporting and conserving renewable energy need to be more effective [1]. Meantime, emphasis on low-carbon technologies would subsist as long as greenhouse gases (GHGs) emissions, which exacerbate anthropogenic climate risks, continue [2].

The increasing economic development across the globe implies that more power supply is needed for homes, offices, industries, mobilities, and public infrastructures. This implies that diminishing fossil fuels may be unsustainable in meeting future energy needs in few centuries ahead. Worst still, the current population of the world which is about 7.3 billion is expected to reach 11.2 billion by 2100 [5]. By 2050, the population of China, India, Indonesia, Nigeria, Pakistan, and the USA may exceed 300 million [5]. Energy infrastructures are key components of 21st century economies and the emerging low-carbon economic development would need clean and smart energy systems to sustain them.

Although the role of energy is critical, sustainable energy supply for economic developments in low income and developing countries (LIDCs) are often hampered by underdeveloped and unreliable power generation, transmission, and distribution infrastructures. For instance, about 580 million people lacked electricity in Sub-Saharan Africa in 2019 and this could be worsened post-COVID-19 pandemic according to the International Energy Agency (IEA) world energy outlook for 2020 [6]. World Bank [7] estimated Nigeria's population to be about 186 million in 2016 but it is currently over 200 million. Yet, Nigeria generates about 7566.2 MW daily which is not sufficient to drive economic development of the country [8]. Meanwhile, distributed renewable energy systems could provide sustainable energy closest to the end-users, without depending on the transmission infrastructure of national grids [9]. Distributed generation also provides an opportunity for hybridisation/integration of two or more generating components into distributed mini- or microgrids.

1.1 Integration of Photovoltaics and Fuel Cells for Power Generation

Generally, the purpose of integrating/hybridising generating components may include increasing the energy and exergy efficiencies, reducing life-cycle cost, reducing system complexity, improving the reliability and stability, reducing the overall GHG emissions, *et cetera* [10, 11]. In this study, pathways to integrate photovoltaic (PV) arrays and fuel cell are explored. Generally, electrical energy from PV systems is stored with batteries or supercapacitors. PV-Battery systems are more appropriate for developed countries where the user can fall back on power supply from the utility and users can also dispatch excess electricity to the grid and be paid under feed-in-tariff scheme. The power demand and supply dynamics of a PV-Battery system would change if it was used as a stand-alone (off-grid) system. First, any excess generation would be wasted, any demand above the capacity of the battery would not be met and if the system happen to run down at night, the user needs to wait till there is solar radiation.

Integrating PV-Batteries and fuel cell (FC) stacks to create a type of an integrated photovoltaic-fuel cell (IPVFC) system could enhance the resilience, reliability, and power quality of the system [12]. This is because the fuel cell can be used to smoothen the energy demand and supply unpredictability in a PV-Battery system. A typical IPVFC system [13] is a clean energy technology (CET) which uses solar energy as the prime mover to generate electrical energy with a photovoltaic component, so that battery/supercapacitor banks can be charged, whilst a portion/excess electricity can be used to generate hydrogen using an electrolyser. Eventually, on demand, hydrogen can be used to generate electricity with fuel cells in the full or partial absence of solar radiation or when the capacity of the battery is exceeded. Depending on the use case, hydrogen from the electrolyser can also be used as an input into chemical processes such as the synthesis of ammonia. Different categories of IPVFC systems representing alternative design methodologies, configurations, and compositions are presented in Chapter 2.

Other generation methodologies include solid oxide fuel cell-microturbine system [11, 14], parabolic dish-Rankine-organic Rankine cycle-fuel cell system [15], photovoltaic-fuel cell-wind turbine system [16, 17], solid oxide fuel cell-thermophotovoltaic system [10], and PV-wind-battery-diesel system [18]. Certainly, integrating multiple generating components adds complexity to the design, power management and control strategy, and may increase the total cost of the system with no guarantee that the integrated efficiency would improve.

In 1988, Rahman and Tam [19] studied the applicability of IPVFC systems for grid and stand-alone applications. Their prototype gave hope that PV modules could be integrated

with fuel cells. Since then, IPVFC systems have been investigated because of their sustainability prospects [20]. Solar-based distributed systems across the globe up to 2009 according to their configurations were reported in [21]. The maximum energy efficiency of IPVFC system was calculated to be 9.7 % whilst the exergy efficiencies was 9.3%. Shaygan et al [22] calculated the exergy efficiency of an IPVFC system to be 21.8% in a recent study. Certainly, these low exergy efficiencies indicate the need to improve the thermodynamic efficiency of IPVFC systems [23]. Although IPVFC systems [22,24–26] can be used for grid and off-grid applications, their modularity suggests that there could be a thermodynamic pathway that could lead to an optimal cost-efficiency-complexity (CEC) benefits. As of it, there is a need to investigate the optimal design and thermodynamics of IPVFC systems to explore the thermodynamic pathways that would yield effective system under distributed stand-alone, as well as grid applications. IPVFC systems can be applied in off-grid rural amenities, off-grid islands, unmanned aerial vehicles (UAVs), hybrid electric vehicles, boats, buildings, telecommunications substation, remote agro-processing factory, remote research stations, microgrids, and for desalination, and synthesis of ammonia.

The basic components of a typical IPVFC system are PV modules, batteries, electrolyser, fuel cell, power conditioning components (converter, inverter, charge controller, maximum power point tracker (MPPT), bus bars) and the ancillaries of these major components (e.g fans, blowers, compressors, tanks, pipes, pumps, humidifiers, sensors for temperature, pressure, humidity, mass flows, etc). Based on functional analysis, the PV generates electrical energy with solar radiation. The maximum power output is extracted from PV module and fuel cell using MPPT algorithms. The voltage of the DC from the PV and fuel cell are conditioned using DC converters. The battery bank stores the DC current from the PV. DC loads such as electrolyser can be fed from the DC bus bar, but AC loads need DC/AC inverters to change the power wave form from DC to AC. Electrolyser generates hydrogen and oxygen with electrical energy from the PV so that they can be stored in tanks. The ability to store hydrogen depends on the capacity of the tank. Lastly, fuel cells generate DC with stored hydrogen and oxygen/air gases.

To underscore the complexity of achieving an optimal CEC benefit of IPVFC system, there is need to highlight that the components may be of many types with different characteristics. For instance, there are many types of solar cells that can be used in the PV component [27]. Solar cell metallic/semiconductors materials (Cu, Zn, Ga, Cd, In, Sb, Te, Se, S, P, Ge, Al, As, Si) can be in pure (e.g. monocrystalline Si) or alloy forms (e.g. SiGeSn). There is also a blend of metals and organic materials (e.g. hybrid perovskites). PV modules can be

integrated with thermal absorber and fluid circulatory system to create a photovoltaic-thermal (PV/T) system. Harnessing electricity and heat from the same surface area of installation means that the energy efficiency of the PV/T module would increase over a PV module [28].

Energy storage with batteries can be done with Li-ion batteries [25] or lead acid batteries [29] or capacitors (SC). Batteries and SC can also be combined to improve the reliability of the system [30,31]. Although this research focuses on proton exchange membrane (PEM) technologies, there are different types of electrolysers (e.g. proton exchange membrane, anion exchange membrane, alkaline, solid oxide) and fuel cells (e.g. proton exchange membrane, solid oxide, phosphoric acid, molten carbonate, alkaline) [32]. A PV module produces electrical energy and waste heat, and the electrical energy can be used by a proton exchange membrane electrolyser (PEME) for water electrolysis to produce hydrogen and oxygen. Again, proton exchange membrane fuel cell (PEMFC) can utilise hydrogen from PEME without further processing. Together, PEME and PEMFC can generate solar hydrogen through water electrolysis (which is a green hydrogen) with zero emission compared to hydrogen from fossil fuels (which is a blue hydrogen) that involves emissions, pollutions, and environmental degradation.

1.2 IPVFC Systems in the Context of a Hydrogen Economy

It has been asserted that renewable hydrogen could change the dynamics of energy and fuel market as the enabling technologies improve [33]. This is because hydrogen will be the main energy vector in a hydrogen economy to provide heat, electricity, energy storage and feedstocks for industrial chemicals and processes [34]. In the foreseeable future, fossil fuels will not be faced out completely, although there is a likelihood that it may be faced down with time and eventually be faced out as combustion fuels. For now, fossil fuels remain the major source of commercial hydrogen [35]. In a hydrogen economy, processes such as water electrolysis using solar energy would be a clean source of hydrogen. Figure 1.1 shows the positioning of IPVFC system for possible integration with diverse energy and feedstocks in a hydrogen economy. Solar hydrogen can be generated through photoelectrolysis, water electrolysis, water thermolysis, and photobiological approaches [21]. The specific use case of an IPVFC system will determine the sizing and configuration of the system.

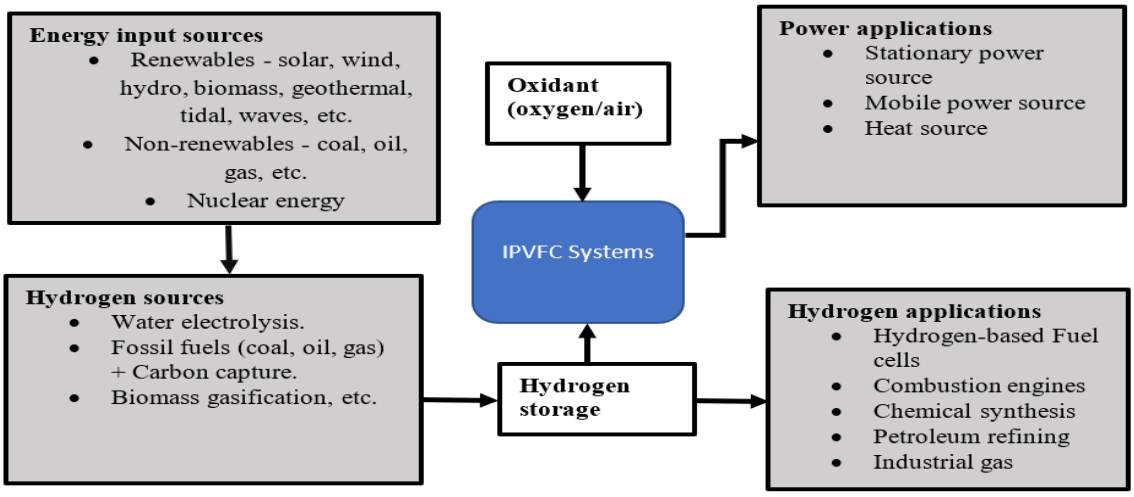

Figure 1.1: Contextualising IPVFC systems in a hydrogen economy [36].

1.3 Thermodynamics of Power Generation

Power generation systems such as IPVFC systems are subject to the laws of thermodynamics. Thermodynamics is from two Greek words "therme" and "dynamis" which means "heat" and "power", respectively. Thus, thermodynamics is defined as the science of energy and energy transformations [37]. Thermodynamics is studied by both physicists and engineers. However, an engineering thermodynamics approach is adopted in this study so that the interaction between components and their environment can be investigated based on the laws of thermodynamics.

The first law of thermodynamics (also referred to as the law of energy conservation) stipulates that the change in the energy of a system is equivalent to energy input minus energy output. The second law of thermodynamics considers both the quality (exergy) and the quantity of energy. Exergy is the maximum theoretical work that a system can perform as it interacts with its surrounding at a reference state [23]. The second law acknowledges the significance of entropy generation which determines the orderliness or disorderliness in a system that is undergoing reversible or irreversible processes. As a system passes from one state to another in a thermodynamic cycle, the sum of the exergy input will differ from the sum of exergy output due to the destruction of exergy in the system and thermodynamic losses. Whereas energy can neither be created nor destroyed but can be transform from one form to another, exergy can be destroyed, and losses can be accumulated. This explains why a thermodynamic system cannot produce 100% output energy from any set of energy and mass inputs into the system. Since exergy analysis measures the degree of imperfections in a system, the second law analysis is better positioned for investigating why and how a system

incurs losses, as well as how insights can be generated to improve the thermodynamic efficiency of the system.

This study proposes exergy-centred design (ExCD) analysis to discover imperfections in IPVFC systems so that the components with the lowest exergy efficiency could be improved to achieve higher overall energy and exergy efficiencies. Later, a description of the thermodynamic system boundaries considered alongside the energy and exergy flow across the boundaries will be defined for the specific contexts investigated.

1.4 Problems of Study

There are versions of IPVFC systems that have been investigated using both experimental and model-based studies as would be shown in Chapter 2. Specifically, this research is investigating the thermodynamic pathways to integrate a PV-based technology and a fuel cell-based technology to create an optimal IPVFC system. This integration creates a design space from which innovative energy systems can be explored. There are no current studies that have critically examined the CEC rationales for adding PEME and PEMFC components to PV-Battery systems using ExCD approach. Contextually, ExCD approach is an inductive process which can be used to improve a parent system to an offspring system if there are rationales to do so. This approach differs from the current approach for performing exergy analysis. Traditional exergy analysis is a deductive process which can only establish the exergy efficiency of a system with disregard to its parent or possible offspring systems. Meanwhile the modularity in design of IPVFC systems could result in several configurations and needs a critical exploration of the design space to investigate how an optimal CEC outcome can be realised.

To illustrate, assuming that the parent system of an IPVFC system is PV-Battery system, and that a PEME and a PEMFC were added to the parent to create an offspring PV-Battery-PEME-PEMFC system. There is a need to understand how the addition of PEME and PEMFC would affect the overall thermodynamic efficiency of the offspring IPVFC system. There could be a thermodynamic improvement or degradation of offspring systems from a parent system within a modularisable design space. The outcome of the improvement or degradation of an offspring over its parent may be “user-inclined” or “thermodynamic-inclined”. The construct referred to as a user-inclined outcome is a rational decision that a user would likely make between the parent system and its offspring system. Such choice could be motivated by a real or perceived CEC benefits. On the other hand, a

thermodynamic-inclined outcome is an outcome that are determined by the physics of the system. Designers and developers can influence thermodynamic-inclined outcomes through energy and exergy efficiencies optimisation to increase the chances of a user accepting a system. From Table 1.1, a rational user would ordinarily prefer a cheap, highly efficient, and less complex system. A mono-objective such as cost, efficiency or complexity can easily be decided. Bi-objectives such as high cost-complexity relationship is natural because the cost of a complex system should be higher than the cost of a simpler system.

Table 1.1: Cost-efficiency-complexity interrelationships

	LOW	MEDIUM	HIGH
Cost	•		
Efficiency			•
Complexity	•		
Cost-efficiency	•		•
Cost- complexity			
Efficiency-complexity	•		•
Cost-efficiency-complexity	•	•	•

Nonetheless, bi-objectives such as cost-efficiency, efficiency-complexity, as well as tri-objective of cost-efficiency-complexity are unpredictable since it is not certain that costly offspring systems are more efficient or that highly complex systems are more efficient or that a costly and complex offspring system will certainly be efficient. These complex interrelationships are of interest in this research because thermodynamic efficiency alone cannot provide a comprehensive view of the sustainability of a system. Thus, this research seeks to develop methodologies and models that can provide CEC decision-making insights into the design, development, and applications of IPVFC systems.

Furthermore, there is a problem of mismatch between cumulative power generated/stored and cumulative power demanded in a PV-Battery system due to the intermittency of solar radiation as illustrated in Figure 1.2. This is an operational problem that could pose reliability risks. Principally, this research considers off-grid scenarios, which implies that the system must be self-sufficient throughout the year. A solution to the reliability problem of a stand-alone PV-battery system could be increasing the PV capacity and adding more battery capacity but the cost of the system would also increase. Moreso, oversizing to guarantee reliable power supply may lead to waste of electricity when the batteries are fully charged. Thus, offspring IPVFC systems investigated in this research are intended to make a parent PV-Battery system operationally robust, resilient, and reliable by smoothening the mismatch

between periods of low power generation that coincide with periods of high demand for power. The mismatch is highly plausible because of the dependency on solar radiation and system failures may be more impactful for stand-alone PV-Battery systems.

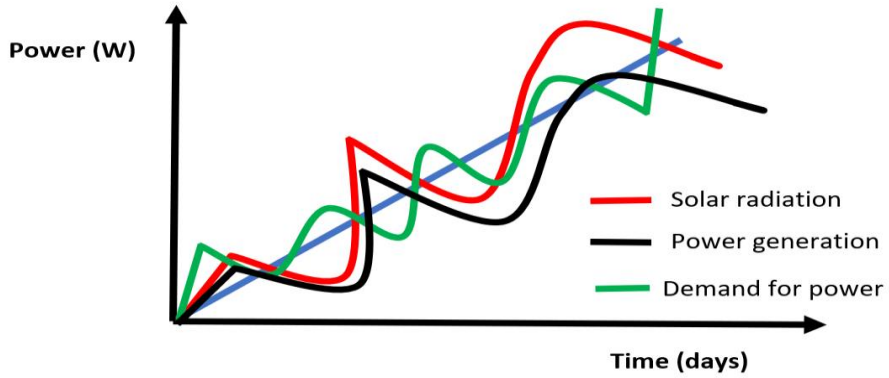

Figure 1.2: Illustration of the mismatch between cumulative solar availability, efficient power generation and demand for power.

This research separates operational efficiency from thermodynamic efficiency. Operational efficiency relates to energy management schemes designed to achieve optimal demand and supply of energy. Thermodynamic efficiency is a scientific ratio of energy/exergy output to energy/exergy input into a system. Thermodynamic efficiency is a function of the environmental variables, functional materials in the system and design composition and configuration of the system. Sustainability of IPVFC systems may be enhanced if high thermodynamic efficiency systems are managed at a high operational efficiency.

Although RETs do not produce GHG emissions during operation, there is a need to consider the entire life-cycle emissions or carbon footprint to ascertain the extent to which the systems satisfy environmental sustainability. RETs may involve an emission of GHGs during the manufacturing processes, transportation, installation, decommissioning, and end-of-life management. As such, this research considers the entire life-cycle carbon footprint of IPVFC system and not just the level of emissions during operation.

1.5 Research Questions

Based on the problems associated with the evolution of PV-Battery systems to IPVFC systems, the following research questions are formulated to be investigated in this work:

Research Question 1: Can exergy-centred design analysis provide insights on how to reduce the conversion and usage losses from a photovoltaic-based energy system?

Research Question 2: What should be an effective approach to overcome the transcendental nature of a photovoltaic model in order to improve its modelling and simulation?

Research Question 3: Can the solar, thermal, and electrical exergies of a photovoltaic module be integrated to create a unified photovoltaic-thermal model?

Research Question 4: How can the radiative heat transfer, power density output, and thermal losses in the core of a thermophotovoltaic system be integrated?

Research Question 5: How can the optimal location among multiple locations for installing a large-scale photovoltaic power generation be determined using a thermodynamic approach?

Research Question 6: Can the power hysteresis effect in a unitized proton exchange membrane fuel cell system be modelled to study its effect on the power generation characteristics of the system?

1.6 Aims and Objectives of this Work

Given the possible variations in the characteristics of offspring IPVFC systems as they evolve from their parent systems, the overarching aim of this study is to realise an IPVFC system with the optimal CEC benefits. To achieve this aim, the specific objectives of this research are as follows:

Research Objective 1: Develop a methodology for exergy-centred design analysis of photovoltaic-based energy systems.

Research Objective 2: Advance a code-based modelling (CBM) approach as a means of overcoming the limitations of a typical block-based modelling (BBM) approach for photovoltaic modelling and simulation.

Research Objective 3: Integrate the solar, thermal, and electrical exergies of a photovoltaic module to gain novel physical insights.

Research Objective 4: Integrate the radiative heat transfer, power density output, and thermal losses in the core of a thermophotovoltaic system to gain novel physical insights.

Research Objective 5: Develop a methodology for determining the optimal location among multiple locations for installing a large-scale photovoltaic power generation using a thermodynamic approach.

Research Objective 6: Model and simulate the power hysteresis effect in a unitized proton exchange membrane fuel cell system as a means of reducing the overpotentials (or thermodynamic irreversibility) in the component.

1.7 Justification of Research

The first justification for undertaking this research is based on the need to establish an advanced inductive ExCD approach to facilitate a scientific approach to rationalise the CEC benefits of PV and fuel cell integration. Currently, it appears that researchers are simply combining different compatible generating components and calculating their integrated energy and exergy efficiencies without recourse to other variables such as cost and complexity. Establishing a practical and scientifically sound basis for justifying system integration is worthwhile beyond the study of IPVFC systems because the methodology can be applied to seek design innovations for any system with a parent-offspring relationship within a design space.

The second justification of this study is that it could provide useful information for deploying photovoltaic-based energy systems in Nigeria to improve the country's power generation. With about 59.3% access to electricity based on population, there is a need to search aggressively for all possible RETs that can be applied to boost power generation in Nigeria to achieve a sustainable development while achieving net-zero targets [8,38]. There is also low renewable energy penetration in Nigeria as only 15.61% of the current generation capacity is from renewable sources while the rest of the 84.39% of energy production is based on fossil fuels [8]. This research was funded by the Petroleum Technology Development Fund (PTDF) Nigeria to contribute to knowledge on how Nigeria can leverage abundant solar energy resources to increase country's power generation. IPVFC systems can be deployed to improve the living standard and productivity of Nigerians without the limitations of the current ineffective power infrastructures. The findings from this study could be useful for other developing countries with weak power generation, transmission, and distribution infrastructures, particularly in Africa, Asia and Middle East, given that solar energy is ubiquitous across the globe.

The technical justification of this study is that optimised IPVFC systems could be applied for power, heat, and hydrogen generation in a hydrogen economy. This research intends to generate an advanced knowledge of IPVFC systems from thermodynamic perspectives. A deeper understanding of the thermodynamic characteristics of the components and at a system level could give new insights on how to design and effectively operate the systems

for diverse power, combined heat and power and hydrogen generation applications. The integration of batteries and hydrogen-based systems would improve the reliability of IPVFC systems over PV-Battery systems since hydrogen has better prospects for large-scale long-term energy storage applications compared to batteries [39]. Again, for stand-alone distributed applications, any excess energy in a PV-battery system would be wasted as it cannot be dispatched to the grid.

There are imminent legal, regulatory, economic, and environmental justifications for studying IPVFC systems. United States, European Union, United kingdom, China, Brazil and other countries are increasingly implementing policies and laws to decarbonise their economies using renewable energy sources [40,41]. This implies that there is an increasing need to expand renewable energy storage capacity and energy storage alternatives given that renewable resources are inherently intermittent. The major disadvantage of battery storage systems is that the marginal value per kWh of storage falls as the storage capacity expands, although the economics of a battery storage may depend on the use case [42].

The justification of the model-based system engineering (MBSE) approach is based on its cost, time-saving and methodological effectiveness in exploring the fundamental physics of IPVFC systems and various components. For instance, the work done in this research could facilitate "computational photovoltaics" so that the design and optimisation of PV cells and systems could be achieved through modelling and simulations before committing resources to the realisation of the project. Thus, the results generated from this research can facilitate further model-based studies, experimental designs, and prototype development.

1.8 Contributions from the Research

There are both original methodological and theoretical contributions realised from this research. Firstly, the proposed code-based modelling (CBM) approach proved effective in overcoming the transcendental nature of photovoltaics, photovoltaic-thermal and thermophotovoltaic modelling and simulation. Secondly, the proposed energy and exergy efficiencies enhancement analysis (E^4A) approach provides a novel ExCD approach to explore CEC interrelationships of integrated energy systems with a parent-offspring relationship. Scientists and engineers can systematically apply it to estimate the opportunity costs of improving the overall thermodynamic efficiencies of an energy system.

Thirdly, the proposed thermodynamic efficiency indices (TEIs) provides a new approach for determining an optimal location among many locations using actual meteorological data.

The selection of an optimal location for a large-scale photovoltaic power generation (LSPPG) can reduce the energy and materials needed to install a photovoltaic-based power generation system.

Fourthly, an integration of solar, thermal, and electrical exergies for a photovoltaic module provided new insights into the thermodynamics of a PV module. The model and the physical insights from the study can be used for model-based and experimental studies of photovoltaic and photovoltaic-thermal systems. Fifthly, an integration of the radiative heat transfer, power density output and thermal losses in the core of a thermophotovoltaic system can facilitate the design and operational improvements of thermophotovoltaic systems. Lastly, the study on the power hysteresis effect (PHE) in a URPEMFC system gave insights into how the efficiency of the system can be enhanced. An improved URPEMFC system could replace PEME and PEMFC to reduce the cost and complexity of the IPVFC system.

1.9 Outline of the Thesis

In this thesis, Chapter 1 presents the overall background, problem of study, research questions, aims and objectives, justification of this research, and the contributions from the research. Chapter 2 presents a systematic review of IPVFC systems in order to establish the research gaps. Chapter 3 presents the overall methodology adopted to realise the aims and objectives. The first aspect of this study focussed on the analysis of photovoltaic-based energy systems as presented in Chapter 4. The E^4A approach provided insights into the CEC interrelationships of the IESs. Since PV component, which is the prime mover of IPVFC systems, was the bottleneck, efforts were made to understand the thermodynamics of PV power generation. Thus, Chapter 5 presents the development of the CBM approach to facilitate the investigation of photovoltaic, photovoltaic-thermal (PV/T) and thermophotovoltaic (TPV) pathways for energy harvesting. Chapter 6 proposes a novel photovoltaic-thermal model and compares it with the Gibbs free energy equation. Chapter 7 proposes a novel thermophotovoltaic model for TPV systems. Chapter 8 presents a proposition to use energy and exergy efficiency indices to determine an optimal location for a LSPPG based on actual meteorological data. In Chapter 9, the phenomenon of PHE in a URPEMFC system was investigated. A critical discussion of the potential pathways to achieve an optimal configuration in the light of the findings in the main chapters were made. Chapter 10 presents the conclusions from the studies, recommendations for further work and the limitations of the research. The appendices and the references are thereafter listed.

Chapter 2: Literature Reviews

This chapter presents a systematic review of literature on the aspects that are relevant to this research. Here, IPVFC systems are categorised based on their composition, configuration, and applications. However, review covered feasibility and demonstration studies, software for design, applications, and limitations of IPVFC systems.

2.1 Compositions and Configurations of IPVFC Systems

Basically, IPVFC systems can be configured to meet end-users' requirements/specifications for a certain application context. There are four categories of IPVFC systems formulated in this study as follows.

Category 1: Photovoltaic-Battery-Electrolyser-Fuel Cell for Power Generation

This design configuration generates power with the PV array as shown in Figure 2.1. Depending on the sizing, part of the power generated from the PV can be used to charge the battery in the first instance. Excess power generated or additional PV capacity is used to generate hydrogen with the electrolyser component. When there is unfavourable weather condition, or at night or when the power demanded from the battery bank exceeds the capacity of the batteries, the stored hydrogen can be reconverted into power using a hydrogen-based fuel cell [29]. The DC from PV modules, fuel cell and battery bank can be conditioned with a DC/DC converter, while a DC/AC inverter changes the DC to AC for AC loads [12]. Tlili et al [43] asserted that adding fuel cells in this design composition enhances its reliability. PEMFC does not make noise during operation due to limited moving parts coupled with the fact that it has zero emission and high energy density per unit area [44,45]. Category 1 can be applied in stationary applications in buildings, in remote off-grid applications, and in mobile applications such as in transportation systems.

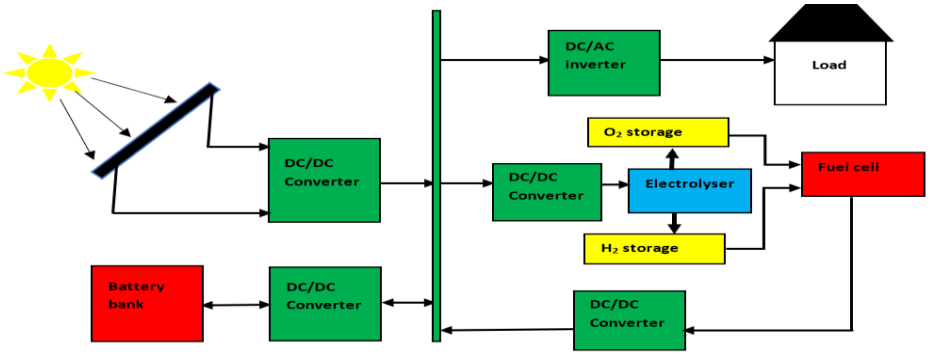

Figure 2.1: IPVFC system including a PV, a battery bank, an electrolyser, and a fuel cell [36].

Category 2: Photovoltaic-Battery-Fuel Cell for Tractive Power Generation

The major difference between Category 1 and Category 2 is that Category 2 has no electrolyser in its design composition as shown in Figure 2.2. Automotive and unmanned aerial vehicles applications can use it to reduce the weight of Category 1. In this configuration, PV module charges the battery bank, and a fuel cell stack uses onboard hydrogen to generate power for charging the battery bank in the absence of solar radiation. The battery provides a stable tractive power source to drive the vehicle. Fuel cells can provide DC for a longer timeframe using hydrogen as energy vector, which increases the reliability of the system even under adverse meteorological conditions. Category 2 can be used in integrated fuel cell hybrid electric vehicles and fuel cell electric vehicles to replace internal combustion engines in the automotive industry [46,47]. The trend will continue because significant emissions come from the automotive sector [48].

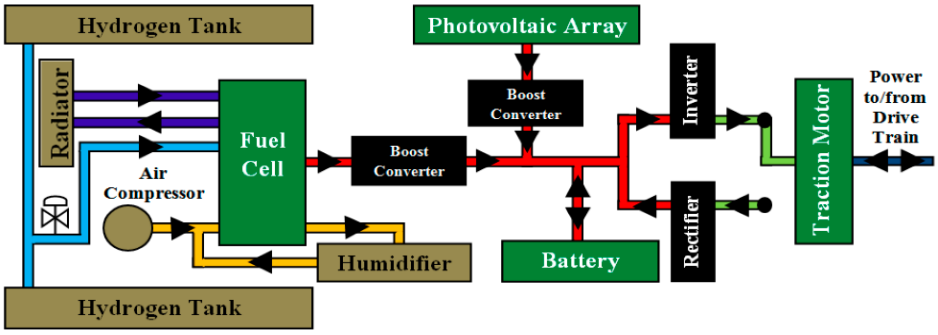

Figure 2.2: IPVFC system for automotive applications [49].

Category 3: Photovoltaic/Thermal-Battery-Electrolyser-Fuel Cell for Cogeneration

This category replaces a PV module in Category 1 with a PV/T module or solar thermal collectors [50] as shown in Figure 2.3. Thus, electricity and hot fluid can be generated, thereby increasing the thermodynamic efficiency of the system. A variation of this configuration may involve harnessing the waste heat from PEMFC, which operates between 70 to 100 °C, to increase the temperature of PEME to facilitate the electrolysis of water. This could save energy from the PV array required to heat the electrolyser. This implies that an improved overall thermodynamic efficiency of the system could be achieved since electricity which has higher exergy would not be consumed to heat PEME and waste heat from the PEMFC could be recycled to achieve additional thermal work.

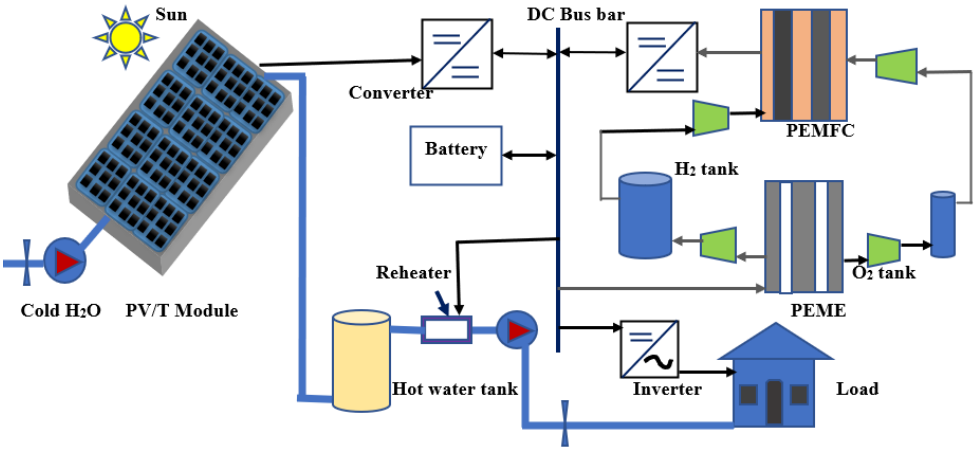

Figure 2.3: IPVFC system including PV/T, battery bank, electrolyser and fuel cell [51]**.**

Category 4: PV-Battery-Unitized Regenerative Fuel Cell System

The fourth category substitutes the electrolyser and fuel cell components with a unitized regenerative fuel cell (URPEMFC) [52]. URPEMFC systems perform the function of an electrolyser and a fuel cell [53] depending on the operating mode. Figure 2.4 shows the diagram of an integration of PV, battery bank, URPEMFC to achieve a more compact design of a mono-generation system. A design variation of Category 4 could be PV/T-Battery-URPEMFC system to create a cogeneration system with an enhanced thermodynamic efficiency, and it can also generate hydrogen for other applications.

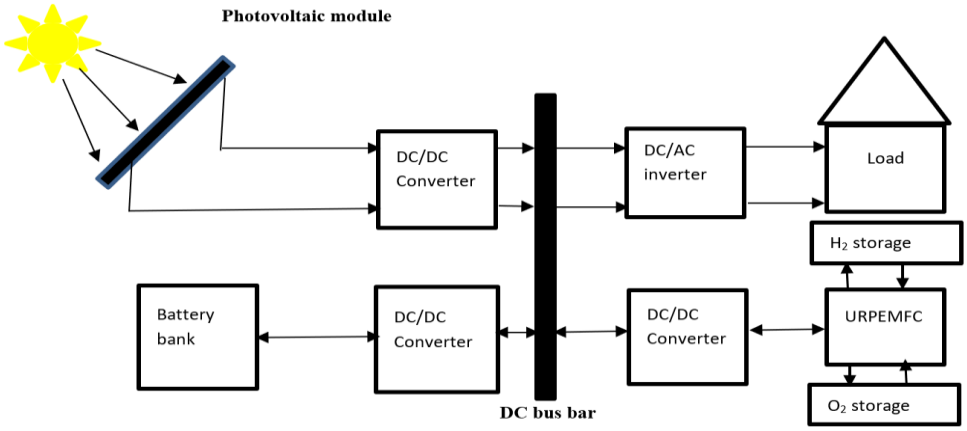

Figure 2.4: An IPVFC system including URPEMFC component [54]**.**

2.2 Feasibility Studies of IPVFC rojects

There have been efforts to design, develop and optimise different versions of IPVFC systems in the last four decades. The timelines and themes on IPVFC systems research and

development since 1980 to date are presented in Table 2.1. It appears that there is growing research on IPVFC system probably because of emphasis on decarbonisation of energy.

Table 2.1: Timelines and themes that dominated the development of IPVFC systems [36].

Decades	1980-1989	1990-1999	2000-2009	2010-2019	2020-2030
Research themes	Initial feasibility studies of solar hydrogen generation.	Demonstration plants for potential industrial scale and commercial applications.	Energy and exergy analysis; Dynamic modelling and simulation; Potential integration with other RETs.	EMS and Controller developments; Size and cost optimisation; Integration with other RETs; Case studies.	Case studies; Implementation for stand-alone and microgrid applications.
References	Rahman and Tam [19]; Kauranen et al [55]; Grasse et al [56];	Meurer et al [29]; Ulleberg [57]; Kauranen et al [55]; Friberg [58]; Goetzberger et al [59];	Yilanci et al [21]; Hwang et al [60]; El-Shatter et al [61]; Choi et al [62]; El-Maaty et al [63]; Zervas et al [64];	Thounthong et al [65]; Silva et al [13]; Hassani et al [26]; Chávez-Ramírez [66]; Ganguly et al [67]; Bambang et al [31]; Karami et al [68]; Padmanaban et al [69]; Touati et al [70]; Lajnef et al [71]; Hajizadeh et al [72]; Dash et al [73]; Majidi et al [74]; Zhang et al [75]; Ghenai et al [76]; Sharma et al [77]; Lee et al [78]; Srisiriwat et al [79]; Castañeda et al [80];	Lokar et al [25]; Hassani et al [81]; Temiz et al [82]; Kafetzis et al. [83]; Elmouatamid et al. [84]; Gonzalez et al. [85].

A demonstration facility in Germany was built to explore the potentials of stationary and mobile applications, and as a source of liquid hydrogen for testing vehicles [86]. A German-Saudi Arabia program gave scientific and engineering feasibility of solar hydrogen production and utilisation [56]. PHOEBUS project implemented at the Central Library in Forschungszentrum Julich in Germany by Ghosh et al [87] and Meurer et al [29] documented evidence of technical feasibility of a self-sufficient IPVFC system. A major finding from the study was that a PEMFC component appeared to be more reliable than an alkaline fuel cell component. Also, PV modules inclined at 40° were better than those inclined at 90°. The actual hydrogen tank has a capacity of 26.8 m^3 at 120 bar, while the 20 m^3 capacity oxygen tank operated at a pressure of 70 bar. A 15 kVA DC-AC converter had an output of 230 V AC as it was integrated with the grid.

Lokar and Virtic [25] used 24 polycrystalline PV modules, a 6.6 kWh Li-ion battery, a 7 kW electrolyser, a 7 kW PEMFC with a power density of 533.3 mW cm^{-2} and a current density

of 800 A cm^{-2} to explore an IPVFC system for grid application. Self-sufficiency is a critical factor for using IPVFC systems for distributed stand-alone applications. Reliability of remote power systems requires them to continuously supply power without frequent backup interventions. Hassani et al [81] used 8 PV modules, 100 Ah batteries, a PEME and a PEMFC with 510 W capacity and concluded that the system can operate as a self-sufficient stand-alone system.

2.3 Software for Design, Modelling, and Simulation of IPVFC Systems

Modelling and simulation is a cost-effective and time-saving means of studying systems before they can be developed fully. Choi et al [62] used fuzzy regression and LabVIEW to acquire data and monitor power generation characteristics of an IPVFC system. MATLAB/Simulink has been used to couple PV modules and PEMFC component by Natarajan et al [88]. El-Aal [63] studied topologies of an IPVFC system for power generation whereas Adi and Chang [89] used temporal flexibility analysis to evaluate the operability of IPVFC system based on energy demand and supply.

With TRNSYS and MATLAB software, Ahmadi et al [90] investigated the transient behaviour and the thermodynamics of an IPVFC system for heating, cooling and power generation. The system indicated an energy and exergy efficiencies of 29% and 36%, respectively. Shaygan et al [22] used meteorological data from Iran to perform energy and exergy analysis of an IPVFC system using MATLAB and concluded that the annual exergy efficiency of the electrolyser, fuel cell, and PV modulus were 11.2%, 32.8% and 10.8%, respectively. Overall, the system indicated an annual average exergy efficiency of 21.8%. Lajnef et al [71] used SimPowerSystems to study the dynamic behaviours of an IPVFC system. They observed that the hydrogen generated from the electrolyser caused the pressure of the storage tank to vary with the power from the PV modules. Amin et al [31] plugged a dSPACE DS1104 board into a PC mainboard to discover that the DC bus voltage was regulated with an overshoot around 6.23% and voltage ripple around 4.25%.

Table 2.2 presents the mathematical models of the components of an IPVFC system. Eqs. (2.1)-(2.5) models the power output from a PV component. Hydrogen is oxidised in PEMFC based on Eq. (2.6) which is the reverse of Eq. (2.19) which shows the water splitting reaction in the PEME. Energy is released from PEMFC; thus, it has a negative Gibbs free energy (see Eq. (2.7) and Eq. (2.8)). In reverse, a PEME has a positive Gibbs free energy because energy is inputted into it during electrolysis (see Eq. (2.20) and Eq. (2.21)).

Table 2.2: Mathematical equations for modelling the components of an IPVFC system [36]

Components	Key equations/Description		References
Photovoltaic module	$E_g(T) = E_g(0) - \frac{\alpha T^2}{T+\beta}$	Eq. (2.1)	Ogbonnaya et al [91]; Unlu [92] ; Bellia et al [93]; Muhammad et al [94]; Zeitoun et al [95]
	$I_{ph} = (I_{sc} + K_i (T_{cell} - T_{ref}) \times \frac{G}{G_{ref}}$	Eq. (2.2)	
	$I_s = I_{s,ref} \left[\frac{T_{cell}}{T_{ref}}\right]^3 \exp\left[\frac{1}{k}\left(\frac{E_g}{T_{ref}} - \frac{E_g}{T_{cell}}\right)\right]$	Eq. (2.3)	
	$I_{pv} = I_{ph} N_p - I_s N_p \left[\exp\left(\frac{qV_{pv}}{AN_s kT}\right) - 1\right]$	Eq. (2.4)	
	$P_{pv} = I_{pv} \times V_{pv}$	Eq. (2.5)	
Fuel cell	$2H_{2(g)} + O_{2(g)} \rightarrow 2H_2O_{(l)} + \text{electricity} + \text{heat}$	Eq. (2.6)	Shaygan et al [22] Ganguly et al [67] Spiegel [96]
	$\Delta\overline{g_{f,FC}} = (\overline{g_f})_{H_2} + \frac{1}{2}(\overline{g_f})_{O_2} - (\overline{g_f})_{H_2O}$	Eq. (2.7)	
	$\Delta G^o_{FC} = -nFE^o$	Eq. (2.8)	
	Electrical efficiency: $\eta_{FC} = \frac{P_{FC}}{\dot{m}_{H_2} HHV_{H_2}}$	Eq. (2.9)	
	Rate of consumption of hydrogen $(\dot{m}_{H_2}) = \frac{P_{FC}}{2 \times V_{FC} \times \eta_{FC} \times F}$	Eq. (2.10)	
	Net Voltage: $V_{FC} = V_{Nernst} - V_{act} - V_{Ohm} - V_{Conc.}$	Eq. (2.11)	
	$E_{Nersnt,FC} = E_{rev} + \frac{RT}{nF} \log\left(\frac{P_{H_2} \times P_{O_2}^{0.5}}{P_{H_2O}}\right)$	Eq. (2.12)	
	Power output: $P_{FC} = I_{FC} \cdot V_{FC} \cdot N_{FC}$	Eq. (2.13)	
	$\eta_{act_{anode}} = \frac{RT}{n\alpha F} \log((i_{loss} + i)/i_{o_{anode}})$	Eq. (2.14)	
	$\eta_{act_{cathode}} = \frac{RT}{n\alpha F} \log((i_{loss} + i)/i_{o_{cathode}})$	Eq. (2.15)	
	$\eta_{Ohm_{total}} = i(R_{elect} + R_{ion} + R_{CR})$	Eq. (2.16)	
	$\eta_{Conc_{anode}} = \frac{RT}{nF} \log(1 - (i/i_{l_{anode}}))$	Eq. (2.17)	
	$\eta_{Conc_{cathode}} = \frac{RT}{nF} \log(1 - (i/i_{l_{cathode}}))$	Eq. (2.18)	
Electrolyser	$2H_2O_{(l)} + \text{electricity} + \text{heat} \rightarrow 2H_{2(g)} + O_{2(g)}$	Eq. (2.19)	Shaygan et al [22] Ganguly et al [67] Ogbonnaya et al [45]
	$\Delta\overline{g_{f,EL}} = (\overline{g_f})_{H_2O} - (\overline{g_f})_{H_2} - \frac{1}{2}(\overline{g_f})_{O_2}$	Eq. (2.20)	
	$\Delta G^o_{EL} = +nFE^o$	Eq. (2.21)	
	Electrical efficiency: $\eta_{EL} = \frac{\dot{m}_{H_2} HHV_{H_2}}{P_{EL}}$	Eq. (2.22)	
	Net Voltage: $V_{EL} = V_{Nernst} + V_{act} + V_{Ohm} + V_{Conc.}$	Eq. (2.23)	
	$E_{Nersnt,EL} = E_{rev} + \frac{RT}{nF} \log\left(\frac{P_{H_2O}}{P_{H_2} \times P_{O_2}^{0.5}}\right)$	Eq. (2.24)	
	Power input: $P_{EL} = I_{EL} \times V_{EL} \times N_{EL}$	Eq. (2.25)	
Battery	State of charge (SOC): $100\left(1 - \frac{it}{Q}\right)$	Eq. (2.26)	Adi and Chang [89]
	Capacity of battery: $C_{batt}(A.h) = \frac{D_{energy} N_{aut}}{V_{batt} \eta_{batt} DOD}$	Eq. (2.27)	
Hydrogen tank	Pressure in the tank: $P_{H_2} - P_{H_{2\_init}} = z\left(\frac{N_{H_2} \times R \times T_{H_2}}{M_{H_2} \times V_{H_2}}\right)$ where $z = \frac{P \times V_m}{T \times R}$	Eq. (2.28)	Hassani et al [81]
Compressor	Power consumed $(\dot{W}_c) = \dot{m}_c \times C_p \times \frac{T_1}{\eta_c} \times \left(\left(\frac{P_{out}}{P_{in}}\right)^{\frac{k-1}{k}}\right)$	Eq. (2.29)	Shaygan et al [22]
Pump	Power for circulating water $(P_{pump}) = \frac{\rho \times g \times Q_w \times H}{\eta_{pump}}$	Eq. (2.30)	Shaygan et al [22]
Load	Energy used per day $(E_{load}) = \sum P_{load} \times t_{load}$	Eq. (2.31)	Hassani et al [26]

The overpotentials (i.e. activation, Ohmic and concentration (or transport)) in the PEMFC and PEME are represented by Eqs. (2.14)-(2.18) [97]. The state of charge (SOC) for the battery component and its capacity are expressed in Eq. (2.26) and Eq. (2.27), respectively. Pressure of the hydrogen tank can be computed with Eq. (28), while the power consumed to compress the gases (hydrogen or oxygen) is given by Eq. (2.29). The rate of water supply to the electrolyser with a pump can be calculated with Eq. (30). Lastly, the load is calculated as the sum of the power rating of each load multiplied by the duration of use.

2.4 Economic Assessment and Optimisation of IPVFC Systems

Due to the modularity in design of IPVFC systems, there is a need to realise configurations with optimal CEC benefits. Khemariya et al [98] studied how an IPVFC system can be used to generate maximum power output at a minimal cost in an Indian village using hybrid optimisation model for electrical renewable (HOMER) software. They concluded that the cost of energy was estimated at $0.1959 per kW. Temiz and Javani [82] stated that an IPVFC system produced about 99.43% of the electricity demand at a levelized cost of electricity of $0.6124/kWh [82].

To achieve a reliable operation, the energy flow between the PV modules, FC stacks, batteries, and the electrolyser need to be balanced. To optimise an IPVFC system, the objective functions may include to minimise emissions, cost of investment, replacement, operation, or maintenance [99]; or to maximise power output, reliability, or integrated efficiency. The constraints of the optimisation may include meteorological variables, duration of operation, load capacity, size of system, cost of the components, efficiency of the components and electrical compatibility of the components. Elgammal and Sharaf [100] investigated an IPVFC system using multi-objective particle swarm optimisation approach to explore hybrid charging with current, voltage, and power in a vehicle-to-grid battery charging stations.

2.5 Current and Emerging Applications of IPVFC Systems

IPVFC systems can be applied in DC Microgrids for data centres, communication systems, building electric systems, and plug-in hybrid electric vehicles [101]. IPVFC can also be applied in the transport sector which contributes a significant portion of emissions [102]. In the upcoming decades, IPVFC systems could be a source of heat, power, and hydrogen gas.

Table 2.3 shows how IPVFC system compares with other RETs. IPVFC systems uses ubiquitous solar energy, and it can be applied for mobile applications which might be difficult for systems containing wind turbines. It has zero emission during operation and the by-products are harmless to the environment. It is more robust in meeting off-design demands compared to PV-battery systems as the stored hydrogen can be reconverted with the fuel cell to provide power under stand-alone application. IPVFC systems can easily be adapted for green chemical production such as ammonia since excess electricity from the PV can be used to generate hydrogen using electrolyser. PV-Battery System does not generate hydrogen, but it is simpler and cheaper than IPVFC system for stationary and

mobile power generation applications. Overall, a typical IPVFC system has median cost and complexity, and further enhancement of the design and thermodynamic efficiency could be useful in a hydrogen economy.

Table 2.3: Comparison between IPVFC systems with emerging competing technologies [36]

Competing methodologies/ technologies	Description of attributes				References
	CO_2 Emission	Operating Temp.	Mobile /Stationary application	Complexity/ CHP	
PV-battery/ supercapacitors system	Zero emission	<100 ˚C	mobile and stationary	Low/ no CHP.	Glavin et al [103]
PV-battery/ supercapacitors-electrolyser-fuel cell system	Zero emission	<100 ˚C	mobile and stationary	Medium/ no CHP	Meurer et al [29]; Ogbonnaya et al [45]; Hassani et al [81].
Photovoltaic/thermal-battery/ Supercapacitors -fuel cell system	Zero emission	<100 ˚C	mobile and stationary	Medium/ with CHP	Goetzberger et al [59]; Ogbonnaya et al [45]
PV-wind-battery/ supercapacitors system	Zero emission	<100 ˚C	stationary	High/ no CHP	Moghaddam et al [99]
PV-wind-battery/ supercapacitors-fuel cell system	Zero emission	<100 ˚C	stationary	High/ no CHP	Bukar et al [17]; Cano et al [16]; Moghaddam [104]
PV-wind-battery/ supercapacitors-diesel system	Emits CO_2	700 ˚C	stationary	Very high/ no CHP	Bukar et al [18] Dufo-Lopez et al [105]
Parabolic dish-Rankine cycle-organic Rankine cycle-fuel cell multigeneration	Zero emission	1000 ˚C	stationary	Very high/ With CHP.	Ozturk et al [15]
SOFC-Microturbine system	emits	750 ˚C	stationary	High/ with CHP	Ferrari et al [11]
SOFC-thermophotovoltaic system	emits	750 ˚C	stationary	High/ with CHP	Rajashekara [10]; Lu et al [106]

2.6 Grid and Off-grid/Stand-alone Applications of IPVFC Systems

Although this study is primarily interested in the off-grid applications of the IPVFC systems, there are many potential grid applications of IPVFC systems. Ghenai and Bettayeb [76] investigated the integration of a 500 kW PV array and a 100 kW PEMFC with the grid for power supply at a University building in Sharjah, UAE. About 26% of the power consumed was purchased from the grid probably because of sub-optimal design and sizing. About 42% of the power from the PV array and 32% from the PEMFC stack were utilised while 5% of the annual output was sold to the grid.

Distributed applications of IPVFC systems can provide power to remote telecommunication infrastructure, agro-processing centres, research sites, sports, and leisure events. Ulleberg [57] studied a stand-alone IPVFC system using TRNSYS and concluded that the system

could provide reliable power. Silva et al [107] investigated the application of IPVFC system at the National Park of Araguaia, Tocantins-Brazil, and the results indicate that the system can be used in public utilities. With data from six remote off-grid Radio Based Stations (RBS), Cordiner et al [108] showed that IPVFC system provided 24/7 quality, autonomous and continuous power supply for RBS. Lee et al [78] achieved 3.8 hrs of test flight of an UAV using experimental and model-based studies at Goheung Aerospace Centre, Korea.

IPVFC system can provide power in inaccessible terrains such as mountainous, island and coastal off-grid cities. For instance, Silva et al [13] demonstrated that IPVFC systems can serve isolated communities as was the case in Amazon region of Brazil. Hassani et al [26] investigated the applicability of IPVFC systems at Bejaia, Algeria. Lokar and Virtic [25] stated that the capacity of PV arrays can be increased to meet annual shortage of hydrogen for IPVFC system, having achieved a self-sufficiency of about 62.13% for the system.

Ganguly et al [67] used the climatic conditions of Kolkata, India to show that the system was self-sufficient as a distributed system for a greenhouse. Seawater electrolysis has been facilitated using an IPVFC system [79]. IPVFC systems can also be used for remote desalination operation to convert seawater, brackish water, fresh water of unknown quality into potable water, and also generate hydrogen and electricity [70].

2.7 Prospects of IPVFC Systems in Developing Countries

Access to continuous, clean, reliable, and affordable energy supply is needed for economic development of the underdeveloped regions of the world. Certainly, the capital cost of new power generation, transmission, and distribution infrastructures could be a huge barrier to energy access in LIDCs. Developing countries require distributed generations because of the inadequacy of the transmission infrastructures required to transmit power generated from distant generation stations to local distribution networks. As of it, distributed applications of IPVFC systems implies that it can be located closest to the end-user, but it can also be connected to the grid where possible. LIDCs may not fast-track energy access using a centralised-to-decentralised strategy since national energy infrastructures are capital intensive. Decentralised-to-centralised strategy could facilitate energy access in developing countries through distributed generation using microgrids independent of the national grid. Patterson et al [109] argued that a relatively smaller scale microgrid mitigates transmission loss, and improves control, security, reliability and design flexibility.

2.8 Limitations of IPVFC Systems

IPVFC systems have huge potentials for both grid and off-grid applications. Notwithstanding, there are challenges that limit the applications of IPVFC systems. Such limitations are discussed as follows:

2.8.1 Challenges of Sizing and Cost Optimisation of IPVFC Systems

IPVFC systems face the same optimal sizing challenges common among solar-based technologies due to the intermittency of meteorological variables [110,111]. This could lead to oversizing or undersizing. Oversizing increases the total cost of the system and waste of energy may be more plausible. Undersizing could cause system failures, low reliability, poor power quality and sub-optimal performance. Hassani et al [81] investigated the optimal sizing and technoeconomic feasibility of a stand-alone IPVFC system. They observed that a particular use case could be economically and environmentally viable at a total net present cost of 61,762.66 euros. Castaneda et al [80] studied both optimal sizing and three control strategies to manage energy flow in an IPVFC system. Optimal sizing and effective control were discovered to be necessary to satisfy the loads; generate hydrogen to meet off-peak loads; and preserve the battery's lifespan through controlled charging and discharging.

The total cost of IPVFC systems can be influenced by the cost of materials such as gold, platinum, silicon, etc. Also, the use of platinum in PEME and PEMFC [10] and gold in PV module contribute to their cost. The capital cost of RETs for the same capacity is currently higher than diesel or gasoline generators [98,105]. Research efforts are made to develop alternative cheaper materials. Cost can also be reduced through design and operations management of the system. Therefore, cost and size optimisations are crucial to reduce the overall costs of energy supply with an IPVFC system.

2.8.2 Operational Challenges of IPVFC Systems

The operational risks in IPVFC systems are caused by the variability of meteorological factors [51]. Ozgirgin et al [112] showed that the power demanded from the grid to support an IPVFC system increased due to a decrease in solar radiation during winter (October to March); but the system was self-sufficient between March and October (summer months).

Operational risk of different categories of IPVFC systems involves the likelihood that possible outputs electricity, hydrogen, oxygen, hot fluid might not be available in the right quality and quantity when demanded. Risk of sizing mismatch between electrolyser and fuel cell may result in overproduction or underproduction of hydrogen based on the available solar resources. Slow response time of PEMFC could pose a risk where quick dispatch of

energy is needed. Fuel cells can be operated at a quasi-steady state while the batteries with better response time can supply power to the transient and off-peak loads to reduce the effect of repetitive stepped loads on the system. Nojavan et al [113] investigated how to satisfy uncertain electrical and thermal loads using an information gap decision theory approach. They suggested that an operator can pay less to purchase electricity from the grid but face the risk of unmet demand. An operator can be risk-averse and purchase excess electricity at a higher cost, but with more certainty of satisfying the loads.

2.8.3 Challenges of Materials and Manufacturability of IPVFC Systems

Functional materials for the PV modules, batteries/supercapacitors, PEME, PEMFC or URPEMFC components will continue to be subjects of intensive research. Advancements in the functional materials could enhance the future competitiveness of IPVFC systems. Solar cells, for instance, appear to be approaching the 33 % efficiency limit of single junction silicon solar cell predicted by Shockley [114]. Mono-crystalline and polycrystalline PV modules [25] are currently in use in IPVFC systems. Emerging perovskite solar cells is quite promising for PV power generation [115,116] and could enhance the prospects of IPVFC systems. Solar hydrogen production via water electrolysis [117] has a positive outlook for a sustainable generation of green hydrogen. Hybrid organic-inorganic metal halide perovskites solar cell could also be used in IPVFC systems because it has high efficiency (which is up to 25%), as well as easy solution-based processing [115]. Phase change materials (PCM) can manage the heat generated in PV modules for improved efficiency and safety [118].

Hydrogen can be stored as compressed gas or in liquid form. While storing hydrogen as gas requires high pressure (up to 700 bar), cryogenic storage of hydrogen requires low temperature (less than 20 K to liquify) [119]. Porous materials such as zeolites, porous carbon, carbon nanotubes, metal-organic frameworks are being considered for hydrogen storage applications [119–121]. Solid metal hydrides for hydrogen storage offer benefits such as high volume efficiency, ease of recovery, high safety, and lower loss [122].

The EL and FC modes of a URPEMFC component was improved by Zhigang et al [123] using 50 wt% Pt + 50 wt% IrO_2, and a catalyst loading of 0.4 mg cm^{-2}. Electrocatalysts based on platinum, rhodium, ruthenium and iridium oxides are increasingly being applied in URPEMFC systems [123,124]. Wang et al [125] used a ratio of 5-7 wt% hydrophobic PTFE and 7-9 wt% hydrophilic Naffion to improve the water management in URPEMFC system.

Manufacturing of IPVFC system requires many components and materials with a wide spectrum of manufacturing process technologies. This creates a complex supply chain network for producing IPVFC systems and this could impact on the cost of the systems.

Manufacturing of IPVFC system appears to need a strategy that integrates the voice of the customers to capture requirements based on the application context. A just-in-time system can be used to reduce inventory cost and lead time given the high cost of the components [126]. Manufacturing process technologies for producing PEME can be used for PEMFC components to reduce tooling cost since both components share some features. Additive manufacturing technology can also facilitate a low-cost manufacturing of the parts of the PEMFC and electrolyser [127]. There is still a need to improve the overall efficiencies of IPVFC systems to make them competitive among RETs [45]. Ezzat and Dincer [128] calculated the energy and exergy efficiencies of an IPVFC system for a vehicle as 39.86% and 56.63%, respectively, at a current density of 150 mA cm^{-2}. Table 2.4 summarises a set of criteria that have been used to assess IPVFC systems. This includes the sustainability index based on the SDGs. Applications and their manufacturability were considered. Overall, it appears that IPVFC systems will continue to receive research and development attention for various applications in the coming years.

Table 2.4: Assessment of critical aspects towards the full commercialisation of IPVFC systems [36].

Criteria of IPVFC systems	Status	References
SDG compliant	Cost reduction required (SDG 7 – Affordable and clean energy). Meets SDG 13 – Climate action.	SDG report 2019 [129].
Grid and microgrid applications	Can be applied as grid-connected and microgrid systems.	Padmanaban et al [69]; Kannayeram et al [101].
Stand-alone applications?	IPVFC system can be applied as a self-sufficient stand-alone generation system.	Hassani et al [81].
Design studies	PHOEBUS.	Ghosh et al [87]; Meurer et al [29].
Control and power management system	PMCS are available.	Kong et al [130]; Sumathi et al [131];Thounthong et al [65].
Application areas	Desalination, Agriculture, Electric Vehicle, seawater electrolysis, buildings, cruise ships, UAVs, telecommunication, chemical synthesis.	Ganguly et al [67]; Zhang et al [75]; Ghenai and Bettayeb [76]; Ghenai et al [132]; Cordiner et al [108]; Touati et al [70].
Demonstration studies	University building, Green cities, National parks, and residential buildings.	Ghosh et al [87]; Cetin et al [24]; Silva et al [107]; Grasse et al [56].
Affordability	Cost of PV, PEME and PEMFC still high. Needs reduction and improved efficiency.	REN21 [133]; Spiegel [134].
Software for design, feasibility, and dynamic modelling studies	MATLAB/, HOMER Pro, PvSys, Aspen plus, TRNSYS, LabVIEW, Simplorer software.	Khemariya et al [98]; Hatti et al [135]; Temiz and Javani [82]; Wu et al [136]; Choi et al [62]; Hwang et al [60];
Manufacturability	More investigations needed on mass commercialisation, smart manufacturing, and integration into a lean supply chain.	Ogbonnaya et al [126].
Circular economic studies.	circular economic studies yet to be done for IPVFC systems. Done for PV and fuel cell components.	Sica et al [137]; Valente et al [138]

2.9 Summary and Direction for Study

This chapter presented a systematic review of IPVFC systems including the design configurations, feasibility and demonstration studies, optimisation strategies, materials for

manufacturing the components, energy management strategies and thermodynamic performance. Their potential applications for grid and off-grid means that they can be used in both developing and developed countries. Key features of IPVFC systems include zero emission during operations; dependency on ubiquitous solar resources; applicability for remote power and hydrogen sources; have no moving parts and could be used as scalable co-generation systems.

From the review of literature, all categories of IPVFC Systems are systems of system. This implies that a component can be isolated and studied in detail. Secondly, the possible interchangeability of the components within the categories suggests that there is modularity in the design space of IPVFC system which could lead to multiple design configurations, compositions, and applications. However, different configurations would yield different energy and exergy efficiencies. Thus, there is a need to extensively explore the design space in which a PV-based technology can be integrated with a fuel cell-based technology in order to investigate the configuration that offers optimal thermodynamic efficiency with reduced cost and complexity.

Consequently, the following gaps and roadmap have been outlined to guide the study presented in the subsequent chapters.

- There is a need to develop a methodology to investigate the thermodynamics of IPVFC systems to gain further insights into CEC interrelationships of the systems. There exist studies on IPVFC systems with specific configurations but the question of what the optimal IPVFC systems looks like is yet to be systematically explored. This study considers modularisation of IPVFC systems within a design space.
- There is a need to study the PV, PEME, PEMFC and URPEMFC components using thermodynamic approach to gain insights into possible design strategies to improve the overall CEC benefits of the optimal IPVFC system.
- Based on exergy approach adopted in this research, optimisation is approached as a location problem given that solar radiation and temperature varies across the globe and IPVFC system needs to interact with its immediate environment.

Chapter 3: Research Methodology

This chapter presents the methods, tools and techniques applied to realise the objectives of the research. Since the project seeks to investigate the potential thermodynamic pathways for the integration of photovoltaics and fuel cells, a Model-Based System Engineering (MBSE) approach was adopted as the overall approach for the study. MBSE is a cost effective and time-saving approach to explore the IPVFC systems design space because of its modularity in design. This approach provided an opportunity to explore an optimal design configurations and composition. MBSE also enables a study of the potential operating benefits and risks using a scientific approach before committing resources to investigate the system experimentally. International Council on Systems Engineering (INCOSE) defined MBSE as "the formalised application of modelling to support system requirements, design, analysis, verification and validation activities beginning in the conceptual design phase and continuing throughout development and later life cycle phases " [139]. The exploration of the CEC benefits of IPVFC systems are well within conceptual design phase as the modularity in design implies that there are multiple thermodynamic pathways to integrate photovoltaics with fuel cells.

The scientific framework for this research is thermodynamics of power generation. Thermodynamic analysis can be used to investigate the energy transformations and maximum theoretical efficiencies of energy systems. In this context, MBSE approach provides a framework for consistent and robust system architecting and engineering [140] within the laws of thermodynamics. The alternative approach would have been an experimental approach, but the question would have been the rationale for developing and optimising any design configuration considering the modularity in design of IPVFC systems. Modularity in design of IPVFC systems implies that a careful procedural study could reveal insights into the design, development, manufacturability, and operations management of the optimal IPVFC system. Therefore, in this research, the model-based approach offers a cost effective and resource efficient means of system engineering, system design analysis, system improvements, system requirements analysis, functional analysis, system application contexts analysis using novel and extant models, theories, and methodologies. To support the MBSE approach, actual meteorological data, experimental data from literature and data from manufacturers product information sheet were used to validate models and procedure proposed in this research.

Given that an IPVFC system is a system of systems (SoS) due to its modularity in design, possible design alternatives are of interests. To explore the design space starting with the basic components (PV, battery, PEME, PEMFC, converts and inverters), a novel E^4A approach was proposed based on the theory of biological evolution, mutation, and inheritance. The principle of evolution implies that a simple PV-battery system can evolve in complexity provided that it utilised photovoltaics and fuel cell. The principle of mutation implies that two or more components within the design space are permitted to be unified if that would provide any CEC benefits. The principle of inheritance implies that an offspring system must have the state-of-the-art components of its parent system. The tripod CEC model shown in Figure 3.1 is an iterative model in which the objective is to focus on multiple objectives of thermodynamic efficiency and the implications of efficiency improvements of parent systems on the cost and complexity of emerging offspring systems.

Figure 3.1: Iterative tripod cost-efficiency-complexity model.

Principally, E^4A approach seeks rational design configurations that could meet optimal CEC benefits. Interestingly, the use of E^4A approach fits into system thinking, system architecting and system engineering because it provides a systematic approach to investigate components of the system in isolation as well as the effects of the components on the integrated system.

Scientifically, IPVFC systems are multi-component and multi-physics system. This creates a challenge with the interface integration of IPVFC systems from a thermodynamic modelling perspective. However, there have been integrated approach to study different aspects of IPVFC systems such as integrated control strategy [131], integrated electrical power generation characteristics [24] and integrated thermodynamic performance [22] of IPVFC systems. The major flaw of high-level integrated systems approach is that of not considering the components first thereby ignoring the causes of inefficiencies which happens

at component levels before they manifest at systems level. In this study, a bottom-up approach is used to understand how the physics of the functional parts contributes to the physics of the components, subsystem, and the integrated system. The potential effects of the physics of parts on the overall system behaviour and characteristics are shown in Figure 3.2. Due to time constraints, the scope of this study focussed on the components that contributed the highest level of exergy destruction since a reduction in their imperfections could potentially improve the overall integrated efficiency of the system.

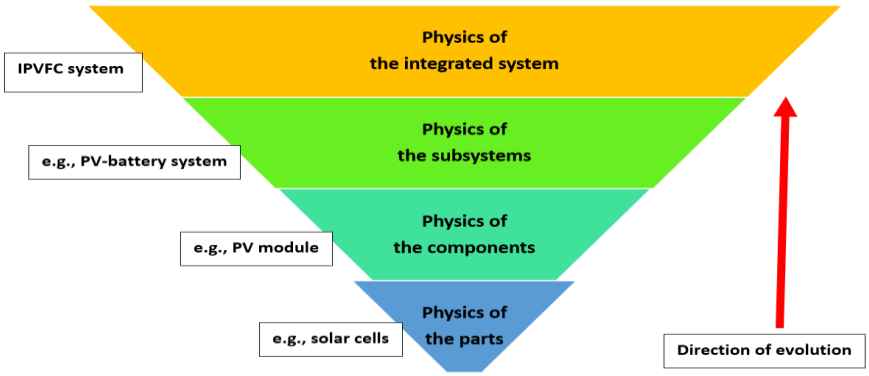

Figure 3.2: Bottom-up approach to Model-based system engineering

Within the overarching MBSE methodology, Figure 3.3 shows the methods, techniques and approaches adopted in the research. There are four major techniques used: Numerical modelling, Computational modelling, Statistical approach, and systems thinking approach.

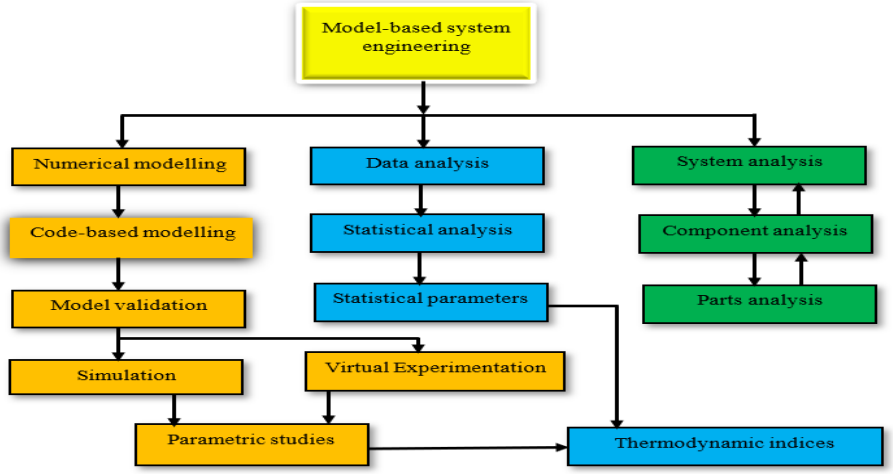

Figure 3.3: Components of Model-based system engineering approach

The first three methods facilitated thermodynamic studies to search for an optimal design configuration and composition to achieve maximum thermodynamic efficiency. As efficiency indices are numbers, they cannot indicate how the thermodynamic evolution from a parent system to an offspring system affects the cost and complexity of the offspring system. Thus, system analysis is necessary to establish the connection between the efficiency indices and the consequent cost and complexity of the integrated system. System thinking also helps to incorporate other aspects of the integrated system such as environmental impacts, reliability, manufacturability, material science and engineering, and social impacts into the whole system analyses. Further description of the applications of the methods and approaches within the context and scope of the current study are presented as follows.

Numerical modelling: This involved the use of mathematical expressions to define theoretical propositions and relationships between parameters of a defined thermodynamic system and its environment. This approach was used to propose a photovoltaic-thermal model presented in Section 6.2; and a thermophotovoltaic model in Section 7.3. Numerical approach was also used to create a code-based model of URPEMFC module presented in Section 9.3.

Code-based modelling approach: MATLAB software was used for this study. As this study is based on computational modelling, numerical models and equations were converted into computational code-based models of the component under study. Algorithms and procedures were used to implement the codes to simulate different processes and contexts. This approach was applied in Chapters 4, 5, 6, 7, 8 and 9 of the thesis.

Model validation with the experimental data from the literature: As stated earlier, the cost implications of using experimental approach at the conceptual design stage of this research is not justifiable because there are different configurations as would be shown in Section 9.5. However, to achieve realistic results, experimental data or rigorously generated indicators from literature and manufacturers' datasheet were used for validations of the proposed models and methodologies. Validations were essential to ensure that the proposed novel numerical models conform to the extant physics of the relevant parts and components before inferences can be drawn on their possible effect on the integrated systems.

Simulation: Simulation of the computational models was crucial for gaining deeper insights into the physics of the components. Based on the bottom-up approach, the effects of the

fundamental physics were used to predict the characteristics of the components in the IPVFC systems. This approach was used for predicting the power generation characteristics of a PV, TPV and URPEMFC models in Sections 5.3, 7.4 and 9.4, respectively. Another use of simulation in the study was to contextualise results with actual meteorological data as applied in Section 8.3 to determine an optimal location among multiple locations.

Parametric studies: Parametric studies were used to gain deeper insights into how changes in the parameters of the system/components, or environmental variables can affect the performance of the system. The parametric studies were performed by simulating the CB model or carrying out a "virtual experiment" within specified boundary conditions. Parametric studies facilitated the validation of the code-based PV model with commercially available modules as presented in Section 5.2. The interest was to ascertain the degree of accuracy of the CB model compared to stated parameters in manufacturers datasheet. Parametric studies were also used to investigate novel insights from the proposed theoretical models. The primary interest was to gain novel insights into the interrelationships of the power generation variables. This approach was applied in Chapters 5, 6, 7 and 9 in this thesis.

Virtual experimentation approach: Although virtual experimentation is a form of parametric studies, its application in this research was necessitated by the need to overcome the inherent transcendental nature of the PV model. Virtual experimentation allows the simulation and visualisation of multi-variables of a system of transcendental equations (SoTEs) simultaneously. For the PV modelling, after a convergence of a simulation which was iterated over the voltage, the parameters under study were extracted from the codes. This process was repeated for the range of the variables or parameters under study. The interrelationships of the extracted parameters can then be post-processed and studied using data analysis tools. The final outputs of virtual experimentations could be used as a decision-making indicator as in Section 8.3 in which thermodynamic efficiencies indices were used to predict the optimal location for installing an LSPPG.

The statistical methods were crucial in integrating actual solar radiation and temperature data into the research. The following statistical techniques were used.

Data analysis: Raw data sourced from Nigerian Meteorological Agency, Abuja were subjected to data analysis and visualisation using Microsoft Excel and MATLAB. It was assessed for the validity of the measured data and the continuity in the dataset. Data processing was also used to convert the raw data into compatible unit system. For instance,

converting the centigrade readings into Kelvin. During the study, simulations and virtual experimentations resulted in enormous amount of data that were studied and visualised using presentation tools such as line plots, graphs, and bar charts.

Statistical analysis: A fundamental statistical basis in dealing with the meteorological data was the central limiting theory (CLT). This theory posits that a large amount of data from the same domain would tend towards a normal distribution. Thus, instead of focusing on hourly distribution of solar radiation and temperature in a location in a day, which is fluctuating across the year, the average values in a day were used. Based on CLT, a location with the higher power generation potential should correlate with the location with the highest sum of daily power generation over a year. This also implies the location with the highest mean power generation. CLT facilitated the generation of statistical mean values (SMVs) that were combined with numerical and computational approaches for decision-making. Although it may appear that the use of hourly data could provide a more accurate result, hourly data would simply show fluctuations in energy and cannot be used to generate a single decision-making index. If daily data was used for generating the SMVs, it would still correlate with daily and annual energy output for the locations. Solar radiation and temperature data were subjected to probability distribution functions fitting to generate the SMVs instead of using simple average. Statistical analysis approach was used to compare the power generation potential of an LSPPG at six different locations (see Section 8.3).

System analysis: The principles of systems theory [141] was implied in this research because a typical IPVFC system is an SoS which must function through a harmonious interaction of its subsystems and the environment. Systems thinking facilitated a study of four different system configurations of PV-led energy systems using energy and exergy analysis as presented in Section 4.5. Systems thinking was also used to perform engineering risk analysis of an integrated photovoltaic-thermal-fuel cell system [51]. Systems analysis was used to predict the performance IPVFC systems in Section 9.5. In the following chapters, a combination of methods, approaches and techniques applied in each of the chapters will be elaborated under research method and approach.

Chapter 4: Energy and Exergy Analysis of Photovoltaic-based Integrated Energy Systems

There are different categories of IPVFC systems as presented in Chapter 2. This chapter addresses Research Objective 1: To develop a methodology for exergy-centred design analysis of photovoltaic-based energy systems. This objective is predicated upon the fact that thermodynamic analysis could provide insights into how energy is generated, used, and lost from IPVFC systems.

Generally, thermodynamic analysis can establish the theoretical performance limit of energy systems. Energy analysis (based on the first law of thermodynamics) excludes losses generated in the system during cycles [142]. Conversely, exergy analysis (based on the second law of thermodynamics) considers the loses and irreversibilities generated in the system [143]. From a broader perspective of resource utilisation efficiency, an energy efficient system is preferred. Yet, it is the exergy efficiency analysis that can uncover the causes of losses and irreversibility in order to improve the energy efficiency of a system [142,144]. Dincer [145] asserted that exergy analysis should be used as an energy policy tool since it measures not only the quantity but also the quality of energy sources.

Winterbone and Turan [146] also inferred that exergy analysis can assist engineers to calculate the maximum work available from a system as it interacts with its environment at a reference state. In a practical system, all the energy input cannot be converted into useful work. Therefore, an exergy analysis is crucial for investigating the sources as well as the causes of exergy destruction and irreversibilities in the system. Exergy efficiency improvement of energy systems could improve their environmental sustainability [147]. Even though solar-based technologies do not emit greenhouse gases during operations, the energy and material usage with respect to overall emissions throughout the life cycle could provide better insights into the sustainability of the systems. The notion of environmentally sustainable energy systems is linked with thermodynamically optimised energy systems with minimal environmental burden across its life cycle. Szargut [148] had argued that the cumulative exergy consumption of the constituent chemical processes should be taken into consideration in determining the degree of perfection of the system.

Although the conversion efficiency of a PV cell has been reported to have reached 46% [149], the conversion efficiency of the PV module can still be improved [150]. A fraction of solar energy received by PV modules is converted into electricity while the rest is lost to the

environment as heat [150]. PV/T modules generate electricity and recover waste heat from PV modules for additional thermal work in order to improve the overall energy efficiency [28]. Aside conversion losses from a PV, electricity generated can be lost due to inaccurate sizing of PV systems vis-à-vis the intermittency of meteorological variables. A PV-battery system, in which the battery stores energy during solar radiation is the simplest version of using PV modules for power generation [151]. If the battery is fully charged, electricity can be wasted under off-grid modes since power cannot be exported to the grid. Overcharging batteries could reduce their long-term performance. Consequently, excess electricity can be used to generate hydrogen with electrolysers so that hydrogen can be utilised to generate electricity with fuel cells at nights or when the demand exceeds the capacity of the battery [29,152].

This chapter aims to establish the configuration and composition with the optimal CEC benefits by exploring the energy and exergy efficiencies of PV-led systems in relation to their cost and complexity. To achieve this, E^4A was proposed to investigate the optimum configuration of a PV-led integrated energy systems (IESs). Attention was paid to the useful energy that can be realised from recovering the thermodynamic and usage losses from a parent system [153]. During thermodynamic optimisation of an energy system, losses can lead to mono-generation [29], co-generation [11], tri-generation [154] and multi-generation [15] systems. E^4A approach for studying PV-led systems is based on the need to recover the losses from the PV [155] and reduce operational risks due to the vagarities of solar radiation [156] or unsteady environmental/atmospheric conditions [157]. The following offspring of the photovoltaic module were studied: a PV-Battery for electricity generation for mono-generation (System 1); a PV/T-Battery for cogeneration (System 2); a PV-Battery-Electrolyser-Fuel cell for electricity generation for mono-generation (System 3); and a PV/T-Battery-Electrolyser-Fuel cell for cogeneration (System 4).

It would appear that recovering the conversion and usage losses from a parent system would improve the overall thermodynamic efficiency of the offspring system. E^4A provides a systematic approach to investigate multiple systems with parent-offspring relationships. Specifically, the following research questions have been formulated to guide the study.

1. To what extent will recovering the conversion and usage losses from a parent system improve the energy and exergy efficiencies of an offspring system?
2. How does the recovery of the conversion and usage losses affect the cost of an offspring system?

3. How does the recovery of the conversion and usage losses affect the complexity of an offspring system?
4. What factors could warrant the development of thermodynamically degraded offspring system?

The answers to these research questions would provide thermodynamic and thermo-economic insights into how PV-led IESs can be improved. The major contribution of this chapter to the field is the introduction of the novel E^4A approach based on ExCD of evolutionary IESs with parent-offspring relationship. Apart from using the methodology to investigate IPVFC systems, it can be used for tracking how improvement in the components might affect the overall efficiency of the systems.

4.1 Description of the Integrated Energy Systems

Figures 4.1(a) – (d) show the four configurations of IESs under study. System 1 in Figure 4.1(a): Integrated PV-battery system composed of a PV module, a DC/DC converter, a battery bank, an inverter, and a load. System 1 ignores the recovery of waste heat from the PV module and excess electricity from the PV module. System 2 in Figure 4.1(b): Integrated PV/T-battery system recovers the waste heat from the PV for heating fluid [158]. It is a co-generation system composed of a PV/T module, a DC/DC converter, a battery bank, an inverter, and a load. This is a direct offspring of System 1 based on waste heat recovery.

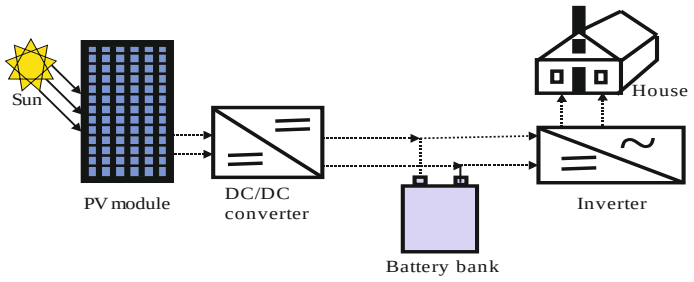

Figure 4.1 (a): Integrated PV-battery system [45]

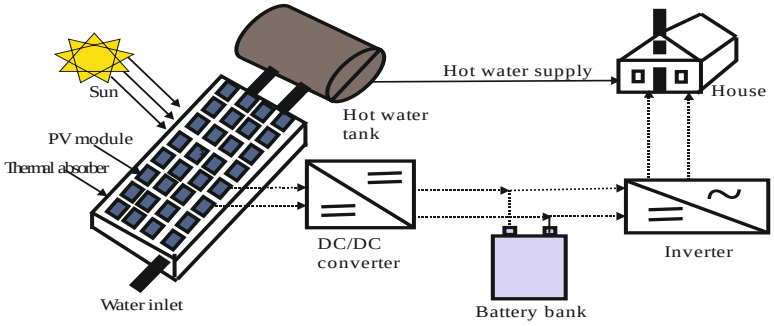

Figure 4.1 (b): Integrated PV/T-battery system [45].

System 3 in Figure 4.1(c): Integrated PV-battery-electrolyser-fuel cell system utilises excess electricity from the PV module to produce hydrogen and oxygen with electrolyser. Fuel cell recombines them for power generation on demand. System 3 ignores the waste heat from the PV module. System 3 is composed of a PV module, a DC/DC converter, a battery bank, a PEME, a PEMFC, a hydrogen tank, an oxygen tank, an inverter, and a load. This is a direct offspring of System 1 based on the recovery of waste electrical energy. Finally, System 4 in Figure 4.1(d): Integrated PV/T-battery-electrolyser-fuel cell system recovers the waste heat from the PV module and excess electricity for cogeneration. System 4 is composed of a PV/T module, a DC/DC converter, a battery bank, a PEME, a PEMFC, a hydrogen tank, an oxygen tank, an inverter, and a load. This is a direct offspring of System 2 targeting waste electrical energy recovery as well as waste heat recovery.

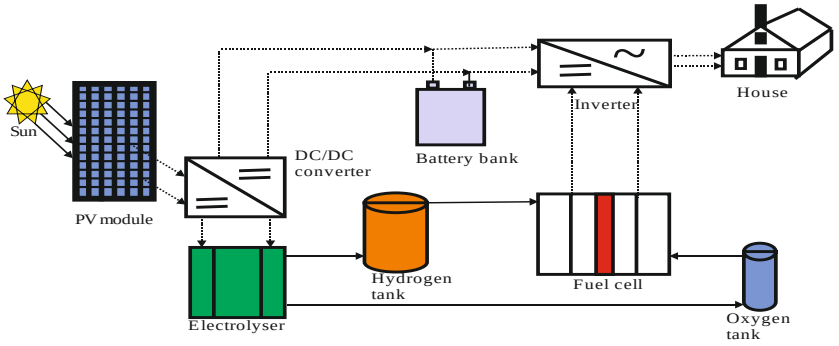

Figure 4.1 (c): Integrated PV-battery-electrolyser-fuel cell system [45].

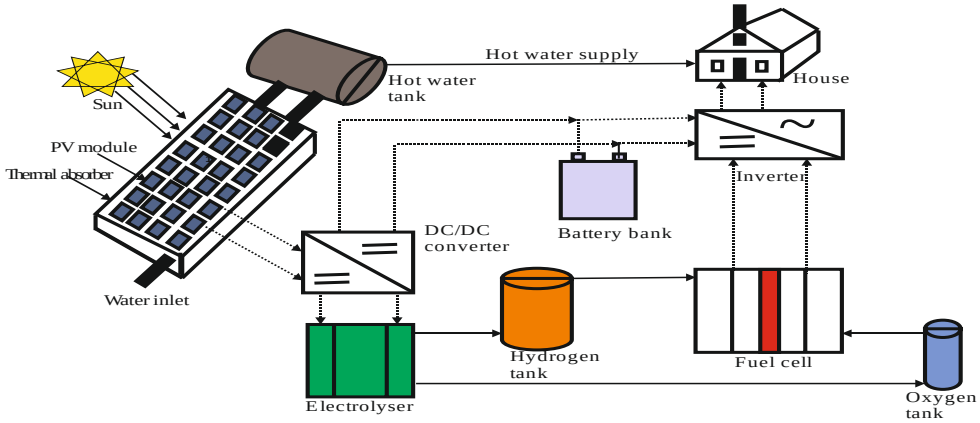

Figure 4.1 (d): Integrated PV/T-battery-electrolyser-fuel cell system [45].

4.2 Research Method and Approach

To evaluate if the offspring systems upgraded or degraded over their direct parent system, the energy and exergy efficiencies for a PV module [150], a PV/T module [159], a PEME [160], a PEMFC [161], a battery [21] and a DC/AC inverter [117] were sourced from

pieces of peer-reviewed literature and applied for the analysis. The interrelationships for recovering the usage losses and conversion losses are shown in Figure 4.2.

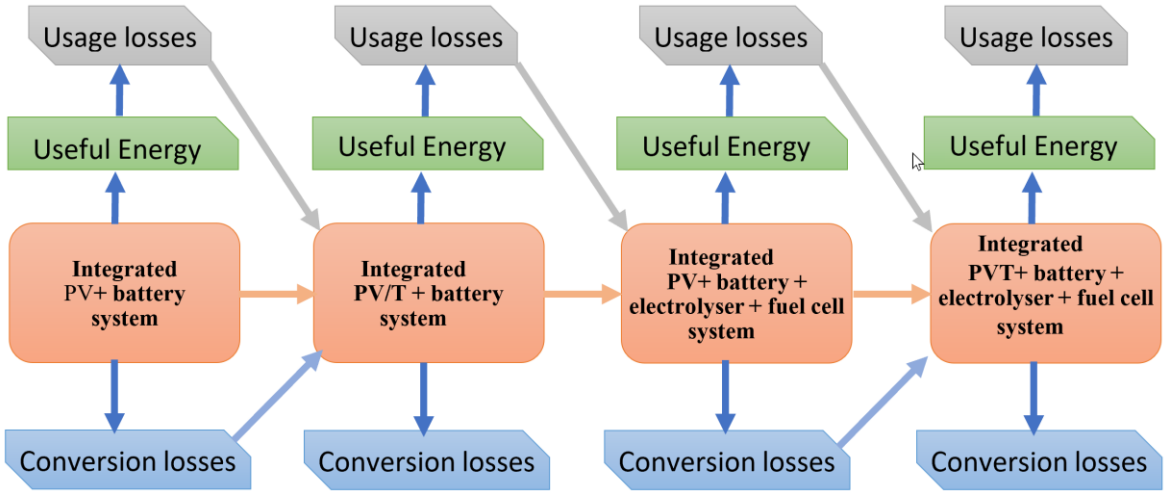

Figure 4.2: Diagram showing conversion and usage losses from a system [45].

The flowchart in Figure 4.3 shows the decision-making process for developing an offspring of a parent system. Rationally, if the losses are insignificant for recovery, the parent system can be optimized instead of developing the offspring system. However, if there are reasonable CEC benefits of the offspring system over its parent system, then it can be optimised and fully developed. This makes the E^4A approach a potential tool for decision-making during energy systems design and development.

To contextualise this study, the actual solar radiation, and temperature data for Kano city in Nigeria, were applied in calculating the exergy efficiencies of the IES. The cost and complexity of the systems in relation to energy and exergy efficiencies were also studied. The interrelationships between efficiencies, cost and complexity were studied using a novel comparative cost approach/analysis (CCA), which is suitable for comparing the cost of systems with parent-offspring relationship. Eventually, discussions were made on the energy loss mechanisms and the prospects of different configurations of the IES in view of other broader issues in the field of renewable energy to address research question 4 in this chapter.

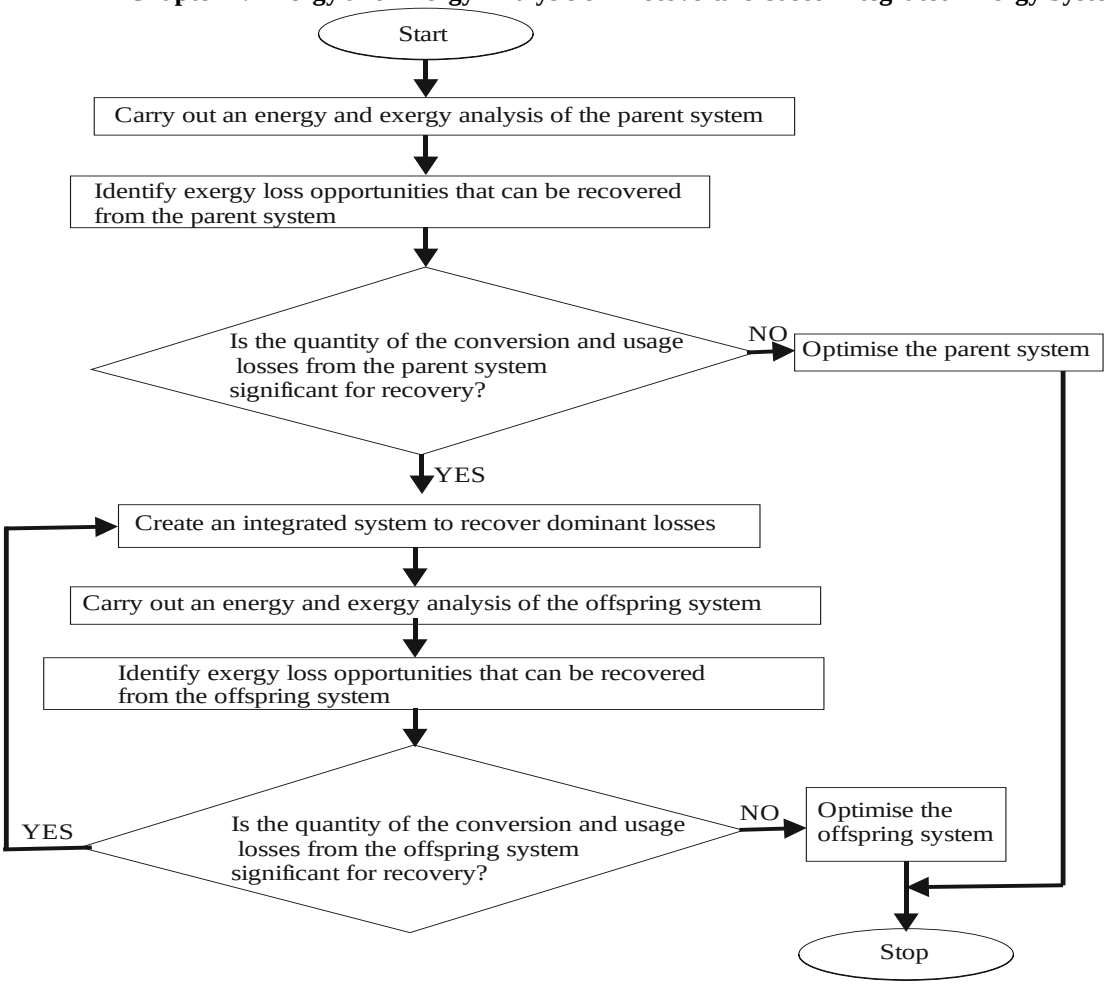

Figure 4.3: Flowchart for implementing energy and exergy efficiencies enhancement analysis [45]**.**

4.3 Energy and Exergy Modelling of the Components of the IESs

The energy and exergy equations for systems can be expressed as Eq. (4.1) and Eq. (4.2), respectively. The energy equation is based on the first law of thermodynamics while the exergy equation is based on the second law of thermodynamics. Energy efficiency (η) of a system is the ratio of the useful energy to the total energy input (Eq. (4.3)) [45]**.**

$$\dot{E}_{in} - \dot{E}_{out} = \frac{dE_{syst}}{dt} \tag{4.1}$$

$$\sum \dot{E}x_{in} = \sum \dot{E}x_{out} + \sum\left(\dot{E}x_{loss} + \dot{E}x_{dest}\right) \tag{4.2}$$

$$\eta = \frac{\dot{E}_{out}}{\dot{E}_{in}} \tag{4.3}$$

Systems 1 and 3 produce electrical energy while Systems 2 and 4 produce electrical and thermal energies. Exergy efficiency (η_{ex}) is the ratio of exergy output to exergy input as the

system interacts reversibly with the environment at reference state as expressed in Eq. (4.4) [162]. Exergy can be destroyed and lost during thermodynamic processes.

$$\eta_{ex} = \frac{\dot{E}x_{out}}{\dot{E}x_{in}} = 1 - \frac{(\dot{E}x_{loss} + \dot{E}x_{dest})}{\dot{E}x_{in}} \quad (4.4)$$

Usage losses include electrical energy wasted because it could not be utilised and electricity that should have been generated with available solar energy after batteries are fully charged. Eqs. (4.5) – (4.8) [45] represent the exergy balances of the IES where $\dot{E}x_{xn}$, $\dot{E}x_{yn}$ and $\dot{E}x_{zn}$ are the exergy input, output, and losses due to conversion and usage losses, respectively. The parent-offspring relationship is inspired by theory of inheritance and genetic evolution in biology. In this context, the driver of evolution of an IES is the proclivity to conserve energy and exergy to remain efficient. A parent system provides exergy input into the offspring system (see Figures 4.2 and 4.3) [45].

System 1: $$\dot{E}x_{x1} = \dot{E}x_{y1} + \dot{E}x_{z1} \quad (4.5)$$

System 2: $$\phi_1 \dot{E}x_{z1} = \dot{E}x_{y2} + \dot{E}x_{z2} \quad (4.6)$$

System 3: $$\phi_2 \dot{E}x_{z2} = \dot{E}x_{y3} + \dot{E}x_{z3} \quad (4.7)$$

System 4: $$\phi_3 \dot{E}x_{z3} = \dot{E}x_{y4} + \dot{E}x_{z4} \quad (4.8)$$

where ϕ_1 is the fraction of System 1 losses recovered as exergy input into System 2. ϕ_2 is the fraction of System 2 losses recovered as exergy input into System 3. ϕ_3 is the fraction of System 3 losses recovered as exergy input into System 4.

Exergy efficiencies (η_{ex}) for the IESs are expressed as Eqs. (4.9) – (4.12) [45], respectively.

$$\eta_{ex_1} = \frac{\dot{E}x_{y1}}{\dot{E}x_{x1}} = 1 - \frac{\dot{E}x_{z1}}{\dot{E}x_{x1}} \quad (4.9)$$

$$\eta_{ex_2} = \frac{\dot{E}x_{y2}}{\phi_1 \dot{E}x_{z1}} = 1 - \frac{\dot{E}x_{z2}}{\phi_1 \dot{E}x_{z1}} \quad (4.10)$$

$$\eta_{ex_3} = \frac{\dot{E}x_{y3}}{\phi_2 \dot{E}x_{z2}} = 1 - \frac{\dot{E}x_{z3}}{\phi_2 \dot{E}x_{z2}} \quad (4.11)$$

$$\eta_{ex_4} = \frac{\dot{E}x_{y4}}{\phi_3 \dot{E}x_{z3}} = 1 - \frac{\dot{E}x_{z4}}{\phi_3 \dot{E}x_{z3}} \quad (4.12)$$

Because the cumulative exergy destroyed by each IES configuration ($\dot{E}x_{zn}$) is composed of the exergy destroyed by the components, the energy and exergy efficiencies of each of the components are further modelled.

4.3.1 Energy and Exergy Modelling of a Photovoltaic Module

Eqs. (4.13) and (4.14), respectively represent the power (η_{PV}) [163] and exergy $\left(\eta_{ex_{pv}}\right)$ [150] efficiencies of a PV module.

$$\eta_{pv} = \frac{I_{sc}V_{oc}FF}{A_{cell} \times G} \tag{4.13}$$

$$\eta_{ex_{pv}} = \frac{I_{sc}V_{oc}FF}{G \times A_{cell} \times \left(1 - \frac{4}{3}\frac{T_a}{T_{sun}} + \frac{1}{3}\left(\frac{T_a}{T_{sun}}\right)^4\right)} \tag{4.14}$$

where FF is the fill factor, A_{cell} is the solar cell area, T_a is the ambient temperature, T_{sun} is the temperature of the sun.

4.3.2 Energy and Exergy Modelling of a PV/T-Water System

The energy efficiency of the PV/T includes electrical and thermal components as expressed in Eq. (5.15) [164]**.** The exergy efficiency can be computed with Eq. (4.16) [159]**.**

$$\eta_{PV/T} = \frac{I_{mpp}V_{mpp} + (\dot{m}C_p(T_{out} - T_{in})}{G \times A_{cell}} \tag{4.15}$$

$$\eta_{ex_{PV/T}} = \frac{I_{mpp}\,V_{mpp} + \left(1 - \frac{T_a}{T_{cell}}\right)\,[h_{ca}A_{cell}(T_{cell} - T_a)]}{G \times A_{cell}\left(1 - \frac{T_a}{T_{sun}}\right)} \tag{4.16}$$

where $\dot{m}$ is the mass flow rate, C_p is the specific heat capacity of the fluid, respectively; h_{ca} is the convective heat transfer coefficient of the surrounding environment (h_{ca} = 5.7 + 3.8v [165]; v is the wind velocity).

4.3.3 Energy and Exergy Modelling of a PEME

The electrochemical reverse process in a PEME yields that of a PEMFC (see Eq. (4.17) and Eq. (4.18)) [134]. At potentials higher than 1.23 V, PEME dissociates water into hydrogen and oxygen using electricity. The energy efficiency of a PEME based on the higher heating

value (HHV) of hydrogen [166] is expressed as Eq. (4.19). Exergy efficiency of a PEME is expressed as a reverse of the exergy efficiency of PEMFC [167] as in Eq. (4.20).

PEME: $$2H_2O + \text{electricity} + \text{heat} \rightarrow 2H_2 + O_2 \quad (4.17)$$

PEMFC: $$2H_2 + O_2 \rightarrow 2H_2O + \text{electricity} + \text{heat} \quad (4.18)$$

$$\eta_{PEME} = \frac{HHV}{\left(\frac{\int_0^{\Delta t} N_{cell} I_{cell} V_{cell} dt}{\int_0^{\Delta t} f_{H_2} dt}\right)} \quad (4.19)$$

$$\eta_{ex_{PEME}} = 1 - \frac{\dot{I}_{PEME}}{(\dot{n} \times b)_{H_2O_{in}}} \quad (4.20)$$

where higher heating value (HHV) of hydrogen is 39.4 kWh kg^{-1} at STP, N_{cell} , I_{cell}, V_{cell} are the number of cell, current and voltage in the cells, respectively; Δt is the duration of operation, f_{H_2} is the flow rate of H_2; $\dot{n}$ is the molar flow rate (mol cm^{-2} s^{-1}), $\dot{I}_{PEME}$ is the thermodynamic irreversibility in the PEME, b is the total specific exergy of water (J mol^{-1}).

4.3.4 Energy and Exergy Modelling of a PEMFC

The thermodynamic losses and irreversibilities in a PEMFC are categorised into activation, Ohmic and concentration (or transport) losses [168,169]. The losses reduce the Nernst voltage (or output voltage) from the fuel cell [170]. Ignoring the thermal losses from the fuel cell, the energy efficiencies of the PEMFC can be calculated with Eq. (4.21) (Spiegel [134]). The exergy efficiency is expressed as Eq. (5.22) [167]**.**

$$\eta_{PEMFC} = \frac{\dot{W}_{PEMFC}}{\dot{m}_{H_{2,in}} \times HHV_{H_2}} \quad (5.21)$$

$$\eta_{ex_{PEMFC}} = 1 - \frac{\dot{I}_{PEMFC}}{(\dot{n} \times b)_{H_{2,in}} + (\dot{n} \times b)_{O_{2,in}}} \quad (5.22)$$

where $\dot{W}_{PEMFC}$ is the power output, $\dot{m}_{H_{2,in}}$ is the mass flow rate of hydrogen, $\dot{n}$ is the molar flow rate (mol cm^{-2} s^{-1}), b is the total specific exergy (J mol^{-1}), $\dot{I}_{PEMFC}$ is the thermodynamic irreversibilities in the PEMFC.

4.3.5 Energy and Exergy Modelling of a Battery

Batteries [171] and supercapacitors [172] are used for energy storage in IESs. The product of current and voltage gives the power of the battery [173]. Efficiency is expressed as the ratio of the total power discharged to the total power utilised for charging the battery. Energy and exergy efficiencies of a battery can be calculated with Eq. (4.23) [16].

$$\eta_{Bat} = \eta_{ex_{Bat}} = \frac{\sum \dot{W}_{DC,discharge}}{\sum \dot{W}_{DC,charge}} = \frac{I_d V_d t_d}{I_c V_c t_c} \quad (4.23)$$

where I_d is the discharge current (Amperes-hrs), V_d is the discharge voltage (V), V_c is the charging voltage (V), I_c is the charging current (Amperes-hours), t_d is the discharge time (hours), t_c is the charging time (hours).

4.3.6 Energy and Exergy Modelling of an Inverter

DC/DC converters and DC/AC inverters condition electricity in the IESs. Energy and exergy efficiencies are assumed to be equal [142] and can be calculated with Eq. (4.24) [21].

$$\eta_{Inv} = \eta_{ex_{Inv}} = \frac{P_{AC,out}}{P_{DC,in}} = \frac{I_{Inv,out} V_{Inv,out}}{I_{Inv,in} V_{Inv,in}} \quad (4.24)$$

where η_{Inv} and $\eta_{ex_{Inv}}$ are energy and exergy efficiencies of an inverter, $P_{AC,out}$ is the alternating power output, $P_{DC,in}$ is the direct power input, $I_{Inv,out}$ is the AC output, $V_{Inv,out}$ is the alternating voltage output, $I_{Inv,in}$ is the DC input and $V_{Inv,in}$ is the direct voltage input.

Heat generated in the battery, converter and inverter were ignored based the logic in Figure 4.3 which implies that losses can be ignored if they are not significant. Waste heat from PEME and PEMFC were ignored because this study focussed on the PV module which is the efficiency bottleneck in IPVFC systems.

4.3.7 Combined Energy and Exergy Efficiencies

E^4A approach uses combined efficiency, which is the product of the components, to rank energy and exergy efficiencies of the systems. The combined energy of the IESs are presented in Eqs. (4.25) - (4.28) [45].

$$\eta_{Syst-1} = \eta_{PV} \times \eta_{Inv} \times \eta_{Bat} \quad (4.25)$$

$$\eta_{Syst-2} = \eta_{PV/T} \times \eta_{Inv} \times \eta_{Bat} \quad (4.26)$$

$$\eta_{Syst-3} = \eta_{PV} \times \eta_{Inv} \times \eta_{Bat} \times \eta_{PEME} \times \eta_{PEMFC} \quad (4.27)$$

$$\eta_{Syst-4} = \eta_{PV/T} \times \eta_{Inv} \times \eta_{Bat} \times \eta_{PEME} \times \eta_{PEMFC} \quad (4.28)$$

The combined exergy efficiency of the IESs are presented in Eqs. (4.29) - (4.32) [45].

$$\eta_{ex_{Syst-1}} = \eta_{ex_{PV}} \times \eta_{ex_{Inv}} \times \eta_{ex_{Bat}} \quad (4.29)$$

$$\eta_{ex_{Syst-2}} = \eta_{ex_{PV/T}} \times \eta_{ex_{Inv}} \times \eta_{ex_{Bat}} \quad (4.30)$$

$$\eta_{ex_{Syst-3}} = \eta_{ex_{PV}} \times \eta_{ex_{Inv}} \times \eta_{ex_{Bat}} \times \eta_{ex_{PEME}} \times \eta_{ex_{PEMFC}} \quad (4.31)$$

$$\eta_{ex_{Syst-4}} = \eta_{ex_{PV/T}} \times \eta_{ex_{Inv}} \times \eta_{ex_{Bat}} \times \eta_{ex_{PEME}} \times \eta_{ex_{PEMFC}} \quad (4.32)$$

Solar radiation and temperature data of Kano city were used to compare the combined energy and exergy efficiency of a PV. The exergy efficiency is based on the model proposed by Petela [174] (Eq. (4.33)). It was assumed that the temperature of the sun (T_{sun}) was 6000 K and the reference temperature (T_a) was 298.15 K. The temperature of the PV was in thermal equilibrium with the ambient temperature.

$$\dot{E}x_{solar} = G \times A_{cell} \times \left(1 - \frac{4}{3}\frac{T_a}{T_{sun}} + \frac{1}{3}\left(\frac{T_a}{T_{sun}}\right)^4\right) \quad (4.33)$$

Updating Eq. (4.33) in Eqs. (4.29) - (4.32) give Eqs. (4.34) – (4.37) which show the effect of the exergy transfer ($\dot{E}x_{Syst}$) to the IESs from the PV or PV/T [45].

$$\dot{E}x_{Syst-1} = G \times A_{cell} \times \left(1 - \frac{4}{3}\frac{T_a}{T_{sun}} + \frac{1}{3}\left(\frac{T_a}{T_{sun}}\right)^4\right) \times \eta_{ex_{PV}} \times \eta_{ex_{Inv}} \times \eta_{ex_{Bat}} \quad (4.34)$$

$$\dot{E}_{Syst-2} = G \times A_{cell} \times \left(1 - \frac{4}{3}\frac{T_a}{T_{sun}} + \frac{1}{3}\left(\frac{T_a}{T_{sun}}\right)^4\right) \times \eta_{ex_{PV/T}} \times \eta_{ex_{Inv}} \times \eta_{ex_{Bat}} \quad (4.35)$$

$$\dot{E}_{Syst-3} = G \times A_{cell} \times \left(1 - \frac{4}{3}\frac{T_a}{T_{sun}} + \frac{1}{3}\left(\frac{T_a}{T_{sun}}\right)^4\right) \times \eta_{ex_{PV}} \times \eta_{ex_{Inv}} \times \eta_{ex_{Bat}} \times \eta_{ex_{PEME}} \times \eta_{ex_{PEMFC}} \quad (4.36)$$

$$\dot{E}_{Syst-4} = G \times A_{cell} \times \left(1 - \frac{4}{3}\frac{T_a}{T_{sun}} + \frac{1}{3}\left(\frac{T_a}{T_{sun}}\right)^4\right) \times \eta_{ex_{PV/T}} \times \eta_{ex_{Inv}} \times \eta_{ex_{Bat}} \times \eta_{ex_{PEME}} \times \eta_{ex_{PEMFC}} \quad (4.37)$$

Entropy generation is expected to be smallest in the system with the smallest exergy destruction rate. Eq. (4.38) shows the entropy balance in System 1 and 3 while Eq. (4.39) shows the entropy balance in System 2 and 4 [45].

$$S_{solar} = S_{elect} + T_0 S_{gen} = \Delta S_{syst-1\ or\ 3} \quad (4.38)$$

$$S_{solar} = S_{elect} + S_{therm} + T_0 S_{gen} = \Delta S_{syst-2\ or\ 4} \quad (4.39)$$

where $T_0 S_{gen}$ represents the solar exergy destroyed by the PV or PV/T at reference state, S_{solar} is the entropy of solar radiation, S_{elect} is the entropy of electrical output and S_{therm} is the entropy of thermal output.

4.4 Comparative Cost Analysis of the Systems

To explore the cost dimension of the CEC interrelationships among the IESs, comparative cost analysis (CCA) is proposed based on the principle of inheritance. This approach assesses the incremental cost or cost reduction of an offspring system compared to its parent. An offspring is assumed to inherit the total cost of its parent in addition to the cost of the components added to create the offspring. Cost of energy (COE) from each IES is categorised into fixed and variable costs. These costs can also be categorised into capital, fuel, operational and maintenance costs [175]. COE can be calculated from Eq. (4.40) [175].

$$\mathrm{COE_{Syst}} = \mathrm{ACC} + \frac{\mathrm{AFC}}{\mathrm{AEP}} \tag{4.40}$$

where ACC is the annualised capital cost (£ kWh^{-1}), AFC is the annual fuel cost (£ yr^{-1}) and AEP is the annual electricity production (kWh yr^{-1}).

ACC is a function of the capital cost of the system and the annual capital recovery factor (CRF). Increment in the capacity of the system can be achieved by scaling up the capacity of the modular components, say, the PV module, PV/T module, PEME and PEMFC stacks which are cell-based. The power output from a PV system can be increased by adding more solar cells in series in a module or more modules in parallel in an array. Volume of hydrogen gas produced from the PEME component can be increased adding more cells in series, while the power output from a PEMFC can be scaled up by adding more fuel cells in series in the stack. There is a cost implication of adding more cells to these components because it will increase the total capital cost of the IES. Eq. (4.41) expresses the ACC of the systems based on the present value of annuity [175].

$$\mathrm{ACC} = \mathrm{COS}\left[\frac{r(1+r)^t}{(1+r)^t - 1}\right] \tag{4.41}$$

where COS is the cost of system (£), r is the discount rate (%) and t is the lifetime of the system in years.

Cost of a component (COC) (i.e. PV, PV/T, battery, inverter, PEME, PEMFC and their subcomponents) can be categorised into component fixed cost (CFC) and component variable cost (CVC) (e.g. $\mathrm{C_{cell}} \times \mathrm{N_{cell}}$) as expressed in Eq. (4.42) [175].

$$\mathrm{COC} = \mathrm{CFC} + \mathrm{C_{cell}} \times \mathrm{N_{cell}} \tag{4.42}$$

where $\mathrm{C_{cell}}$ is the cost per cell (£ $cell^{-1}$), $\mathrm{N_{cell}}$ is the number of cells.

Substituting Eqs. (4.41) and (4.42) into Eq. (4.40) gives Eq. (4.43) [45], which represents the annualised cost of energy from each of the IESs based on the present value of annuity.

$$\mathrm{COE_{IES}} = \sum_{\mathrm{j}=1}^{12} \left\{ \sum_{i=1}^{n} COC_i \left[\frac{r(1+r)^t}{(1+r)^t - 1} \right] + \frac{\mathrm{AFC}}{\mathrm{AEP}} \right\} \qquad (4.43)$$

where j is the monthly capital and fuel cost amortisation, n is the number of components, i represents an individual component of the IES.

Since Systems 1 and 2 do not incur fuel cost but System 3 and 4 do, Eq. (4.43) can be adjusted to represent those contexts. If hydrogen was sourced from a hydrogen gas infrastructure, the cost of generating the hydrogen with a PEME stack would be replaced with the cost of fuelling from gas grid of filling station.

4.5 Results and Discussion

4.5.1 Analysis of the Combined Energy and Exergy Efficiencies of the IESs

Table 4.1 presents the combined energy and exergy efficiencies of the IESs based on Eqs (4.25) - (4.28) and Eqs (4.29) - (4.32). To adopt a systematic approach, the precondition for choosing the energy and exergy efficiency was that both must be derived together through experimental or analytical methods. This is because energy and exergy efficiencies from random sources may be inconsistent. Thus, the energy and exergy efficiencies are not indicators of the overall efficiencies of the IESs because the technologies are continuously evolving. The E^4A approach provides a comparative energy and exergy efficiency of parent-offspring systems so that the CEC benefits can be evaluated within a design space. It can show that the energy and exergy efficiencies of an offspring upgraded or otherwise degraded over its parent based on the combined energy and exergy efficiencies.

Table 4.1: Combined energy and exergy efficiencies of the systems [45]**.**

Component	Energy efficiency (%)	Exergy efficiency (%)	References
PV	6.4	8.5	Sudhakar et al [150]
PV/T	45	16	Joshi et al [159]
PEME	77	67	Rosen [160]
PEMFC	42.32	49.59	Hussain et al [161]
Battery	85	85	Yilanci et al [21]
DC/AC Inverter	85	85	Dincer and Joshi [117]
Combined efficiency:			
System 1:	4.62	6.14	
System 2:	32.51	11.56	
System 3:	1.51	2.04	
System 4:	10.59	3.84	

To ascertain the direction of the upgrade or degradation of an offspring system, an energy and exergy efficiencies enhancement matrix (E^4M) is hereby proposed and applied. Upgrade/enhancement (en) or degradation (de) of the systems are presented in Table 4.2. As a convention, 'cell (r, c)' represents the current performance of an IES. 'r' and 'c' are the row and column number of the cell, respectively. Thus, en(27.89) on cell (1, 2) indicates that the overall efficiency of System 2 upgraded over System 1 by 27.89%. Contrarily, de(21.92) on cell (2, 4) indicates that the energy efficiency of System 4 degraded by 21.92% over System 2. The reversal of a degraded offspring to its parent system reverses its degraded energy or exergy efficiency. For instance, cell (2, 3) shows that System 3 degraded by 31% over System 2. Returning System 3 to System 2 as shown by cell (3, 2) would result in 31% upgrade in the overall energy performance. Comparatively, System 2 improved over System 1. This implies that recovering waste heat from the PV module can improve the overall efficiency of System 2 over System 1. This agrees with the findings in [28]. System 4 upgraded over System 3 because waste heat from the PV module was recovered for thermal work. However, the addition of a PEME and a PEMFC to System 1 and 2 to create System 3 and 4, respectively may have introduced higher entropy generations. Consequently, energy and exergy efficiencies of System 3 and 4 degraded over System 2.

Table 4.2: Energy and exergy efficiencies enhancement matrix (EEEEM) for the IESs [45]**.**

	System 1	**System 2**	**System 3**	**System 4**
Energy				
System 1	4.62	en(27.89)	de(3.11)	en(5.97)
System 2	de(27.89)	32.51	de(31.00)	de(21.92)
System 3	en(3.11)	en(31.00)	1.51	en(9.08)
System 4	de(5.97)	en(21.92)	de(9.08)	10.59
Exergy				
System 1	6.14	en(5.42)	de(4.10)	de(2.30)
System 2	de (5.42)	11.56	de(9.52)	de(7.72)
System 3	en(4.10)	en(9.52)	2.04	en(1.80)
System 4	en(2.30)	en(7.72)	de(1.80)	3.84

Interestingly, System 4 upgraded over System 1 although System 3 was still below the performance of System 1. Entropy generation in the PEME and PEMFC when electrical energy from the PV module, which has the highest energy quality was recycled through electrochemical processes may have contributed to the degradation (see Eq. (4.38) and (4.39)). Eqs. (4.34) – (4.37) were implemented in MATALAB to investigate how solar radiation and temperature variations on the PV and PV/T affected the performance of the systems. Table 4.3 presents the simulations of monthly solar exergy input for Kano city in Nigeria. The monthly exergy destruction rates were computed using Eqs. (4.5) – (4.8).

Table 4.3: Combined exergy efficiencies of the systems [45].

Month	[a]Average Temp. (K)	[b]Monthly Solar Radiation (MJ m^{-2} day^{-1})	Solar exergy input (MJ day^{-1})	System 1 Exergy flow (MJ day^{-1})	System 2 Exergy flow (MJ day^{-1})	System 3 Exergy flow (MJ day^{-1})	System 4 Exergy flow (MJ day^{-1})
Jan.	298.25	15.73	14.687	0.902	1.698	0.299	0.564
Feb.	301.05	18.08	16.870	1.308	1.950	0.344	0.648
Mar.	304.68	24.45	22.795	1.400	2.635	0.465	0.875
Apr.	305.90	25.26	23.543	1.445	2.722	0.480	0.904
May	304.27	22.84	21.296	1.308	2.461	0.434	0.818
Jun.	301.50	19.28	17.988	1.105	2.079	0.367	0.691
Jul.	300.20	16.98	15.847	0.973	1.832	0.323	0.608
Aug.	299.22	16.16	15.086	0.926	1.744	0.308	0.579
Sept.	300.48	19.58	18.272	1.122	2.112	0.373	0.702
Oct.	302.34	23.39	21.819	1.340	2.522	0.445	0.838
Nov.	302.39	20.34	18.973	1.165	2.193	0.387	0.728
Dec.	299.87	17.36	16.203	0.995	1.873	0.331	0.622

(Source of a and b is the Nigerian Meteorological Agency, Abuja)

Figure 4.4 presents the extent of utilisation of the available solar exergy at the location by the systems. It appears that the exergy transfer from the PV/T module in System 2 is higher than the exergy transfer of the PV module in System 1. Likewise, the exergy transfer from the PV/T module in System 4 is higher than the exergy transfer of the PV module in System 3. This shows that replacing PV with PV/T in their direct parents improved the thermodynamics of the offspring systems. Clearly, the four systems performed well below the solar exergy input. This indicates that the systems can be improved to harness more of the available solar radiation at the location. The wider design implication is that PV/T is a more efficient prime mover than PV in terms of energy and exergy efficiencies. This can be used to logically navigate the thermodynamic pathways within the design space of IPVFC system to establish the optimal CEC benefits.

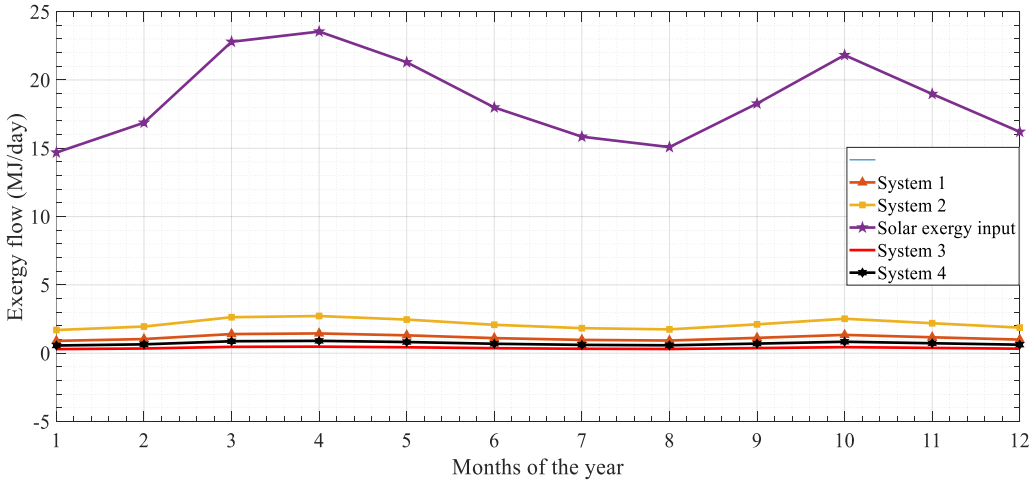

Figure 4.4: Monthly solar exergy utilisation by System 1: PV-Battery; System 2: PV/T-Battery; System 3: PV-Battery-Electrolyser-Fuel cell; and System 4: PV/T-Battery-Electrolyser-Fuel cell [45].

From Figure 4.5, System 2 destroyed lesser solar exergy input than System 1; whereas System 4 destroyed lesser exergy than System 3 as shown in Figure 4.6. Overall, System 2 appears to be the optimum design stage of evolution for these IESs since System 1 had lower energy and exergy efficiencies due to unrecovered losses while Systems 3 and 4 were degraded because of the recycling of quality electrical energy though loss-prone electrochemical processes. System 2 would therefore require improved storage components to improve the system reliability. Since this system is based on the principles of inheritance and evolution, what is certain so far is that PV/T is more fit than PV in terms of producing offspring IESs with improved thermodynamic efficiencies. Inferentially, a PV/T-Battery-URPEMFC system will have higher energy and exergy efficiencies compared to PV-Battery-URPEMFC system. This will be discussed in detail in Section 9.5. Again, replacing PEME and PEMFC with URPEMFC could lower both cost and complexity of the offspring system. Interestingly, URPEMFC could achieve up a power efficiency of 44% [54] compared to the combined power efficiency of 33% when using separate PEME and PEMFC. Consequently, PV/T-Battery-URPEMFC system would be more thermodynamically efficient than System 3 (PV-Battery-PEME-PEMFC system) and System 4 (PV/T-Battery-PEME-PEMFC system). In Chapter 9, up to 24 IESs that can be configured within the design space of IPVFC systems are listed.

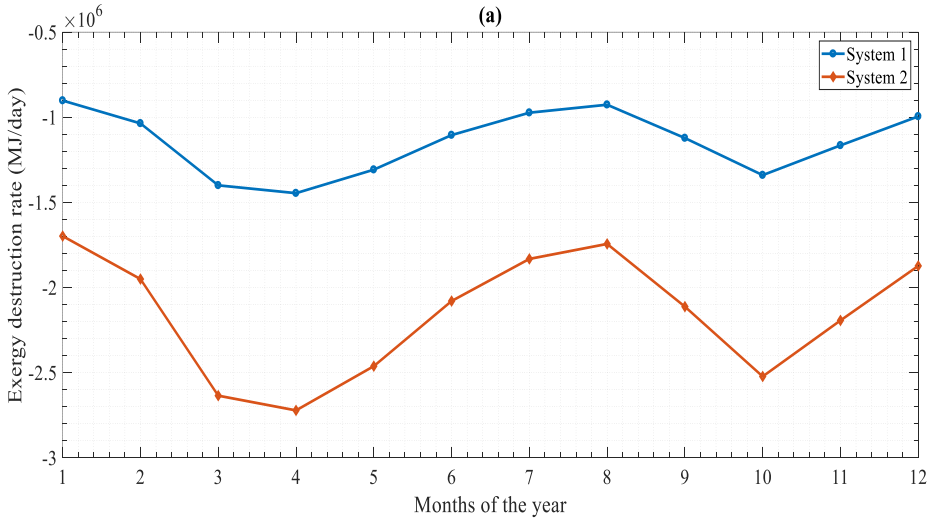

Figure 4.5: Monthly exergy destruction flow for System 1 and System 2 [45].

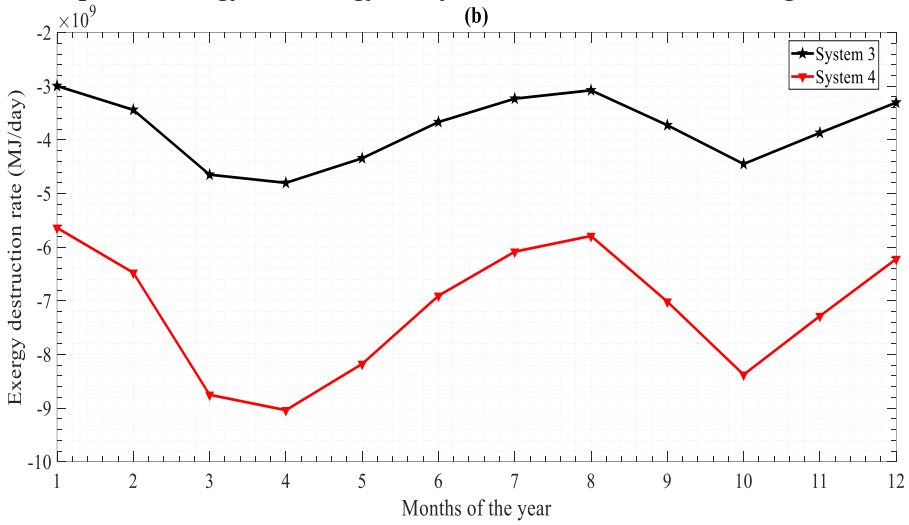

Figure 4.6: Monthly exergy destruction flow for System 3 and System 4 [45].

4.5.2 Discussion on the Comparative Cost Analysis of the Proposed Four Systems

Figure 4.7 shows the comparative costs of the IESs based on benchmarked cost of components with respect to Eq. (4.43). A benchmarked cost indicates the cost of a component which can be inherited by the direct offspring system. The size of the PV module was the baseline so that the size of other components depends on the size of the PV array. System 4 has the highest cost and complexity; but the increased cost and complexity did not translate into higher energy and exergy efficiencies. Therefore, an increase in the complexity of an offspring system seems to correlate with its total cost but not integrated efficiency.

It can therefore be stated that energy and exergy efficiencies of the IESs have no continuous direct proportional relationship with cost and complexity which are incurred in pursuit of recovery of conversion and usage losses. Exergy efficiencies depend on the cumulative exergy transfer between the components of the IESs. Thus, replacing a component with high exergy destruction with a component with a lower exergy destruction could improve the overall thermodynamic efficiency of the system.

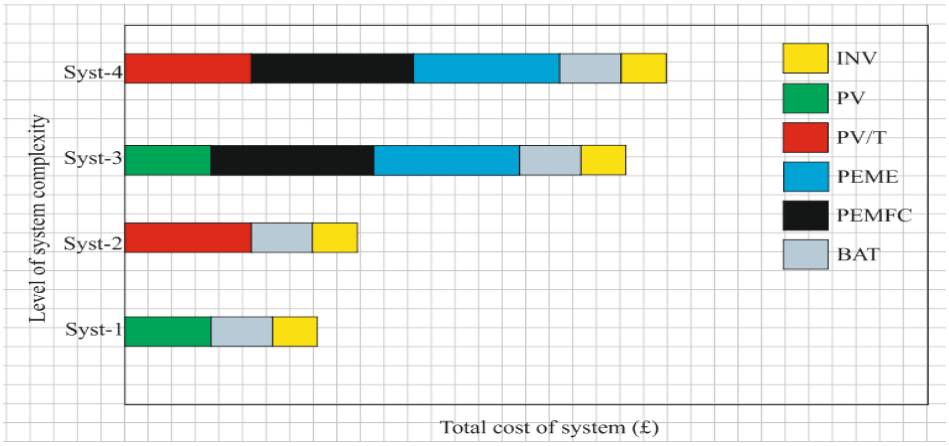

Figure 4.7: Comparative cost analysis of the IESs using benchmarked component cost [45].

Rosen and Bulucea [142] asserted that the development of IESs does not depend on their thermodynamic performance alone. Other factors that matter include trade-offs in the economics of the system, its environmental impact, and ingenuity in applying exergy to improve the systems. Likewise, the development of System 3 and 4 cannot be justified based on their thermodynamic performance alone. From a CEC benefits point of view, they increased in cost and complexity over System 1and 2. However, a critical analysis of the use context suggests that System 2 with the highest thermodynamic improvement could be applicable for stationary power due to the additional need for cold water inflow. In comparison, System 3 with a lower thermodynamic efficiency could be applied for both stationary and mobile applications [169,176]. Although complexity does correlate consistently with efficiency, complexity of a system may be accepted if that can improve the reliability of the system, where reliability is a performance objective. In terms of reliability, System 3 and 4 appear better than System 1 and 2 since they contain fuel cell in addition to batteries to ensure that demand for power is continuously met. In the context of a hydrogen economy, System 2 is not equipped to generate hydrogen whereas System 3 and 4 can generate clean and sustainable solar hydrogen which can be used for power generation or as an input in industrial processes.

Lastly, laws and legislations against the use of fossil fuels favour all the IESs. As research and development efforts continue, the design space of IPVFC systems could be improved as the processes and technologies of the components improve. To reduce the cost and complexity of Systems 3 and 4, aspects that can be considered include system automation, manufacturability, maintainability, scalability, and safety.

4.5.3 Further Discussions on the Exergy Destruction Mechanisms in the Component

It is important to investigate further the causes of exergy destruction in the components**.** Dupre et al [177] classified PV conversion losses into losses occurring below bandgap energy, and losses due to thermalisation, emission, Carnot, angle of mismatch, non-radiative receiver, reflection, shunts and series resistance. Solar exergy destroyed by the PV module represents the losses due to the fact the entire solar spectrum cannot be converted to electricity [178]. Thermalisation of electrons occur during generation and recombination processes because all electrons cannot be collected from the p-n junction of solar cells [178]. This can be reduced through bandgap engineering using approaches such as up-conversion, down-conversion or quantum dots [178]. Multi-junction solar cells can also increase the solar spectrum harnessed to produce electrical energy [27].

In a PV/T module, exergy destruction could be due to low flow rates of the working fluids, high temperature of the inlet working fluid, inappropriate insulation and poor thermal conductivity of the thermal absorber [179]. Jafarkazemi and Ahmadifard [179] suggested an increase in the mass flow rate to avoid heat transfer from the fluid to the absorber plate. Also, fluids with low inlet temperature should be used to reduce the exergy losses due to the temperature difference between absorber plate and the reference temperature [179]. This agrees with Florschuetz [180] that showed that the electrical efficiency of the flat plate collector reduces with a significant increase in cell temperature above the reference temperature. Again, the cooling effect of the working fluid in a PV/T module has been reported to improve the electrical efficiency [181–183]. Yet, there exist an inherent thermodynamic contradiction in attempting to simultaneously improve the electrical and thermal efficiencies of a PV/T module. High operating temperature degrades electricity generation of the PV [180]; whereas the thermal quality of a PV/T module can be improved by increasing the thermal content of the PV/T module.

Batteries are critical components of IPVFC systems. However, batteries incur losses and irreversibilities common to all electrochemical devices. Charging and discharging patterns could influence the overall performance of batteries. As example, deep discharge of batteries could lead to mechanical stresses in the plate and could lead to shedding, poor conductivities and diminished lifetime [184]. Poor current distribution due to electrochemical reactions, imbalance in the transport phenomena during charging and discharging, internal resistance, as well as poor heat dissipation could be sources of exergy destruction in a battery [184].

Theoretical thermodynamic efficiency of PEMFC is about 83% (i.e. 1.229/1.482); but the practical efficiency is below 60% due to activation, concentration and Ohmic losses [134]. Wang et al [168] observed that an increase in temperature (from 50 $^{\circ}$C to 70 $^{\circ}$C) improved the performance of a fuel cell because the membrane conductivity increased. Contrarily, high temperature above the humidification temperature could dehydrate the surface of the catalyst, and this could increase activation losses. They also observed that increasing the pressure between 1 to 3.72 atm improved the performance of a PEMFC. Transport losses can be reduced by increasing the partial pressure of the gases in the system [96]. Transport losses can also be minimised with a well-designed transport channels [185]. Ohmic losses in the PEMFC can be reduced by using conductive electrodes and membrane with high ionic conductivity whilst preventing electron transport [186].

4.5.4 Design Methodology Implications of the E^{4}A Approach

E^{4}A approach seeks to optimise the CEC benefits of an optimal design from the IPVFC design space. Based on the components within the design space, some components can be unified. For instance, boosting and inversion of low-voltage unregulated output from the FC can be done with a boost-inverter with a bidirectional backup battery storage [187]. A bidirectional converter and a boost converter can manage the flow of current in an IPVFC system so that the current/voltage from the FC can be regulated by a boost converter, while the bidirectional converter can regulate the current/voltage from the battery [31].

4.6 Summary

In this chapter, E^{4}A approach was proposed and applied to assess the evolution of PV-led IESs. The major findings include that the energy and exergy efficiencies of System 2 upgraded by 27.89% and 5.42%, respectively, compared to System 1. Moreover, the energy efficiency of system 4 was increased by 5.97% compared to System 1 but degraded in exergy efficiency by 2.3% due to the irreversibilities in the PEME and PEMFC. The energy and exergy efficiencies of System 3 degraded by 3.11% and 4.10%, respectively, over System 1; while the energy and exergy efficiencies of System 4 also degraded by 21.92% and 7.72%, respectively, over System 2. Among the systems investigated, System 2 appeared to have the highest potential for harnessing monthly solar exergy at Kano city because it utilised the highest portion of the solar exergy input for cogeneration, followed by Systems 4, 1 and 3. Cost also increased as the complexity of the system increased.

Chapter 5: Robust Code-based Modelling and Simulation of Photovoltaic systems

The E^4A methodology implemented in Chapter 4 revealed that optimising the efficiency of IPVFC systems depends on improving the components of the system. From ExCD perspectives, the IPVFC systems need a reduction in the conversion and usage losses in the PV; a reduction in the losses due to overpotentials in the PEME and PEMFC; and a reduction in the overall cost and complexity of the systems by seeking plausible optimal design configuration within the design space. Since a PV module is the prime mover, this chapter focuses on developing a robust PV modelling approach to investigate its thermodynamics to realise Research Objective 2.

The Renewables 2021 Global Status Report (GSR) [188] indicated that solar PV added as much as 139 GW in 2020, bringing the global solar PV capacity to about 760 GW. Utilisation of PV modules may continue to increase due to its applicability for power generation [29,112,189]. PV module is critical in generating electrical energy in PV/T systems [28,158].

The major challenge with attempting to predict the performance of a PV module is that manufacturers list few electrical and thermal properties of PV modules [190]. Thus, an effective computational modelling of PV module is required to predict the generation characteristics. Here, PV modelling approaches are categorised into block-based modelling (BBM) [93,191–195], code-based modelling (CBM) [196], electrical circuit modelling (ECM) [197] and Numerical modelling (NM) [198,199]. Each of the categories involves iteration due to the transcendental form of the photovoltaic model.

To investigate IPVFC systems further, there is a need to explore a predictive and prescriptive approach for PV modelling. Predictive PV model can predict the effects of changes in the materials, operating or environmental variables [200]. Prescriptive PV model enables developers to generate PV design options to facilitate decision-making. During PV modelling, parameters of interest are selected. As example, five-parameter model has been proposed [196]. Another approach used open circuit voltage (V_{oc}), short circuit current (I_{sc}), output current (I_o), and voltage at maximum power point (V_{mpp}) [201].

There are different pieces of software for modelling and simulating different aspect of PV systems. National Renewable Energy Laboratory developed System Advisor Model for

techno-economic study of renewable energy systems [202,203]. Transient system simulation (TRNSYS) by University of Wisconsin Madison can be used to study the transient behaviour of systems based on user-defined function (UDF) [204]. Fraunhofer Institute for Solar Energy Systems bases its computer simulation chain based on two-diode model [205]; but PVsyst uses single diode model. Sentaurus Technology computer-aided design simulates the wafer fabrication, operation and reliability of semiconductor devices [206]. Other PV modelling and simulation tools are EnergyPlus, RETScreen, SolDesigner, SolarPro, T*SOL, WATSUN, Polysun, F-Chart [207] and PV Lighthouse [208].

In the overall research on IPVFC system, the thermodynamics of a PV module from fundamental physics was explored. BBM approach appears complex because it is difficult to trace linkages between equations, variables, and constants; and this could be confusing and time-consuming. Although traceability can be improved by creating subsystems, the problem of accessibility of variables remains. Again, including UDF in BBM is difficult. Table 5.1 presents PV modelling approaches adopted for studies on PV modules or systems. In particular, the overarching aim of this chapter is to advance the CBM approach to facilitate the modelling and simulation of photovoltaics. The specific objectives are to:

1. Create a robust code-based model of photovoltaic module.

2. Validate the CB model with commercially available PV modules.

3. Show that the CBM approach is more robust than the BBM approach.

Table 5.1: Photovoltaic modelling and simulation approaches [209]**.**

References	Approach	Focus of study/remarks
Vinod et al [210]	BBM /Simulink	model and simulate irradiation and temperature of PV module with single diode.
Gilman [202,203]	CBM /SAM	can be used for techno-economic decision-making.
Fatehi and Sauer [211]	CBM /PVSys	temperature and solar radiation dependence of PV.
Aryal and Bhattarai [212]	CBM /PVSys	studied 115.2 kWp PV system connected to the grid.
Abdulkadir et al [213]	BBM /Simulink	radiation and temperature effects on 36 W module.
Keles et al [214]	BBM /Simulink	current and voltage potential of PV module for a given solar radiation and temperature
Motahhir et al [191]	BBM /Simulink	effects of parameters on PV with modified incremental conductance algorithm.
[197]Fernandes et al [197]	circuit /PSPICE	effect of shading of PV based on some string layouts.
Lo Brano et al [196]	CBM/Visual Basic	studied PV module characteristics with five parameters approach.
Gupta et al [201]	BBM / Simulink	Studied PV generation with four parameters approach.
Morshed et al [215]	HOMER,PVsys, SolarMAT	studied 2 kW stand-alone PV system with 3 methods.
Mohammed et al [216]	CBM /TRNSYS	studied direct solar water heating system
Tan et al [217]	Simulink	dynamic simulation of PV system.
El Hassouni et al [195]	BBM /Simulink	studied 4.2 kW PV system for agricultural purpose.
Elkholy et al [199]	Numerical /Simulink/Excel	PV modules and arrays modelling
Pagrut et al [218]	BBM /Simulink	effects of environmental factors on PV system.
Mahmood et al [219]	BBM /Simulink	used four parameters approach to PV modelling.
Krismadinata et al [192]	BBM /Simulink	effect of temperature and irradiations on PV.
Acakpovi and Hagan [220]	BBM /Simulink	effect of irradiations and temperature on PV.

This study demonstrates how the CBM approach could help overcome the limitations of the BBM approach. The robustness can facilitate new theoretical models and algorithms, the study of thermophotovoltaics, and an enrichment of PV modelling and simulation tools/software. This could contribute towards low risk, timely and cost-effective PV systems development. Thus, this could contribute to advancing computational photovoltaics which entails the use computational modelling and simulation to improve the performance of PV, PV/T, and TPV systems.

5.1 Research Methods and Approach

Computational photovoltaics in which a CBM approach was used to create a computational model of the physical PV was the approach adopted in this study. The CB model was created to reflect the physical parameters of a PV module. Validation against the parameters in the datasheet of manufacturers was adopted. After validation, the CB model was used for simulation or virtual experimentation.

First, extant PV equations used to create the CB model involves a system of transcendental equation (SoTE), which is a set of simultaneous equations including at least a transcendental equation. Examples of transcendental equation are x = 2x - 2, y = Sin(2y) + 4, etc. Transcendental equations are better solved using computational iterations. For instance, the values of x or y cannot be determined through explicit solution. A certain value of x or y can be selected; and then, the right-hand side of the equation can be evaluated. The complexities of modelling and simulating SoTEs are presented in [221]. To calculate the power output of a PV module, voltage must be calculated. To avoid unnecessary repetition within the thesis, the step-by-step details on how the SoTE for a PV module was created will be presented in Section 6.2. The basic CB model is included in this thesis as Appendix A.

Table 5.2 presents the summary of equations used to create the basic SoTE for a PV module. Eq. (5.1) connects bandgap and temperature. Eq. (5.2) connects photocurrent and solar radiation, while Eq. (5.3) connects saturation current, bandgap and temperature. Eq. (5.4) shows how voltage depends on the number of cells in series in the PV and number of PV in parallel in the array. Lastly, Eq. (5.5) expresses the power output of a PV module. There is no direct expression for calculating voltage output (V_0) and (I_0) from Eq. (5.4) such that both can be substituted into Eq. (5.5) without creating a SoTE. The strategy adopted to implement the SoTE was to iterate over voltage since the open circuit voltage will be equal to the point the current-voltage curve cuts the voltage axis; and that is also the value of the voltage at the point of full convergence of the SoTE. The power outputs of the PV, including MPP, can be determined by the product of the current and the corresponding voltage on the curve.

Table 5.2: Equations for creating the CB model of a PV module [209]**.**

References	Equations	Equation Number
Unlu [92]	$E_g(T) = E_g(0) - \frac{\Theta_1 T^2}{T + \Theta_2}$	(5.1)
Bellia et al [93]	$I_{ph} = (I_{sc} + K_i (T_{cell} - T_{ref}) \times \frac{G}{G_{ref}}$	(5.2)
Mohammed et al [216]	$I_s = I_{s,ref} \left[\frac{T_{cell}}{T_{ref}}\right]^3 \exp\left[\frac{1}{k}\left(\frac{E_g}{T_{ref}} - \frac{E_g}{T_{cell}}\right)\right]$	(5.3)
Zeotouny et al [95]	$I_0 = I_{ph} N_p - I_s N_p \left[\exp\left(\frac{qV_0}{AN_s kT}\right) - 1\right]$	(5.4)
Power output equation	$P_o = I_o \times V_o$	(5.5)

5.2 Validation of the Proposed Code-Based Model and CBM Approach

Table 5.3 presents the data from peer-reviewed literature used for training the CB module of the PV model. Researchers often validate a PV model by comparing the model-predicted outputs with the manufacturers' stated values [196,201,218,222]. Adopting such approach, the CB model was herein validated with Solarex MSX-60 [191] and Shell S140 [223].

Table 5.3: Parameters and operating data for training the CB model [209]**.**

Parameters	Values	Units	References
Open circuit Voltage (V_{oc})	21.1	V	Motahhir et al [191]
Short circuit current (I_{sc})	3.8	A	Motahhir et al [191]
Saturation current (I_s)	5.39×10^{-5}	A	Meyer [224]
Maximum Power Point(P_{mp})	60	Watts	Motahhir et al [191]
Maximum Voltage Point(V_{mp})	17.1	V	Motahhir et al [191]
Maximum Current Point(I_{mp})	3.5	A	Motahhir et al [191]
Ideality factor (A)	2.83		Meyer [224]
Band gap (Silicon) at 0 K	1.1557-1.295	eV	Shi and Kioupakis [226]; Varshni [225]
Solar cell material constant (Θ_1)	7.021×10^{-4}		Varshni [225]
Solar cell material constant (Θ_2)	1108		Varshni [225]
Reference Temperature (T_{ref})	25	^oC	Villalva et al [190]
Temperature Coefficient at I_{sc} (K_i)	0.065	%/^oC	Motahhir et al [191]
Temperature Coefficient at V_{oc} (K_v)	-0.38	%/^oC	Motahhir et al [191]
Number of cells in series(N_s)	36		Motahhir et al [191]
Number of cells in parallel (N_p)	1		
Reference Insolation(G_{ref})	1000		Villalva et al [190]
Boltzmann constant (k)	1.38×10^{-23}	$J\ K^{-1}$	constant
Electron Charge (q)	1.602×10^{-19}	C	constant

The parameters that were compared were the MPP, short circuit current and the open circuit voltage (see Table 5.4). Here, the positive deviation '+' indicates where the model-predicted values were greater than the manufacturers' stated values in the data sheet, while negative deviation '-' indicates the opposite. Figures 5.1 (a) and (b) compared the parameters predicted by the CB model with values stated by the manufacturers of Solarex MSX-60 and Shell S140 modules. Information needed but not stated by the manufacturer were sourced from literatures or standard physical properties of the PV cell to populate the CB model.

The CB model predicted the I_{sc} with 100% accuracy because it was one of the input parameters. The percentage deviation in the MPP for the modules was below 2% while the percentage deviation in the V_{oc} approached 10%. The high deviation in the V_{oc} was because the CBM approach iterates over voltage and thus the predicted V_{oc} was mostly affected. In other words, the residual errors during cycles of iterations affected the voltage most and consequently the V_{oc} (the point where the I-V curve cuts the voltage axis). The deviation in the V_{oc} did not go in one direction for the two modules because the PV modules were made

from different solar cell materials. The accuracy of the CB model prediction may be affected by the accuracy of the laboratory measurements reported in the manufacturers data sheet. Unfortunately, there is no way to verify the accuracy of the laboratory measurements by manufacturers and the prediction can only be based on the available parameters on the datasheet. Nonetheless, the level of accuracy of the predictions of the CB model is adjudged acceptable for investigating thermodynamics of PV generation assuming that losses and irreversibilities are accounted as waste heat under practical applications.

Table 5.4: Percentage deviation of the model from Manufacturers' specifications [209]**.**

Parameters/PV modules	Solarex MSX-60	Shell S140
MPP(W) (manufacturer's spec)	60.0	40.0
MPP (W) (Model predicted)	59.00	39.51
% deviation of MPP	-1.7	-1.2
I_{sc}(A) (manufacturer's spec)	3.8	2.68
I_{sc} (A) (model predicted)	3.8	2.68
% deviation of I_{sc}	0.0	0.0
V_{oc} (V) (manufacturer's spec)	21.1	23.3
V_{oc} (V) (model predicted)	23.1	22.6
% deviation of V_{oc} (V)	+9.4	-3.0

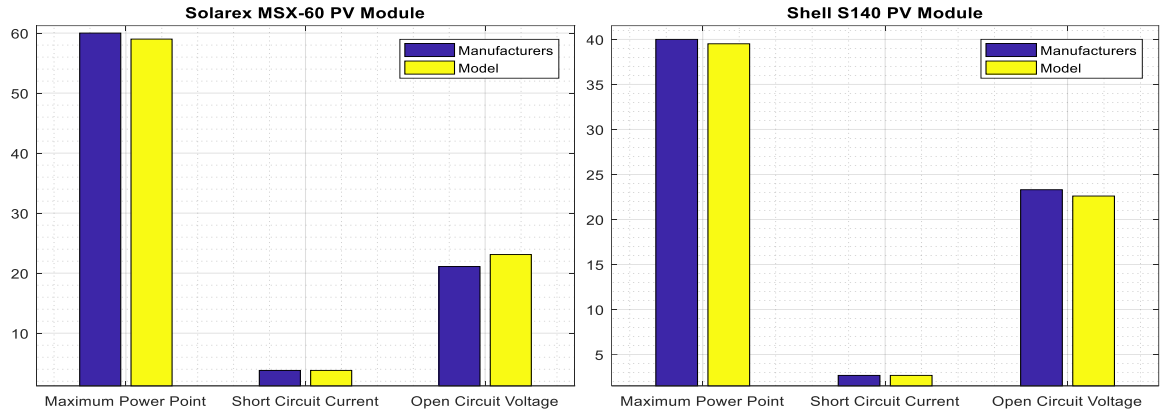

Figure 5.1: Prediction of parameters for Solarex MSX-60 and Shell S140 [209]**.**

5.2.1 Comparison of CBM and BBM Approaches

There were two processes adopted to establish the robustness of CBM approach over BBM approach. The first process validated the accuracy of the CB model using commercial PV modules (see Table 5.4). The second process implemented investigations considered to be computationally difficult with BBM approach.

First, CB and BB models were used to predict the MPP of four PV modules at STC as shown in Figure 5.2. Comparing the CB model with the BB model in MATLAB [227] eliminates possible effect of software type on the prediction. Clearly, from Figure 5.2, there was not

much difference between the MPP predicted by the two approaches. Therefore, CBM approach matches the accuracy of the prevalent BBM approach. This comparison benchmarked the CB model with the BB model. The second process tests for the robustness of the CBM approach over the BBM approach. The structure, algorithm and UDF features of the CB model make it suitable for "virtual experimentation". A UDF may be a function of PV material properties, environmental variables, costs, and so on as shown in Figure 5.3. PV modelling and simulation approaches reported in Table 5.1 focuses on the level of the PV module or system characteristics. Meantime, modelling of photovoltaic physics, thermodynamics, applications can be facilitated by a more robust and flexible approaches such as the proposed CBM approach. This could contribute to advance the frontiers of computational photovoltaics.

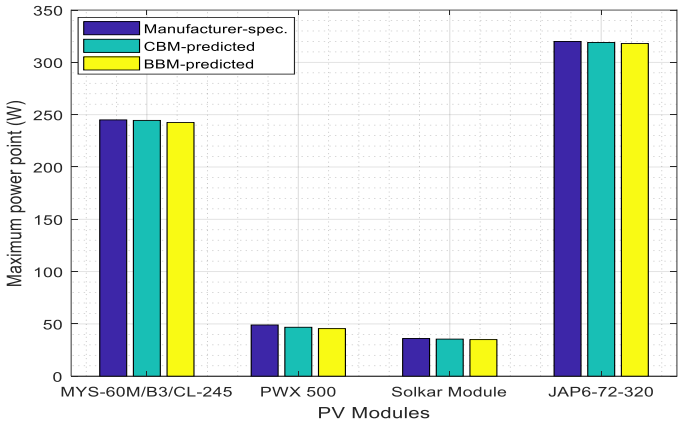

Figure 5.2: Comparison of the predictions of the MPP of commercial modules [209]**.**

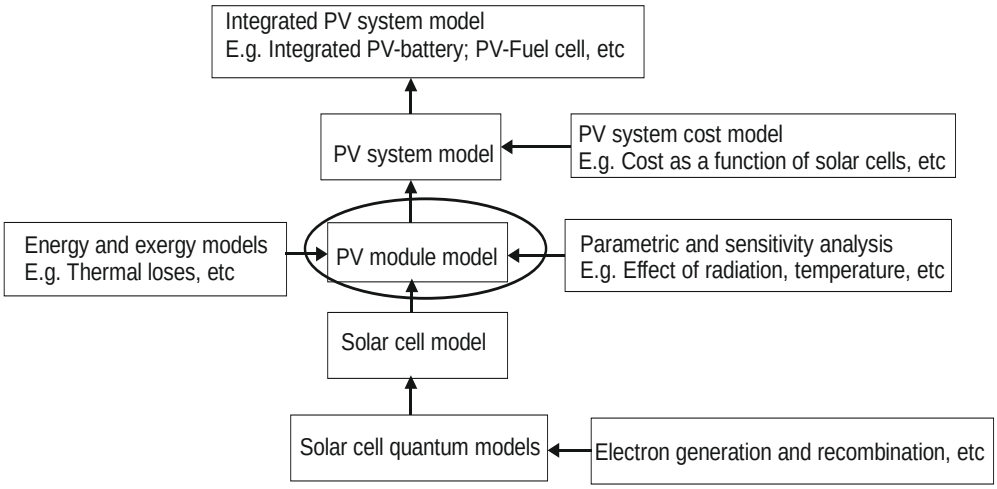

Figure 5.3: Potential applications of the CBM approach [209]**.**

5.3 Results and Discussion

This section presents the results generated using the "virtual experimentation" approach. It includes PV thermodynamics analysis, module characteristics, and system design. Detailed applications of the CBM approach are presented in Chapter 6 and 7.

5.3.1 Photovoltaic-Thermal Modelling Using CBM Approach

Thermalisation during generation and recombination of carriers reduces the conversion efficiency of PV modules [228]. Quantifying this thermal evolution in PV modules could deepen the understanding of how to reduce it or recover it for useful low temperature thermal work. CBM approach facilitated the proposed photovoltaic-thermal model presented in Chapter 6; as well as the proposed thermophotovoltaic model presented in Chapter 7. As of it, the CBM approach exhibited the robustness to facilitate an advanced thermodynamics study of PV and TPV systems. Thermodynamics of photovoltaics is beyond the capability of the BBM approach because of the UDFs and algorithm required to implement the integrated models. Moreover, off the shelf PV modelling and simulation software are usually constrained by an in-built pre-defined algorithm even when they accept UDFs. The algorithm of the CBM approach can easily be adjusted and this makes it suitable for aspects of PV modelling involving UDF including developing novel theoretical models.

5.3.2 Characterisation of PV Modules Using CBM Approach

The ideality factor (A) of a PV module describes the extent to which a solar cell matches the Shockley or an ideal forward-biased diode. To investigate the effect of ideality factor on power generation, the ideality factor of a 40 W PV module was varied from 0.5 to 2.83 to observe the effects on the accuracy of the model predicted MPP. From Figure 5.4, the accuracy of prediction (at constant number of iterations at 500) increases as the ideality factor approached 2.83. During the simulation, there was not noticeable improvement in prediction accuracy beyond 500 iterations, but the total computing time was proportional to the number of iterations. As a result, the number of iterations should be slightly above the saturation point to save computational time since the accuracy and precision of the prediction will not be jeopardised.

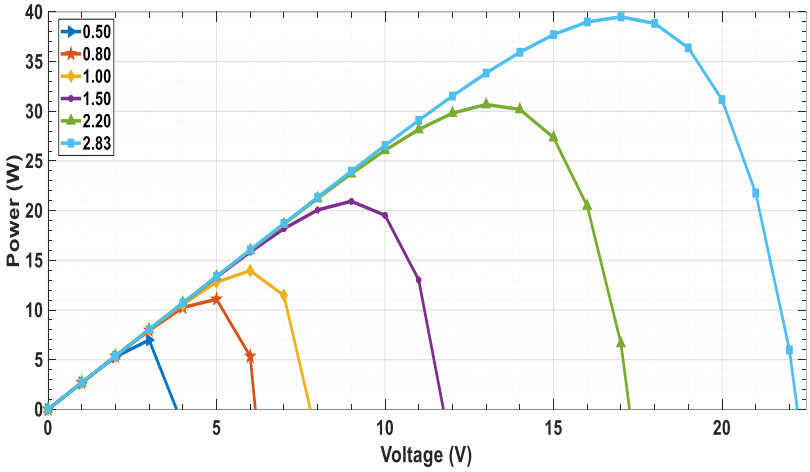

Figure 5.4: Predicted P - V curves for different ideality factors [209].

The PV module current is affected by the ideality factor according to Eq. (5.4). The short circuit current, which is the current through the solar cell when the voltage across the solar cell is zero, is related with the conversion efficiency by (Eq. (5.7)) [228]. The "rectangularness" of the I-V curve is a function of the fill factor (FF). FF depends on the level of resistances in series connection, as well as on the shunt resistance in the solar cells [229]. FF close to unity indicates high conversion efficiency and optimal open circuit voltage based on Eq. (5.7). Thus, increasing the ideality factor of a solar cell may involve the use of materials with low resistivity. The implication is that the relationship between FF, A and V_{oc} could be used to seek optimal PV design for improved efficiency.

$$\eta_{pv} = \frac{I_{sc}V_{oc}FF}{G \times A_{cell}} \qquad (5.7)$$

Increase in temperature can also affect V_{oc} as shown in Figure 5.5. This agrees with Dupre et al [230] and Chenni et al [222] that reported deterioration of the performance of PV modules with an increase in operating temperature. Compared with low temperature solar cells, high temperature solar cell (HTSC) should withstand generation and recombination of carriers (without degrading the V_{oc}) since electrical efficiency varies inversely with the operating temperature [231,232]. Notwithstanding, HTSC may require tuning of the thermal capacity of solar cell materials to withstand the degradation effects of increasing temperature. Varshni's model relating bandgap and temperature [225] in Eq. (5.1) means that bandgap engineering could be used to increase the amount of solar spectrum utilised for generation, as well as reduce the degradation of the V_{oc} by reducing the thermalisation of carriers in the valence-conduction bands [178].

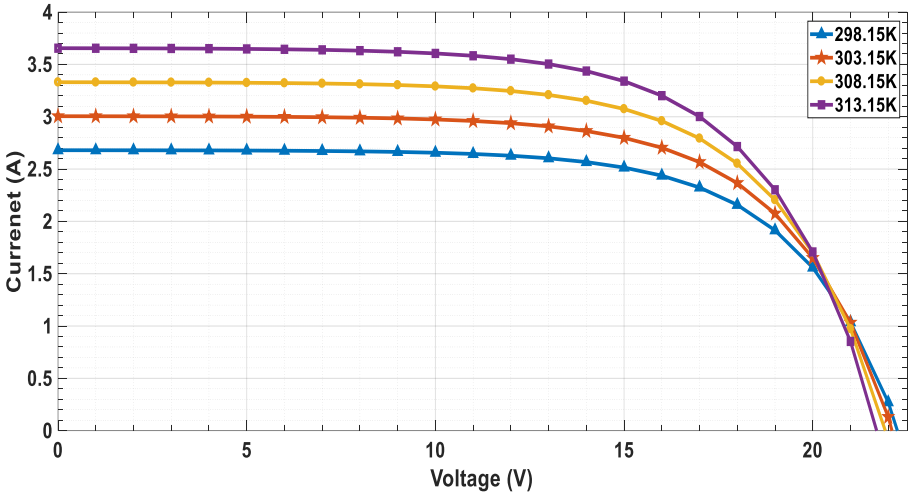

Figure 5.5: Predicted I - V curves for 15 ºC increment over reference [209].

5.3.3 Modelling and Simulating of PV Systems

High voltage or high current can be generated from PV array depending on the design [173]. CBM approach was applied to explore how the solar cell string designs and modules configurations affect power generation. Figure 5.6 shows a simulation of a PV module designs with 36, 38, 40 and 42 solar cells. The current is constant while the voltage across the cells in series increased (i.e. $V_{module} = V_1 + V_2 + \ldots + V_n$). This capability of the CBM approach is a predictive application for establishing solar cell strings design. This could also facilitate sizing of a PV module to produce a specific MPP.

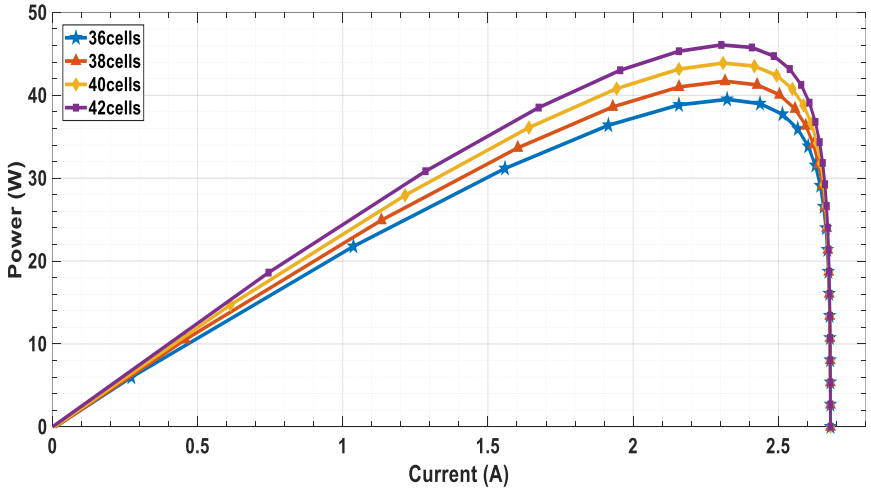

Figure 5.6: Predicted P - I curves for module design with different solar cell strings in series [209].

In Chapter 8 [233], CBM approach was used to create a large-scale photovoltaic power generation (LSPPG) and virtually deploy it at six different locations to determine the optimal

location. Eq. (5.8) predicts the number of PV modules, of equal MPP rating, that can be used to construct a LSPPG system.

$$P_{system} = P_{Pv} + P_{Pv}(N_P - 1) \quad (5.8)$$

where P_{system} is MPP of the array, P_{Pv} is MPP of a PV module and N_P is the number of PV modules connected in parallel.

From Figure 5.7, the voltage of a PV array (V_{array}) is constant but the current increments (i. e. $I_{array} = I_1 + I_2 + \ldots + I_n$) to give the total current of the array. This is clear in connecting 40 W PV module in parallel to create a160 W PV array.

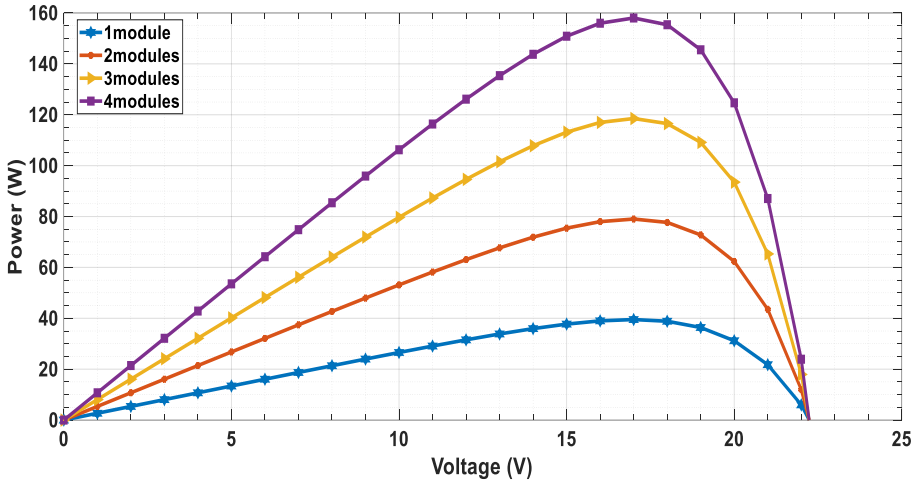

Figure 5.7: Code-based model predicted P - V curves for **PV modules in arrays** [209].

The output voltage from Figure 5.7 remains constant whilst the output current varies with the number of modules in the array. This feature of the CB model can be used to estimate the number of PV modules that can be used to generate certain amount of power based on the prevailing meteorological variables in a location.

Solar radiation is a critical meteorological variable for PV power generation. Figure 5.8 shows the effect of solar radiation variations on a 50 kW PV array at STC. This consists of 1,250 PV modules, 45,000 solar cells with an area of 312.5 m^2. The PV array was simulated at between 200 and 1000 Wm^{-2}. The output of the model conforms with Eq. (5.2) and the findings from extant literature in Table 5.1.

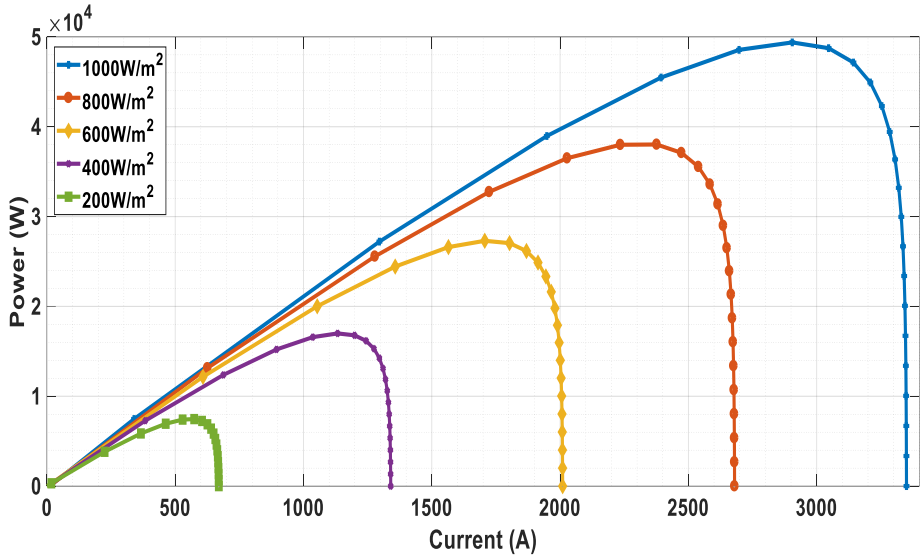

Figure 5.8: Predicted P - I curves for a large PV array [209].

Power output increases proportionally with the solar cell active area as shown in Figure 5.9 (a). The number of solar cells in series increases with the number of modules in the array as shown in Figure 5.9 (b). Power output of a PV module depends on the conversion efficiency of the type of solar cell. Designing and modelling of PV systems can be facilitated with Eq. (5.8). The ability to establish design scenarios is a prescriptive application of the CBM approach. It can enable decision-making on whether to use higher number of solar cells per module to reduce the number of modules or use lower number of solar cells and higher number of modules. Furthermore, cost of PV systems can be modelled if the total cost function for materials is included in Eq. (5.8).

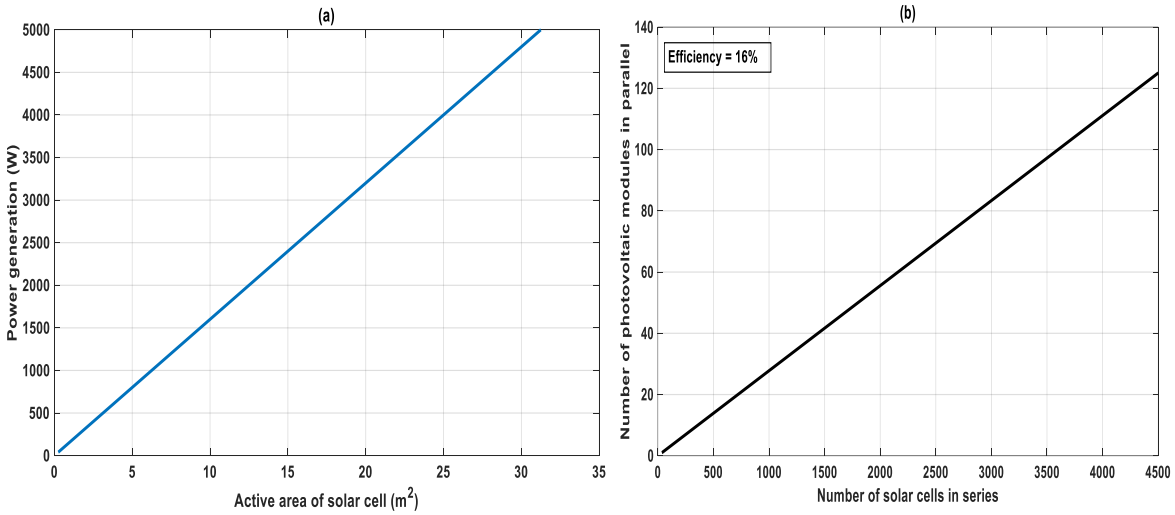

Figure 5.9: 5 kW PV system (a) MPP versus active area of solar cell. (b) Solar cells in series in the module versus the number of PV modules [209].

5.3.4 Potential of CBM Approach for Multiple Variables Simulation

Figure 5.10 shows daily mean power generation based on mean temperature and solar radiation. In Sections 5.4.2 and 5.4.3, the effect of one input variable on the PV power geneartion characteristics was simulated. Now, solar radiation and temperature effects on PV systems was studied using actual meteorological data from 1st to 31st January, 2016 for Enugu in Nigeria. The effect was observed from the simulation of a 50 kW PV system presented in Section 5.4.3. This feature of the CBM approach can give insights into the sizing of a PV system using two meteorolgical variables. The reliabilityof PV systems can improve with appropriate sizing. Accurate sizing could also reduce overall system cost and energy waste since the MBSE is done at the design stage.

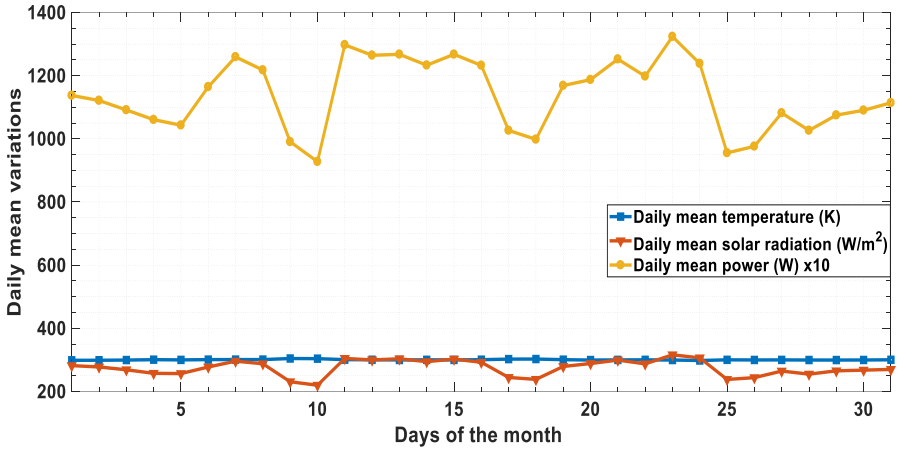

Figure 5.10: Simulation of MPP of PV system using CBM approach based on actual data [209].

5.4 Summary

This chapter presented a CBM approach as a potential approach to advance computational photovoltaics which can be combined with an experimental approach to improve the applications of PV-based power systems. A CB model of a PV module was created using MATLAB codes, and it was validated with commercial PV modules. The CB model consistently predicted the I_{sc}, MPP, V_{oc} with deviations of 0%, <2% and <10%, respectively. This level of accuracy is acceptable for thermodynamic modelling in which losses are accounted for as waste heat. The CB model was further demonstrated to be robust as it can accept UDF and can be applied for predictive and prescriptive studies. Overall, the proposed CBM approach exhibits robustness for modelling and simulating photovoltaics beyond the capability of the prevalent BBM approach. Chapters 6, 7 and 8 present how the CB model and CBM approach was applied to achieve the objectives of this research.

Chapter 6: Numerical Integration of Solar, Thermal and Electrical Exergies of a Photovoltaic Module

The E^4A implemented in Chapter 4 indicated that more energy needs to be harnessed from the PV module. Consequently, the CBM approach presented in Chapter 5 was developed to further investigate the thermodynamic characteristics of photovoltaics. This chapter focuses on the integration of solar, electrical, and thermal exergies to quantify the thermal losses from a PV module pursuant Research Objective 3.

Electrical energy efficiency of PV devices drops with an increase in the temperature of solar cells [192,220]. Gaitho [234] observed that the efficiency of the silicon solar cell was high for a range of 297-360 K; whereas higher temperatures degraded the efficiency. Thus, to improve the conversion efficiency of PV devices, the sensitivity of V_{oc} and I_{sc} to temperature needs to be better understood [230]. An experimental study showed that the electrical efficiency of a PV dropped by 8.5% when the temperature increased to 68 ^{o}C [182]. It has also been shown that V_{oc}, MPP, FF and efficiency of a PV module decreased with an increase in temperature [235]. A finite element analysis of a PV module showed that its efficiency degraded at higher temperature and this could induce thermal stress in a PV [231].

Generally, extracting the heat generated from solar cells by cooling, during power generation under high solar radiation, improves electrical and thermal efficiency of PV/T systems [181,236]. Researchers [177] and [150] assert that insights into the physics of PV as a function of temperature is essential for optimising it for thermophotovoltaic applications. To address this, a macroscopic energy and entropy equations for a PV [237] were derived. This chapter, therefore, purposes to integrate the solar, electrical, and thermal exergies of a PV module to deepen the understanding of thermodynamics of PV power generation.

The energy and exergy characteristics of solar radiation have been studied [174]. Shockley predicted the electrical energy efficiency limit of the silicon solar cell [114]. Interestingly, thermodynamics of a PV module could provide insights into how thermal exergy flow within the PV module can be converted into useful work as it interacts with the environment. Given that solar cells generate power through direct conversion unlike other thermodynamic cycles (e.g. Rankine, Brayton), PV-based technologies will be crucial in any imaginable renewable energy mix. PV power generation is subject to the laws of thermodynamics [146]. For instance, if the sun's temperature is 6000 K and PV module's temperature is 300 K, the

Carnot efficiency would be 95%. As a heat engine, PV modules can harness more energy from the sun since the actual conversion efficiency is still less than 50% [238].

Conceptualising a PV module as a Carnot engine does not account for the losses or irreversibilities because the Carnot efficiency is an energy analysis approach which is based on the first law of thermodynamics. Exergy analysis, based on the second law of thermodynamics, considers thermodynamic losses and irreversibilities. Exergy is " the shaft work or electrical energy necessary to produce a material in its specified state from materials common in the environment in a reversible way, heat being exchanged only with the environment at T_o" [143]. Photovoltaic devices interact with solar radiation and the ambient temperature as it generates electrical energy and exchange waste heat to the environment.

The overarching aim of this study is to integrate the solar, thermal, and electrical exergies of a PV module so that the waste heat generated during a photovoltaic process can be quantified. The integration is expected to generate a theoretical model to deepen the understanding of the physics of a PV module. To this end, the specific objectives are to:

1. Derive an integrated solar, electrical, and thermal exergy model of a PV module.
2. Create a CB model of the integrated model in objective 1.
3. Perform parametric studies to gain physical insights into the thermodynamics of photovoltaic power generation.

To integrate the solar, electrical, and thermal exergies of a PV module, some assumptions were made. First, re-radiated energy on the glass surface was excluded in the analysis and this was factored into the modelling by including transmissivity as a penalty for losses that occurred on the surface. There were no internal re-radiations within the PV module. CB model of the PV module was created at STC [239]. Useful work of the solar radiation is equal to the radiation exergy input into the module [174]. Exergy destruction and irreversibilities during conversion process are lost to the environment as heat alone. First and second laws of thermodynamic were obeyed. Electrical energy efficiency is different from electrical exergy efficiency. Lastly, there was no other heat inflow into the system besides photon energy and the heat outflow was limited to the heat from the PV module.

Quantifying the heat generated from a PV module can enable designers estimate the amount of heat source from a PV module for heating fluids as in PV/T applications [240]. Already, the extended Hottel-Whillier model [180] enables a thermal analysis of a flat plate collectors and this has been applied to study PV/T systems [28]. As of it, quantifying the heat generated

from a PV can give insights into how different materials and PV designs destroy solar exergy. In this study, it is expected that the reduction in thermal generation in a PV module will result in higher electrical energy generation based on the first law of thermodynamics. Based on the second law of thermodynamics, thermal energy generation indicates conversion imperfections in a PV module. Thus, inhibiting thermal evolution would increase the perfection with which the PV module would convert solar exergy into electrical exergy.

6.1 Research Method and Approach

Initially, a CB model of a 45 W PV was created with parameters presented in Table 6.1. It was then validated to ensure that it predicts the MPP at STC as shown in Figure 6.1. The scope of the work done in Chapter 5 was to create the CB model which can only predict the power characteristics of a PV module, which was based on the first law of thermodynamics.

Table 6.1: Parameters of the CB model of a PV module [91].

Parameters	Values	Units
Open circuit Voltage (V_{oc})	22.2	V
Short circuit current (I_{sc})	3.0	A
Maximum Power Point(P_{mp})	45	Watts
Maximum Voltage Point(V_{mp})	14.98	V
Ideality factor (A)	2.83	
Temperature of the sun (T_{sun})	6000	K
Transmissivity of glass cover (τ_{glass})	0.8	
Number of cells in series (N_s)	36	

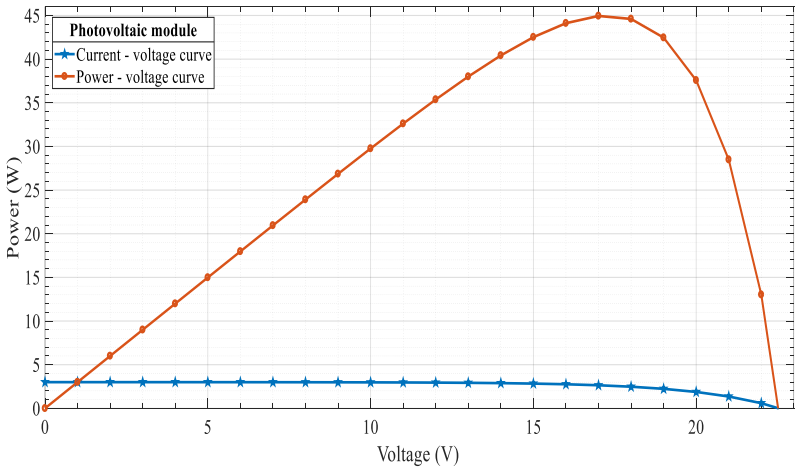

Figure 6.1: P – V and I – V curves of a 45 W PV module [91].

To facilitate exergy analysis of a PV module, the thermal and solar exergy components of a PV module were incorporated into the power generation model which was the focus of Chapter 5. In this study, solar exergy model proposed by Petela [174] was adopted to create a computational black box model in which solar exergy inputs that did not come out as electrical exergy was assumed to be the thermal loss.

The integrated model was used to perform parametric study to understand the effect of temperature and solar radiation on the functional parameters of the PV. A wide range of solar radiation and temperature was used to perform virtual experimentation. The results of the simulations were tabulated, plotted, and interpreted based on the principles of photovoltaic physics and the laws of thermodynamics.

6.2 Numerical Modelling of the Proposed Photovoltaic-Thermal Model

Energy of a system is usually conserved (i. e. $E_{in} = E_{out}$) based on the first law of thermodynamics. For a PV module, input solar energy is conservatively converted into electrical and thermal energies. Here, the sum of the output electrical and thermal energies equals the solar energy input into the PV module. There are two approaches to conceptualising the thermodynamic modelling of a photovoltaic model: the two-level solar cell model [241]; and as an infinite tandem system [242] in which a PV cell is modelled as an infinite stack of p-n junctions with continuously decreasing bandgap.

In calculating the electrical energy efficiency of a PV module, the output thermal energy is usually excluded as it is regarded as a by-product. This neglect of the thermal component of the input solar energy cannot give insight into the maximum theoretical efficiency limit of a PV model, which the exergy analysis (second law of thermodynamics) can provide insights into. Exergy analysis focuses on the quality of the electrical energy produced by a PV module as it interacts with the environment at the reference state. Baruch et al [243] stated that the theoretical conversion efficiency of solar cell can be derived through energy and entropy balance or through balancing of carriers generation and recombination in PV cells. The earlier approach was adopted in this study to balance the entropy of a PV module.

Thus, solar exergy input ($\dot{E}x_{Solar}$) into a PV module was converted into electrical energy ($\dot{W}_{elect}$) and heat ($\dot{Q}_{loss}$) as expressed in Eq. (6.1). The term ($\dot{Q}_{loss}$) represents the exergy loss and irreversibilities in a PV module. Eq. (6.1) appears analogous to the Gibbs

free energy equation ($\Delta G = \Delta H - T\Delta S$) which describes the thermodynamic state of a spontaneous system. Later, in Section 6.4.3, further comparisons would be drawn.

$$\dot{Q}_{loss} = \dot{E}x_{Solar} - \dot{W}_{elect} \quad (6.1)$$

Up to nine categories of PV conversion losses [177] have been identified but this study focuses on the actual solar exergy inflow through the PV module surface. To incorporate the potential solar exergy destruction at the glass surface, transmissivity of the glass top (τ_{glass}) was included as a penalty for the optical properties of the PV module (see Figure 6.2). The balance of the solar exergy input that reaches the PV cells is converted into useful electrical exergy and waste thermal exergy, which represents an opportunity for improvement.

Landsberg and Baruch [244] proposed that the upper limit of thermodynamic efficiency (η_L) of energy conversion of radiation into other forms of energy as in photovoltaics, photochemistry and photobiology can be expressed as Eq. (6.2); assuming that the temperature of the pump (i.e. sun) will be greater than the temperature of the converter (i.e. PV cells) and the temperature of the sink (i.e. surrounding of the PV cells); and the temperature of the converter is almost the same as the temperature of the environment.

$$\eta_L = 1 - \frac{4}{3}\left(\frac{T_s}{T_p}\right) + \frac{1}{3}\left(\frac{T_s}{T_p}\right)^4 \qquad T_c \approx T_s \text{ and } T_p \geq T_c \geq T_s \quad (6.2)$$

where T_s is the sink temperature, T_c is the temperature of the converter and T_p is the black body radiation temperature of the pump.

Petela [174] proposed that a unified efficiency expression for a converter (η_c), where the useful work is equal to the radiation exergy, can be expressed as Eq. (6.3).

$$\eta_c = 1 - \frac{4}{3}\left(\frac{T_0}{T}\right) + \frac{1}{3}\left(\frac{T_0}{T}\right)^4 \qquad T_2 = T_0 \quad (6.3)$$

where T_0 is the sink temperature, T_2 is the temperature of the converter and T is the black body radiation temperature of the sun (approximately 6000 K).

The model by Landsberg and Baruch is equivalent to that of Petela, but Petela used exergy approach and highlighted that the heat generated was due to entropy generation. Solar exergy input, based on the model by Petela [174], through the PV surface area (A_{cell}) at a specific solar radiation intensity (G) and taking into consideration the optical properties of the PV surface (τ_{glass}) can be expressed as Eq. (6.4). So, the useful work of solar radiation is equivalent to the radiative exergy, while the temperature of the surface of the PV is equal to the ambient temperature.

$$\dot{E}x_{Solar} = G \times A_{cell} \times \tau_{glass} \left(1 - \frac{4}{3}\frac{T}{T_{sun}} + \frac{1}{3}\left(\frac{T}{T_{sun}}\right)^4\right) \quad (6.4)$$

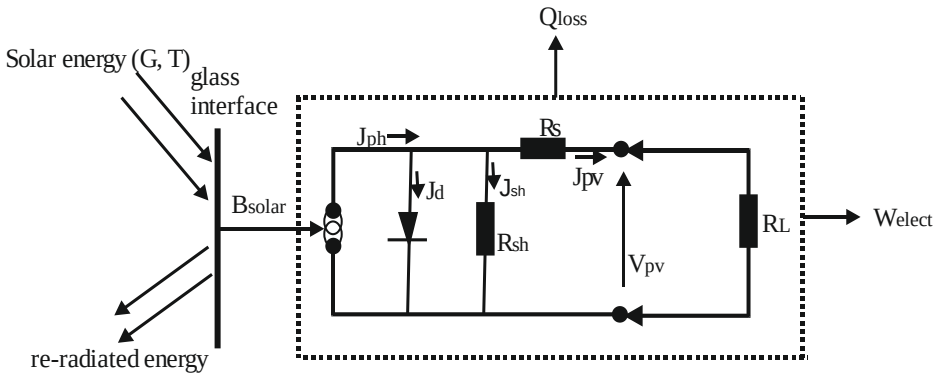

Figure 6.2: Diagram of exergy flow in a photovoltaic module [91].

The electrical exergy flow ($\dot{W}_{elect}$) of a PV module is the product of the current (I_{pv}) and the voltage (V_{pv}) across the terminals as expressed in Eq. (6.5).

$$\dot{W}_{elect} = I_{pv} \times V_{pv} \quad (6.5)$$

In accordance with Kirchhoff's current law, the current output of a PV module (I_{pv}) equals the photo-induced current (I_{ph}) minus the current due to the forward biased diode (I_d) characteristic of the solar cell and the shunt current representing current flowing through the material (I_{sh}) (Eq. (6.6)).

$$I_{pv} = I_{ph} - I_d - I_{sh} \quad (6.6)$$

Photocurrent (I_{ph}) depends on the solar radiation intensity, thermal properties expressed as thermal coefficient (K_i) and the temperature gradient between the PV cells and the reference temperature as in Eq. (6.7) [93].

$$I_{ph} = (I_{sc} + K_i (T_{cell} - T_{ref}) \times \frac{G}{G_{ref}} \quad (6.7)$$

where I_{ph} is the light induced current, K_i is the thermal coefficient at short circuit current and G_{ref} is the reference insolation at STC (1000 W m^{-2}, 25 ^{o}C, AM1.5).

Shockley [114] proposed the forward biased diodes characterisation of solar cells as (Eq. (6.8). Solar cells behave like forward biased diodes because they permit current to only flow in forward direction when they receive photon energy.

$$I_d = I_s\left(\exp^{\left(\frac{qV_d}{AkT}\right)} - 1\right) \quad (6.8)$$

Ohms law accounts for the effect of the resistance of solar cells material to the photocurrent given the potential difference across the terminals during generation and combination of electrons. Both shunt resistance (R_{sh}) and the resistance due to the series connections of solar cells (R_s) are sources of electrical exergy destruction classified as Ohmic losses expressed in Eq. (6.9). Since the load is connected in series with the PV module, the current output from a PV module is equal to the current input into external load (I_L).

$$V_L = I_{sh}R_{sh} - R_sI_L \text{ or } V_d = I_{sh}R_{sh} = V_L + R_sI_L \quad (6.9)$$

where $I_{sh} = \frac{V_L + R_sI_L}{R_{sh}}$

Substituting Eq. (6.7) - (6.9) into Eq. (6.6) results in Eq. (6.10).

$$I_{pv} = I_{ph} - I_s\left(\exp^{\left(\frac{q(V_L + R_sI_L)}{AN_skT}\right)} - 1\right) - \frac{V_L + R_sI_L}{R_{sh}} \quad (6.10)$$

To create a PV module, PV cells are connected in series. The PV modules connected in parallel (N_p) increase the output current while PV cells connected in series within the module (N_s) increase the output voltage of the PV module. A PV array can be created by connecting PV modules in parallel. Thus, Eq. (6.11) can be used to compute the output current (I_{pv}) from the PV module ($N_p = 1$) or PV array ($N_p > 1$).

$$I_{pv} = I_{ph}N_p - I_sN_p\left[\exp\left(\frac{qV_{pv}}{AN_skT}\right) - 1\right] \quad (6.11)$$

The bandgap energy (E_g) of a PV cell is an important material property in modelling a PV module. From Eq. (6.11), saturation current (I_s) for a PV module with a certain bandgap energy, operating between the minimum and maximum solar radiation for a spectral energy distribution at air mass AM1.5 has been expressed as Eq. (6.12) [94,95].

$$I_s = I_{s,ref}\left[\frac{T_{cell}}{T_{ref}}\right]^3 \exp\left[\frac{1}{k}\left(\frac{E_g}{T_{ref}} - \frac{E_g}{T_{cell}}\right)\right] \quad (6.12)$$

where $I_{s,ref}$ is the reference saturation current of the semiconductor and $\frac{kT}{q}$ is 26 mV at 300 K [245].

Varshni's empirical model (Eq. (6.13)) expresses the relationship between the bandgap energy, solar cells material properties and the saturation current as a function of temperature [92,225]. Different solar materials have different bandgap energy and material constants.

$$E_g(T) = E_g(0) - \frac{\theta_1 T^2}{T + \theta_2} \tag{6.13}$$

$E_g(0)$ is energy gap at 0 K, $E_g(T)$ is direct or indirect energy gap at temperature T and θ_1 and θ_2 are constants (for silicon: θ_1 = 7.021x10^{-4} and $\theta_2 = 1108$); these values are obtained experimentally [225].

The computation of the voltage of PV modules (V_{pv}) in Eq. (6.11) creates a transcendental equation because the voltage must be calculated first before it can be substituted into Eq. (6.5) to calculate electrical power. Here, the transcendental nature of the CB model is effectively solved by computational iteration over the voltage. The CB model which was developed and validated using commercially available PV to implement Eq. (6.4), (6.5), (6.7), (6.11), (6.12) and (6.13) helps to realise the proposed photovoltaic-thermal model expressed in Eq. (6.14).

$$\dot{Q}_{loss} = \left[G \times A_{cell} \times \tau_{glass}\left(1 - \frac{4}{3}\frac{T}{T_{sun}} + \frac{1}{3}\left(\frac{T}{T_{sun}}\right)^4\right)\right] - \left(I_{ph}N_p - I_s N_p\left[\exp\left(\frac{qV_{pv}}{AN_s kT}\right) - 1\right]\right) \times V_{pv} \tag{6.14}$$

Eq. (6.15) is generated by substituting Eqs. (6.7) and Eq. (6.12) into Eq. (6.14). A manual calculation of Eq. (6.14) can be done using Eq. (6.15). Otherwise, an algorithm can be used to determine the computational procedure of implementing the SoTE. My study [221] provides a generalised step-by-step procedure of implementing SoTEs.

$$\dot{Q}_{loss} = \left[G \times A_{cell} \times \tau_{glass}\left(1 - \frac{4}{3}\frac{T}{T_{sun}} + \frac{1}{3}\left(\frac{T}{T_{sun}}\right)^4\right)\right] - \left(N_p\left[\left(I_{sc} + K_i\left(T_{cell} - T_{ref}\right) \times \frac{G}{G_{ref}}\right] - \left[I_{s,ref}\left[\frac{T_{cell}}{T_{ref}}\right]^3 \exp\left[\frac{1}{k}\left(\frac{E_g}{T_{ref}} - \frac{E_g}{T_{cell}}\right)\right]\right] \times N_p\left[\exp\left(\frac{qV_{pv}}{AN_s kT}\right) - 1\right]\right) \times V_{pv} \tag{6.15}$$

Eq. (6.16) [246] was used to calculate the electrical energy efficiency (η_{elect}) of a PV module without the transmissivity of the glass but it was added here as a penalty for solar

flux due to the optical nature of PV module surface. Similarly, transmissivity was included in the Petela model [174] in the calculation of exergy efficiency (η_{ex}) as in Eq. (6.17).

$$\eta_{elect} = \frac{\dot{W}_{elect}}{G \times A_{cell} \times \tau_{glass}} \tag{6.16}$$

$$\eta_{ex} = \frac{\dot{W}_{elect}}{G \times A_{cell} \times \tau_{glass}\left(1-\frac{4}{3}\frac{T}{T_{sun}}+\frac{1}{3}\left(\frac{T}{T_{sun}}\right)^4\right)} \tag{6.17}$$

6.3 Results and Discussion

This section was divided into three major parts: effects of temperature, effects of solar radiation and a comparison between the proposed model and Gibbs free energy equation.

6.3.1 Effects of Temperature on the Performance Parameters of Photovoltaic Module

The CB model was simulated between 5 and 350 K using virtual experimentation approach to gain insights into the physical behaviours of the PV module over a wide range of temperature variations. Figure 6.3 presents the effect of temperature on photocurrent generation, solar exergy flow and voltage of the PV module. Clearly, the voltage of the PV module increased with temperature up to 250 K before it started to deteriorate. This agrees with a finding that power generation increased up to a maximum point after which degradation sets in [150]. The open circuit voltage was not significant below 200 K; probably because there is a minimum heat content of a PV module that can facilitate efficient power generation based on kinetic theory perspective. Such critical point could be likened to the activation energy in chemical processes. The sudden fall in the voltage agrees with findings in [230] in which the sensitivity of open-circuit voltage in connection with the balance between generation and recombination as a function temperature variation was established. The sensitivity of short circuit current to temperature was driven by the dependence of bandgap on temperature, as well as the nature of incident spectrum and the conversion efficiency of the PV module [225,230].

The thermal conductivity of PV cells can also influence their thermal capacity and thermal behaviours as the thermal content of a PV module change. It was reported that there was a rapid decrease in thermal conductivity of zinc oxide coated single solar cell from 1.26×10^3 $Wm^{-1}K^{-1}$ to 9.63×10^2 $Wm^{-1}K^{-1}$ as the temperature increased from 297 K to 320 K [234]. With no dissipation of heat generated from the module, the deterioration of the open circuit voltage of the PV module in this study was in agreement with a study [235]. Electrons and holes which are excited above and below the bandgap respectively will be thermalised.

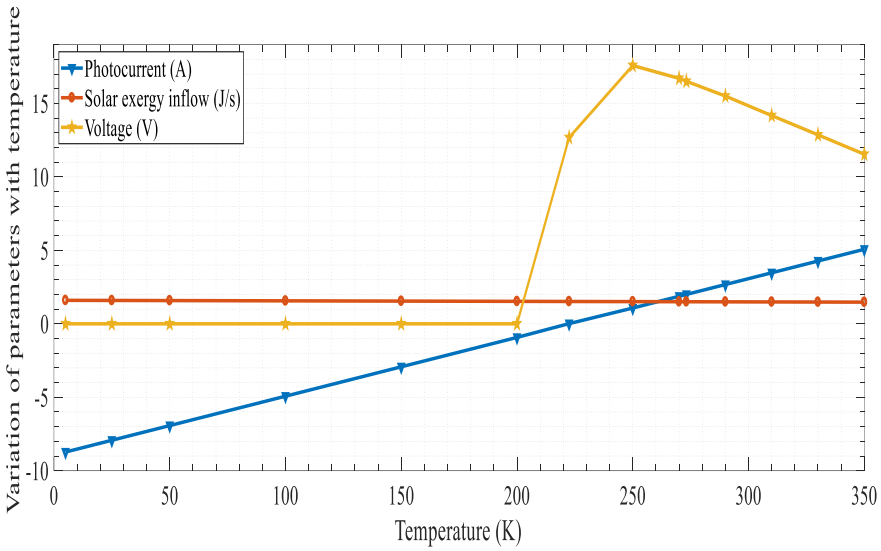

Figure 6.3: PV temperature variation effects on the photocurrent and voltage [91].

Thermalisation of electrons and holes contribute to the increase the thermal content of the module [178]. Supposing that a special case of a thermally isolated PV system, as in space, is considered. The absorption of photons and the thermalisation of the carriers will result in self-heating. This self-heating will occur rapidly in the thermally isolated system until currents can flow and electrical energy can be extracted. Once current flows, then there will be a thermal balance reached between the rate at which electrical energy is extracted and the thermalisation rate of the above/below gap carriers.

Figure 6.4 shows a sub-linear increase in the electrical and thermal exergy beyond 223.50 K. Clearly, thermal exergy flow increased with temperature, an indication that the quality of thermal energy available for useful thermal work increased as the temperature gradient widens over the reference state (298.15 K). However, there are two possible implications of an increase in thermal exergy as the temperature increases. Firstly, increasing thermal generation degrades its electrical energy efficiency [220] because of the negative temperature coefficient of PV cells. To hedge against V_o deterioration (also see Figure 6.3) and sustain electrical exergy flow, thermal management [182,183] of the PV module is often used. For instance, heat generated in the PV module can also be managed or dissipated using phase change materials such as polyethylene glycol 1000 (PEG1000) [247], cooling with air using forced convection [182] and cooling with water [248].

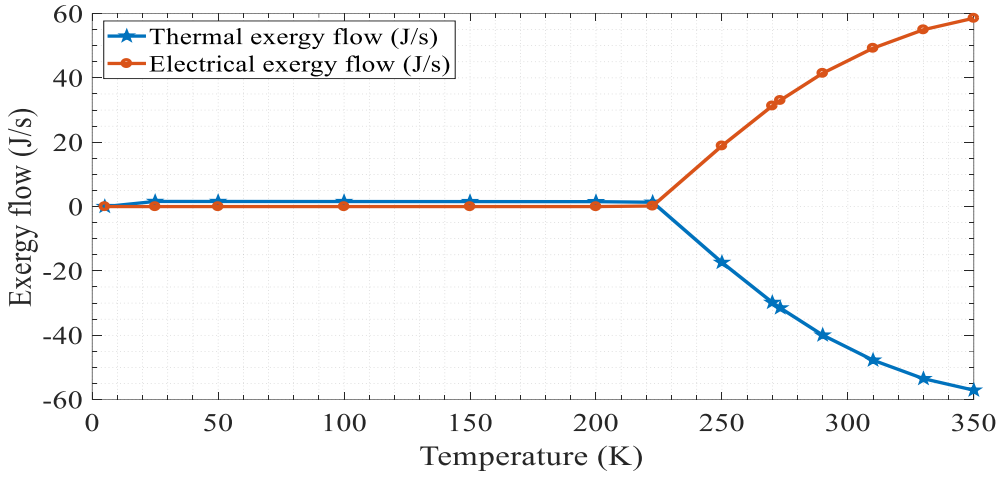

Figure 6.4: PV temperature variations effects on the thermal and electrical exergy flows [91].

Secondly, increasing thermal exergy of the PV module indicates the quantity of heat that can be recovered for additional useful thermal work in PV/T systems [28,249]. While in Figure 6.4, the temperature of the PV needs to exceed a critical temperature (in this case 223.5 K) before it can generate electrical energy and exchange heat with the environment; In the case of PV/T systems, heat generated ($\dot{Q}_{loss}$) will be utilised to heat working fluid. For PV/T modules, thermal extraction will improve electrical efficiency [250]. By utilising the waste heat, the overall energy and exergy efficiencies will improve. This implies that heat dissipation to the environment should be enhanced in PV applications while heat recovery should be enhanced in PV/T applications. Here, at a temperature of 290 K, the electrical exergy from the 45 W PV was 41.46 J s^{-1} and the overall improvement in exergy could be up to 51% if the $\dot{Q}_{loss}$ is utilised for useful thermal work in PV/T systems. Details of the simulation results at 1000 W m^{-2} and varying temperature are presented in Table 6.2.

Table 6.2: Effects of PV temperature on the parameters of the module [91].

Temp. (K)	Solar exergy inflow (J s^{-1})	Photocurrent (A)	Electrical exergy flow (J s^{-1})	Voltage (V)	Thermal exergy outflow (J s^{-1})	Electrical energy efficiency (%)	Electrical exergy efficiency (%)
5.00	1.598	-8.726	0.000	0.0000	0.0000	0.0000	0.0000
25.00	1.591	-7.926	0.0000	0.0000	1.5911	0.0000	0.0000
50.00	1.582	-6.926	0.0000	0.0000	1.5822	0.0000	0.0000
100.00	1.564	-4.926	0.0000	0.0000	1.5644	0.0000	0.0000
150.00	1.547	-2.926	0.0000	0.0000	1.5467	0.0000	0.0000
200.00	1.529	-0.926	0.0000	0.0000	1.5289	0.0000	0.0000
223.50	1.521	0.014	0.1775	12.6786	1.3430	0.0011	0.0012
250.00	1.511	1.074	18.8823	17.5813	-17.5813	0.1180	0.1250
270.00	1.504	1.874	31.3058	16.7053	-29.8018	0.1957	0.2082
273.15	1.503	2.000	33.0176	16.5088	-31.5147	0.2064	0.2197
290.00	1.497	2.674	41.4572	15.5038	-39.9603	0.2591	0.2770
310.00	1.490	3.474	49.2427	14.1746	-47.7529	0.3078	0.3305
330.00	1.483	4.274	54.9790	12.8636	-53.4963	0.3436	0.3708
350.00	1.476	5.074	58.5604	11.5413	-57.0848	0.3660	0.3969

6.3.2 Effects of Changes in Solar Radiation on the PV Module Performance

Solar radiation between 0 and 1000 W m^{-2} as the temperature of the PV module was kept at 298.15 K was simulated using virtual experimentation approach. Here, 0 W m^{-2} represents no solar radiation (e.g. at night) while 1000 W m^{-2} represents high solar radiation (e.g. afternoon of a typical summer day). From Eq. (6.7), an increase in the solar radiation can increase the photocurrent generation in a PV module as shown in Figure 6.5. Clearly, the voltage of the PV module increases with an increase in solar radiation from 0 to 1000 W m^{-2} at constant temperature. Likewise, the photocurrent increased with an increase in solar exergy input based on Eq. (6.7). This implies that PV power generation would increase with increasing solar exergy as both photocurrent and voltage of the PV module would increase at a constant temperature. As already highlighted, cooling improves electrical power generation [247] and this finding corresponds to the practical applications in which thermal management is used to control the temperature of a PV module.

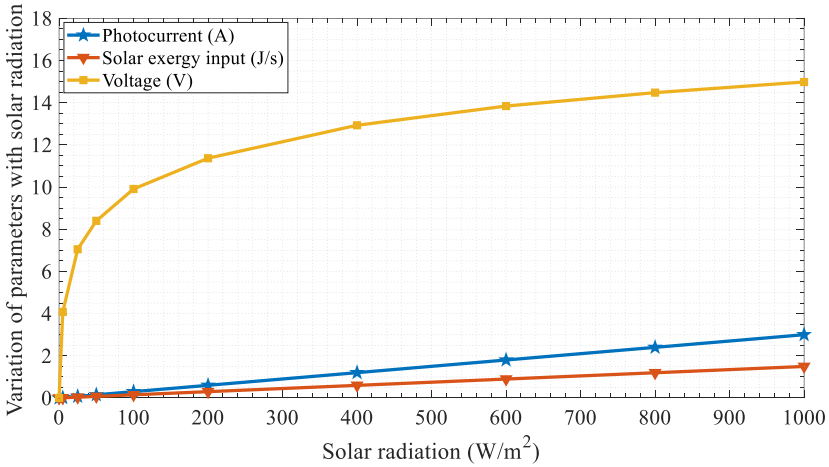

Figure 6.5: Solar radiation effects on the photocurrent and voltage of the PV module [91].

Figure 6.6 indicates that the electrical and thermal exergy flow from the PV module will increase with an increase in solar radiation. Whereas increasing temperature degrades electrical exergy of a PV module, increase in solar radiation improves it. This is because entropy generation in any thermodynamic system generally depends on temperature (i.e. $T_0 S_{gen}$). Figure 6.6 suggests that keeping the temperature of the PV module low and constant could potentially enable both electrical and thermal exergy to evolve gradually.

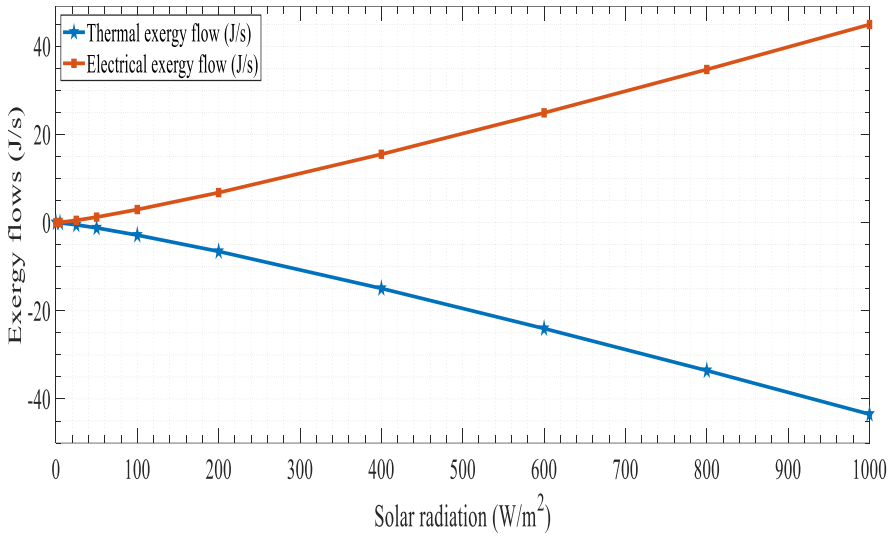

Figure 6.6: Solar radiation effects on the thermal and electrical exergy flow in a PV module [91].

On the other hand, high electrical exergy efficiency of a PV module implies lesser heat generation because exergy destruction results in heat generation. This agrees with a previous finding that the cell temperature, electrical power and thermal energy increased for every 100 W m^{-2} increase in solar radiation for a PV/T system [181]. This is evident in the widening of the electrical and thermal exergy flows as solar radiation increased at constant temperature. The electrical conversion efficiency would have a negative slope if the temperature was allowed to increase in accordance with the extended Hottel-Whillier model [180] expressed in Eq. (6.18).

$$\eta_{elect} = \eta_{ref}[1 - \beta_{ref}(T - T_{ref})] \qquad (6.18)$$

where η_{elect} is electrical efficiency of the PV/T system, η_{ref} is efficiency at a reference point, T_{ref} is reference temperature, β_{ref} is a material constant.

There is an inherent thermodynamic contradiction in attempting to simultaneously optimise the electrical and thermal exergies for a PV module. This should be taken into consideration during design of PV and PV/T systems. Details of the simulation results at constant temperature (298.15 K) as solar radiation varies are presented in Table 6.3.

Table 6.3: Solar radiation effects on the PV module performance [91].

Solar radiation (W/m^2)	100	200	400	600	800	1000
Solar exergy inflow (J/s)	0.1494	0.2988	0.5976	0.8964	1.1952	1.4940
Electrical exergy flow (J/s)	2.9729	6.8206	15.5166	24.9146	34.7468	44.9468
Thermal exergy flow (J/s)	-2.8235	-6.5218	-14.9190	-24.0182	-33.5516	-43.4528
Photocurrent (A)	0.3000	0.6000	1.2000	1.8000	2.4000	3.0000
Voltage (V)	9.9097	11.3677	12.9305	13.8414	14.4778	14.9823

From Figure 6.7, the electrical energy and exergy efficiencies of the PV module (see Eq. (6.16) and (6.17), respectively) were initially similar at lower temperature but the difference widened as temperature increased. This shows that the electrical exergy ($\dot{W}_{elect}$) component of the proposed model could represent electrical energy if the heat generated is not considered. For PV/T systems, the effect of extraction of $\dot{Q}_{loss}$ at the reference temperature needs to be considered. The electrical energy output from a PV/T module would be higher than that of a PV module because of the cooling effect of $\dot{Q}_{loss}$ extraction from the PV/T module by the working fluid which enables power generation to occur at a higher insolation without incremental heat generation. Since there is potential utilisation of $\dot{Q}_{loss}$ for useful thermal work in PV/T modules, it can be inferred that PV/T-led systems would be more efficient than PV-led systems as shown in Chapter 4 in which PV/T-Battery-PEME-PEMFC system was more efficient than PV-Battery-PEME-PEMFC system and PV/T-Battery system was more efficient than PV-Battery system.

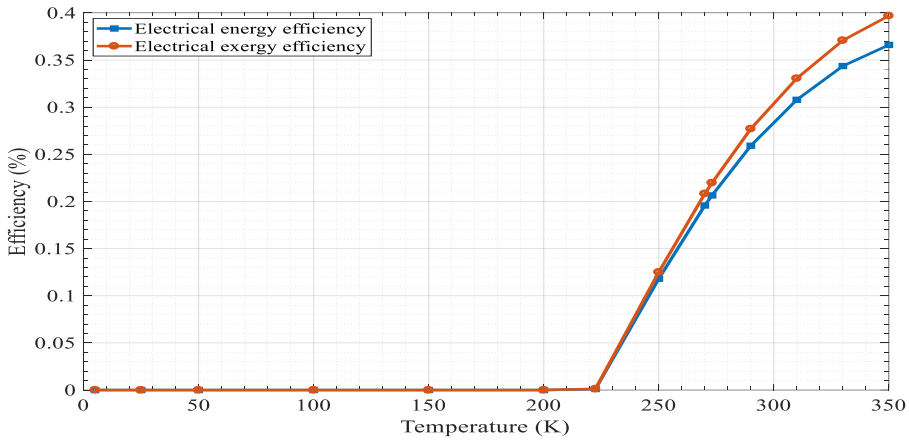

Figure 6.7: Temperature variation effects on energy and exergy efficiencies of the PV module [91].

6.3.3 Comparison Between Gibbs Free Energy Model and the Proposed Model

This section compares the proposed photovoltaic-thermal model with the Gibbs free energy equation. Gibbs free energy is an important equation in thermodynamics because it determines the spontaneity of thermodynamic processes [146]. Table 6.4 gives more comparisons between the two equations. Based on an analogous comparison of $\Delta G = \Delta H - T\Delta S$ and $\dot{Q}_{loss} = \dot{E}x_{Solar} - \dot{W}_{elect}$, the Gibbs free energy (which indicates the maximum non-expansion work that can be extracted from a closed thermodynamic system) is equivalent to the thermal losses from the PV (which also indicates the maximum thermal work that can be converted to power or thermal work). The solar exergy input which is equivalent to the enthalpy in Gibbs model has two components (light and heat). The

wavelength of the light spectrum needs to be within the bandgap energy of the PV cells for an effective generation. The thermal content of the solar energy contributes to raise the PV cells to a critical temperature where an absorption of photons can easily excite the electrons and holes in the semiconductor. However, excessive thermal energy exposure could increase the kinetic energy of the electrons and holes thereby reducing the power output due to entropic thermalisation of carriers that would been excited above/below the bandgap.

Table 6.4: Comparison between Gibbs free energy and the photovoltaic-thermal equations [91].

Gibbs free energy equation	**Photovoltaic-thermal equation**
Similarities	
For exothermic processes, the same amount of energy is lost to the environment.	Heat generated in the PV module is lost to the environment for the PV module and transferred to the fluid in the case of PV/T system. During power generation, PV process appears to be exothermic.
Enthalpy of the system decreases for spontaneous system at constant entropy.	Input solar exergy into the PV module is transformed into electrical energy even at constant entropy. Only solar exergy that finally reach the solar cell contribute to the enthalpy of the PV module. Solar radiation affects the generation and recombination of carriers. If entropy is the disorderliness of a system, then the degradation in the electrical exergy, propagated by temperature, is entropic in nature.
Temperature propagates entropy in thermodynamic process.	Temperature propagates deterioration of electrical exergy of a PV because of the negative temperature coefficient of a PV module.
Gibbs free energy is applied to chemical systems as in electrochemical fuel cell [134])	The proposed thermophotovoltaic model leads to electrical energy generation; although in a photovoltaic process.
Differences	
Applies to pressure-volume-temperature system	Applies to a quantum-mechanical process involving photon and solid-state physics of solar cells (semiconductors).
It is widely applied to thermodynamic processes	This is limited to the thermodynamics of PV modules.

Plank's equation connects bandgap energy (E_g) and wavelength of light spectrum, $E_g = hv = hc/\lambda$ (where h is Plank constant, c is speed of light and λ is wavelength). E_g of the PV cell is usually measured at AM1.5D solar spectrum. The thermal component of solar energy, based on Stefan law of radiative energy of a black body emitter, is $E = \delta T^4$, (where δ is Stefan-Boltzmann constant and T is temperature of the sun). Stefan equation can also be derived from Plank equation for spectral energy density. Comparatively, $\dot{E}x_{Solar}$ term indicates the enthalpy of solar radiation in relation to its spectral energy density that needs to match the PV material property (particularly bandgap energy).

The $T\Delta S$ term is analogous to the power output term (P = IV) in the PV module. T is analogous to I (or photocurrent) and S is analogous to V (or potential difference set up due to the flow of photocurrent). Thus, entropy generation reduces the value of P by degradation of potential difference setup by the flow of carriers. Increasing I (which also depends on $\dot{E}x_{Solar}$) implies increasing the value of P. In Gibbs model, if $\Delta G = 0$, then $\Delta H = -T\Delta S$.

Similarly, if $\dot{Q}_{loss} = 0$, then $\dot{Ex}_{Solar} = \dot{W}_{elect}$. This implies that inhibiting thermal losses from a PV module would cause nearly all the solar exergy received by the PV module to be converted into power; assuming that there is a perfect match between solar spectrum and the PV cell bandgap, and that the generation and recombination of carriers result in all the electrons flowing reversibly (without thermalisation) around the circuit. This is highly idealistic and would run contrary to the second law of thermodynamics that predict that entropy generation is propagated as a system moves from one state to another.

From Figure 6.5, solar exergy of 1.52 J s^{-1} was enough to generate the least thermal exergy based on the conversion efficiency of the PV module. Controlling solar exergy inflow into the PV module can be achieved with photosensitive surface. Optimal control of solar exergy inflow would ensure that excess solar exergy input is not transmitted since excess solar exergy would lead to heat generation which would ultimately degrade the PV conversion efficiency. If optimal heat dissipation and effective optical surface control of the PV are addressed, the performance of a PV module might be improved.

Controlling the heat dissipation through natural convection depends on the thermal design of a PV module. A PV module compose of the top glass cover, solar cells, bus bars, ethylvinylacetate and tedlar back sheet [231] and each of these materials has different heat capacities. Further analysis of the materials to substitute those that retains heat with those materials that can facilitate fast thermal dissipations could improve cooling and ultimately the efficiency of the PV module. Wind speed around the module [251] can also influence thermal dissipation rate through natural convective heat transfer.

6.4 Summary

In this chapter, a CBM approach was applied to integrate the solar, electrical, and thermal exergies of photovoltaic module to create a novel photovoltaic-thermal model. Notably, from the results, the temperature of the solar cell needs to exceed a critical temperature (in this case 223.5 K) before it can generate electrical energy. However, extremely high operating temperatures degraded the open circuit voltage thereby reducing the conversion efficiency of a PV module. An improvement of 51% for a 45 W PV module used in this study could be realised if the waste heat generated was utilised for useful thermal work. Overall, the findings contribute towards a better understanding of the thermodynamics of photovoltaic power generation and could be useful in material and design optimisation of photovoltaic and photovoltaic-thermal components.

Chapter 7: Radiation-Thermodynamic Modelling and Simulating of a Thermophotovoltaic System

In Chapter 6, the CBM approach facilitated a creation of a photovoltaic-thermal model based on solar radiation. In this chapter, CBM approach was used to create a novel thermophotovoltaic model to realise Research Objective 4. The difference between the photovoltaic-thermal model and thermophotovoltaic model is that the former uses solar radiation as the source of photon energy whereas the later can use artificial radiative energy from a radiator as photon source. The similarity between photovoltaic-thermal system and thermophotovoltaic system is that both involve the use of radiative energy to cause the photovoltaic process in PV cells.

Thermophotovoltaics can be applied in military hardware, boats, vehicles, recovery of waste heat and so on [252]. TPV systems have lightweight, emit zero pollution, does not depend on solar radiation, have high gravimetric/volumetric power density output, have fuel versatility with low maintenance cost, in addition to being portable, silent during operation, long-lasting during operation; while some can use high temperature sources [253,254]. Currently, research and development of TPV systems [255] is increasing although the thermophotovoltaic process was first suggested in 1950s [254]. A review by Coutts [253] showed that TPV systems could play a role in clean electricity generation. Bauer [252] explored the principles and concepts of TPV systems design. TPV systems have low conversion efficiency [256]. A prototype by Paul Scherrer Institute has a diameter of 17 cm and produces 56 W. The prototype by JX Crystals (Midnight sun®) generated 500 W-h/day, which is about the daily output of a 200 W PV module [257].

Some studies have investigated the design, material characterisation and theoretical efficiency of TPV systems through model-based or/and experimental studies. As examples, Harder and Wurfel [258] predicted the theoretical limit of a TPV module to be up to 60%, and Ferrari et al [259] used an analytical approach to estimate the efficiencies of different components of a TPV system. A study of the use of high temperature source for a TPV and thermal energy storage was done by Seyf and Henry [260]. Butcher et al [261] studied a TPV system which generates heat with oil. They observed that an increase in the burner firing rate resulted in an increase in the output power, although the PV cells' temperature increased over time. Lu et al [106] demonstrated the possibility of generating power with TPV systems

at temperatures below 1000 K. Gentillon et al [262] generated 1 W of electrical power from 24 GaSb PV cells with an erbia coated emitter. As research efforts on TPV applications intensify, there is a need to understand its energy conversion processes to improve the overall performance through appropriate material selection, design optimisation, and optimal operating conditions. Since the surface properties of the sun differ from the artificial radiators, the overarching aim of the study is to integrate radiative heat transfer, power density output and thermal losses in within the core of a TPV system to facilitate new physical insights into effects of artificial radiation on the photovoltaic process.

As a heat engine, radiative heat flux from the hot reservoir will interact with the PV cells at the cold reservoir to generate power. Here, the laws of thermodynamics, radiation, and photovoltaics were applied to create the proposed thermophotovoltaic model. Contextually, the TPV core under consideration is between the radiator and the PV cells.

To achieve the aim of this study, the specific objectives are to:

1. Derive a thermophotovoltaic model for a TPV system.
2. Study how changes in the temperatures of the radiator and the PV cells affect TPV generation.
3. Study how efficiency varies with the radiator and TPV cells temperatures.
4. Evaluate the interrelationships among TPV generation variables.

This study contributes to deeper understanding of the thermodynamics of thermophotovoltaic power generation. The proposed radiation-thermodynamic model for the core of TPV systems is new. TPV systems design and development can be improved using modelling and experiments. Moreover, sub-models of the proposed TPV model can be expanded towards an improvement in the performance of TPV system and cogeneration systems. Lastly, the TPV model can be used as an energy conservative model in software.

7.1 Description of Thermophotovoltaic System Description and Operation

TPV systems may compose of a heat source, a radiator/emitter, PV cells, reflector for recovering photons below/above bandgap, spectral filters, a heat sink, and a DC power conditioning system [252,253]. A TPV system may be a near-field TPV [263], a nano-gap TPV [264] or a micro-TPV [252]. This categorisation is based on the core distance of the TPV . The micro-TPV type studied here uses dielectric medium in the core of the system.

PV cells convert the radiative energy within its bandgap energy to electrical energy in accordance with the photovoltaic process (see Chapters 5 and 6). Radiators can be of silicon carbide, micro-structure tungsten or welsbach mantle [254]. In TPV system, selective filter and a reflector can be used to recirculate incident photons with energy below or above the bandgap energy. Recirculation of photon could be done using dielectric filters, plasma filters (a transparent conducting oxide), resonant antennae arrays, or back-surface reflectors [257]. Silicon, Gallium antimonide, copper indium gallium diselenide, Indium gallium arsenide, and Germanium can be applied as TPV cells [257].

TPV systems can generate heat from sources such as chemical, waste heat, solar thermal sources, nuclear, heat from biomass plants, and so on [265]. From Figure 7.1, radiative heat transfer ($\dot{H}_{rad}$) from the radiator, electrical power ($\dot{P}_{elect}$) and the thermal losses ($\dot{Q}_{losses}$) are shown. Heat losses to the sink can be recovered for additional work such as heating of water or air. The TPV model used a refractive index between 1.0 and 1.5 to incorporate the effect of a dielectric medium [252].

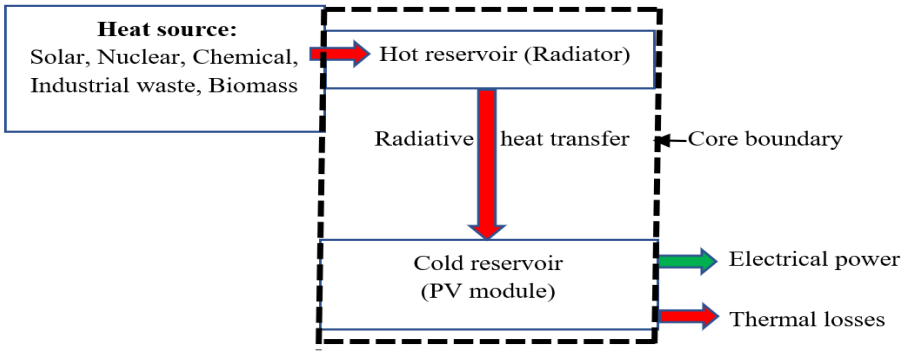

Figure 7.1: Flow of energy across the core of a TPV system [266].

7.2 Research Method and Approach

The CBM approach presented in Chapter 5 was used to create a SoTE representing a TPV model. The components of the radiative heat transfer, power density output and thermal losses were integrated. The model was validated with experimental data from a peer-reviewed literature. The simulation was performed using virtual experimentation approach. Firstly, the temperature of the radiator temperature varied from 500 to 6000 K whilst maintaining the temperature of the PV cells at 300, 400 and 500 K. Values for the photocurrent, maximum voltage, power density output and thermal losses were extracted from the simulation after the convergence of 700 iterations. The interrelationships were

further investigated. Next, the temperature of the PV cells was varied from 300 to 700 K whilst the temperature of the radiator was at 1000, 1800 and 2500 K. The photocurrent, maximum voltage, and power density output were extracted, and their interrelationships were studied.

7.3 Modelling of the Core of a TPV System

Under a steady state, the following assumptions were made: thermal losses from the core equals the difference between the radiative heat flux and power density output; the radiator and emitter were in thermal equilibrium; thermodynamics and radiations laws were obeyed [146]; and thermal losses exit to the heat sink [267].

In accordance with the First law of thermodynamics, $\dot{H}_{rad}$ is conservatively converted into $\dot{P}_{elect}$ and $\dot{Q}_{losses}$ based on Eq. (7.1). Classical thermodynamic approach was used in lieu of statistical or quantum thermodynamics approaches to avoid accounting for the behaviours of each photon, electron, and the microstructure of the materials. Classical thermodynamics remains an acceptable approach in modern engineering science because it can provide a global insight into the thermodynamics of systems [268].

$$\dot{Q}_{losses} = \dot{H}_{rad} - \dot{P}_{elect} \quad (7.1)$$

Stefan-Boltzmann's law, expressed in Eq. (7.2) [253], shows the total energy radiated (E_{rad}) by a radiator with a temperature (T_{rad}), emissivity(ε), and area (A_R).

$$E_{rad} = \varepsilon\sigma A_R T_{rad}^4 \quad (7.2)$$

where σ is the Stefan-Boltzmann's constant (5.7 x 10^{-8} W m^{-2} K^{-4}).

The radiative heat transfer for parallel orientation of the radiator and the TPV cells (also referred to as PV cells here) was calculated using Eq. (7.3) [253]. *n* is the refractive index of the medium in the core of the system.

$$\dot{H}_{rad} = n^2 \varepsilon\sigma F A_R (T_{rad}^4 - T_{pv}^4) \quad (7.3)$$

where F is the view factor relating to orientation and T_{pv} is the temperature of the cells.

A TPV cell is a p-n junction semiconductor which can generate electron-hole pairs when excited by radiative energy [263,264]. $\dot{P}_{elect}$ equals the product of current output (I_{pv}) and the voltage (V_{pv}) across the terminals of the TPV system as in Eq. (7.4).

$$\dot{P}_{elect} = I_{pv} \times V_{pv} \quad (7.4)$$

photocurrent (I_{ph}) induced by radiative heat flux is analogous to the photocurrent induced by the solar radiation in solar PV system. The photocurrent and the reference radiative heat flux are analogous to the I_{ph} in an SPV system by Bellia et al [93] as expressed by Eq. (7.5).

$$I_{ph} = (I_{sc} + K_i (T_{pv} - T_{ref})) \times \frac{H_{rad}}{H_{ref}} \quad (7.5)$$

where I_{sc} is the short circuit current, K_i is the thermal coefficient at short circuit current, T_{ref} is the reference temperature (298.15 K), and H_{ref} is the reference radiative heat flux (1000 W m^{-2}).

TPV array with TPV modules connected in parallel (N_p) has high output current. TPV cells in each TPV module are connected in series (N_s) to increase the output voltage. Thus, Eq. (7.6) can be used to compute I_{pv} from the TPV system. Substituting Eq. (7.6) into (7.4); so that its resultant equation is substituted into Eq. (7.1) with Eq. (7.3), yields Eq. (7.8).

$$I_{pv} = I_{ph}N_p - I_sN_p \left[\exp\left(\frac{qV_{pv}}{AN_skT_{pv}}\right) - 1\right] \quad (7.6)$$

Where the saturation current is the same with the expressed as Eq. (7.7) [94,95].

$$I_s = I_{s,ref}\left[\frac{T_{cell}}{T_{ref}}\right]^3 \exp\left[\frac{1}{k}\left(\frac{E_g}{T_{ref}} - \frac{E_g}{T_{cell}}\right)\right] \quad (7.7)$$

$$\dot{Q}_{losses} = \left[n^2\varepsilon\sigma FA_R(T_{rad}^4 - T_{pv}^4)\right] - \left(I_{ph}N_p - I_sN_p\left[\exp\left(\frac{qV_{pv}}{AN_skT_{pv}}\right) - 1\right]\right) \times V_{pv} \quad (7.8)$$

Whereas Eq. (7.8) is the simplified version of the CB model of the TPV model and was implemented as a SoTE, an expanded equation can be realised by substituting Eqs. (7.5) and (7.7) into Eq. (7.8) to realise Eq. (7.9).

$$\dot{Q}_{loss} = \left[n^2\varepsilon\sigma FA_R(T_{rad}^4 - T_{pv}^4)\right] - \left(N_p\left[I_{sc} + K_i(T_{pv} - T_{ref})) \times \frac{H_{rad}}{H_{ref}}\right] - \left[I_{s,ref}\left[\frac{T_{cell}}{T_{ref}}\right]^3 \exp\left[\frac{1}{k}\left(\frac{E_g}{T_{ref}} - \frac{E_g}{T_{cell}}\right)\right]\right] \times N_p\left[\exp\left(\frac{qV_{pv}}{AN_skT}\right) - 1\right]\right) \times V_{pv} \quad (7.9)$$

The temperature of the two reservoirs of a Carnot engine determine the thermodynamic efficiency of a TPV system [146]. Thus, Eq. (7.10) can be used to calculate the thermal efficiency of a TPV system using the temperatures of the reservoirs [253].

$$\eta_{Th} = 1 - \frac{T_{PV}}{T_{rad}} \quad (7.10)$$

7.4 Results and Discussion

This section presents the validation of the TPV model, and a discussion of the results generated from the virtual experimentation simulations. The extracted variables were plotted to facilitate the analyses of their interrelationships. The physical insights gained were used to predict the possible overall power generation characteristics of a TPV system.

7.4.1 Validation of the TPV Model

The parameters of the TPV cells can be stated at STC [269]. Table 7.1 presents the design and operational information on the TPV system used for this study. Data were sourced from peer-reviewed literature.

Photovoltaic modelling and simulation code (PVMSIC) used in Chapter 5 and 6 facilitated the CBM process. The PVMSIC provided the platform to utilise some of the features of the photovoltaic-thermal model to create the TPV model. Initially, the proposed TPV model was validated with two tests. Firstly, the effect of $\dot{H}_{rad}$ in Eq. (7.5) on the proposed CB model was validated. The aim was to confirm that the proposed TPV model conformed with the extant PV cell physics.

Table 7.1: Parameters and operating conditions of a TPV module [266]**.**

Parameters	Values	Units	References
Temperature of the radiator (T_R)	1800	K	Bauer [254]
Temperature of the TPV cells (T_{pv})	300	K	Bauer [254]
Maximum Power Point (at $T_R = 1800$ K, $T_{PV} = 300$ K)	116	W	PVMIC [209]
Reference temperature (T_{ref})	298.15	K	Bauer [254]
Refractive index (n)	1.5		Bauer [254]
View factor (parallel configuration) (F)	1		Bauer [254]
Reference radiative heat transfer (H_{ref})	1000	W m^{-2}	PVMIC [209]
Emissivity of the radiator (ε_R)	1		Bauer [254]
Short circuit current of TPV cells (I_{sc})	2.68	A	PVMIC [209]
Saturation current of the TPV cells (I_s)	5.39×10^{-5}	A	Meyer [224]
Maximum Power Point (P_{mp}) (at STC)	80	Watts	PVMIC [209]
Maximum Voltage Point(V_{mp})	35	V	PVMIC [209]
Ideality factor (A)	2.85		PVMIC [209]
Band gap (Silicon) at 0 K	1.17	eV	Varshni [225]
Number of cells in series (N_s)	72		PVMIC [209]
Number of cells in parallel (N_p)	1		PVMIC [209]
Boltzmann constant (k)	1.38×10^{-23}	J K^{-1}	Coutts [253]
Electron Charge (q)	1.602×10^{-19}	C	Coutts [253]
Stefan-Boltzmann constant (σ)	5.67×10^{-8}	W m^{-2} K^{-4}	Coutts [253]
Number of simulation iterations	700		PVMIC [209]

A silicon-based 80 W PV module was created in the PVMSIC and validated at STC. The TPV module used PV cells parameters. Simulation was performed at a radiator and TPV cells temperatures of 1800 K and 300 K, respectively. Figure 7.2 shows that the open circuit voltage for TPV was greater than the open circuit voltage of the SPV at STC. Again, the MPP of the SPV and that of the TPV module were 80 W and 116 W, respectively. This implies about 45% improvement in power density output PV cell was used as TPV cell.

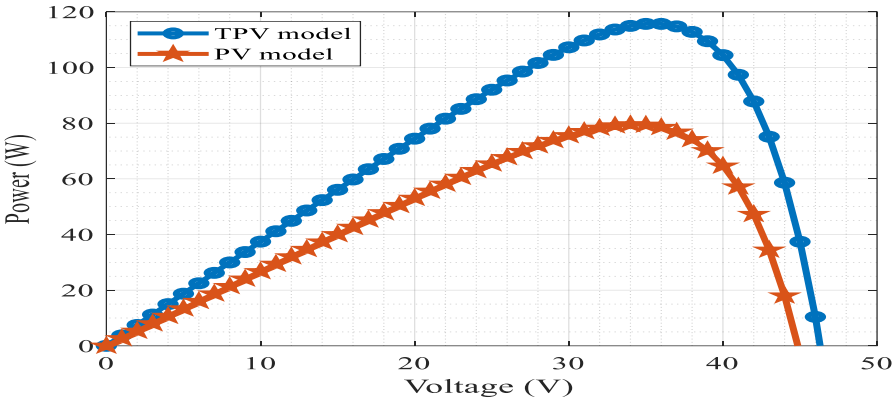

Figure 7.2: Power – voltage curves for SPV and TPV CB models [266].

The second validation test attempted to use the TPV model to predict the parameters of a GaSb-based TPV module, with a bandgap of 1.441 eV at 300 K, reported in Coutts [253]. I_{sc} (13.18 A), MPP (400 W), V_{oc} (44.2 V), number of cells (48) and the temperature of the radiator (1700 K) were provided. From Figure 7.3, the CB model predicted 399.13 W and 45.84 V, respectively in comparison with the 400 W and OCV of 44.2 V (Coutts [253]). The CB model predicted the MPP and OCV at 0.87 W and 1.64 V deviations, respectively, which is acceptable for this type of study.

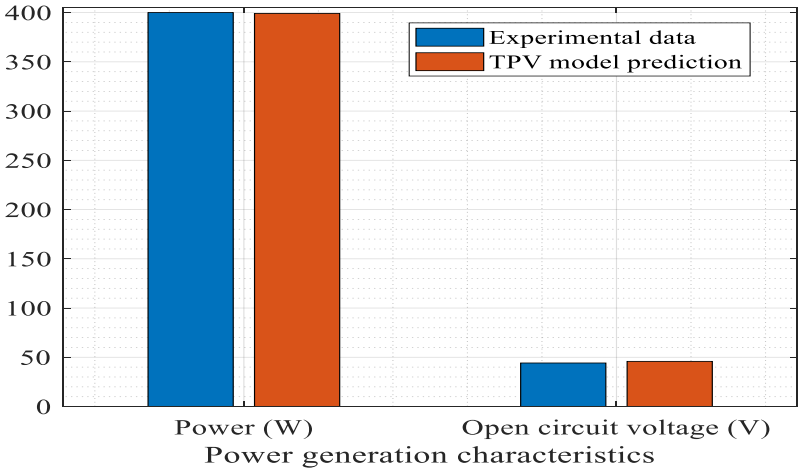

Figure 7.3: Predicted and experimental power and open circuit voltage [266].

7.4.2 Radiator Temperature Variation Effects on the Power Density Output

Figure 7.4 (a) and (b) presents the effects of increasing the radiator temperature from 500 to 6000 K while maintaining the temperature of the TPV cells at 300, 400 and 500 K, respectively. Radiant energy that initiates the photovoltaic process depends on temperature [253]. Again, the temperature of the radiator varies with the radiative heat flux to the fourth power as based on Stefan-Boltzmann law expressed in Eq. (7.2). Based on the principles of thermophotovoltaic process, the power density output increased as radiator temperature increased. Inferentially, photocurrent varied with power density output as the radiator temperature increased whilst the TPV cells were kept at 300 K.

Also, the photocurrent increased sub-linearly with the temperature of the radiator as shown in Figure 7.4 (a). Since Si-based TPV require higher radiator temperature compared to GaSb-based TPV [270], the implication for the design process is that the radiator temperature needs to be matched with the optimal cell temperature. This is in tandem with studies that indicated that the performance of the TPV system depends on temperature [252,253]. The power density output was higher when the PV cells was at 500 K than when it was at 300 K. Consequently, high temperature cells are needed for TPV applications operating at high temperature. The core of TPV exposes the PV cells to higher temperature compared to the level of temperature exposure of solar PV cells. From the findings in Chapters 5 and 6, high temperature TPV cells may be needed to forestall the degradation of the open circuit voltage, which exhibits high sensitivity to temperature [209].

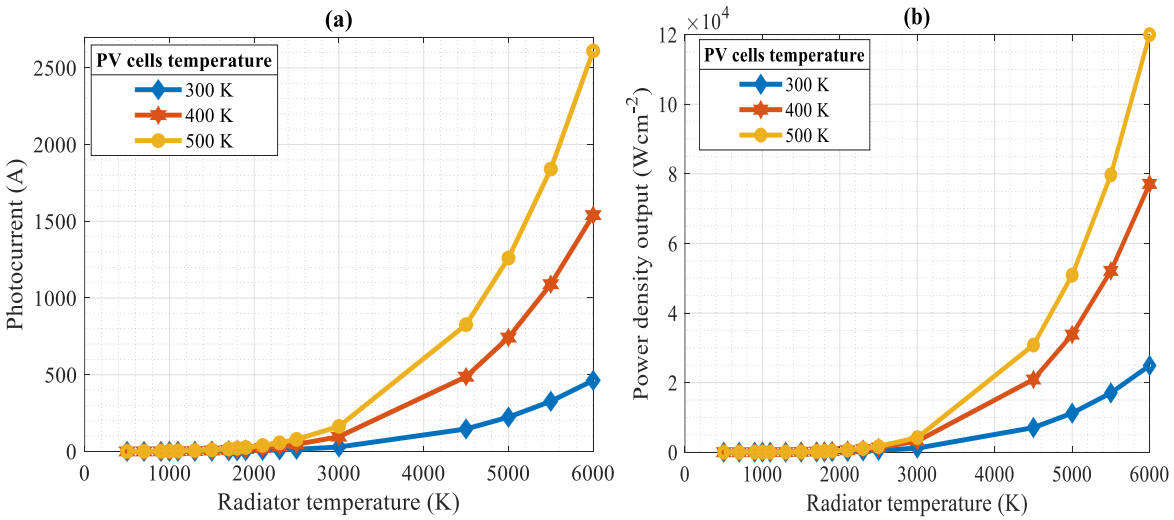

Figure 7.4: Plot of radiator temperature and (a) photocurrent (b) power density output [266].

In practice, high temperature could induce thermal stresses in the parts with low heat capacities. TPV systems operating at significantly high temperature such as that of the sun

(i.e. 6000 K) may face material constraints. Thus, applications of TPV system for space missions near the sun or satellites requires optimal thermal designs. Datas and Marfi [271] explored the potential applications of TPV systems in space technologies including those near the sun.

From Figure 7.5 (a), photocurrent increased with the radiative heat flux. This result agrees with the photovoltaic effect in which photons create electron-hole (E-H) pairs. E-H pairs generated varies with the energy flux on the PV cells [209]. Based on Figures 7.4(a), 7.4(b), 7.5(a) and 7.5(b), the voltage of the TPV system appeared to be sensitive and exhibited a non-linear variation. This result agrees with that of Jiang et al [272] that the voltage of a PV decreases with an increase in the ambient temperature. The sub-linearity of the power density output when the radiator temperature increased is based on Eq. (7.8). Butcher et al [261] observed that the power output density of an oil-fired TPV system increased with the burner firing rate, which influences the radiative heat transfer.

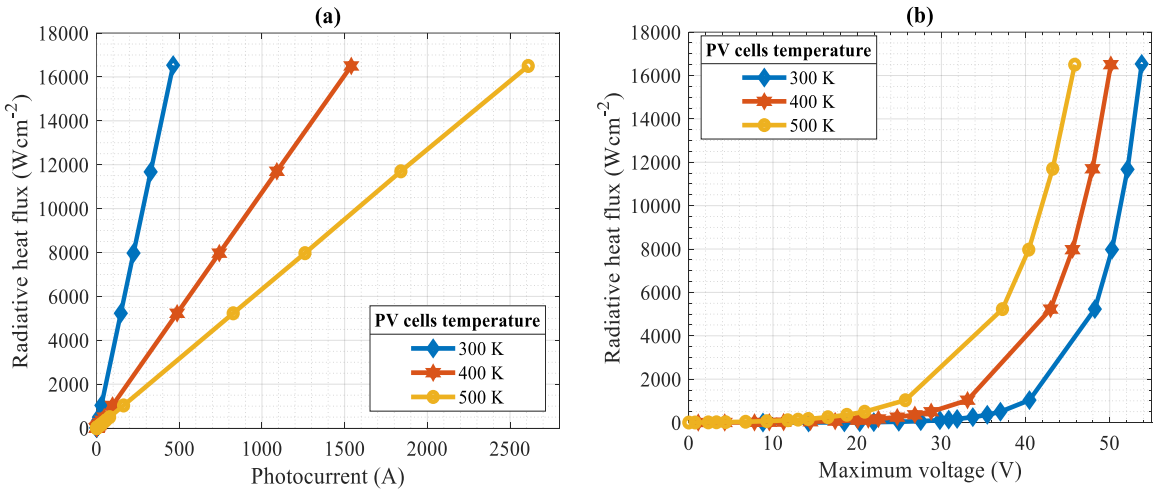

Figure 7.5: Plots between radiative heat flux and (a) photocurrent (b) maximum voltage [266].

Figure 7.6 shows how power density output varies with the thermal losses flux. The power density output as well as the thermal losses flux increased as the PV cells temperature increased which agrees with the 1st Law of thermodynamics (Eq. (7.1)). The use of higher temperature heat source results in high thermal losses as shown in Figure 7.6. Consequently, co-generation design of TPV system must consider the mechanisms for dissipating $\dot{Q}_{losses}$ into the working fluid so that the temperature of the core can be operated below a critical TPV cells temperature above which the open circuit voltage will degrade. Furthermore, the spectral filter and reflector can be used to reduce the $\dot{Q}_{losses}$ exiting into the heat sink.

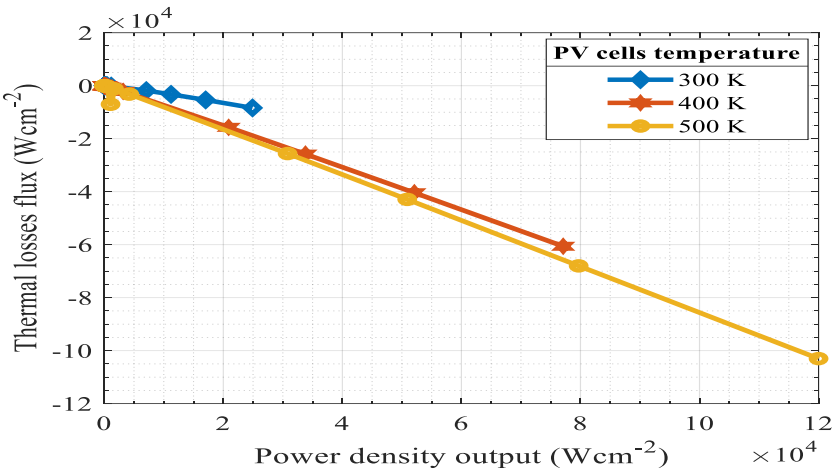

Figure 7.6: Plot of power density output versus thermal heat flux [266].

7.4.3 TPV Cells Temperature Change Effect on Power Generation

Simulation of the TPV model when the radiator was at 1000, 1800 and 2500 K and the PV cells temperature was varied from 300 to 700 K was investigated. From Figure 7.7, photocurrent varied linearly with PV cells temperature when the radiator temperature was constant. Together with Figure 7.5 (a), photocurrent appear to have a linear relationship with radiative heat flux, and this suggests that photocurrent generation increased when the radiator and PV cells temperatures increased.

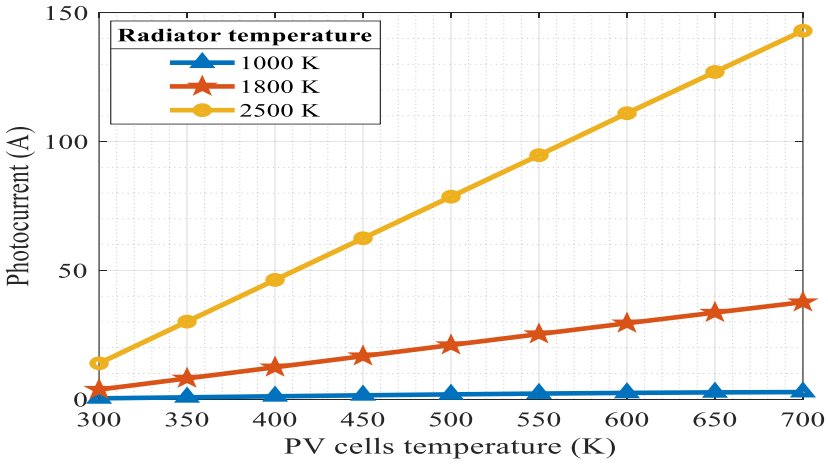

Figure 7.7: Plot of PV cells temperature and photocurrent [266].

Based on the negative linear relationship of photocurrent and temperature of the PV cells, Figure 7.8 showed that the voltage of the TPV system decreased as the PV cells temperature increased. Fundamental physics of PV cells indicates that electron generation in the p-n junction varies with the photon energy level [228]. Thus, the radiative energy increased with a radiator temperature increase. So, photocurrent increased as the radiator temperature increased from 1000 to 2500 K. Howbeit, the voltage output degraded. Nonetheless, the

results conform with current knowledge of PV cells physics which is that higher temperatures of the PV cells degrade the open circuit voltage and ultimately the power output of the PV module [273].

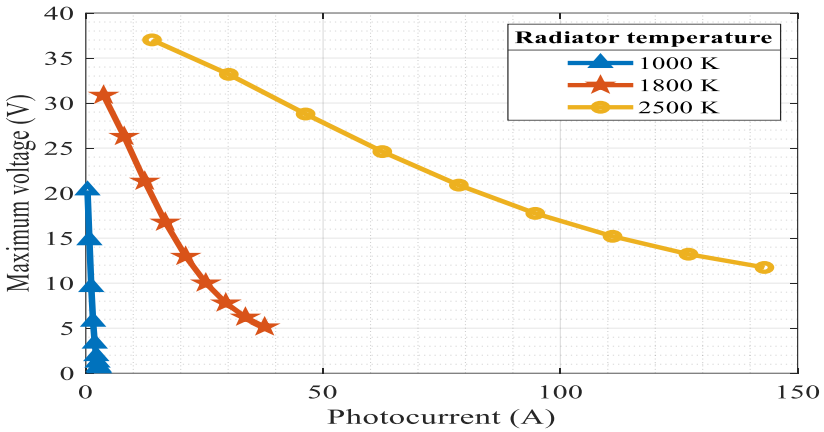

Figure 7.8: Plot of photocurrent and maximum voltage as the temperature of the radiator was constant whilst the PV cells temperature changed [266]**.**

Furthermore, the voltage decreased when the radiator temperature was at 1000, 1800 or 2500 K whilst the PV cells temperature increased as in Figure 7.9 (a). From Figure 7.9 (b)**,** at 1800 K, the power density output increased until 450 K before it dramatically degraded. This agreed with the findings of Durisch et al [269] in which MPP of a TPV system decreased from 20.2 W to 15.6 W when temperature of the TPV cells increased from 25 to 55 ˚C. This suggests that effective thermal management such as cooling is required to maintain optimal TPV cells temperature for high temperature radiators. The stability of power density output in Figure 7.9 (b) was higher at 1800 K compared to when it was at 2500 K, considering the shape of the curve. Thus, operating at 1800 K gave a better stability and factor of safety considering the bell shape or normal distribution of the power density output.

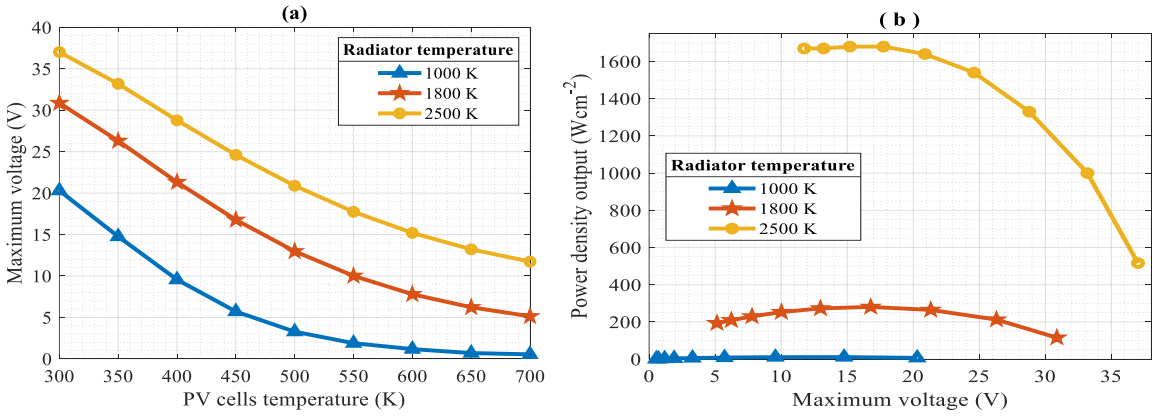

Figure 7.9: Plot of maximum voltage and (a) PV cells temperature (b) power density outputs [266]**.**

7.4.4 Thermal Efficiency of a TPV System

Based on Eq. (7.10), and from Figure 7.10 (a), thermal efficiency of a TPV system increased when the PV cells temperature reduced. Again, thermal efficiency was higher when the PV cells temperature was lower whilst maintaining the radiator temperature at 1800 K. From Figure 7.10 (b), the thermal efficiency increased when the radiator temperature increased if the PV cells temperature was at 300 K. Juxtaposing the two results, higher efficiency requires adequate matching between the radiator and TPV cells temperatures. In practical terms, optimal design should seek the critical radiator and PV cells temperatures beyond which the open circuit voltage would degrade. Moreover, TPV system has additional complexity as a heat engine because altering the temperature of the reservoirs could affect the open circuit voltage of the TPV cells.

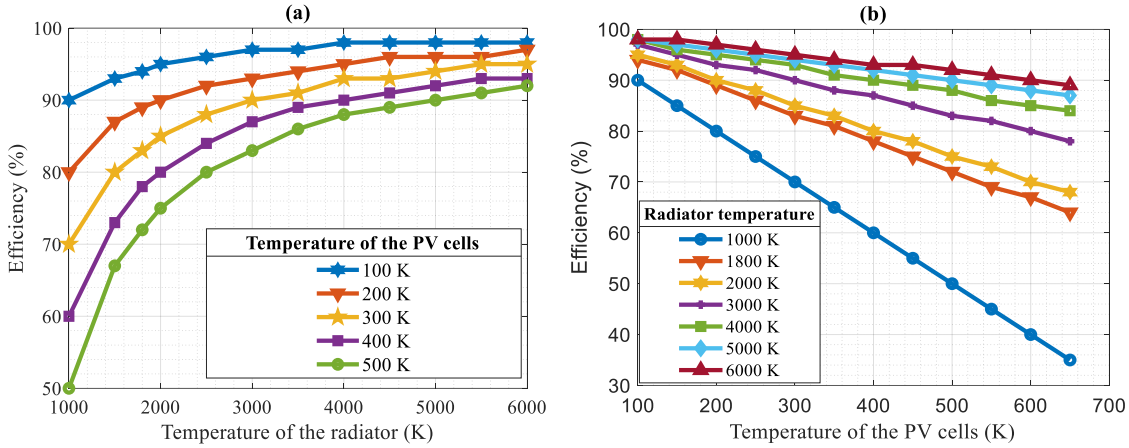

Figure 7.10: Thermal energy efficiency of a TPV system (a) Effects of radiator temperature, (b) Effects the PV cells temperature [266]**.**

7.5. Summary

This chapter proposes a novel thermophotovoltaic model for modelling and simulating a TPV system using a combined CBM and virtual experimentation approaches. When the radiator and PV cells temperatures were at 1800 K and 300 K respectively, the TPV model predicted the power density output, thermal losses, and maximum voltage of the TPV system as 115.68 W cm^{-2}, 18.14 W cm^{-2} and 36 V, respectively. The 80 W TPV module used in this study showed a potential 45% improvement in power generation capacity compared to applying it in a solar PV at STC. Within the limits of the assumptions in this study, the proposed TPV model did not deviate from the extant laws and theories. It is, therefore recommended to scientists and engineers for consideration in model-based and experimental studies of TPV systems.

Chapter 8: Determination of an Optimal Location for a LSPPG using Thermodynamics Approach

This Chapter focuses on the use of thermodynamics approach to determine an optimal location for a large-scale photovoltaic power generation (LSPPG) to realise Research Objective 5. The performance of an optimised PV-based energy system such as the IPVFC system still depends on the location of installation. There is an assumption that commercial PV modules rated under laboratory environment will generate power at the same efficiency regardless of the location of deployment. This study interrogates this assumption using a thermodynamic approach and virtual experimentation approach because solar radiation and temperature fluctuates with seasons and time of the day and affect power generation of PV systems [190,198,220,230]. Intermittency of solar resources poses challenge for designing, sizing, optimising, and operating solar-based technologies such as the IPVFC system.

STC measurements of PV modules based on the International Electrochemical Commission IEC 61215 [239] excludes actual field data in its procedure and cannot show a comparative performance of a PV system at different locations across the globe. It may be convenient to rate PV modules at STC (1000 W m^{-2} , 25 $^{\circ}$C, and AM1.5 [274] in order to compare the efficiency of different solar cells. However, in a real-world application, Figure 8.1 shows that global horizontal irradiation for Nigeria is not constant across the states. Solar energy harvesting is promising in Nigeria [275–278]. A study of over 26 years for 25 locations from the 5 climatic zones in Nigeria indicated that the range of the average daily solar irradiation is 15.01 to 25.01 MJ m^{-2} day^{-1} [279]. Nigeria has a land mass of 923,768 km^2 and it is located in the west coast of Africa between latitudes $4^{o}16'$N and $13^{o}53'$N and longitudes $2^{o}40'$E and $14^{o}41'$ E [280]. Bridge et al [281] suggested that low carbon energy transition policy should be recast as a geographical process instead of viewing it as a process that affect a geography. Thus, improved renewable power generation in Nigeria depends on the processes of their utilisation.

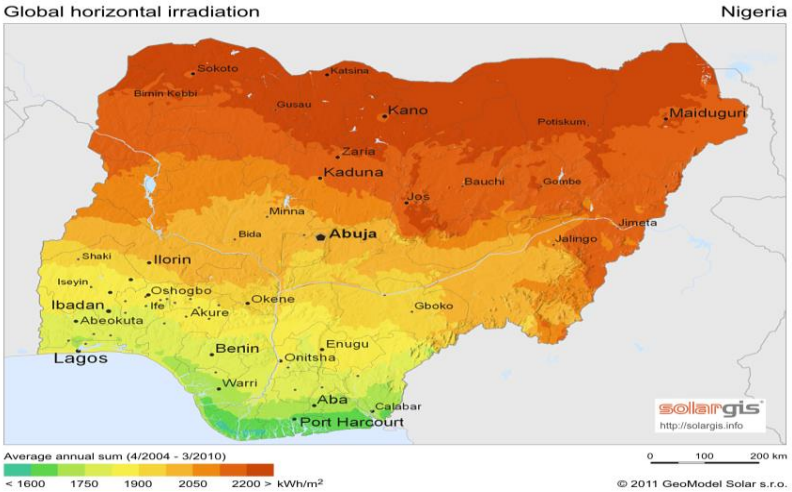

Figure 8.1: The global horizontal irradiation map of Nigeria [282]

Because solar radiation and temperature fluctuate, the current laboratory based STC specifications need to be modified for strategic decisions involving optimal locations for LSPPG in a real-world operating environment. IEC 61853 ("Photovoltaic Module Performance Testing and Energy Rating") advocates for explicit power rating of PV modules [274]. Again, reproducible, operational, probabilistic or physically-based, ensemble, and skill (ROPES) [283] describes future solar forecasting studies that considers actual data.

Here, the overall aim of this chapter is to develop a novel approach for choosing a location from multiple locations to install an LSPPG based on actual data, STC specification and the laws of thermodynamics. The following research questions have been posed for investigation:

1. Do the stochastic distributions of solar radiation and temperature affect the generation of an LSPPG at different locations?
2. Are there significant differences between mean photovoltaic power generations at six spatially distributed locations in Nigeria?
3. Can thermodynamic efficiency indices (TEI) unambiguously rank generation potential of LSPPG using solar radiation and temperature data?
4. Can the thermo-economic analysis of an LSPPG be facilitated by TEI?

These research questions connect with the four research objectives in this chapter. On the optimal location question for an LSPPG, the specific objectives are to:

1. Normalise the solar radiation and temperature data for the locations to generate statistical mean value (SMV) for TEI analysis.
2. Formulate thermodynamic efficiency indices for strategic decision-making.

3. Link TEI with return on capital employed (ROCE) for thermo-economic analysis.
4. Compare the performance of a 5 MW PV in six distributed locations in Nigeria.

The major contribution of this study to the field is the development of a new approach for comparative analysis of the performance of an LSPPG to determine an optimum generation location from multiple potential locations. It can be used as a solar energy planning tool by energy policymakers or energy companies seeking to maximise power generation and return on capital employed (ROCE) with limited resources. From an environmental perspective, deploying an LSPPG at the optimal location could reduce the overall life-cycle emissions because of the potential reduction in materials and energy inputs. Thus, the overall environmental [284] and economic sustainability of PV application for power generation can be maximised by choosing the optimal location.

Secondly, TEI methodology may improve mutual trust and understanding among stakeholders (end-users, public, governments, energy companies, manufacturers, and investors) because it communicates a more realistic PV performance as a function of field data. Harjanne and Korhonen [285] argued that framing of renewable energy properly could improve renewable energy policy-making. Consequently, complementing STC specification with actual data-driven methodology could promote a more vibrant ecosystem for diverse investments in PV-based technologies.

8.1 Justification of Study

Renewable energy resources (RERs) abound in Nigeria (see Aliyu [286] and Mas'ud et al [287]), although Nigeria depends on a centralised energy infrastructure powered by fossil-fuel [288]. Currently, Nigeria generates about 7566.2 MW. Yet, Nigeria can generate 100% of its energy demand from renewables with the right technologies and policies [289,290]. Renewable energy resources such as solar energy can be utilised under distributed applications to overcome the constraints posed by long distant grid transmission of power [246,291–293]. National energy planning requires a scientific and systematic approach to decide where to establish LSPPG for maximum solar energy harvesting. Energy Commission of Nigeria (ECN) [294] projected that the electricity demand, and the supply sources to meet the demand by 2050 as Figures 8.2 and 8.3, respectively.

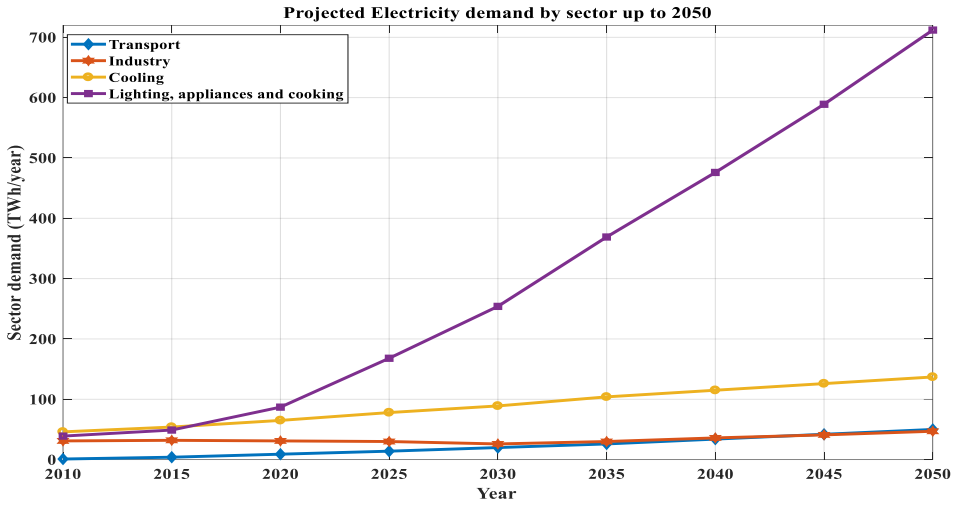

Figure 8.2: Electricity demand in Nigeria up to 2050 (Source: Energy Commission of Nigeria) [294].

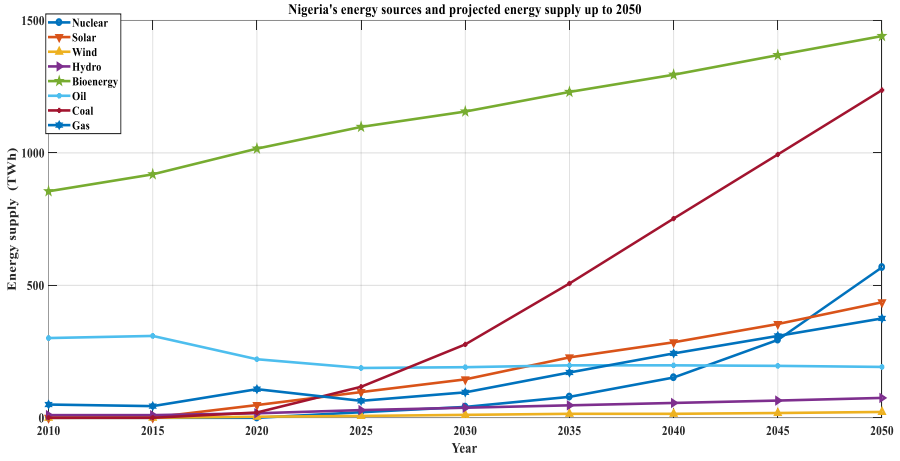

Figure 8.3: Electricity supply in Nigeria up to 2050 (Source: Energy Commission of Nigeria) [294].

From Figure 8.3, it is expected that PV power generation would contribute a significant amount of clean energy in Nigeria's energy mix up to 2050. Although solar resources on which PV power generation depends on fluctuate, PV power generation can be forecast a day ahead for short-term operational decision-making [295–298]. To support short-term forecasting of PV power generation, this study focuses on long-term forecast using thermodynamic indices in conjunction with actual meteorological data. The proposed long-term forecasting precedes short-term forecasting because an LSPPG should be installed at the optimal location before short-term optimum generation can be realistic. In United States, Data-driven solar energy generation approach was explored by the National Renewable Energy Laboratory (NREL) and National Climate Data Base (NSRDB) [299]. Data-driven short-term operational forecasting and long-term strategic forecasting would improve

decision-making on PV-based technologies. Thus, this study uses data-driven approach to generate input parameters into the thermodynamic analysis.

Although PV systems do not emit greenhouse gases during operation, there is a concern that PV waste may surge in the next 20-30 years as the current installations reach their end-of-life (EoL). Santos and Alonso-Garcia [300] estimated that about 700,000 tonnes of PV wastes may be generated in Spain by 2050. Chen et al [301] used life cycle assessment (LCA) to demonstrate that there could be future concerns in China regarding the impacts of mono-Si PV generation due to possible human toxicity, marine ecotoxicity and depletion of precious metals. PV waste management by landfilling might be cheap, but it could introduce toxic chemicals (e.g. Pb, Cd and Te) into the environment. Recycling appears better than landfilling since PV wastes material value could be about USD 15 billion by 2050 [302]. Researchers [303–306] have considered recycling approaches and techno-economic implications of recycling PV modules such as Si, copper indium gallium selenide (CIGS), and cadmium telluride (CdTe).

A cradle-to-cradle circular economic analysis of PV systems [307] can reduce the environmental impacts throughout the life cycle. Prieto-Sandoval et al [308] defined circular economy as " an economic system that represents a change of paradigm in the way that human society is interrelated with nature and aims to prevent the depletion of resources, close energy and material loops, and facilitate sustainable development through its implementation at the micro, meso and macro levels". With a circular economic approach, Sica et al [137] recommended that the use of materials such as Si, Al, and Ag in PV systems should be reduced. The overarching methodological implication of the proposed approach is to reduce the quantity of resources for LSPPG by making informed decision on location. The reduction strategy in circular economy framework is a waste prevention strategy while the recycling is a waste recovery strategy. Waste prevention is superior to waste recovery because resources saved can be utilised for other uses. Thus, choosing an optimal location for LSPPG favours economic and environmental sustainability, as well as utilisation efficiency which is the ratio of the power generated to total capital employed to build the LSPPG.

8.2 Research Method and Approach

This section presents the steps used to achieve the research objectives. It includes a formulation of the optimal location problem; description of the approach for data collection and analysis; an explanation of the design methodology for a 5 MW LSPPG; a derivation of thermodynamic indices; and a description of the simulation approach.

8.2.1 Formulation of an Optimal Location Problem

Assuming that a decision is to be made to choose a location from multiple locations for installing LSPPG using a large non-zero independent and identically distributed data of solar radiation and temperature. If the efficiency of 40 W PV modules was 16%; and it was used to construct the 5 MW LSPPG (covering an area of 31,250 m^2). Given that solar radiation and temperature fluctuate, let the objective function be to determine the location with optimal power generation as in Eq. (8.1) subject to Eq. (8.2) to (8.9). Then the optimal location problem for the LSPPG is as follows:

$$\text{Maximize } P_{LSPPG,PV} = P_{pv} + P_{pv}(N_p - 1) \quad (8.1)$$

Subject to:

$$P_{LSPPG,PV} = \eta_{En} \times A_{cell} \times G_{SMV} \quad (8.2)$$

$$P_{LSPPG,PV} = \eta_{Ex} \times A_{cell} \times G_{SMV} \times \left(1 - \frac{4}{3}\frac{T}{T_{sun}} + \frac{1}{3}\left(\frac{T}{T_{sun}}\right)^4\right) \quad (8.3)$$

$$G_{SMV} > 0 \quad (8.4)$$

$$T_{SMV} > 0 \quad (8.5)$$

$$N_p = 125{,}000 \quad (8.6)$$

$$A_{cell} = 31{,}250\ m^2 \quad (8.7)$$

$$P_{PV} = 40\ W \quad (8.8)$$

$$\eta_{En} = 16\% \quad (8.9)$$

where $P_{LSPPG,PV}$ is the total power output, P_{pv} is the power rating of the PV module, N_p is the number of PV modules, η_{En} is the energy efficiency at statistical mean value (SMV), η_{Ex} is the exergy efficiency at SMV, G_{SMV} and T_{SMV} are the SMV solar radiation and temperature, respectively, and T_{sun} is the temperature of the sun.

Figure 8.4 shows the systematic procedure from data collection stage to the stage of decision-making. The key tasks in the flowchart are further elucidated. Raw daily solar radiation and temperature data were obtained from Nigerian Meteorological Agency, Abuja. Then, statistical probability distribution functions were used to generate the SMVs for all the

locations. The CB model of the LSPPG was created in MATLAB and was then subjected to virtual experimentation using SMVs and STC values of solar radiation and temperatures. Heat generation rate was computed while economic analysis was considered. Finally, the LSPPG performance at the six locations were ranked to determine the optimal location.

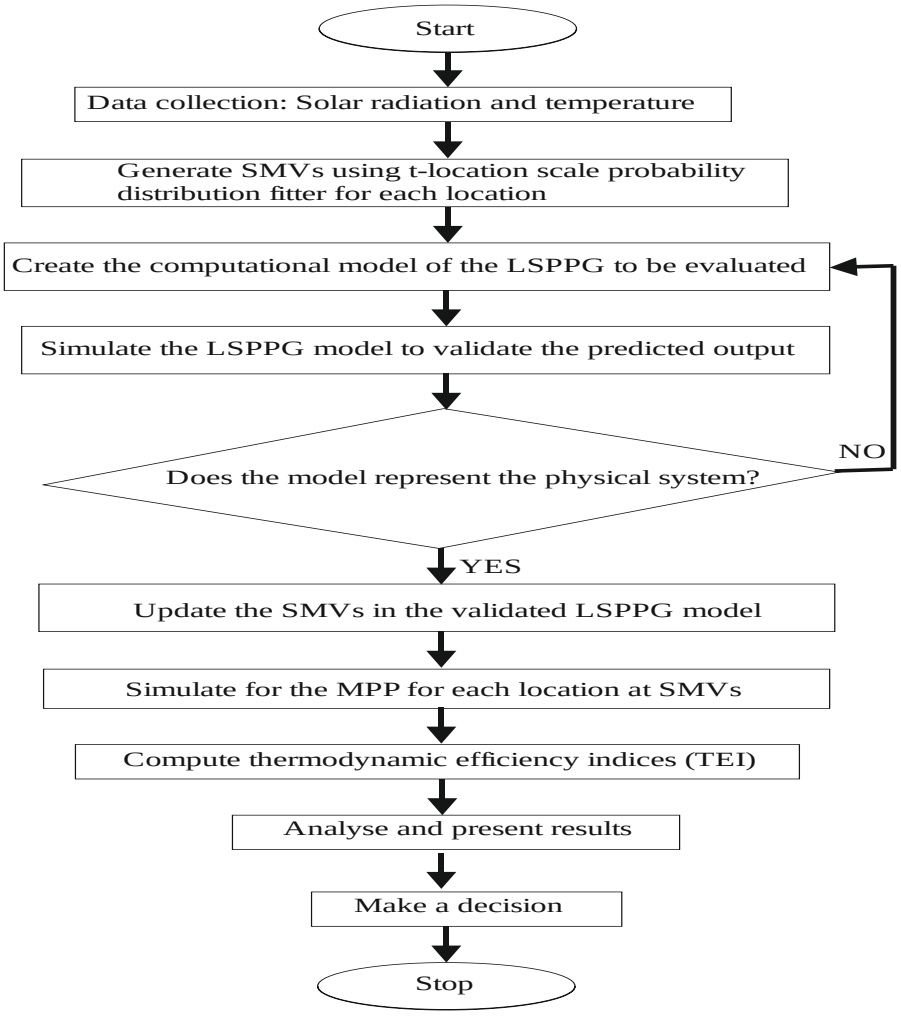

Figure 8.4: Flowchart for choosing an optimum location for LSPPG installation [233].

8.2.2 Collection and Analysis of Data

Data for one state from each of the six geopolitical regions of Nigeria were collected to maintain spread. The locations, which are visible in Figure 8.1, are Abuja, Calabar, Enugu, Gombe, Lagos - Ikeja and Kano.

Classical almost sure central limit theorem (ASCLT) [309] predicts that the distribution of a very large discrete data from the same domain would tend to form a normal distribution. The mathematical statements of ASCLT for the SMVs using solar radiation and temperature data are expressed as follows:

Let $\{X, X_n; n \geq 1\}$ be a collection of independent and identically distributed (i.i.d) random solar radiation or temperature data (X); where S is the sum, M is the mean and n is the total count. The sum and mean of solar radiation and temperature from the first non-zero variable "k" can be expressed as Eq. (8.10).

$$S_n = \sum_{k=1}^{n} X_k,\ M_n = \max_{1 \leq k \leq n} X_k, n \geq 1. \quad (8.10)$$

If E(X) = 0, and E(X^2) = 1, the ASCLT data can be expressed as Eq. (8.11).

$$\lim_{n \to \infty} \frac{1}{\log n} \sum_{k=1}^{n} \frac{1}{k} \left(\frac{S_k}{\sqrt{k}} \leq x \right) = \phi(x) \text{ (a.s.) for all } x \in R, \quad (8.11)$$

where $a_k > 0$ and $b_k \in R$ satisfy Eq. (8.12),

$$P\left(\frac{M_k - b_k}{a_k} \leq x \right) \rightarrow G(x) \text{ a.s. for all } x \in R, \quad (8.12)$$

for any continuity point x of G. If G represents solar radiation and temperature data source.

The daily solar radiation and temperature data for the six locations are presented in Appendix B. Mean values for the minimum and maximum daily temperatures for 731 days (January 1, 2015 to December 31, 2016) were computed using Excel. Then, the Excel was imported into MATLAB. Each of the dataset was vectorised by plotting a histogram before applying different "*distributionfitter*" on the vectorised data. After considering different fitting models, t-location scale and stable fit were considered further as shown in Appendix C. The t-location scale was finally selected because solar radiation and temperature data have tails compared to stable and normal distribution. SMVs for solar radiation and temperature for each location were generated and applied in this study.

8.2.3 Design and Modelling of 5 MW LSPPG

A 5 MW LSPPG was created with CBM approach described in Chapter 5. Figure 8.5 shows the predicted MPP of the LSPPG at STC. This validated that the total output of the PV array was up to 5 MW before it was deployed virtually to each of the locations.

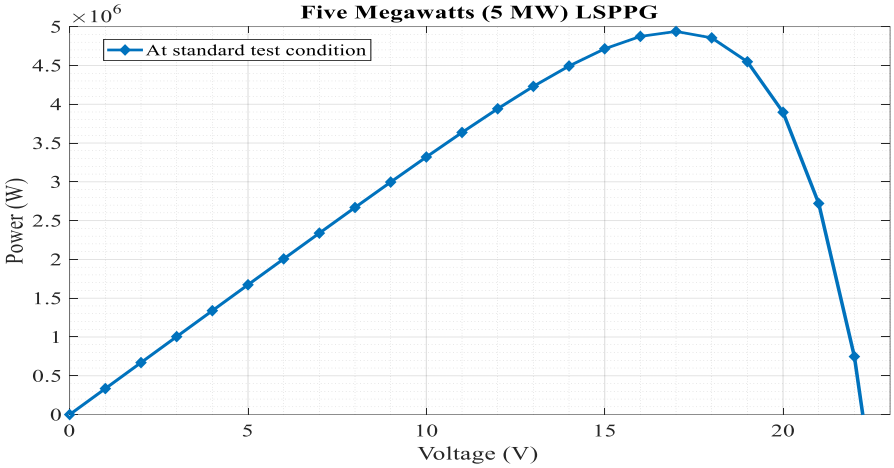

Figure 8.5: Predicted MPP of the 5 MW PV array at STC [233].

8.2.4 Formulation of the Thermodynamic Efficiency Indices

The energy efficiency index (EnEI) focuses on the efficiency of solar-electrical energy conversion based on the first law of thermodynamics. The heat loss which cannot be accounted for by the first law was accounted for using the second law based on Eq. (8.13) [91]**,** which was the focus of Chapter 6.

$$\dot{Q}_{loss} = \left[G \times A_{cell} \times \tau_{glass}\left(1 - \frac{4}{3}\frac{T}{T_{sun}} + \frac{1}{3}\left(\frac{T}{T_{sun}}\right)^4\right)\right] - \left(I_{ph}N_p - I_s N_p\left[\exp\left(\frac{qV_{pv}}{AN_s kT}\right) - 1\right]\right) \times V_{pv} \quad (8.13)$$

The energy efficiency by Park [163] (Eq. (8.14)) and exergy efficiency by Sudhakar and Srivastava [150] (Eq. (8.15)) for a photovoltaic module at STC were applied in this study.

$$\eta_{En,STC} = \frac{P_{STC}}{A_{cell} \times G_{STC}} \quad (8.14)$$

$$\eta_{Ex,STC} = \frac{P_{STC}}{A_{cell} \times G_{STC} \times \left(1 - \frac{4}{3}\frac{T}{T_{sun}} + \frac{1}{3}\left(\frac{T}{T_{sun}}\right)^4\right)} \quad (8.15)$$

By substituting the STC terms with SMV terms, energy and exergy efficiencies of the PV module at SMVs can be expressed as Eq. (8.16) and (8.17), respectively.

$$\eta_{En,SMV} = \frac{P_{SMV}}{A_{cell} \times G_{SMV}} \quad (8.16)$$

$$\eta_{Ex,SMV} = \frac{P_{SMV}}{A_{cell} \times G_{SMV} \times \left(1 - \frac{4T_{SMV}}{3T_{sun}} + \frac{1}{3}\left(\frac{T_{SMV}}{T_{sun}}\right)^4\right)} \quad (6.17)$$

Here, energy efficiency index (EnEI) and exergy efficiency Index (ExEI) are defined as the ratios of the STC efficiencies to SMV efficiencies as expressed in Eq. (8.18) and (8.19),

respectively. Eq. (8.18) and (8.19) integrate actual meteorological data with STC measurements of PV modules. Thus, EnEI is an indicator for power generation potential of an LSPPG at STC and SMV of solar radiation and temperature data.

$$\text{EnEI} = \frac{\eta_{\text{En,STC}}}{\eta_{\text{En,SMV}}} \tag{8.18}$$

$$\text{ExEI} = \frac{\eta_{\text{Ex,STC}}}{\eta_{\text{Ex,SMV}}} \tag{8.19}$$

Suppose that power output varies directly with operating profit under commercial setting. EnEI can be expressed in terms of power generation and solar radiation as in Eq. (8.20). Also, EnEI can be combined with return on capital employed (ROCE) as in Eq. (8.21) to indicate a thermodynamic moderated return on capital employed (TEI-ROCE) expressed in Eq. (8.22). TEI-ROCE compares the potential economic performance of an LSPPG at different locations since profitability varies with power output (all things being equal).

$$\text{EnEI} = \frac{\text{P}_{\text{STC}} \text{ x } \text{G}_{\text{SMV}}}{\text{G}_{\text{STC}} \text{ x P }_{\text{SMV}}} \tag{8.20}$$

$$\text{ROCE} = \frac{\text{operating profit}}{\text{Capital employed for the LSPPG}} \text{ x } 100 \tag{8.21}$$

$$\text{TEI-ROCE} = \frac{\text{operating profit (OP)}}{\text{Capital employed for the LSPPG (CE) x EnEI}} \text{ x } 100 \tag{8.22}$$

The TEI-ROCE can be stated explicitly in terms of Eq. (8.20) as Eq. (8.23).

$$\text{TEI-ROCE} = \frac{\text{OP x } \text{G}_{\text{STC}} \text{ x P }_{\text{SMV}}}{\text{CE x P}_{\text{STC}} \text{ x G}_{\text{SMV}}} \text{ x } 100 \tag{8.23}$$

Other factors such as licencing, taxation, logistics, cost of installation, maintenance cost, replacement cost, etc can affect capital employed (CE) for LSPPG operations. The TEI-ROCE can combine the STC, SMV and CE to perform economic analysis of LSPPG. In Section 8.4, CE is kept constant with an assumption that CE across the locations would be approximately the same.

8.2.5 Simulation of the 5 MW PV System

Virtual experimentation was used to simulate the performance of the 5 MW LSPPG considering the SMVs of the solar radiation and temperature. Virtual experimentation approach offered a robust approach to deploy the LSPPG at the six locations by updating the meteorological data in the CB model of the LSPPG.

8.3 Results and Discussion

This section presents the results from the virtual experimentation of the 5 MW LSPPG and the implications for PV power generation. Figures 8.6 (a) and 8.6 (b) presents the power-voltage and current-voltage outputs for the LSPPG at the six locations under study. The results are based on the SMVs of solar radiation and temperature. Clearly, different locations generated power based on the stochastic distribution of solar radiation and temperature at the location. Apparently, no location generated up to 5 MW at SMV since the solar radiation and temperature are different from the STC values used to characterise the module.

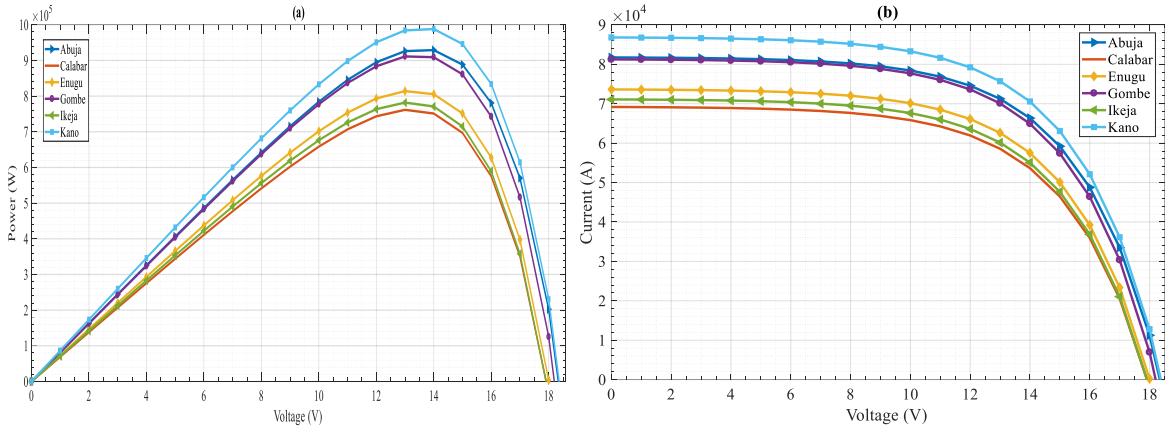

Figure 8.6: Prediction of 5 MW LSPPG: (a) Power-Voltage curves (b) Current-Voltage curves [233].

Table 8.1 presented the results based on Eqs. (8.18) and (8.19). A factor of coverage (FC) is defined in this study as the ratio of the SMV solar radiation to the SMV power generation. FC represents the effective active area of the PV cell used for power generation. As such, power generation increases with an increase in the active area of the PV cell at a constant solar radiation. If the PV cell area increases, the overall material input will increase and so will the cost of the system, energy input and emissions throughout the life cycle of the LSPPG. Implicitly, to generate the same amount of power with a low conversion efficiency PV cell, larger active area is required. The PV cells used to create the 5 MW LSPPG has 16% conversion efficiency and covered 31,250 m^2. Higher conversion efficiency PV cell would have achieved the same amount of power with lesser active area.

Table 8.1: Characteristics of LSPPG deployment in six states in Nigeria [233].

Regions	**North Central**	**South-South**	**South-East**	**North-East**	**South-West**	**North-West**
States	Abuja	Calabar	Enugu	Gombe	Ikeja	Kano
Temperature (SMV) (K)	300.05	300.25	301.05	301.35	300.95	301.25
Solar radiation (SMV) (W m^{-2})	237.27	200.23	210.65	231.48	203.70	247.69
Solar exergy flow (SMV) (J s^{-1})	2.92e+6	5.84e+5	6.14e+5	6.74e+5	5.94e+5	7.22e+5
Power (SMV) (W)	9.29e+5	7.61e+5	8.14e+5	9.11e+5	7.81e+5	9.88e+5
Heat generation rate (J s^{-1})	2.37e+5	1.78e+5	2.00e+5	2.36e+5	1.88e+5	2.66e+5
Energy efficiency (SMV) (%)	12.53	12.17	12.37	12.60	12.28	12.76
Exergy efficiency (SMV) (%)	13.42	13.04	13.25	13.50	13.16	13.68
Energy efficiency (STC) (%)	16	16	16	16	16	16
Exergy efficiency (STC) (%)	16.92	16.92	16.92	16.92	16.92	16.92
Energy efficiency Index (EnEI)	1.277	1.315	1.293	1.270	1.303	1.254
Exergy efficiency index (ExEI)	1.261	1.298	1.277	1.253	1.286	1.237
Factor of coverage (m^{-2})	0.2554	0.2629	0.2588	0.2540	0.2605	0.2507

Based on exergy analysis with Eq. (8.13), power and heat generated at SMV at Kano was the highest as shown in Figure 8.7. The average power generation for the locations was between 0.76 and 0.99 MW. The solar exergy flow at the six locations suggests that solar-based technologies, such as IPVFC systems, PV/T systems and solar thermal plants [15,28,278] have huge potentials at the locations studied. The descending order of power generation potential are as follows: Kano, Abuja, Gombe, Enugu, Ikeja and Calabar. This agreed with the global solar radiation in Figure 8.1 and the iso-irradiation map of Nigeria by Ojosu [275]. The benefit of the proposed thermodynamic approach is that it uses numerical values to rank the locations. Thus, it appeared that solar radiation and temperature data were sufficient for ranking the performance of the LSPPG at the locations studied.

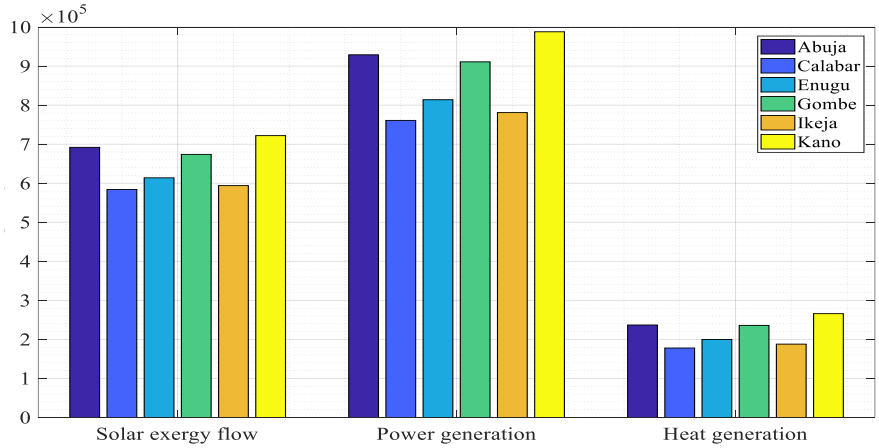

Figure 8.7: Solar, power and heat generations at SMV at the six locations in Nigeria [233].

From Figure 8.8, there is a clear distinction between the energy and exergy efficiency indices at SMV for the locations. Explicitly, the SMVs of the solar radiation and temperature in conjunction with the STC values yielded distinct TEI at different locations for the same

LSPPG system. Inductively, if locations X and Y are considered with Kano's performance such that the daily mean solar radiation and mean temperature of X for 731 days were higher than the SMVs for Kano; while those of Y were less than the SMVs for Kano, location X would generate more power than Kano whereas location Y would generate lesser power than Kano. Since the differences between the SMV of solar radiation and mean temperature across the locations studied were not significant, the LSPPG is viable at the locations.

However, if the size of the LSPPG and the number of years of operation were considered, there will be a signifant difference between the power generation potential among the locations. As an illustration, suppose that the 5 MW LSPPG in this study was operated for 10 years at SMV, the difference between the power output of Kano (9.9 MW) and Calabar (7.6 MW) would be 2.3 MW. This will increase if the size of the LSPPG increases. This finding does not necessarily mean that a significant power would not be generated from Calabar; however, it means that Kano has a better potential than Calabar. The energy efficiency index (EnEI) ranged from 1.254 to 1.315; while the exergy efficiency index (ExEI) ranged from 1.237 to 1.298. Locations with higher power generation potential would tend towards 1.0 because the EnEI value at the STC is unity. The closeness among the TEIs is probably due to the homogenenous tropical climate in Nigeria.

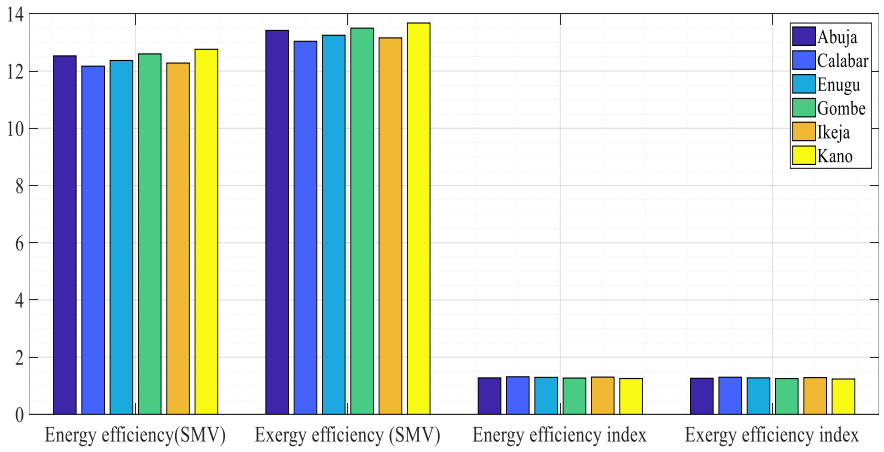

Figure 8.8: Thermodynamic efficiency indices of 5 MW PV array [233].

From Figure 8.9, Abuja performed better than Gombe due to the stochastic distributions of the solar radiation and temperature at the two locations. Abuja has higher solar radiation (237.27 W m^{-2}) and lower temperature (300.05 K) compared to that of Gombe with lower solar radiation and higher temperature of 231.48 W m^{-2} and 301.35 K.

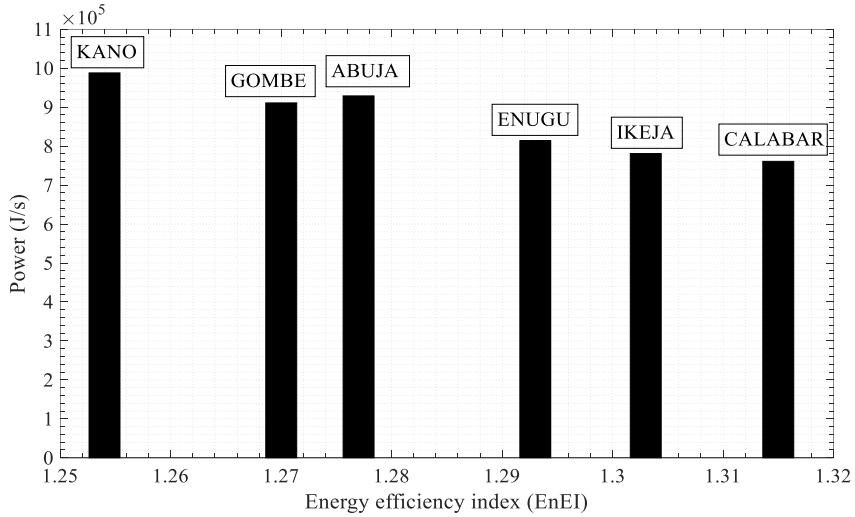

Figure 8.9: Power output versus EnEI for the six locations [233].

To compare multiple countries, the plot of EnEI versus FC can be used. Homogeneous climatic conditions will tend to produce a linear EnEI-FC plot. The gradient of the line of best fit gives the ratio of the power outputs of the LSPPG system to solar radiation at STC based on Eq. (8.20). Figure 8.10 presents a plot of the EnEI versus FC for the LSPPG for the six locations in Nigeria. Suppose that similar data from other countries are plotted on the same graph, lines steeper than that of Nigeria are countries with higher EnEI than Nigeria.

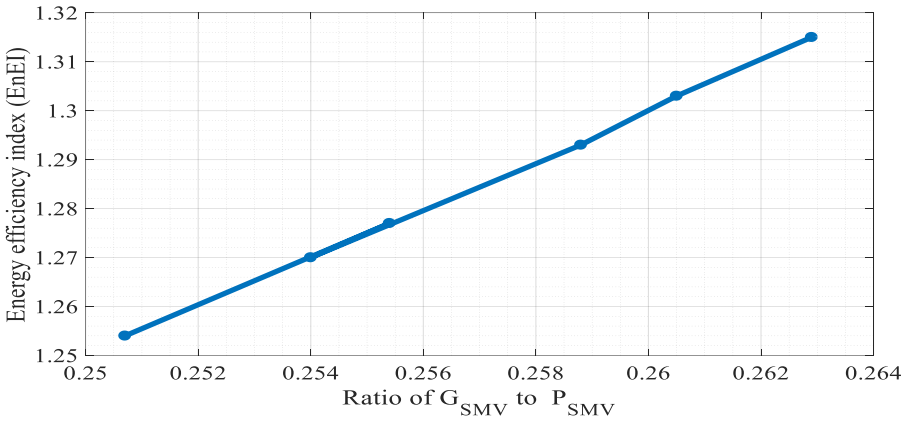

Figure 8.10: Plot of EnEI versus factor of coverage for Nigeria [233].

Inferentially, the positive gradient of the EnEI-FC plot based on Eq. (8.23) would always result in lower EnEI and higher TEI-ROCE. If the CE is constant, then operating profit would vary with the power output. Therefore, TEI-ROCE will increase when the EnEI decreases, implying that the location with the lowest EnEI will yield the highest TEI-ROCE. Suppose that the CE for the 5 MW LSPPG is constant, Kano would potentially be the optimal location for the LSPPG because its lowest EnEI would produce the maximum TEI-ROCE.

8.4 Summary and Policy Implications

This chapter presented a novel thermodynamic efficiency indices approach for strategic decision-making on the optimal location for installing an LSPPG system as a resource reduction strategy to manage the environmental impacts of the system. The energy and exergy efficiency indices range from 1.315 to 1.298 and 1.298 to 1.237, respectively. Of the cities in Nigeria studied, Kano had the highest generation potential. If the waste heat from a 5 MW LSPPG was used for thermal processes, Kano city would produce an additional power of 2.66 E+6 J s^{-1}. Overall, the proposed thermodynamic efficiency indices ranked the power generation potentials of multiple locations using solar radiation and temperature, which is a valuable piece of information for strategic decision-making on LSPPG deployments.

Chapter 9: Modelling and Simulation of a Unitized Regenerative Proton Exchange Membrane Fuel Cell System

The upcoming "hydrogen economy" [310] in which hydrogen would play a crucial role as energy vector has become a subject of intensive research. Hydrogen generates environment friendly heat and water as by-products during combustion. Although the major sources of hydrogen production remains steam reforming and water gas shift reaction with fossil fuels as feedstocks [311,312], there is an emerging potential to generate hydrogen from water electrolysis using renewable energy. In Chapter 4, the need to reduce the cost and complexity of IPVFC systems was emphasised. This Chapter 9 explores the possibility of replacing PEME and PEMFC with a Unitized Regenerative Proton Exchange Membrane Fuel Cell (URPEMFC) to perform the electrolytic and power generation functions by simply switching it from electrolyser mode (EL mode) or fuel cell mode (FC mode) and vice versa [313]. This is intended to reduce the cost and complexity of IPVFC systems, as well as improve their integrated efficiency. This is the focus of Research Objective 6.

Although URPEMFC system can be integrated with PV module [66], it is important to investigate its electrolytic and galvanic characteristics to enhance its integration with renewable energy resources in a hydrogen economy [314,315]. According to Grigoriev et al [316], the nominal power and voltage of a URPEMFC system was about 1562 W and 12.2 V in EL mode and 492 W and 3.85 V in FC mode. The FC output translated into 31.5% of the power used in the EL mode. Guo et al [317] reported that switching between modes resulted in an increase in the total response time to 4 seconds before achieving stability. Considering the thermodynamic characteristics of URPEMFC, efficiency can be improved by narrowing the gap between the power consumed during electrolytic process and the power generated during the galvanic process. Currently, there is a power hysteresis effect (PHE) in the URPEMFC which has been observed to occur during "up-scanning" and "down scanning" in the URPEMFC system [315]. The hysteresis effect in URPEMFC has been reported to be promoted by entrapped gases, dry interfaces, loose membrane and wet electrode backing [318]. Hysteresis is common with mechanisms, cycles, reactions, or processes that appear irreversible [319,320]. The Preisach model describes a classical hysteresis model [321] while rate-dependent hysteresis is a dynamic lag between an input and output that disappears if the input is varied more slowly [319].

Figure 9.1 shows an illustration of how PHE in URPEMFC creates a power hysteresis loop (PHL) from the point electrical energy dissociates water in the EL mode to the point stored hydrogen is converted into electrical energy in the FC mode. Thermodynamically, the imperfections in both electrolytic and galvanic process manifests as overpotentials or irreversibilities. The goal of electrochemical and thermodynamic improvement of URPMEFC systems is to flatten the PHL to align with the zero-loss line, where the power generated in the FC mode would be equal to the power consumed in the EL mode. This is practically infeasible due to the second law of thermodynamics, but the aim is to achieve the optimal point where the efficiency of the system can be maximised.

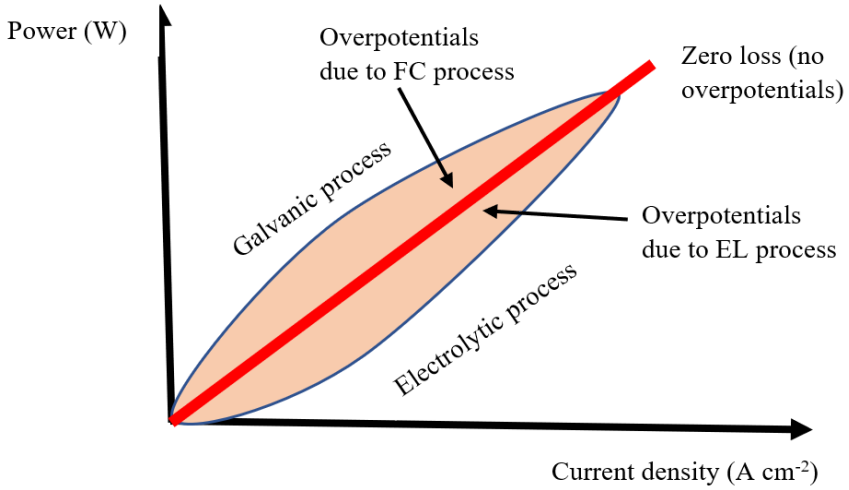

Figure 9.1: Power – Current graph of hysteresis effect in URPEMFC system

Since the phenomenon of PHE in URPEMFC is not yet fully understood, this study aims to investigate the PHE in URPEMFC system using a model-based approach. A deeper understanding of PHE could facilitate optimal design, enhanced performance, and reliable operations. The specific objectives are to:

1. Create a CB model of a URPEMFC system.
2. Investigate PHE in URPEMFC system using parametric studies.
3. Evaluate the wider implications of findings on the CEC benefits of IPVFC systems.

This study contributes towards generating insights that can facilitate the replacement of PEME and PEMFC with URPEMFC component to improve the overall design and performance of IPVFC system. PHE could provide insights on how to manage power consumption and generation in URPEMFC system as direct consequences of hydrogen generation and consumption, respectively. Thus, this could support electrochemical

engineering design, fluid dynamics, materials innovation, energy and mass transfer, electrochemistry, and catalysis of a URPEMFC system. The findings from this chapter are combined with results from the previous chapters to discuss potential design configurations in the light of the proposed CEC interrelationships.

9.1 Description of a Typical URPEMFC System

A URPEMFC system unifies the electrolytic process in PEME and galvanic process in PEMFC in a single system. Whenever the system is in the EL mode, it produces and stores hydrogen and oxygen with water using electrical energy. When it is in the FC mode, the system converts the stored hydrogen and oxygen (or air) into electrical energy. Bifunctional electrode and switching system are crucial in reversing the electrochemical processes in the component [123]. A URPEMFC system also uses power control and management units, communication units, and health monitoring units to ensure that it is reliable and efficient [52]. Ancillary components might be used to monitor or control operating temperature, pressure, reactants feed rate, water flooding and power quality.

URPEMFC system can be integrated into an IPVFC systems for power-to-gas applications to generate hydrogen [322]. As a component of an IPVFC system in conjunction with renewable energy sources [323], the overall system is clean and does not pose any environmental burden during operations. Hydrogen from a URPEMFC system can be used in hydrogen combustion engines, distributed power and gas generation, hydrogen filling stations, and in synthesis of methane [324]. A URPEMFC system can be used as a back-up power source in boats, automobiles, drones, homes, offices, aircraft, etc.

9.2 Research Method and Approach

In this study, the electrochemical and thermodynamic characteristics of a URPEMFC system were coupled using CBM approach in MATLAB so that the phenomenon of PHE can be investigated. The CB model was validated using the experimental results from Grigoriev et al [316]. Thereafter, virtual experimental approach was used to investigate the effect of the operating variables on a URPEMFC system. Table 9.1 presents the parameters used for modelling of the URPEMFC model.

Table 9.1: Parameters of the URPEMFC systems [46,96]

Parameters	Values	Units
Reversible potential	1.23	V
Number of cells in the stack	10	
Active cell area	100	cm^2
Cell current density ($i_{FC\ mode}$)	0.5	Acm^{-2}
Cell current density ($i_{EL\ mode}$)	0.5	Acm^{-2}
Mean stack voltage at EL mode	59	V
Mean stack voltage at FC mode	18	V
Mean stack power consumed at EL mode	3090	W
Mean stack power produced at FC mode	728	W
Temperature of ($T_{URPEMFC}$)	353.15	K
Anode activation constant (A_{anode})	0.0304	V
Cathode activation constant ($A_{cathode}$)	0.0507	V
Lost internal current density (i_{loss})	0.008	Acm^{-2}
Anode exchange current density ($i_{o,anode}$)	0.15	Acm^{-2}
Area specific ion resistance (R_{ion})	0.01	Ωm^{-2}
Area specific contact resistance (R_{CR})	0.03	Ωm^{-2}
Anode empirical constant (B_{anode})	0.0152	V
Cathode empirical constant ($B_{cathode}$)	0.0152	V
Anode limiting current density ($i_{l,anode}$)	15	Acm^{-2}
Cathode limiting current density ($i_{l,cathode}$)	2.5	Acm^{-2}
Hydrogen partial pressure in (P_{H_2})	1	atm
Water partial pressure (P_{H_2O})	1	atm
Oxygen partial pressure (P_{O_2})	0.21	atm
Gas constant (R)	8.3145	$Jmol^{-1}K^{-1}$
Faraday's constant (F)	96485	$Cmol^{-1}$
Number of electrons (n)	2	

9.3 Mathematical Modelling of a URPEMFC Stack

PEM technologies such as PEME, PEMFC and URPEMFC are studied using Gibbs free energy theory, Nernst equation, Tafel equation, Faraday law of electrolysis, Butler-Volmer equation, laws of thermodynamics, fluid dynamics, electrochemical polarisation model, and theory of hysteresis [134,319]. Winterbone and Turan [146] stated that Gibbs free energy is the available energy to do maximum external work by a system. Enthalpy represents the sum of the Gibbs free energy and energy due to entropy. To model a URPEMFC system, Nernst equation is useful to predict the maximum theoretical voltage if there were no activation, Ohmic and concentration overpotentials in the system.

The assumptions made here include that: (a) Overpotentials can either be activation, Ohmic or concentration overpotentials; (b) thermodynamics and electrochemical laws were obeyed; (c) there was no crossover of electrons across the PEM during switching; (d) a steady state and ideal gas conditions were applied.

From Figure 9.2, the amount of hydrogen produced during electrolytic process is twice the volume of oxygen produced under an ideal Faradaic efficiency. Similarly, the amount of

hydrogen used in the FC mode is twice the volume of oxygen. Theoretically, in EL mode, at least 1.23 V should be applied across the electrodes at 298 K and 1 bar to dissociate water at standard enthalpy of 285.8 kJ mole^{-1} [325]. In the FC mode, hydrogen is catalytically oxidized by oxygen (or air) to generate electrical energy.

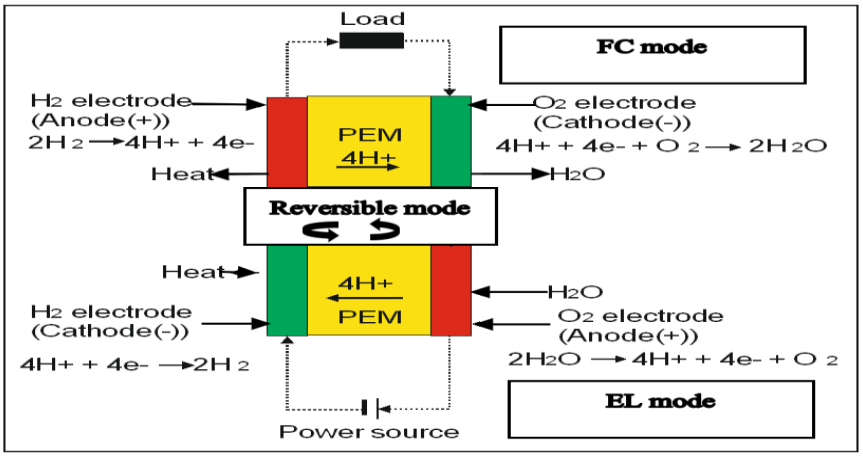

Figure 9.2: Schematic diagram of the EL and FC modes of a URPEMFC system [54].

A positive change in the Gibbs free energy promotes hydrogen generation in the EL mode (Eq. (9.1)), while negative change in the Gibbs free energy promotes water formation in the FC mode (Eq. (9.2)).

$$2H_2O_{(l)} + \text{electricity} + \text{heat} \rightarrow 2H_{2(g)} + O_{2(g)} \qquad [\Delta G^o_{EL} = +nFE^o] \quad (9.1)$$

$$2H_{2(g)} + O_{2(g)} \rightarrow 2H_2O_{(l)} + \text{electricity} + \text{heat} \qquad [\Delta G^o_{FC} = -nFE^o] \quad (9.2)$$

In the URPEMFC system, the overpotentials in the EL mode and the FC mode are categorised into activation ($E_{act_{total}}$) , Ohmic ($E_{Ohm_{total}}$) and concentration ($E_{Conc_{total}}$) and added to Nernst potential (Eq. (9.3)) to realise the net voltage in the EL mode but deducted in the FC mode (Eq. (9.4)).

$$E_{Nersnt,EL} = E_{rev} + \frac{RT}{nF}\log\left(\frac{P_{H_2O}}{P_{H_2} \times P_{O_2}{}^{0.5}}\right) + E_{act_{total}} + E_{Ohm_{total}} + E_{Conc_{total}} \quad (9.3)$$

$$E_{Nersnt,FC} = E_{rev} + \frac{RT}{nF}\log\left(\frac{P_{H_2} \times P_{O_2}{}^{0.5}}{P_{H_2O}}\right) - E_{act_{total}} - E_{Ohm_{total}} - E_{Conc_{total}} \quad (9.4)$$

The activation overpotential represents energy loss or irreversibilities due to electrochemical reaction. Tafel equation was preferred in this study but Butler-Volmer equation [96] is an

alternative approach. Factors such as nature and loading of catalyst, reactants distribution, temperature, reactants utilisation rate, and pressure could affect the activation overpotential [326]. The total activation overpotential ($E_{act_{total}}$) is expressed in Eq. (9.5).

$$E_{act_{total}} = \frac{RT}{n\alpha F}\left[\log((i_{loss} + i)/i_{o_{anode}}) + \log((i_{loss} + i)/i_{o_{cathode}})\right] \quad (9.5)$$

where the activation constant is equivalent to $\frac{RT}{n\alpha F}$; i_{loss} is the lost internal current density; α is the charge transfer coefficient; i is the current density; $i_{o_{anode}}$ and $i_{o_{cathode}}$ are anode and cathode exchange current density, respectively.

The irreversibilities due to the Ohmic resistances in the URPEMFC system were classified as resistance to electricity passing through the electrical plates and connections (R_{elect}); resistance to the transport of H^+ through PEM (R_{ion}); and the Ohmic resistance due to specific contacts (R_{CR}). Total Ohmic resistance ($E_{Ohm_{total}}$) is express as (Eq. (9.6)).

$$E_{Ohm_{total}} = i(R_{elect} + R_{ion} + R_{CR}) \quad (9.6)$$

Concentration overpotentials are due to the transportation of the reactants, products, and ions in URPEMFC system. The concentration of H^+ in the PEM depends on the operating conditions. Water formation in the FC mode needs an efficient diffusion of H^+ through the PEM from the positive electrode to the negative electrode. Overall concentration overpotential ($E_{Conc_{total}}$) in the system is expressed as Eq. (9.7).

$$E_{Conc_{total}} = \frac{RT}{nF}\left[\log(1 - (i/i_{l_{anode}})) + \log(1 - (i/i_{l_{cathode}}))\right] \quad (9.7)$$

where the empirical constant for the electrodes is equivalent to $\frac{RT}{nF}$; $i_{l_{anode}}$ and $i_{l_{cathode}}$ represent the electrodes limiting current density.

The overall CB model of URPEMFC was created as a system of equations representing the polarisation curves for the electrolytic and galvanic processes. Polarisation curves are useful for visualising the current-voltage characteristics in PEME [325], PEMFC [168] and URPEMFC system [315]. To investigate the PHE in this study, PHL is used to visualise the power-current density characteristics of the system. Eq. (9.8) represents the PHL of a single cell of URPEMFC system.

$$\mathrm{PHL} = \begin{cases} \mathrm{E_{EL}} = \mathrm{E_{Nersnt}} + \mathrm{E_{act_{total}}} + \mathrm{E_{Ohm_{total}}} + \mathrm{E_{Conc_{total}}}; \text{for EL mode} \\ \mathrm{P_{EL}} = \mathrm{i_{EL}} \times \mathrm{E_{EL}}\ ; \\ \mathrm{E_{FC}} = \mathrm{E_{Nersnt}} - \mathrm{E_{act_{total}}} - \mathrm{E_{Ohm_{total}}} - \mathrm{E_{Conc_{total}}}; \text{for FC mode} \\ \mathrm{P_{FC}} = \mathrm{i_{FC}} \times \mathrm{E_{FC}}. \end{cases} \quad (9.8)$$

A fundamental benefit of URPEMFC system is its modularity in design which facilitates its scalability. To increase the capacity of a URPEMFC system, the membrane electrode assembly (MEA) is connected in series. Eq. (9.9) represents the power utilised in the EL mode and the power generated in the FC mode.

$$\mathrm{P_{URPEMFC_{stack}}} = \begin{cases} \mathrm{P_{EL}} = \mathrm{N_{cell}} \times \mathrm{A_{cell}} \times \mathrm{i_{EL}} \times \mathrm{E_{EL}} & \text{Power consumed in the EL mode.} \\ \mathrm{P_{FC}} = \mathrm{N_{cell}} \times \mathrm{A_{cell}} \times \mathrm{i_{FC}} \times \mathrm{E_{FC}} & \text{Power produced in the FC mode.} \end{cases} \quad (9.9)$$

where $\mathrm{N_{cell}}$ is the number of cells in the stack, $\mathrm{A_{cell}}$ is the active area of the URPEMFC cell.

Eq. (9.10) represents the net balances of hydrogen in the stack ($\mathrm{PHL_{stack}}$) under different operating scenarios of URPEMFC system.

$$\mathrm{PHL_{stack}} = \begin{cases} \mathrm{H_{2_{EL}}} > \mathrm{H_{2_{FC}}} & \mathrm{H_2} \text{ produced in EL mode} > \mathrm{H_2} \text{ consumed in FC mode} \\ \mathrm{H_{2_{EL}}} = \mathrm{H_{2_{FC}}} & \mathrm{H_2} \text{ produced in EL mode} = \mathrm{H_2} \text{ consumed in FC mode} \\ \mathrm{H_{2_{EL}}} < \mathrm{H_{2_{FC}}} & \mathrm{H_2} \text{ produced in EL mode} < \mathrm{H_2} \text{ consumed in FC mode} \end{cases} \quad (9.10)$$

where $\mathrm{H_{2_{EL}}}$ is the hydrogen generated in EL mode and $\mathrm{H_{2_{FC}}}$ is the hydrogen utilised in FC mode.

The integrated efficiency of a URPEMFC system ($\omega_{\mathrm{URPEMFC,Power}}$) for power-to-power application is the percentage of the power produced in the FC mode compared to the power consumed in the EL mode as in Eq. (9.11). For applications where both power and hydrogen are of interest, the efficiency calculation includes the equivalent higher heating value (HHV) of hydrogen produced as expressed in Eq. (9.12).

$$\omega_{\mathrm{URPEMFC,Power}} = \frac{\dot{\mathrm{W}}_{\mathrm{FC\,mode}}}{\dot{\mathrm{W}}_{\mathrm{EL\,mode}}} \times 100\% \quad (9.11)$$

$$\omega_{\mathrm{URPEMFC,Hybrid}} = \frac{\dot{\mathrm{W}}_{\mathrm{FC\,mode}} + \emptyset\, \dot{m}_{\mathrm{H_2}}\, \mathrm{HHV_{H_2}}}{\dot{\mathrm{W}}_{\mathrm{EL\,mode}}} \times 100\% \quad (9.12)$$

where $\dot{W}_{Fc\ mode}$ is the maximum power output in the FC mode; $\dot{W}_{EL\ mode}$ is the maximum power input in the EL mode; $\emptyset$ is a hydrogen-power conversion factor; $\dot{m}_{H_2}$ is the mass flow rate.

9.4 Results and Discussion

In this section, the validation of URPEMFC model was presented before the simulation results on the effects of lost internal current density, number of cells in the stack and the total resistance on power generation characteristics were presented. The implications of the results were then discussed within the context of design methodologies to achieve optimal design configuration of IPVFC systems.

9.4.1 Validation of the URPEMFC Model

The model predicted polarisation curves were compared with the polarisation curves from Grigoriev et al [316] to confirm that the CB model exhibited temporal behaviours of a URPEMFC system in EL and FC modes. Figure 9.3 presents the predicted polarisation curves with those of Grigoriev et al [316].

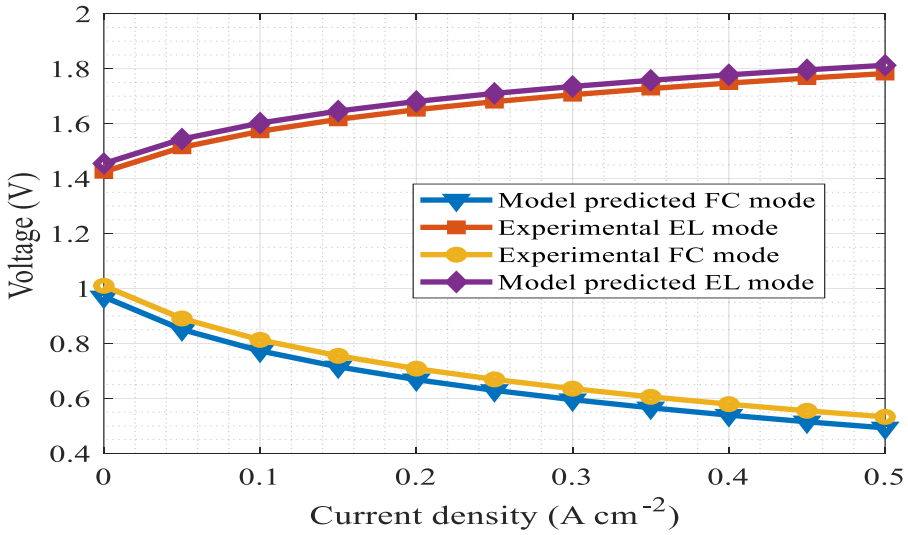

Figure 9.3: URPEMFC model validation using (Grigoriev et al. [316]**)** [54].

9.4.2 Reversibility of the URPEMFC System

Figure 9.4 shows the PHL of a URPEMFC system that is reversible. This is an ideal condition in which there is no PHE. Practically, overpotentials must occur in a URPEMFC system as consequences of electrochemical and thermodynamic processes. PHE contributed by the activation overpotential can be reduced by optimising the electrocatalysis and operating conditions of the system. Reduction in activation overpotentials will reduce the

activation energy needed to be exceeded to promote effective electrolytic process in the EL mode. Also, reducing the activation overpotentials will reduce the activation energy needed to facilitate galvanic process in the FC mode.

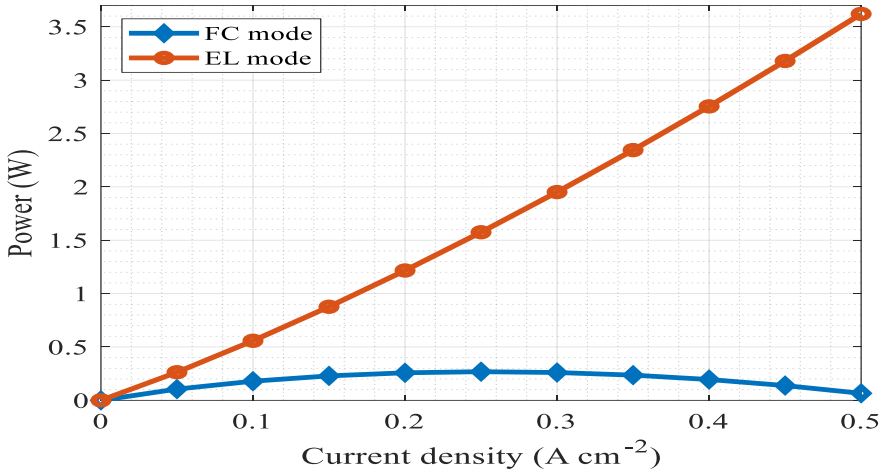

Figure 9.4: Reversible URPEMFC system without PHE [54].

The CB model of a URPEMFC stack containing 10 cells with an active area of 100 cm^2 and current density of 2 Acm^{-2} was created. The potential difference in the EL mode was increased from 1.2, 2.2, 3.2, 4.2 to 5.2 V over the FC mode in Figure 9.5. The size of the PHL decreased as the voltage in the EL mode increased. Grigoriev et al [316] achieved similar results when their result indicated the power and voltage of a URPEMFC system in the EL mode was 1562 W and 12.2 V whilst the power and voltage in the FC mode was 492 W and 3.85 V, respectively. The PHE can be reduced with effective electrocatalysts, optimal operating conditions, high conducting materials for PEM and collector plates, effective heat dissipation and water flooding management.

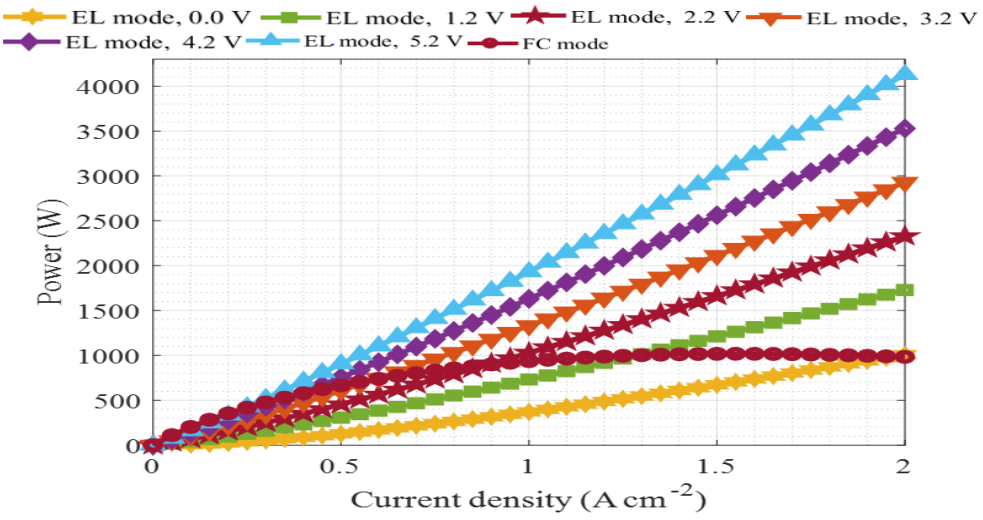

Figure 9.5: Effect of increasing potential difference between the EL and the FC modes [54].

Ohmic overpotential is a linear function that describes the overall resistance to flow of electrons, ions, and species in the system. The effect of increasing the Ohmic resistance from 0.5, 1.5, 2.5 to 3.0 Ohms on the performance of the system is shown in Figure 9.6. Clearly, the overall overpotential increased as the total Ohmic resistance increased. This caused the steepness of the linear portion of the polarisation curve to increase. Generally, Ohmic overpotential for PEM technologies can be reduced by utilising highly conductive materials for the current collectors, by reducing the thickness of the PEM, by improving the humidity of the membrane (which enhances ionic conductivity) and by eliminating water flooding [134]. Spiegel [96] observed that poly(tetrafluoroethylene) (PTFE) and Perfluorosulfonic acid (PFSA) membranes have a low cell resistance (0.05 Q cm^2) for a 100-mm-thick membrane with a voltage loss of 50 mV at 1 A cm^{-2}. Yet, the limitations of PFSA membranes include a high cost of materials, weaker supporting structure, and poor thermal capacity.

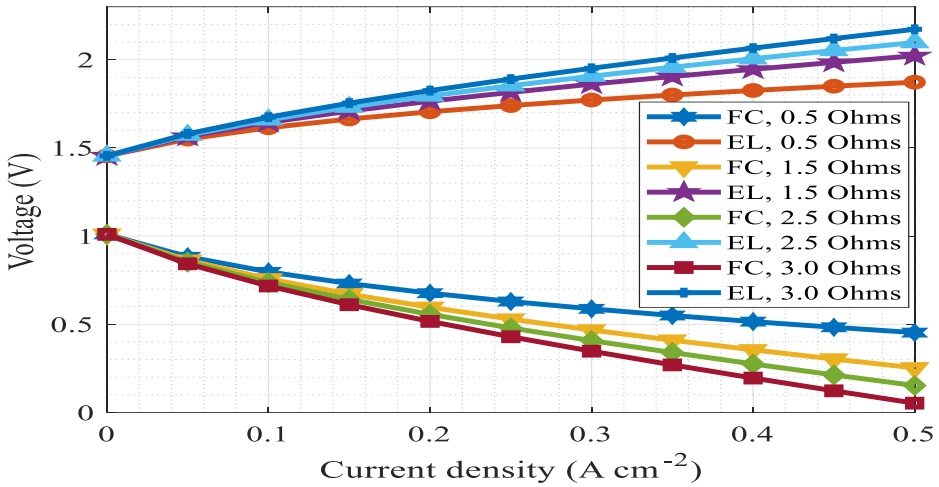

Figure 9.6: Effect of total Ohmic resistance on the URPEMFC cell [54].

9.4.3 Effects of Lost Internal Current Density

The lost internal current density was increased by a factor of 10 in order to investigate its effect on the open circuit voltage (OCV) in the EL and FC modes. From Figure 9.7, an increase in the lost internal current density from 0.008 to 0.8 A cm^{-2} increased the OCV in EL mode but reduced the OCV in FC mode. This result implies that lost internal current density of a URPEMFC system should be reduced to increase the OCV in the FC mode, but reduced in the EL mode. In a PEMFC system, Spiegel [96] observed that the kinetics was sluggish, and that the activation overpotential grew larger if the exchange current density of a PEMFC was low. Yet, the kinetics was fast, and the activation overpotential was reduced when the exchange current density was large. If the exchange current density was extremely

small, then significant current will not flow unless a large activation overpotential was applied. Therefore, reducing the overall lost internal current density could improve the performance of a URPEMFC system.

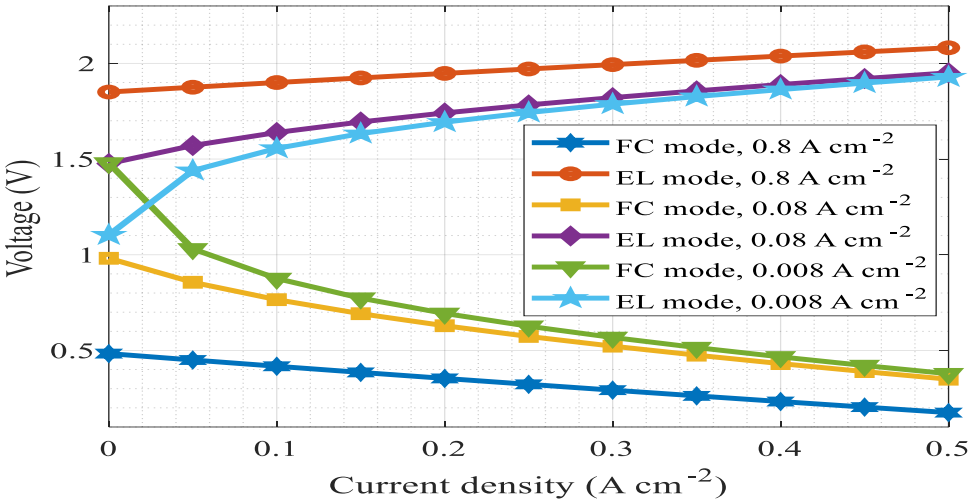

Figure 9.7: Effects of lost internal current density on the URPEMFC system [54].

Scalability of URPEMFC system can be achieved by connecting MEA in series. Figure 9.8 shows an increase in the number of cells from 1 to 10 based on Eq. (9.11). Indeed, scaling up the URPEMFC system did not eliminate the PHE. This indicated that PHE was part of the electrochemical and thermodynamic attributes of a URPEMFC system. In this study, for a current density of 0.5 A cm^{-2} and 10 cells, 990 W was utilised in the EL mode while 440 W was generated in the FC mode, which translated into a power conversion efficiency of 44%. The aim of investigating the PHE is to understand how the power difference in the EL mode and in the FC mode can be reduced so that the efficiency can be improved.

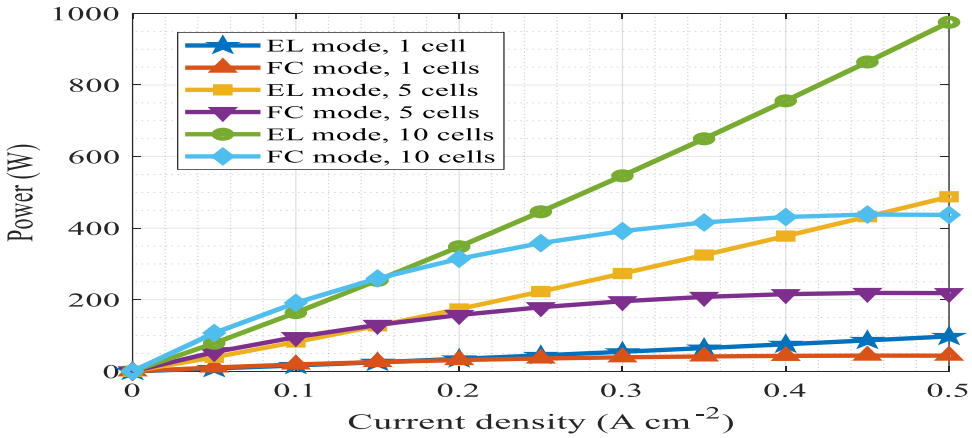

Figure 9.8: Effect of increasing the number of cells on the URPEMFC system [54].

9.4.4 Thermodynamic Efficiency of a URPEMFC System

For a reversible URPEMFC system in which PHE is non-existent, howbeit idealistic, the electrical energy consumed in the EL mode equals the electrical energy generated in the FC mode. The theoretical thermodynamic efficiency of a URPEMFC system involves input electrical energy in the EL mode that is equivalent to the enthalpy of formation of hydrogen and oxygen, whereas the output electrical energy in the FC mode is equivalent to the enthalpy of formation of water. At STP, $\overline{g_{f_{H_2O}}}$ was -237.2 kJ mole^{-1} and the reversible potential was 1.23 V [327]. Therefore, the theoretical thermodynamic efficiency in the FC mode is the level of change in the Gibbs free energy at STP that equals the enthalpy of formation of water (i.e. 237.2/285. 84 = 0.8298 or 83%). Therefore, the integrated theoretical thermodynamic efficiency of the URPEMFC system is about 0.6886 (or 69%). This shows that there is still room to improve the system considering that Grigoriev et al [316] achieved 31.5% power conversion efficiency and this study predicted 44%. Thermodynamic efficiency improvements of a URPEMFC system need systematic reduction in the activation, Ohmic and concentration overpotentials. Based on the E^4A approach adopted for thermodynamic investigation of IPVFC systems, an improved URPEMFC component will improve the integrated thermodynamic efficiency.

9.4.5 Modularisation of a URPEMFC System

Considering that switching from one mode to another could magnify the PHE as shown by Dhar [318] and Rabih et al [315], the design insights from this study is that the operational efficiency of the system could be improved by leveraging its modularity in design. Currently, integrated PV-URPEMFC systems will not utilise solar resources efficiently because it can only be in the EL mode, or in the FC mode or in OFF mode at a time. Contextually, suppose that a PV-URPEMFC system was generating power when solar radiation became available. The system will need to forego generating hydrogen. Modularisation and effective control mechanisms can enable a fourth mode herein termed “dynamic mode” in which the system can be generating both power and hydrogen simultaneously. Figures 9.9 (a) and (b) shows the polarisation and PHL curves, respectively, of a 10-cell modularised URPEMFC system. Three scenarios were contemplated: (a) a state in which 5 cells were in the EL mode and 5 cells were in the FC mode; (b) a state in which 8 cells are in the EL mode and 2 cells were in the FC mode; (c) a state in which 2 cells were in the EL mode and 8 cells were in the FC mode. From Figure 9.9 (a), the OCV increased with an increase in the number of cells. The availability of hydrogen in the system can then be moderated by maintaining the system at an adequate ratio. Figure 9.9 (b) shows that the maximum power was generated when the

number of the cells in the FC mode was 8. Yet, the operational implication is that higher amount of power will be consumed in the EL mode when the number of cells are in the EL mode increases, but generation of hydrogen will also increase. If the number of cells in the FC mode increases over the number of cells in the EL mode, more power will be generated although the stored hydrogen would deplete faster (see Eq. (9.10)).

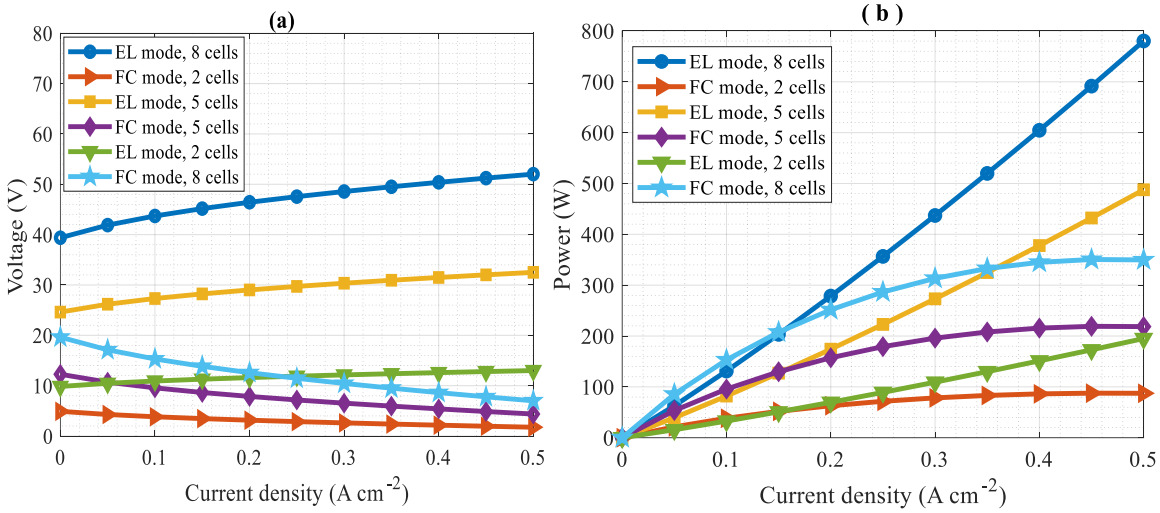

Figure 9.9: Modularisation of URPEMFC system. (a) Polarisation curves (b) PHL [54].

9.5 Discussion on the Implications of Integrating PV with Fuel Cells

This section presents the synthesis, evaluation, and creation of different design configurations of IPVFC systems based on the findings from Chapter 4, 5, 6, 7, 8 and 9. Initially, this research set out to establish methodologies for integrating PV and fuel cells for distributed applications using thermodynamic approach and other relevant techniques, laws, and theories. A preliminary analysis of a typical IPVFC system showed that the PV was inclined to generating electrical energy. Thus, if a PV module was to be integrated with a fuel cell, there was a need to tap into the electrical energy output. This required using an electrolyser as an intermediary component to generate hydrogen which can then be utilised by the fuel cell for power generation. Based on the exergy efficiency analysis of an IPVFC system, there was also a need to harness waste heat from the PV module to perform thermal work in form of a PV/T cogeneration system. Thus, attempting to recover waste heat and unutilised power from the PV module could lead to the creation of PV-PEME-Fuel-Cell system and PV/T-PEME-Fuel-Cell system. This system could as well utilise batteries which currently has higher efficiency than fuel cell to create PV-Battery-PEME-Fuel-Cell and PV/T-Battery-PEME-Fuel-Cell systems.

Obviously, the modularity in the design of IPVFC systems implies that there could be many configurations of an IPVFC system. The implementation of the E^4A showed that there was a possibility of alternative design configurations with different cost implications and consequential system complexity as the number of components increase. Therefore, a systematic exploration of the design space for IPVFC systems was needed to determine what could be the optimal design configuration from the modules based on exergy-centred design. There were two key findings. First, the PV module is the most important component of all categories of IPVFC systems, but it was equally the component with the lowest thermodynamic efficiency. The second finding was that the CEC interrelationships of integrated energy systems could be predicted if the complexity is analysed based on the principle of inheritance. As the complexity and cost of energy system increase, the efficiency improvement is not guaranteed because it depends on the cumulative exergy destruction of exergy flow in the system.

Figure 9.10 shows several components in the IPVFC systems design space that make modularisation feasible. Through a systematic inductive application of CEC interrelationships, there are several possible IPVFC systems that can be created from this design space under study. The design space also represents an innovation space in which alternative design configurations of IPVFC system can be considered for diverse use cases.

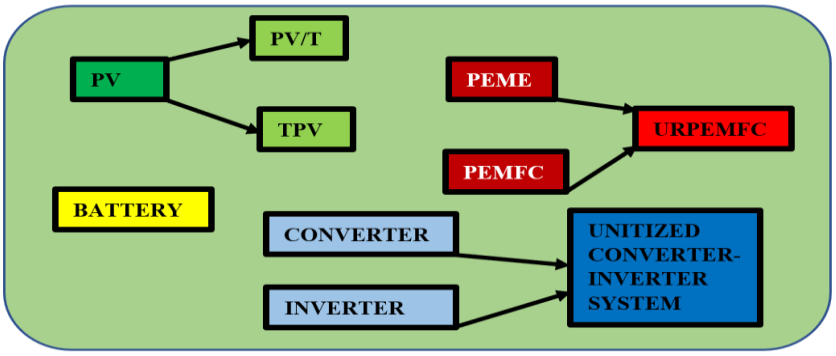

Figure 9.10: Design space with major modules that can be used to create an IPVFC system

Table 9.2 shows that there are several IPVFC systems that could be configured from the design space under consideration. It was reckoned that each of configurations has different CEC characteristics and may be suitable for different use cases and applications. However, the current analysis focuses on exploring the thermodynamic pathway that can realise the optimal CEC benefits based on the energy and exergy efficiencies. This was based on the

foreknowledge from the thermodynamic characteristics of the components and their possible effects on the integrated systems.

Table 9.2: Possible IPVFC systems Configurations using different PV-based prime movers

Prime Movers	Possible IPVFC Systems Configurations
PV	PV-Battery-Converter-Inverter-PEME-PEMFC system; PV-Converter-Inverter-PEME-PEMFC system; PV-Battery-Converter-Inverter-URPEMFC system; PV-Converter-Inverter-URPEMFC system; PV-Battery-Unitized Converter-Inverter-PEME-PEMFC system; PV-Unitized Converter-Inverter-PEME-PEMFC system; PV-Battery-Unitized Converter-Inverter-URPEMFC system; PV-Unitized Converter-Inverter-URPEMFC system.
PV/T	PV/T-Battery-Converter-Inverter-PEME-PEMFC system; PV/T-Converter-Inverter-PEME-PEMFC system; PV/T-Battery-Converter-Inverter-URPEMFC system; PV/T-Converter-Inverter-URPEMFC system; PV/T-Battery- Unitized Converter-Inverter-PEME-PEMFC system; PV/T-Unitized Converter-Inverter-PEME-PEMFC system; PV/T-Battery- Unitized Converter-Inverter-URPEMFC system; PV/T-Unitized Converter-Inverter-URPEMFC system.
TPV	TPV-Battery-Converter-Inverter-PEME-PEMFC system; TPV-Converter-Inverter-PEME-PEMFC system; TPV-Battery-Converter-Inverter-URPEMFC system; TPV-Converter-Inverter-URPEMFC system; TPV-Battery-Unitized Converter-Inverter-PEME-PEMFC system; TPV-Unitized Converter-Inverter-PEME-PEMFC system; TPV-Battery-Unitized Converter-Inverter-URPEMFC system; TPV-Unitized Converter-Inverter-URPEMFC system.
Total	24

The components of IPVFC systems are shown in Figure 9.11. Further analysis was performed to explore the thermodynamic pathway that might provide an optimal CEC benefit. TPV module was excluded because it is not a solar-based technology. The E^4A in this study was based on solar energy. Moreover, the findings from Chapter 7 also indicated that PV and PV/T were more efficient first movers based on their current state-of-the-art.

Figure 9.11: Modules in the design space of IPVFC systems.

Based on the E^4A approach, the major weaknesses of the design configuration of the PV-Battery-Converter-Inverter-PEME-PEMFC system in Figure 9.12 was that the system was complex and heat generated from the PV and PEMFC could still be used to preheat the PEME so that the overall system efficiency can be improved.

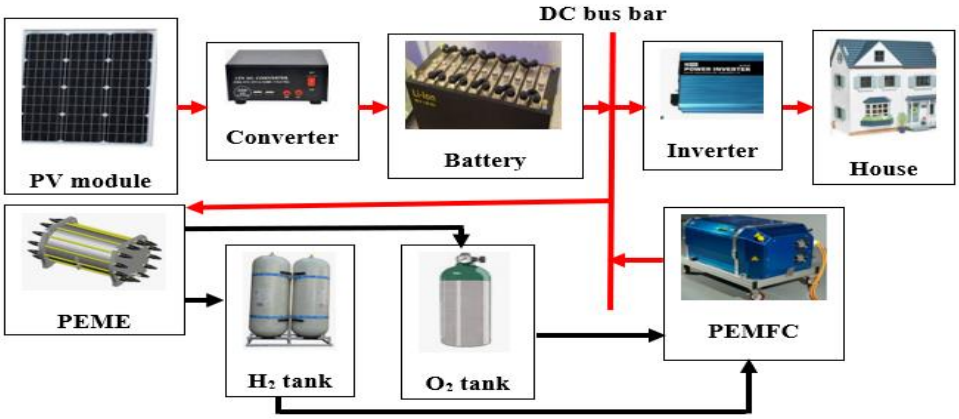

Figure 9.12: Integrated PV-Battery-PEME-PEMFC system

Harnessing the waste heat from the system in Figure 9.12 can lead to the creation of PV/T-Converter-Inverter-PEME-PEMFC system in Figure 9.13. This would achieve higher thermodynamic efficiency, but the cost and complexity of the system would also increase. The additional complexities include the process required to circulate the water in the PV/T component and transport the hot fluid extracted at high quality thermal energy to the house. Nonetheless, the system would provide hot water in addition to electricity. As discussed earlier in Chapter 5, the cooling effects of the fluid in PV/T improves the electrical efficiency of the PV component. With the additional thermal energy and improved electrical energy efficiency, it could be inferred that the offspring system in Figure 9.13 will have an enhanced overall integrated efficiency compared to its parent system in Figure 9.12. This was also based on the findings from Chapter 4.

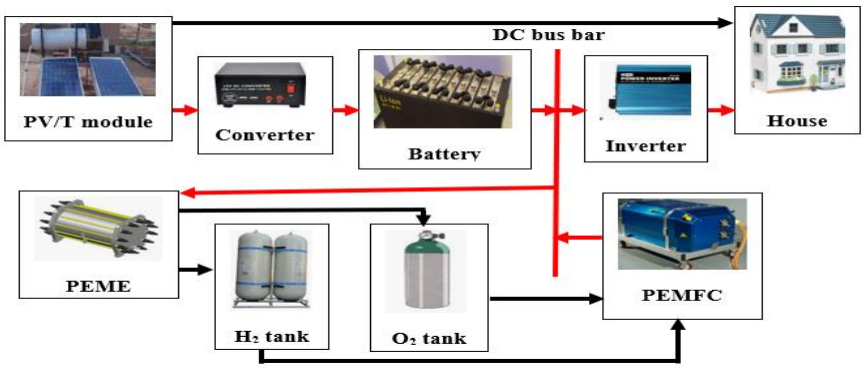

Figure 9.13: Integrated PV/T-Battery-PEME-PEMFC system

With the potential improvement in the thermodynamic efficiency of the offspring system, the growing cost and complexity need to be addressed to achieve optimal CEC benefits within the design space under consideration. Even if alternative components (say, using a cheaper PV module or cheaper battery, etc) are used to substitute the current components, total cost might reduce but the complexity will remain the same.

The substitution of a component with an alternative that can perform the same function could affect the overall behaviour of the system as well. Take for instance, batteries can be replaced with supercapacitors. Although both can be used to store electrical energy from the PV module, their behaviours during operation might not be applicable for all use cases of IPVFC systems. Both can be included but it may also add complexity and cost. Chapter 9 of this thesis explored the URPEMFC component as a potential replacement of PEME and PEMFC to reduce the cost and complexity of IPVFC systems. The converter and the inverter can also be unitized to reduce their cost and complexity. The E^4A approach could inspire designers to explore leaner design pathway after establishing the zone of optimal thermodynamic efficiency. Thus, the unitization of PEME and PEMFC, as well as the unitization of converter and inverter in the offspring Figure 9.13 could lead to a new offspring (PV/T-Battery-Unitized Converter-Inverter-URPEMFC system) shown in Figure 9.14, which is a grandchild of the IPVFC system in Figure 9.12. Certainly, the cost and complexity of the system have reduced, and it may well be that the efficiency would improve because Ohmic and transportation losses in the new offspring would be reduced. At this point, the alternative pathway is PV-Battery- Unitized Converter-Inverter-URPEMFC system, but a PV/T-Battery- Unitized Converter-Inverter-URPEMFC system is certainly more efficient because of the recovery of thermal losses from the PV component.

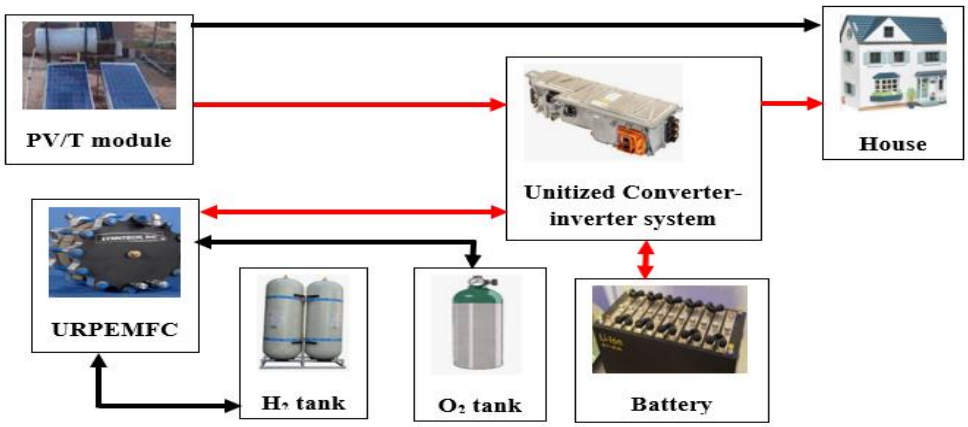

Figure 9.14: Integrated PV/T-Battery-URPEMFC system with unitized converter and inverter

It is important to highlight that this study used MBSE approach to explore the potential optimal design for IPVFC system. With the foregoing analysis, the system that can be investigated further using experimental process would be a PV/T-Battery-URPEMFC system with unitized converter-inverter unit. The reduction in complexity has huge manufacturing benefits because more components would create complex supply chain network which could impact on the delivery of IPVFC systems. The significance of the E^4A approach is that it can be applied to systematically improve the design and operational efficiency of other energy systems with parent-offspring relationships as demonstrated in this study. Overall, it provides insights on how the recovery of exergy losses and irreversibilities can improve the overall energy and exergy efficiencies of IESs.

9.6 Summary

In this chapter, the electrochemical and thermodynamic characteristics of a URPEMFC system were coupled and visualised using polarisation curves and power hysteresis. The aim was to explore if a URPEMFC system can be used to replace PEME and PEMFC components in an IPVFC system to reduce the cost and complexity of the offspring system within the design space. Fundamentally, there was a problem of power hysteresis effect which will occur as the system switches from the EL mode to the FC mode, and vice versa. Parametric studies indicated that PHE occurred at all the scales of a URPEMFC system. Overpotentials in the URPEMFC system increased when the lost internal current density and the total resistance increased. The theoretical thermodynamic efficiency of a URPEMFC system was calculated as 68.86%, but the power efficiency realised from the current study was 44%. Overall, a PV/T-Battery-URPEMFC system with unitized converter-inverter unit appeared to be the optimal ExCD configuration in the design space of a PV-based prime mover and fuel cell integration for distributed applications.

Chapter 10: Conclusions, Recommendations and Limitations of Study

This chapter presents the major conclusions from the research with regards to the research objectives set out in Chapter 1. Recommendations for further study were also made, and the limitations of the research and how they impacted the research process were outlined.

10.1 Conclusions

Although there were experimental and model-based studies on different categories of IPVFC systems (based on the review of literature), the major problem was that there was no existing systematic approach to establish the optimal design configuration considering the modularity in design. The modularity in design and the implications for cost, efficiency, manufacturability, operations, and environmental impact of IPVFC systems were systematically explored in this research. An MBSE approach was adopted as the focal research methodology. The proposed E^4A approach facilitated an evidence generation to support thermodynamic inferences within the IPVFC design space. Overall, the following conclusions can be drawn from the work presented in Chapters 4, 5, 6, 7, 8, and 9 in pursuit of the research objectives stated in Chapter 1. The conclusions based on the set objectives are presented as follows:

Objective 1: Develop a methodology for exergy-centred design analysis of a photovoltaic-based energy system.

E^4A approach was proposed as a systematic and systemic approach to study the CEC interrelationships of PV-based integrated energy systems (System 1: PV-Battery; System 2: PV/T-Battery; System 3: PV-Battery-Electrolyser-Fuel cell; System 4: PV/T-Battery-Electrolyser-Fuel cell). The findings revealed that System 4 was more efficient than System 3 because waste heat from the PV in System 4 can be utilised for some useful thermal work. However, in addition to the increased complexity, the efficiency of System 4 degraded over System 2 due to the irreversibilities incurred by passing electrical energy, which has the highest exergy, through electrochemical processes in the PEME and PEMFC. These findings gave insights into the need to investigate the thermodynamics of PV cells, as well as the necessity to create pathways to reduce the cost and complexity of IPVFC systems.

Objective 2: Advance the code-based modelling (CBM) approach as a means of overcoming the limitations of the block-based modelling (BBM) approach for photovoltaic modelling and simulation.

The prevalent BBM approach for model-based study of PV modules was not robust enough to implement extensive investigation of the thermodynamics of a PV module due to its constraints in accepting user-defined functions and algorithms. Consequently, the CBM approach was improved and applied in this study. The CB model consistently predicted the short circuit current, maximum power point, open circuit voltage with 0%, <2% and <10% deviations, respectively. This degree of accuracy was acceptable because exergy destruction in a PV module would produce some waste heat. The CBM approach facilitated the creation of novel photovoltaic-thermal and thermophotovoltaic models.

Objective 3: Integrate the solar, thermal, and electrical exergies of a photovoltaic module in order to gain novel physical insights.

PV module is the prime mover of all IPVFC systems. Unfortunately, of all the components in the design space under study, the PV module has the least thermodynamic efficiency. This makes the PV module act as a bottleneck in the system. To gain deeper physical insights into the thermodynamics of a PV module, the CBM approach facilitated an integration of the solar, electrical, and thermal exergies of a PV module. Major findings include that the temperature of the PV module needs to exceed a critical temperature before it can generate electrical energy sub-linearly. However, extreme operating temperatures could degrade the open circuit voltage and reduce the conversion efficiency of a PV module. Harnessing the waste heat from a 45 W PV module used in this study for useful thermal work could improve it by 51%. This implies that a PV/T module of the same surface area with a PV module will harness more solar energy for power and heat generation.

Objective 4: Integrate the radiative heat transfer, power density output, and thermal losses in the core of a thermophotovoltaic system in order to gain novel physical insights.

Beside the use of PV cells in solar PV systems, PV cells can also be used in TPV systems for power generation. The CBM approach also facilitated an integration of the radiative heat transfer, thermal losses, and power density output in the core of a thermophotovoltaic system. In the TPV system, increasing the operating temperature from 300 to 700 K degraded the open circuit voltage which agrees with the findings in Chapter 5. At a radiator

temperature of 1800 K and TPV cells temperature of 300 K, the TPV model predicted the power density output, thermal losses, and maximum voltage of a TPV system as 115.68 W cm^{-2}, 18.14 W cm^{-2} and 36 V, respectively. The power generation capacity of a 80 W solar PV module in this study could improve by 45% at a radiator temperature of 1800 K and TPV cells temperature of 300 K. Based on the current state-of-the-art the PV-based technologies, a PV/T module appears to be more thermodynamically efficient than a TPV module due to the need to match the radiative source with the PV characteristics. Thus, this study focussed on a PV/T instead on a TPV design pathway.

Objective 5: Develop a methodology for determining an optimal location among multiple locations for installing a large-scale photovoltaic power generation using a thermodynamic approach.

An optimised IPVFC system cannot generate the same amount of energy wheresoever as it is deployed across the globe due to the variability of solar resources. To address this issue, novel thermodynamic efficiency indices based on actual meteorological data were proposed to investigate six states from Nigeria to determine a location that will yield an optimal power generation for a 5 MW LSPPG. This was crucial because the amount of power generated from the PV component could affect the amount stored in the battery as well as the amount used for hydrogen generation with the PEME or URPEMFC component. The energy and exergy efficiency indices across the six geopolitical regions of Nigeria range from 1.315 to 1.298 and 1.298 to1.237, respectively. This finding implies that IPVFC systems will generate different amount of energy depending on the location of deployment. Interestingly, the results suggests that LSPPG systems can be sustainable across all the locations studied.

Objective 6: Model and simulate the power hysteresis effect in a unitized proton exchange membrane fuel cell system as a means of reducing the overpotentials in the component.

To address the problem of CEC interrelationships of IPVFC systems as they evolve to recover thermodynamic and usage losses, the unitization of the PEME and the PEMFC to create a URPEMFC system was investigated. The results showed that the power efficiency of a URPEMFC was 44%. This implies that the URPEMFC component can replace a PEME and a PEMFC to achieve a reduced cost and lesser complexity, whilst the integrated efficiency could increase. Through E^4A approach and modules unitization, a PV/T-Battery-

URPEMFC system with unitized converter and inverter might be the optimal design configuration within an IPVFC design space in terms of the CEC benefits.

10.2 Recommendations for Future Works

This work started from a global exploration of the most effective approach to integrate a PV and a fuel cell for distributed applications. Although a PV/T-Battery-URPEMFC system with unitized converter and inverter might be the optimal design configuration within IPVFC design space in terms of the CEC benefits, the following recommendations for further work are made to enable researchers to advance or to apply the outcomes realised in this research.

- The proposed PV/T-Battery-URPEMFC system with unitized converter and inverter for trigeneration of power, heat and hydrogen should be investigated experimentally to establish its reliability as well as to improve it for distributed applications.
- The proposed CBM approach can be explored further for modelling and simulation of photovoltaics and thermophotovoltaics since the approach accept user-defined functions and algorithms. The realised theoretical models can be used for experimental or numerical studies to improve the overall conversion efficiency of photovoltaic and thermophotovoltaic systems. The models can also be considered for inclusion in a PV software for photovoltaic, photovoltaic-thermal and thermophotovoltaic modelling and simulation.
- Additional sub-models of the proposed models can be pursued to include parameters such as the wavelength of the radiation, material parameters, surface characteristics of the PV cells to expand the scope and application of the proposed models. Heat transfer models can be included to investigate the mechanisms of heat dissipations or retention in the PV modules or in the core of thermophotovoltaic systems.
- Given the sublinear increase in electrical energy output and the reduction in V_{oc} for the proposed photovoltaic-thermal model in Chapter 6 in Figure 6.3, there is a need to investigate the characteristics of the generation at temperatures above 450 K.
- A dynamic mode for a URPEMFC system to simultaneously operate it in EL and FC modes should be investigated using an experimental approach. Insights from such study could provide insights into how the modularisation and an energy management strategy and control could reduce the PHE if PV or PV/T were integrated with a URPEMFC component.

- The proposed E^4A approach can be applied beyond photovoltaic-based energy systems to explore CEC benefits and innovations in designs provided that the systems have a parent-offspring relationships.
- The policy implication of this research for Nigeria is that photovoltaic and photovoltaic-thermal generation are viable across the six geopolitical zones of Nigeria. Given the poor transmission infrastructures in Nigeria, the use of different categories of IPVFC systems for different use cases could improve power generation. However, the government, research institutions, and industrialists need to collaborate to develop indigenous solar-based technologies to contribute towards reducing the current energy poverty in Nigeria. The insights from exploring the IPVFC design space has shown that there could be several design configurations and compositions for possible grid-connected and off-grid applications. This research provides useful information for manufacturing companies on how they can exploit the modularity in design of IPVFC systems to produce customised and standardised versions that will meet customer requirements and specifications.

10.3: Limitations of the Study

Overall, the scope of this research is limited to conceptual studies of designs and development pathways for IPVFC systems using thermodynamics-based model-based systems engineering. Although interesting insights and results have emerged from the research, there were limitations and constraints that could have possibly made a difference in the outcomes of this research.

- Although the MBSE approach offered a cost effective and time-saving approach to study the IPVFC system design space, experimental setup of the PV/T-Battery-URPEMFC system with unitized converter and inverter would have been an interesting study. This could not be done because of funding and time limitations.
- The CEC indicators are not static but evolving as the state-of-the-art of the components evolve. This means that results from the E^4A methodology will be influenced by the time of the analysis as energy and exergy efficiency depends on the state-of-the-art of the components. Therefore, developments in the components should be monitored to see if there will be less complex, more efficient, and cheaper components that can be utilised in the IPVFC systems to improve the CEC benefits.

- Incomplete data for components such as PV, PV/T, TPV and URPEFC from the manufacturers resulted in the missing data being sourced from peer-reviewed literature and the standard tables for physical parameters of the components.
- The statistical approach used to generate SMVs for solar radiation and temperature was based on daily data that was available at the Nigerian Meteorological Agency Abuja. Using minute or hourly data would have provided higher resolution in visualising the power generation. However, the outcome would have been the same since the TEI depended on the mean values of solar radiation and temperature.
- The E^4A approach predicts the system with the optimal CEC benefits with an assumption that the efficiency of the state-of-the-art components within the design space are the same and that an offspring system must inherit the efficiency, costs, and complexity of the parents.

Appendices

Appendix A: A sample of the CB model for a PV module. The codes require input parameters of the specific PV cell type and module characteristics being modelled.

```
%PV module Inputs
T= 298.15;% Operating temperature
Tr=298.15;% Reference temperature
ki=0.065;% Temperature coefficient of Isc
Iscr=2.68; % Short circuit current (A)
Irr= 0.000539;
A = 2.83;% Ideality factor
Ego = 1.17; % Band gap of Silicon at 0K
alpha =7.021*10^(-4); % Material constant
beta=1108;% Material constant
S = [100]; % Irradiation
K = 1.38065*10^(-23); % Boltzmann's constant
q = 1.6022*10^(-19); % electron charge
Np= 1;% Solar cells in parallel
Ns=36;% Number of cells in series
Vo= [0:1:500]; % number of iteration over voltage
% find the values for all the suns.
for i =1:1
    Eg = Ego - (alpha*T*T)/(T+beta)*q; % Band gap energy
    Iph = (Iscr+ki*(T-Tr))*((S(i))/100); %Photocurrent
    Irs = Irr*((T/Tr)^3)*exp(q*Eg/(K*A)*((1/Tr)-(1/T)));%Saturation current
    Io= Np*Iph-Np*Irs*(exp(q/(K*T*A)*Vo./Ns)-1); %output current
    Po = Vo.*Io; % Output power
    figure(2) % Voltage versus Current
    plot(Vo,Io);
    axis([0 25 0 3.5])
    xlabel('Voltage in Volts')
    ylabel('Currenet in Amperes')
    title('Photovoltaic module')
    grid on
    grid minor
    legend 1000W/m^2 800W/m^2 600W/m^2 400W/m^2 200W/m^2
    set(findall(gca, 'Type', 'Line'),'LineWidth',2);
    hold on
    figure(3); % Voltage versus Power
    plot(Vo,Po);
    axis([ 0 25 0 40]);
    xlabel('Voltage in Volts')
    ylabel('Power in Watts')
    title('Photovoltaic module')
    grid on
    grid minor
    legend 1000W/m^2 800W/m^2 600W/m^2 400W/m^2 200W/m^2
    set(findall(gca, 'Type', 'Line'),'LineWidth',2);
    hold on
    figure(4)% Current versus Power
    plot(Io,Po);
    axis([0 3.5 0 40]);
    xlabel('Current in Amperes')
    ylabel('Power in Watts')
    title('Photovoltaic module')
    grid on
    grid minor
    legend 1000W/m^2 800W/m^2 600W/m^2 400W/m^2 200W/m^2
    hold on
    set(findall(gca, 'Type', 'Line'),'LineWidth',2);
end
```

Appendix B: Solar radiation and temperature data for the six locations under study (Source of data: Nigerian Meteorological Agency, Abuja, Nigeria).

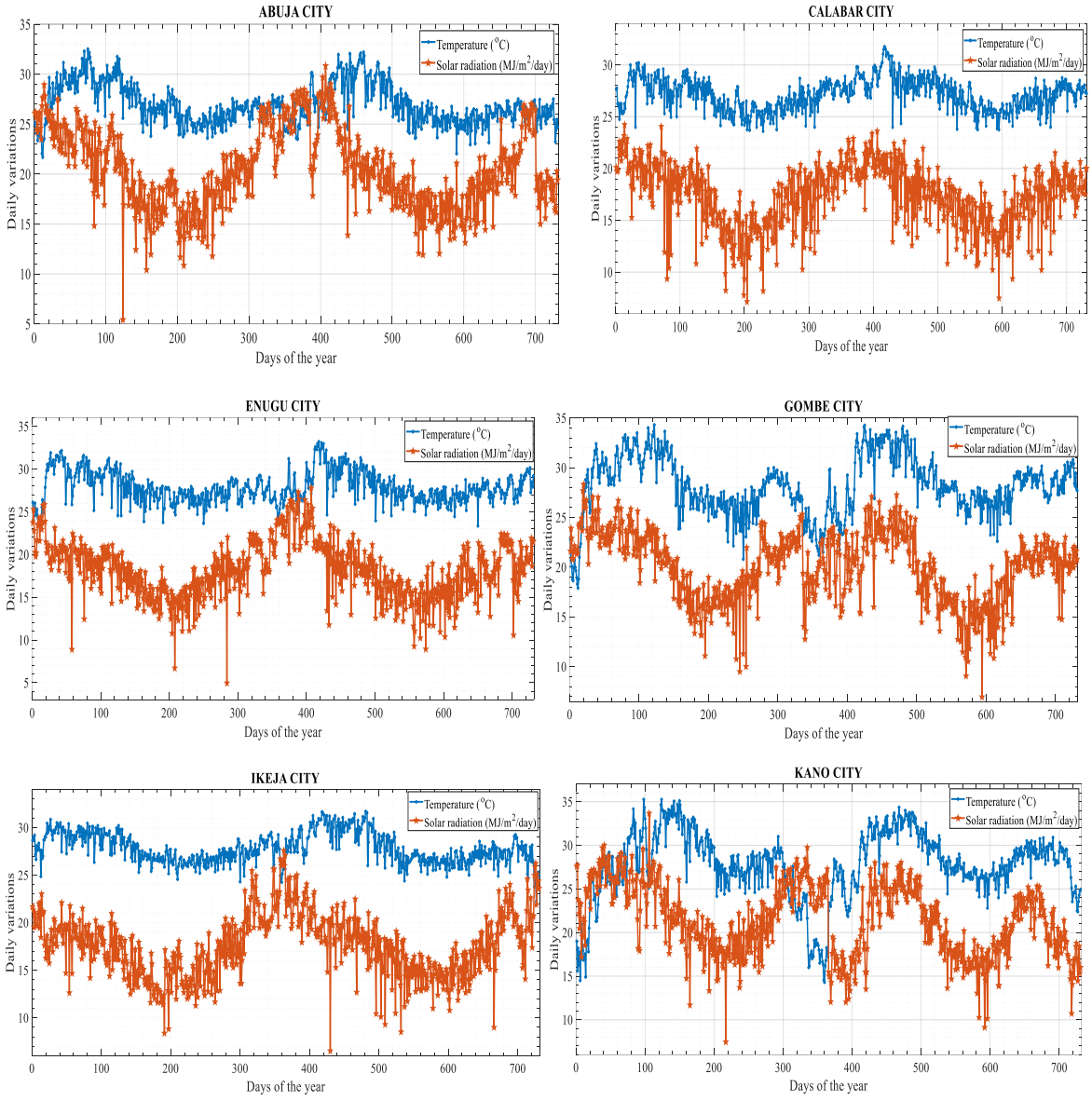

Appendix C: t-location scale and stable probability distribution function (PDF) of solar radiation and temperature data for the six locations under study (Source of data: Nigerian Meteorological Agency, Abuja, Nigeria)

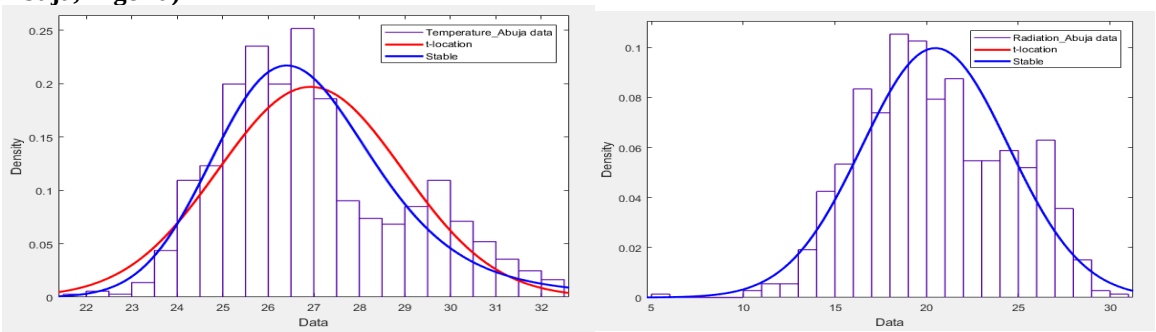

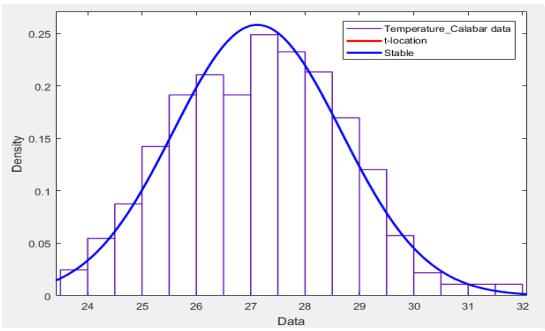
Temperature_Calabar data
t-location
Stable
Density
Data

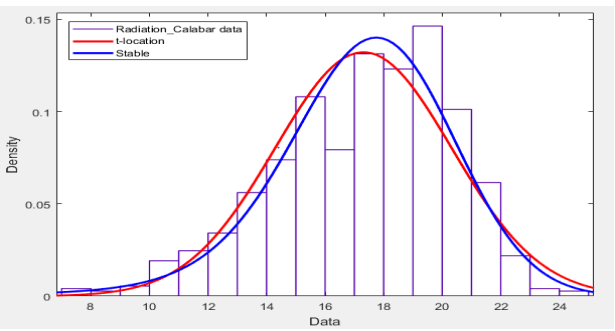
Radiation_Calabar data
t-location
Stable
Density
Data

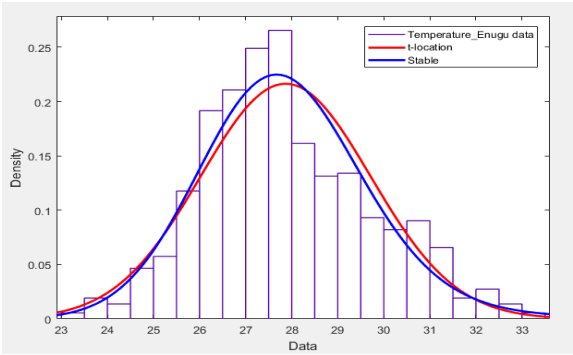
Temperature_Enugu data
t-location
Stable
Density
Data

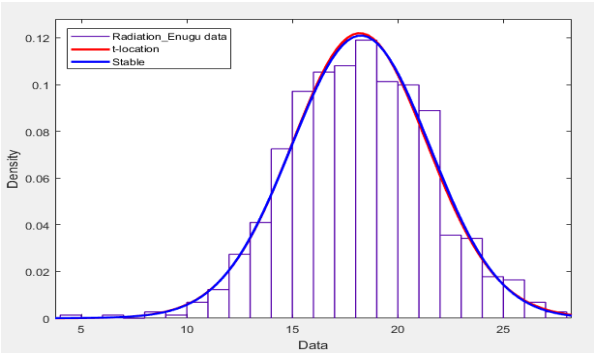
Radiation_Enugu data
t-location
Stable
Density
Data

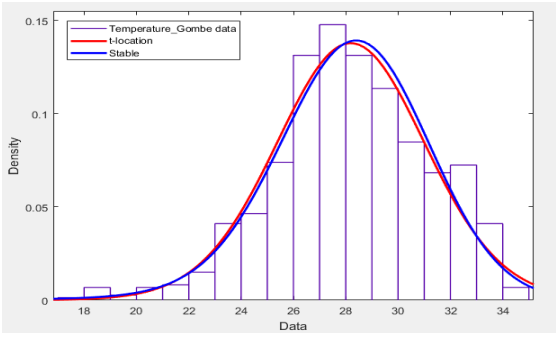
Temperature_Gombe data
t-location
Stable
Density
Data

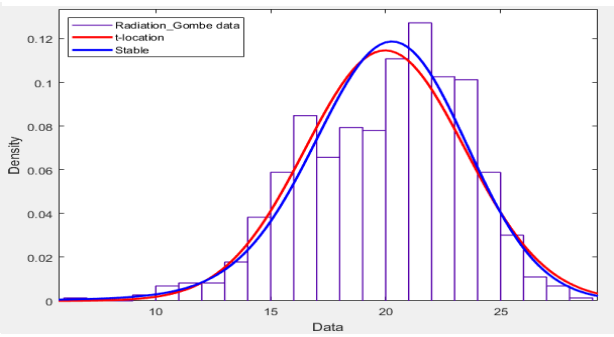
Radiation_Gombe data
t-location
Stable
Density
Data

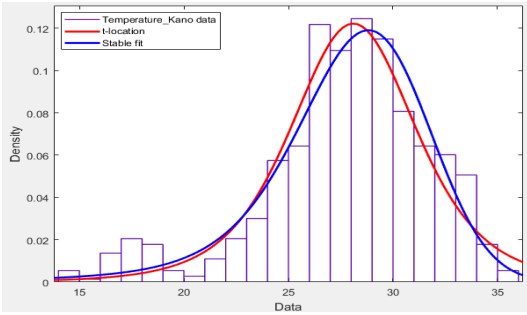
Temperature_Kano data
t-location
Stable fit
Density
Data

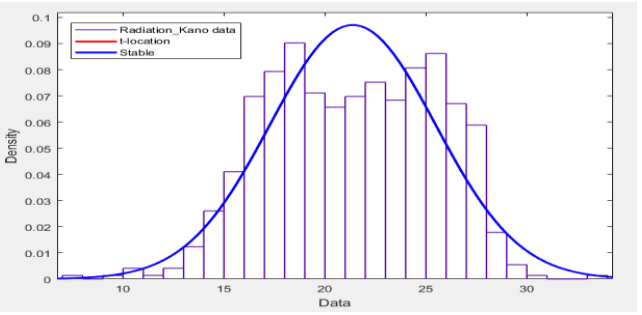
Radiation_Kano data
t-location
Stable
Density
Data

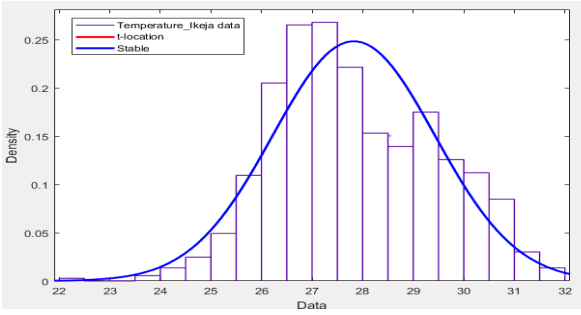
Temperature_Ikeja data
t-location
Stable
Density
Data

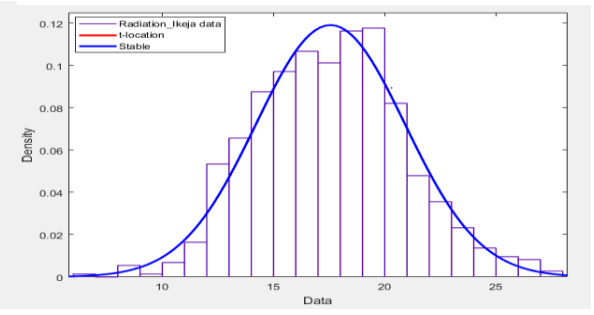
Radiation_Ikeja data
t-location
Stable
Density
Data

Journal of Energy Storage 26 (2019) 101029

Contents lists available at ScienceDirect

Journal of Energy Storage

journal homepage: www.elsevier.com/locate/est

Energy and exergy efficiencies enhancement analysis of integrated photovoltaic-based energy systems

C. Ogbonnaya[a,c,*], A. Turan[a], C. Abeykoon[b]

[a] School of Mechanical, Aerospace and Civil Engineering, The University of Manchester, M60 1QD, UK
[b] Aerospace Research Institute, School of Materials, The University of Manchester, Oxford Road, M13 9PL, UK
[c] Faculty of Engineering and Technology, Alex Ekwueme Federal University Ndufu-Alike Ikwo, P.M.B. 1010, Nigeria

ARTICLE INFO

Keywords:
Exergy control design
Integrated energy systems
Photovoltaics
Distributed systems
Energy and exergy analysis

ABSTRACT

Integrated energy systems (IESs) take advantage of the complementarity of their subsystems to improve the overall system functionality, sustainability and performance. Presently, the cost of the recovery of thermodynamic losses from photovoltaic modules has not been addressed. In this study, novel energy and exergy efficiencies enhancement analysis (EEEEA) is proposed for the study of the implications of recovering the conversion and usage losses from a photovoltaic (PV) module. Four evolutionary IES were analysed: a PV-Battery (System 1); a Photovoltaic-thermal (PV/T)-Battery (System 2); a PV-Battery-Electrolyser-Fuel cell (System 3) and a PV/T-Battery-Electrolyser-Fuel cell (System 4). Actual solar radiation and temperature data coupled with synthesised data were applied. Results show that both the energy and exergy efficiencies of System 2 upgraded by 37.89% and 5.42%, respectively, over System 1. The energy and exergy efficiencies of System 3 degraded by 3.11% and 4.10%, respectively, over System 1; whereas the energy and exergy efficiencies of System 4 degraded by 21.92% and 7.72%, respectively, over System 2. Furthermore, the thermodynamic efficiencies of the IESs did not naturally upgrade with system complexity. The EEEEA can help scientists, engineers and policymakers to analyse IESs with a parent-offspring relationship in order to establish the optimum efficiency and thermo-economics.

1. Introduction

Solar energy has a potential to contribute more useful energy than it is currently providing [1]. Most of the technologies that depend on solar energy do not emit greenhouse gases (e.g. CO_2, methane, CFCs, NO_x); yet, solar energy resource is globally ubiquitous, 100% clean, renewable, and convertible with varieties of solar-based technologies (e.g. photovoltaics, solar thermal plants, photovoltaic-thermal systems and their hybrids). These features have made solar energy one of the most intensive areas of research for future energy source for the inhabitants of the earth. Presently, it is advocated by the United Nations Framework Convention on Climate Change (UNFCCC) [2] that member countries should use efficient and sustainable energy systems in order to reduce the global carbon footprint, greenhouse gas emissions and pollution.

Scientists and engineers apply thermodynamic analysis to establish the theoretical performance limit of energy systems. The energy analysis, which is based on the first law of thermodynamics, has been criticised for not including losses generated in the system in the course of energy production [3]. On the other hand, energy analysis, which is based on the second law of thermodynamics, includes the loses and irreversibilities generated in the system [4]. Thus, these thermodynamic analyses can be used to evaluate the theoretical performance of systems at research and development phase. From a global perspective of resource utilisation efficiency of energy systems, a system that converts the available resources into high quality energy is preferred because it generates lower losses and irreversibilities. Dincer [5] argued that energy should be used as an energy policy tool since it measures both the quantity and quality of energy sources.

Winterbone and Turan [6] stated that exergy analysis helps engineers to estimate the maximum amount of work available from a system as it interacts with its surroundings. In practice, where all the energy input into a system cannot be converted to useful work, an exergy analysis becomes essential for investigating the sources and causes of exergy destruction and irreversibilities in the system. This would then help engineers to improve the overall system efficiency [3,7]. Broadly, increasing the exergetic efficiency of energy systems could improve environmental sustainability [8]. For instance, the

* Corresponding author at: School of Mechanical, Aerospace and Civil Engineering, The University of Manchester, M60 1QD, UK.
E-mail addresses: chukwuma.ogbonnaya@manchester.ac.uk, chukwuma.ogbonnaya2@gmail.com (C. Ogbonnaya).

https://doi.org/10.1016/j.est.2019.101029
Received 29 June 2019; Received in revised form 30 September 2019; Accepted 21 October 2019
Available online 29 October 2019
2352-152X/

Journal of Cleaner Production 249 (2020) 119405

Contents lists available at ScienceDirect

Journal of Cleaner Production

journal homepage: www.elsevier.com/locate/jclepro

Novel thermodynamic efficiency indices for choosing an optimal location for large-scale photovoltaic power generation

C. Ogbonnaya [a, c, *], A. Turan [a], C. Abeykoon [b]

[a] Department of Mechanical, Aerospace and Civil Engineering, The University of Manchester, M60 1QD, UK
[b] Aerospace Research Institute, Department of Materials, The University of Manchester, Oxford Road, M13 9PL, UK
[c] Faculty of Engineering and Technology, Alex Ekwueme Federal University Ndufu-Alike Ikwo, Nigeria

ARTICLE INFO

Article history:
Received 14 August 2019
Received in revised form
19 November 2019
Accepted 20 November 2019
Available online 21 November 2019

Handling editor: Giorgio Besagni

Keywords:
Solar energy
Photovoltaic modules
Thermodynamic efficiency indices
Modeling and simulation
Nigeria

ABSTRACT

Sustainable energy is a current key priority across the globe. Hence, renewable energy sources have been widely accepted as potential substitutes for fossil fuels in the existing energy infrastructures. A recent report showed that photovoltaic power generation constituted around 100 GW out of 2378 GW of the global renewable power capacity installed in 2018. Consequently, various researchers are investigating how the increasing utilisation of photovoltaics can be handled in order to reduce future environmental impacts; whilst leveraging their operational zero-emission. From a circular economic paradigm, recycling, reuse and reduction strategies are often adopted to improve the sustainability of systems. This study proposes novel thermodynamic efficiency indices as a resources reduction strategy. By selecting an optimal location for large-scale photovoltaic power generation (LSPPG), the same amount of resources (such as land space, materials, energy) will achieve higher utilisation efficiency. In this study, actual two-year solar radiation and temperature data were sourced from Nigerian Meteorological Agency, Abuja. A probability distribution modeling was used to generate statistical mean values for solar radiation and temperature based on the classical almost sure central limit theory. Then, Photovoltaic modeling and simulation code was used to simulate the power generation characteristics of the LSPPG. Comparative analyses of the results for a 5 MW (MW) LSPPG showed that statistical mean value of power generation, energy efficiency index and exergy efficiency index range from 0.76 to 0.99 MW, 1.315 to1.254 and 1.298 to1.237, respectively, across the locations studied. Overall, the thermodynamic efficiency indices can complement the current laboratory-based rating of the photovoltaic modules in order to establish the environmental, economic and policy rationales for sitting a LSPPG. This would ultimately improve the cradle-to-cradle management of LSPPG installations based on resources reduction strategy.

1. Introduction

Sustainable energy supply portfolio of the future would certainly include solar energy technologies because solar energy is environmentally benign, ubiquitous, renewable and vast in applications (Bukar and Tan, 2019; C. Ogbonnaya et al., 2019a; Penga et al., 2019). Notably, the subsisting Sustainable Development Goals (SDGs) of United Nations (UN, 2015) has specifically stated that renewable and clean energy should be explored for meeting diverse human needs. In particular, Goals 1 and 2 which focus on ending poverty and hunger would need energy as a critical enabler, particularly in developing countries. Goal 7 focuses on providing affordable and clean energy. Energy is crucial for furthering economic growth and industrial developments as expressed in Goals 8 and 9. Goal 12 focuses on achieving responsible consumption and production based on sustainable energy source; while Goal 13 focuses on the reduction of environmental impacts of energy production including climate change and global warming. In order to realise these goals, there is an urgent need to shift from the dependence on fossil fuels (e.g. coal, oil, gas) to renewable energy sources (solar, wind, geothermal, biomass, hydro, tidal, etc) (MacKay, 2009). Consequently, the utilisation of renewable energy resources would be fundamental in every country if the global goal of future 100% renewable energy supply must be achieved.

Recently, the Renewables 2019 Global Status Report (GSR) (REN21, 2018) indicates that solar photovoltaic (PV) constitutes

* Corresponding author. Department of Mechanical, Aerospace and Civil Engineering, The University of Manchester, M60 1QD, UK.
E-mail address: chukwuma.ogbonnaya@manchester.ac.uk (C. Ogbonnaya).

https://doi.org/10.1016/j.jclepro.2019.119405
0959-6526/

Solar Energy 185 (2019) 298–306

Contents lists available at ScienceDirect

Solar Energy

journal homepage: www.elsevier.com/locate/solener

Numerical integration of solar, electrical and thermal exergies of photovoltaic module: A novel thermophotovoltaic model

C. Ogbonnaya[a,c,*], A. Turan[a], C. Abeykoon[b]

[a] School of Mechanical, Aerospace and Civil Engineering, The University of Manchester, M60 1QD, UK
[b] Aerospace Research Institute, School of Materials, The University of Manchester, Oxford Road, M13 9PL, UK
[c] Faculty of Engineering and Technology, Alex Ekwueme Federal University Ndufu-Alike Ikwo, P.M.B. 1010, Nigeria

ARTICLE INFO

Keywords:
Photovoltaic module
Photovoltaic-thermal module
Modelling
Simulation
Thermodynamic analysis
Parametric study

ABSTRACT

Over the years, there have been efforts to understand the thermodynamics of solar cells so that the physics can be better improved. Heat generation in photovoltaic (PV) modules (which contain solar cells for direct electrical energy generation) has been acknowledged in many literatures as a key power degradation parameter. At the moment, an accurate modeling of photovoltaic power generation requires a computational iterative model since the output voltage of a PV creates a transcendental equation. This study uses code-based model (CBM) which allows user defined codes to implement a novel integration of solar, electrical and thermal exergies of photovoltaic module in order to create a thermophotovoltaic model. After integrating the proposed model in MATLAB, parametric studies were carried out to understand how changes in temperature and solar radiation affect the electrical and thermal exergy flows during power generation. Interestingly, results show that heat is essential for power generation although it should not exceed the critical value beyond which the voltage would start deteriorating. At 290 K, the electrical exergy flow of the 45 W PV module used in this study was 41.46 J/s and the overall improvement in exergy could be up to 51% if the waste heat generated is utilised for useful thermal work. The energy and exergy efficiencies of the PV module were initially the same but the energy efficiency degraded because of the reduction in the open circuit voltage (V_{oc}) as temperature increased. Lastly, insights from this study is purposed to increase the understanding of how electrical and thermal exergy flow pattern in the PV module can be managed to either stabilise its temperature through cooling and surface treatment or facilitate its heat recovery for photovoltaic-thermal applications.

1. Introduction

The growing interests and activities in renewable energy are strongly connected to the potential of renewable energy to complement and potentially substitute fossil fuels as energy sources (Akuru et al., 2017; Taibi et al., 2012). This is because greenhouse emissions from the combustion of fossil fuels during energy production are the major contributors to global warming and climate change (MacKay, 2009). Solar energy harvesting is often without emission during operation. Again, solar energy is the most sustainable, ubiquitous and clean renewable energy source (Eilabban et al., 2014). This explains the increasing focus on solar energy harvesting using different solar based technologies including solar thermal systems (Ozturk and Dincer, 2013) and photovoltaic systems (Roger and Jerry, 2005). Photovoltaic module (hereinafter referred to as either PV, PV module or module) has also been investigated by many researchers for its potential integration with electrolyser and fuel cell in hybrid systems for constant power generation (Ganguly et al., 2010; Meurer et al., 1999; Rekioua et al., 2014). Furthermore, the waste heat from the photovoltaic module has been targeted for recovery for useful thermal work such as heating water or air (Chow, 2010; Michael et al., 2015; Tripanagnostopoulos, 2007).

Presently, the major challenge with harvesting electrical energy with photovoltaic devices is that the electrical conversion efficiency drops with an increase in the temperature of solar cell (Acakpovi and Ben Hagan, 2013; Krismadinata et al., 2013). A study, (Gaitho et al., 2009), investigated the effect of thermal conductivity on the power characteristics of a single solar cell and observed that the efficiency of the silicon solar cell was high at mid-temperatures for a range of 297–360 K; while higher temperatures degraded its performance. Another study (Olivier Dupré et al., 2017) asserts that the temperature sensitivity of the open-circuit voltage (V_{oc}) and short circuit current (I_{sc}) needs a better understanding in order to tune the temperature

* Corresponding author at: School of Mechanical, Aerospace and Civil Engineering, The University of Manchester, M60 1QD, UK.
E-mail address: chukwuma.ogbonnaya@manchester.ac.uk (C. Ogbonnaya).

https://doi.org/10.1016/j.solener.2019.04.058
Received 22 February 2019; Received in revised form 1 April 2019; Accepted 16 April 2019
Available online 30 April 2019

Solar Energy 199 (2020) 521–529

Contents lists available at ScienceDirect

Solar Energy

journal homepage: www.elsevier.com/locate/solener

Robust code-based modeling approach for advanced photovoltaics of the future

C. Ogbonnaya[a,c,*], A. Turan[a], C. Abeykoon[b]

[a] Department of Mechanical, Aerospace and Civil Engineering, The University of Manchester, M13 9PL, UK
[b] Aerospace Research Institute, Department of Materials, The University of Manchester, Oxford Road, M13 9PL, UK
[c] Faculty of Engineering and Technology, Alex Ekwueme Federal University Ndufu-Alike Ikwo, P.M.B. 1010, Nigeria

ARTICLE INFO

Keywords:
Photovoltaic systems
Photovoltaic tools
Code-based modeling
Block-based modeling
Simulation

ABSTRACT

Modeling and simulation of photovoltaics help to reduce development costs, design turnaround time and facilitates better techno-economic decisions. However, there is a current need to generate new theories, algorithms, applications and software in order to increase the contribution of solar energy to the global energy supply. For future advancements in the field of photovoltaics, robust techniques for PV modeling, simulation, visualisation and design are required to overcome the limitations of the current approaches. This study proposes the Code-Based Modeling (CBM) approach as a potent approach to facilitate the study of PV technologies. Experimental data were synthesised and used for coding and training of the code-based (CB) model; followed by a validation of the trained model using commercial PV modules. Results clearly show that the model can repeatedly and reliably predict the short circuit current, maximum power point, open circuit voltage with 0%, < 2% and < 10% deviations, respectively. Furthermore, instances of the applicability of the CBM approach in the study of the thermodynamics of PV, solar cell materials characterisation, PV systems design and power monitoring were presented. Above all, CBM approach accepts user-defined functions and therefore presents new opportunities for scientists and engineers to advance model-based investigations of the photovoltaics beyond the current state-of-the-art.

1. Introduction

Research is actively being carried out on how photovoltaics can be applied as a clean source of energy because it does not emit greenhouse gases during operation (Bukar and Tan, 2019; Ogbonnaya et al., 2019a). The Renewables 2019 Global Status Report (GSR) (REN21, 2018) indicates that solar photovoltaic (PV) constitutes around 100 GW out of 2378 GW global renewable power capacity installed in 2018; which represents 55% of the renewable capacity additions in the year, followed by wind power (28%) and hydropower (11%). Apart from direct power generation with PV systems, PV could also become a primary power subsystem in integrated systems in the future. For instance, PV modules have been studied for integration with electrolysers, fuel cells and batteries for reliable power generation (Lehman and Chamberlin, 1991; Meurer et al., 1999; Özgirgin et al., 2015). Also, PV modules have been integrated with thermal absorbers to create photovoltaic-thermal (PV/T) systems to supply electricity and hot water (Avezov et al., 2011; Michael et al., 2015). The present trends in integrating PV as a power source; or as a subsystem of a hybrid system, suggest that the demand for software including PV models would increase in the future. As an example, the possibility of integrating a maximum power point tracking (MPPT) algorithm with an automotive-based software to optimise solar energy harvesting was designed and verified by (Cheddadi et al., 2018). Kolhe et al. (2019) also experimented with the use of PV systems for power ventilation system of electric cars. It is expected that more application-based studies would be facilitated by robust modeling and simulation approaches; howbeit, complemented by theoretical models and experimental results.

Presently, manufacturers provide limited information on the electrical and thermal characteristics of PV modules whilst omitting other useful information such as bandgap energy, photon-generated current, diode reverse saturation current, shunt resistance and ideality factor of the semiconductors (Villalva et al., 2009). So, in order to generate more information on the module, an accurate, repeatable and reliable computational model is required. Here, PV modeling approaches are classified into block-based modeling (BBM) (Bellia et al., 2014; El Hassouni et al., 2017; Krismadinata et al., 2013; Motahhir et al., 2018; Patel and Sharma, 2013; Zainal and Yusoff, 2016), code-based modeling (CBM)

* Corresponding author at: Department of Mechanical, Aerospace and Civil Engineering, The University of Manchester, M13 9PL, UK.
E-mail address: chukwuma.ogbonnaya@manchester.ac.uk (C. Ogbonnaya).

https://doi.org/10.1016/j.solener.2020.02.043
Received 22 June 2019; Received in revised form 29 November 2019; Accepted 10 February 2020

Thermal Science and Engineering Progress 13 (2019) 100390

Contents lists available at ScienceDirect

Thermal Science and Engineering Progress

journal homepage: www.elsevier.com/locate/tsep

The current and emerging renewable energy technologies for power generation in Nigeria: A review

C. Ogbonnaya[a,c,*], C. Abeykoon[b], U.M. Damo[a], A. Turan[a]

[a] School of Mechanical, Aerospace and Civil Engineering, The University of Manchester, M13 9PL, UK
[b] Aerospace Research Institute and Northwest Composite Centre, School of Materials, The University of Manchester, Oxford Road, M13 9PL, UK
[c] Faculty of Engineering and Technology, Alex Ekwueme Federal University Ndufu-Alike Ikwo, Nigeria

ARTICLE INFO

Keywords:
Renewable energy
Power generation
Distributed generation
Fuel cell
Hydrogen economy
Nigeria

ABSTRACT

Nigeria is the most populous country and the largest economy in the African continent; but its power sector is currently underdeveloped. Remarkably, its economic and energy security depend on dwindling fossil fuel reserves. Yet, the Nigerian landscape experiences an average daily solar intensity of 20.1 MJ/m^2/day; and the wind speed across the states ranges from 1.5 to 4.1 ms^{-1}; with potential for harnessing energy from biomass, geothermal and water. With a projected population of 300 million by 2050, the current 7566.2 MW electricity generation capacity would continue to impede socio-economic development of the nation. Presently, few studies have reported on the suitable renewable energy technologies (RETs) for Nigeria. This study, therefore, updates the current and emerging RETs for harnessing the abundant renewable energy resources in Nigeria. Furthermore, a critical discussion is made on the application of RETs in achieving sustainable development in the imminent hydrogen economy. Eventually, some recommendations are made; and, it can be stated that the RETs, particularly distributed hybrid/integrated power systems, should be promoted in Nigeria based on the availability of diverse renewable sources. Undoubtedly, it is timely for the Nigerian government to investigate the possible applications of the RETs to improve the nation's power generation capacity.

1. Introduction

Future energy supply needs to satisfy factors such as sustainability, economy, efficiency and low environmental impact in order to reduce global energy crises, climate change and energy poverty, simultaneously [1,2]. Presently, the efficiency of some of the renewable energy technologies (RETs) are yet to be optimised; but, demand for renewable energy (RE) sources has continued to increase globally because of its clean, sustainable, futuristic, environmentally benign and inexhaustible nature [1,3]. Focus on RETs by governments, industrialists and users means that the advancements of functional materials, technologies for harvesting, converting, storing and conserving energy from renewable sources would continue to increase [4]. Also, the attention on low carbon development would subsist as long as the emissions of greenhouse gases (GHG), which cause anthropogenic interferences on the climate system continue [2].

Meantime, the increasing world population and the escalating need to power more homes, offices, industries and public infrastructures have put more pressure on the conventional energy resources such as coal, lignite, natural gas, crude oil, etc. For instance, the current world population of 7.3 billion is expected to reach 8.5 billion by 2030, 9.7 billion by 2050 and 11.2 billion by 2100, according to UN DESA report [5]. In the same report, it was projected that India would become the largest country in population size surpassing China by 2022, while Nigeria could surpass the United States by 2050. Again, by 2050, six countries are expected to exceed 300 million: China, India, Indonesia, Nigeria, Pakistan, and the USA. World Bank [6] estimates that Nigeria has a population of 186 million as of 2016. Undoubtedly, these countries would have to expand the capacity of their energy infrastructure to cater for the growing population majorly with sustainable energy technologies suitable for low carbon development.

The current power generation capacity of Nigeria stands at 7,566.2 MW; and only 15.61% of this is generated from renewable sources while the rest is based on fossil fuels [7]. This capacity is certainly too small considering the potential of Nigeria for both conventional and renewable energy utilisation. In the last decade, some studies have been conducted to assess the potential of renewable energy resources (RERs) in Nigeria. Aliyu [8] and Mas'ud et al. [9] showed that RERs are available in African countries including Nigeria; but the failure to deploy suitable RETs is the greatest drawback in using RE to

* Corresponding author at: School of Mechanical, Aerospace and Civil Engineering, The University of Manchester, M13 9PL, UK.
E-mail address: chukwuma.ogbonnaya@manchester.ac.uk (C. Ogbonnaya).

https://doi.org/10.1016/j.tsep.2019.100390
Received 27 April 2019; Received in revised form 19 June 2019; Accepted 3 August 2019

Cleaner Environmental Systems 2 (2021) 100021

Contents lists available at ScienceDirect

Cleaner Environmental Systems

journal homepage: www.journals.elsevier.com/cleaner-environmental-systems

Engineering risk assessment of photovoltaic-thermal-fuel cell system using classical failure modes, effects and criticality analyses

C. Ogbonnaya [a,c,*], C. Abeykoon [b], A. Nasser [a], C.S. Ume [c], U.M. Damo [d], A. Turan [e]

[a] Department of Mechanical, Aerospace and Civil Engineering, The University of Manchester, M60 1QD, UK
[b] Aerospace Research Institute, Department of Materials, The University of Manchester, Oxford Road, M13 9PL, UK
[c] Faculty of Engineering and Technology, Alex Ekwueme Federal University Ndufu-Alike Ikwo, P.M.B. 1010, Nigeria
[d] Department of Mechanical, Aerospace and Civil Engineering, The University of Manchester, M13 9PL, UK
[e] Independent Researcher, Manchester, M22 4RS, Lancashire, UK

ARTICLE INFO

Keywords:
Renewable energy technology
Integrated photovoltaic-thermal-fuel cell system
Solar energy
Failure mode and effect analysis
Criticality analysis
Reliability

ABSTRACT

As renewable energy technologies (RETs) replace fossil fuel-based energy systems, the need to address the risks and reliability of emerging RETs suitable for integration into energy infrastructures becomes urgent. The intermittency of renewable energy sources and individual characteristics of the components of RETs are potential causes of power curtailment, system failure, techno-economic costs, and the inertia to transit to renewable energy utilisation. Here, we applied the classical failure modes, effects, and criticality analyses to assess the effects of failure modes of the components of an integrated photovoltaic-thermal-fuel cell system. Risk items were identified with their possible failure modes, mechanisms, and effects to generate risk priority numbers and Criticality values. Results showed that the risk of no solar radiation, hydrogen leakage, failure of photovoltaic module, leakage of oxygen had risk priority number of 450, 270, 240, 240 whilst their corresponding Criticality values were 90, 54, 80, 48, respectively. Generating power with both battery and fuel cell may improve the overall reliability of the system. Eventually, some recommendations were made to improve the system for off-grid and grid-connected applications to supply electrical energy and hot water. Therefore, addressing the identified risk items could significantly improve the reliability and operational efficiency the system.

1. Introduction

Solar energy technologies are probably the most sustainable renewable energy technologies (RETs) because of the ubiquity of solar radiation across the globe and the capability of solar energy technologies to operate with zero or minimal amount of greenhouse gases emissions (Ogbonnaya et al., 2019a; Schram et al., 2019). Nevertheless, the intermittent nature of solar radiation appears to pose prima facie risk and reliability concerns (Ogbonnaya et al., 2020a,b,c) given that reliability is a key component of users' requirements (Kececioglu et al., 2020). Over the last four decades, there have been research efforts to model, design, develop and optimise integrated photovoltaic-fuel cell systems for both grid (Lajnef et al., 2013) and off-grid applications (Dash and Bajpai, 2015; Rekioua et al., 2014) because of their environmental friendliness and relevance in the upcoming hydrogen economy. Photovoltaic-led energy systems will continue to dominate the composition of RETs for transition into 100% renewable energy infrastructure across the globe because of the decreasing cost of PV modules and promising conversion efficiencies of PV cells (IEA, 2020; Ogbonnaya et al., 2019a,b,c,d). An energy and exergy analysis of photovoltaic-led energy systems including photovoltaic-battery, photovoltaic-thermal-battery, photovoltaic-battery-fuel cell and photovoltaic-thermal-battery-fuel cell system showed that combining photovoltaic-thermal modules, batteries and fuel cell components could provide a robust energy storage system (Ogbonnaya et al., 2019a,b,c,d).

Although the risk and reliability aspects of an integrated photovoltaic-fuel cell (IPVFC) systems are often mentioned or implied as an important factor in their commercialisation and uptake (Ghosh et al., 2003; Volken et al., 2019), there are scarce studies that have systematically investigated their risks and reliability. An engineering risk analysis of RETs may focus on detailed analysis of the parts of a key component as exemplified by an engineering risk analysis of wind turbine (Colli, 2015; Kahrobaee and Asgarpoor, 2011) and PV module (Arabian-Hoseynabadi et al., 2010). Another approach, which is not common so far, is to consider all the active components of the system and their parts,

* Corresponding author. Department of Mechanical, Aerospace and Civil Engineering, The University of Manchester, M60 1QD, UK.
E-mail address: chukwuma.ogbonnaya@manchester.ac.uk (C. Ogbonnaya).

https://doi.org/10.1016/j.cesys.2021.100021
Received 13 January 2021; Received in revised form 29 January 2021; Accepted 26 February 2021

energies

MDPI

Article

Radiation-Thermodynamic Modelling and Simulating the Core of a Thermophotovoltaic System

Chukwuma Ogbonnaya [1,2,*], Chamil Abeykoon [3], Adel Nasser [1] and Ali Turan [4]

[1] Department of Mechanical, Aerospace and Civil Engineering, The University of Manchester, Manchester M60 1QD, UK; a.g.nasser@manchester.ac.uk
[2] Faculty of Engineering and Technology, Alex Ekwueme Federal University, Ndufu Alike Ikwo, Abakaliki PMB 1010, Nigeria
[3] Department of Materials, Aerospace Research Institute, The University of Manchester, Manchester M13 9PL, UK; chamil.abeykoon@manchester.ac.uk
[4] Independent Researcher, Manchester M22 4ES, Lancashire, UK; a.turan@ntlworld.com
* Correspondence: chukwuma.ogbonnaya@manchester.ac.uk; Tel.: +44-016-1306-3712

Received: 31 October 2020; Accepted: 20 November 2020; Published: 23 November 2020

check for updates

Abstract: Thermophotovoltaic (TPV) systems generate electricity without the limitations of radiation intermittency, which is the case in solar photovoltaic systems. As energy demands steadily increase, there is a need to improve the conversion dynamics of TPV systems. Consequently, this study proposes a novel radiation-thermodynamic model to gain insights into the thermodynamics of TPV systems. After validating the model, parametric studies were performed to study the dependence of power generation attributes on the radiator and PV cell temperatures. Our results indicated that a silicon-based photovoltaic (PV) module could produce a power density output, thermal losses, and maximum voltage of 115.68 W cm^{-2}, 18.14 W cm^{-2}, and 36 V, respectively, at a radiator and PV cell temperature of 1800 K and 300 K. Power density output increased when the radiator temperature increased; however, the open circuit voltage degraded when the temperature of the TPV cells increased. Overall, for an 80 W PV module, there was a potential for improving the power generation capacity by 45% if the TPV system operated at a radiator and PV cell temperature of 1800 K and 300 K, respectively. The thermal efficiency of the TPV system varied with the temperature of the PV cell and radiator.

Keywords: power generation; thermophotovoltaics; thermodynamics; radiation; parametric study

1. Introduction

Decarbonized energy infrastructure is urgently needed to reduce greenhouse gas emissions in order to mitigate the current impacts of global warming and climate change [1]. MacKay [2] stated that energy production processes are the highest contributor to greenhouse gas emissions. This is understandable because modern civilization cannot exist as it has without different forms of energy. However, the importance of generating energy sustainably has gone beyond academia to influence political, environmental, and economic decisions across the globe. This has motivated an aggressive search for clean energy technologies in order to implement the Paris Agreement, which seeks to reduce the threats of climate change by keeping the global temperature rise this century below 2 °C above pre-industrial levels and to limit the global temperature rise to 1.5 °C [3]. Ultimately, low-carbon energy technologies will strengthen the global response during the upcoming transition from fossil fuels to low-carbon energy infrastructure [4].

In the last three decades, the extraordinary innovations in photovoltaics have contributed to a reduction in life-cycle greenhouse gas emissions across the globe [5]. There has been intensive research development and novel applications of photovoltaics for harvesting energy because of their simple

mathematics

MDPI

Article

A Computational Approach to Solve a System of Transcendental Equations with Multi-Functions and Multi-Variables

Chukwuma Ogbonnaya [1,2,*], Chamil Abeykoon [3], Adel Nasser [1] and Ali Turan [4]

[1] Department of Mechanical, Aerospace and Civil Engineering, The University of Manchester, Manchester M13 9PL, UK; a.g.nasser@manchester.ac.uk
[2] Faculty of Engineering and Technology, Alex Ekwueme Federal University, Ndufu Alike Ikwo, Abakaliki PMB 1010, Nigeria
[3] Aerospace Research Institute and Northwest Composites Centre, School of Materials, The University of Manchester, Manchester M13 9PL, UK; chamil.abeykoon@manchester.ac.uk
[4] Independent Researcher, Manchester M22 4ES, Lancashire, UK; a.turan@ntlworld.com
* Correspondence: chukwuma.ogbonnaya@manchester.ac.uk; Tel.: +44-(0)74-3850-3799

Abstract: A system of transcendental equations (SoTE) is a set of simultaneous equations containing at least a transcendental function. Solutions involving transcendental equations are often problematic, particularly in the form of a system of equations. This challenge has limited the number of equations, with inter-related multi-functions and multi-variables, often included in the mathematical modelling of physical systems during problem formulation. Here, we presented detailed steps for using a code-based modelling approach for solving SoTEs that may be encountered in science and engineering problems. A SoTE comprising six functions, including Sine-Gordon wave functions, was used to illustrate the steps. Parametric studies were performed to visualize how a change in the variables affected the superposition of the waves as the independent variable varies from x_1 = 1:0.0005:100 to x_1 = 1:5:100. The application of the proposed approach in modelling and simulation of photovoltaic and thermophotovoltaic systems were also highlighted. Overall, solutions to SoTEs present new opportunities for including more functions and variables in numerical models of systems, which will ultimately lead to a more robust representation of physical systems.

Keywords: system of transcendental equation; computational solutions; code-based modelling approach; numerical analysis; Sine-Gordon equations; photovoltaics; thermophotovoltaics; solar energy

Citation: Ogbonnaya, C.; Abeykoon, C.; Nasser, A.; Turan, A. A Computational Approach to Solve a System of Transcendental Equations with Multi-Functions and Multi-Variables. *Mathematics* **2021**, *9*, 920. https://doi.org/10.3390/math9090920

Academic Editor: Maria Luminita Scutaru

Received: 2 April 2021
Accepted: 19 April 2021
Published: 21 April 2021

1. Introduction

The advent of the computer has made explicit solution and visualization of transcendental equations (TE) easier [1]. Computing has, indeed, expanded the possibilities of modelling and simulation of complex phenomena, processes, and systems [2]. However, encountering non-zero TE of the form f(x) = g(x) in science and engineering poses challenges, particularly when the TE is included in a system of equations to create a system of transcendental equations (SoTE). A TE may have many roots which may require explicit method to find their roots using Cauchy's integral theorem [3]. The computational solution to SoTE may result in a single output in a case where some functions act as functions of the output function. The output function can be represented graphically to visualize and analyze how it changes with respect to some system variables or functions in the SoTE.

In order to increase the number of variables and parameters of a physical system captured during numerical modelling, multi-functions may be required to be solved simultaneously. Consequently, more methods/techniques for solving SoTEs are required to facilitate numerical solutions of physical systems involving TE. Over the years, the need to solve problems involving TEs or SoTEs caused scientists and engineers to use different methods/techniques to find solutions to them [4]. For instance, Artificial Neural Network (ANN) has been proposed for solving SoTEs [5]. A Chebyshev series has been added

Cleaner Engineering and Technology 4 (2021) 100241

Contents lists available at ScienceDirect

Cleaner Engineering and Technology

journal homepage: www.sciencedirect.com/journal/cleaner-engineering-and-technology

Unitized regenerative proton exchange membrane fuel cell system for renewable power and hydrogen generation: Modelling, simulation, and a case study

C. Ogbonnaya [a,c,*], C. Abeykoon [b], A. Nasser [a], A. Turan [d]

[a] Department of Mechanical, Aerospace and Civil Engineering, The University of Manchester, M13 9PL, UK
[b] Aerospace Research Institute, Department of Materials, The University of Manchester, Oxford Road, M13 9PL, UK
[c] Faculty of Engineering and Technology, Alex Ekwueme Federal University Ndufu-Alike Ikwo, P.M.B. 1010, Nigeria
[d] Independent Researcher, Manchester, Lancashire, M22 4ES, United Kingdom

ARTICLE INFO

Keywords:
Power hysteresis effect
Unitized regenerative proton exchange membrane fuel cells
Modelling and simulation
Hydrogen energy
Zero emission
Photovoltaic

ABSTRACT

Unitized regenerative proton exchange membrane fuel cell (URPEMFC) performs the functions of an electrolyser and a fuel cell. Currently, power hysteresis effect (PHE) is a key technological challenge for the URPEMFC because it reduces the efficiency of the system as it switches from electrolyser mode to fuel cell mode and vice versa. Here, a modelling and simulation approach is used to investigate the PHE based on its thermodynamic and electrochemical attributes. URPEMFC model was validated against an experimental study and then used for parametric studies. The results indicate that the PHE occurs when the number of cells is 1, 5 and 10. Moreover, an increase in the lost internal current density and total resistance resulted in an increase in overpotentials of the system. Although the theoretical thermodynamic efficiency of a URPEMFC is about 68.86%, the current study predicted an efficiency of 44% for a stack of 10 cells at current density of 0.5 A cm^{-2}. A case study of an integrated photovoltaic-URPEMFC system for power generation using actual meteorological data is also presented. If optimised, URPEMFC can be applied with renewable energy sources for power-to-gas technologies, power-to-power technologies, hydrogen filling stations or distributed hybrid energy systems.

1. Introduction

Hydrogen presents an opportunity for sustainable energy generation particularly in conjunction with renewable energy sources such as solar energy and feedstocks such as water or biomass (Dinçer and Joshi, 2013). Hydrogen exists in nature in organic (coal, oil, gas, biomass, etc) and inorganic (water) compounds because of its high reactivity. The imminent "hydrogen economy" (Muradov and Veziroğ;lu, 2005) in which energy supply would depend on hydrogen is attractive because the combustion of hydrogen produces water and heat, which will not have a substantial adverse environmental impact. This implies that the anthropogenic impact of fossil fuel production (Umar et al., 2021) and combustion including pollution, global warming and climate change can be ameliorated by using renewable hydrogen-based energy systems. However, there are current issues with the storage and transportation of hydrogen from the point of production to the end-users; hence, the so-called "hydrogen economy" still faces huge infrastructural challenges (Ogden, 1999). Thus, the limitations posed by current means of hydrogen production, storage, transportation, and utilisation are current issues (Abdalla et al., 2018).

Nevertheless, the ubiquity of renewable energy sources particularly solar energy and the future direction of solar hydrogen indicates that hydrogen can be produced using distributed systems such that hydrogen can be generated at the location where it is needed (Aouali et al., 2014), without relying on a central hydrogen infrastructure. Currently, steam reforming process and water gas shift reaction using feedstocks such as gas, oil, coal, and biomass remain the major sources of hydrogen production (Izquierdo et al., 2012). Gnanapragasam et al. (2010) proposed that carbon capture can be used to reduce the emission of CO_2 during hydrogen production through coal gasification. Nowadays, in order to reduce the associated greenhouse gas emissions from hydrogen production using fossil fuels, the use of renewable resources and environment friendly feedstocks have become subjects of intensive research (Joshi et al., 2011).

* Corresponding author. Department of Mechanical, Aerospace and Civil Engineering, The University of Manchester, M13 9PL, UK.
E-mail address: chukwuma.ogbonnaya@manchester.ac.uk (C. Ogbonnaya).

https://doi.org/10.1016/j.clet.2021.100241
Received 14 October 2020; Received in revised form 8 June 2021; Accepted 6 August 2021
Available online 8 August 2021

energies

MDPI

Review

Prospects of Integrated Photovoltaic-Fuel Cell Systems in a Hydrogen Economy: A Comprehensive Review

Chukwuma Ogbonnaya [1,2,*], Chamil Abeykoon [3], Adel Nasser [1], Ali Turan [4] and Cyril Sunday Ume [2]

[1] Department of Mechanical, Aerospace and Civil Engineering, The University of Manchester, Manchester M60 1QD, UK; a.g.nasser@manchester.ac.uk
[2] Faculty of Engineering and Technology, Alex Ekwueme, Federal University Ndufu Alike Ikwo, Abakaliki PMB 1010, Nigeria; cyril.ume@funai.edu.ng
[3] Department of Materials, Aerospace Research Institute, The University of Manchester, Oxford Road, Manchester M13 9PL, UK; chamil.abeykoon@manchester.ac.uk
[4] Independent Researcher, Manchester M22 4ES, UK; a.turan@ntlworld.com
* Correspondence: chukwuma.ogbonnaya@manchester.ac.uk; Tel.: +44-0-74385-03799; Fax: +44-0-16130-63712

Abstract: Integrated photovoltaic-fuel cell (IPVFC) systems, amongst other integrated energy generation methodologies are renewable and clean energy technologies that have received diverse research and development attentions over the last few decades due to their potential applications in a hydrogen economy. This article systematically updates the state-of-the-art of IPVFC systems and provides critical insights into the research and development gaps needed to be filled/addressed to advance these systems towards full commercialization. Design methodologies, renewable energy-based microgrid and off-grid applications, energy management strategies, optimizations and the prospects as self-sustaining power sources were covered. IPVFC systems could play an important role in the upcoming hydrogen economy since they depend on solar hydrogen which has almost zero emissions during operation. Highlighted herein are the advances as well as the technical challenges to be surmounted to realize numerous potential applications of IPVFC systems in unmanned aerial vehicles, hybrid electric vehicles, agricultural applications, telecommunications, desalination, synthesis of ammonia, boats, buildings, and distributed microgrid applications.

Keywords: solar energy; photovoltaic-fuel cell system; integrated energy system; power generation; hydrogen energy; hydrogen economy; zero emissions; photovoltaics; fuel cells

Citation: Ogbonnaya, C.; Abeykoon, C.; Nasser, A.; Turan, A.; Ume, C.S. Prospects of Integrated Photovoltaic-Fuel Cell Systems in a Hydrogen Economy: A Comprehensive Review. *Energies* **2021**, *14*, 6827. https://doi.org/10.3390/en14206827

Academic Editor: Adalgisa Sinicropi

Received: 27 September 2021
Accepted: 8 October 2021
Published: 19 October 2021

1. Introduction

Globally, there is an increasing emphasis on the decarbonization of economies and a quicker transition from the use of fossil fuels to renewable energy resources to mitigate the unravelling risks posed by the anthropogenic interferences on the climatic systems from the inception of the first industrial revolution. As the political will to adopt and scale-up clean energy technologies (CETs) increases across the globe, there is an urgent need to facilitate the technological transition by developing novel CETs or optimizing the existing ones. Of all the renewable energy resources available to mankind (including solar, hydro, wind, geothermal, biomass, tidal, etc.), solar energy appears to be the most sustainable because it is inexhaustible, ubiquitous across the globe, and it is not subject to price controls, unlike fossil fuels. Because of this, renewable energy technologies (RETs) that use solar energy as a prime mover will continue to attract research and development attention because they can be deployed across the globe. One of such RETs is integrated photovoltaic-fuel cell (IPVFC) system, which uses photovoltaics and fuel cells to majorly generate power and hydrogen, using solar energy as the prime mover.

In 1988, Rahman and Tam [1] investigated the feasibility of grid-connected and stand-alone applications of IPVFC systems and reported that their prototype, which was tested in the United States and Japan, could create new possibilities of combining photovoltaic (PV)

References

[1] Bollen M, Hassan F. Integration of Distributed Generation in the Power System. 2011. https://doi.org/10.1002/9781118029039.

[2] Greene LA. United nations framework convention on climate change. Environ Health Perspect 2000;108.

[3] REN21. Renewables 2017: global status report. vol. 72. 2017. https://doi.org/10.1016/j.rser.2016.09.082.

[4] Morales Pedraza J. Electrical Energy Generation in Europe. 2015. https://doi.org/10.1007/978-3-319-16083-2.

[5] General Assembly, United Nations. Transforming our world: The 2030 agenda for sustainable development. Https//SustainabledevelopmentUnOrg/Content/Documents/7891Transforming%20Our%20World Pdf 2015:1–5. https://doi.org/10.1007/s13398-014-0173-7.2.

[6] IEA. World Energy Outlook. Paris: 2020.

[7] World Bank. World Development Indicators 2013. 2013. https://doi.org/10.1596/978-0-8213-9824-1.

[8] TCN. National statistics for power generation and supply. Transm Co Niger 2018. http://www.tcnorg.com/ (accessed April 12, 2018).

[9] Comodi G, Bartolini A, Carducci F, Nagaranjan B, Romagnoli A. Achieving low carbon local energy communities in hot climates by exploiting networks synergies in multi energy systems. Appl Energy 2019. https://doi.org/10.1016/j.apenergy.2019.113901.

[10] Rajashekara K. Hybrid fuel-cell strategies for clean power generation. IEEE Trans Ind Appl 2005. https://doi.org/10.1109/TIA.2005.847293.

[11] Mario L. Ferrari, Usman M. Damo, Ali Turan DS. Hybrid Systems Based on Solid Oxide Fuel Cells: Modelling and Design. Wiley 2017.

[12] Gebre TS. Fuel Cell Assisted PhotoVoltaic Power Systems. Norwegian University of Science and Technology, 2012.

[13] Silva SB, Severino MM, De Oliveira MAG. A stand-alone hybrid photovoltaic, fuel cell and battery system: A case study of Tocantins, Brazil. Renew Energy 2013. https://doi.org/10.1016/j.renene.2013.02.004.

[14] Damo UM, Ferrari ML, Turan A, Massardo AF. Solid oxide fuel cell hybrid system: A detailed review of an environmentally clean and efficient source of energy. Energy 2019:235–46. https://doi.org/10.1016/j.energy.2018.11.091.

[15] Ozturk M, Dincer I. Thermodynamic analysis of a solar-based multi-generation system with hydrogen production. Appl Therm Eng 2013;51:1235–44. https://doi.org/10.1016/j.applthermaleng.2012.11.042.

[16] Cano A, Jurado F, Sánchez H, Fernández LM, Castañeda M. Optimal sizing of stand-alone hybrid systems based on PV/WT/FC by using several methodologies. J Energy Inst 2014. https://doi.org/10.1016/j.joei.2014.03.028.

[17] Bukar AL, Tan CW. A review on stand-alone photovoltaic-wind energy system with fuel cell: System optimization and energy management strategy. J Clean Prod 2019;221:73–88. https://doi.org/10.1016/j.jclepro.2019.02.228.

[18] Bukar AL, Tan CW, Lau KY. Optimal sizing of an autonomous photovoltaic/wind/battery/diesel generator microgrid using grasshopper optimization algorithm. Sol Energy 2019;188:685–96. https://doi.org/10.1016/j.solener.2019.06.050.

[19] Rahman S, Tam K sur. A feasibility study of photovoltaic-fuel cell hybrid energy system. IEEE Trans Energy Convers 1988;3:50–5. https://doi.org/10.1109/60.4199.

[20] Contino F, Moret S, Limpens G, Jeanmart H. Whole-energy system models: The advisors for the energy transition. Prog Energy Combust Sci 2020. https://doi.org/10.1016/j.pecs.2020.100872.

[21] Yilanci A, Dincer I, Ozturk HK. A review on solar-hydrogen/fuel cell hybrid energy systems for stationary applications. Prog Energy Combust Sci 2009;35:231–44. https://doi.org/10.1016/j.pecs.2008.07.004.

[22] Shaygan M, Ehyaei MA, Ahmadi A, Assad MEH, Silveira JL. Energy, exergy, advanced exergy and economic analyses of hybrid polymer electrolyte membrane (PEM) fuel cell and photovoltaic cells to produce hydrogen and electricity. J Clean Prod 2019. https://doi.org/10.1016/j.jclepro.2019.06.298.

[23] Winterbone DE, Turan A. Availability and Exergy. 2015. https://doi.org/10.1016/B978-0-444-63373-6.00004-6.

[24] Cetin E, Yilanci A, Oner Y, Colak M, Kasikci I, Ozturk HK. Electrical analysis of a hybrid photovoltaic-hydrogen/fuel cell energy system in Denizli, Turkey. Energy Build 2009. https://doi.org/10.1016/j.enbuild.2009.04.004.

[25] Lokar J, Virtič P. The potential for integration of hydrogen for complete energy self-sufficiency in residential buildings with photovoltaic and battery storage systems. Int J Hydrogen Energy 2020. https://doi.org/10.1016/j.ijhydene.2020.04.170.

[26] Hassani H, Rekioua D, Aissou S, Bacha S, Zaouche F. Hybrid stand-alone photovoltaic/batteries/fuel cells system for green cities. Proc. 2018 6th Int. Renew. Sustain. Energy Conf. IRSEC 2018, 2018. https://doi.org/10.1109/IRSEC.2018.8702278.

[27] Mohammad Bagher A. Types of Solar Cells and Application. Am J Opt Photonics 2015;3:94. https://doi.org/10.11648/j.ajop.20150305.17.

[28] Michael JJ, S I, Goic R. Flat plate solar photovoltaic-thermal (PV/T) systems: A reference guide. Renew Sustain Energy Rev 2015;51:62–88. https://doi.org/10.1016/j.rser.2015.06.022.

[29] Meurer C, Barthels H, Brocke WA, Emonts B, Groehn HG. PHOEBUS—an autonomous supply system with renewable energy: six years of operational experience and advanced concepts. Sol Energy 1999;67:131–8. https://doi.org/10.1016/S0038-092X(00)00043-8.

[30] Jayalakshmi NS. Study of hybrid photovoltaic/fuel cell system for stand-alone applications. Curr. Trends Futur. Dev. Membr. Renew. Energy Integr. with Membr. Oper., 2018. https://doi.org/10.1016/B978-0-12-813545-7.00009-X.

[31] Amin, Bambang RT, Rohman AS, Dronkers CJ, Ortega R, Sasongko A. Energy

management of fuel cell/battery/supercapacitor hybrid power sources using model predictive control. IEEE Trans Ind Informatics 2014. https://doi.org/10.1109/TII.2014.2333873.

[32] Ferrari ML, Damo UM, Turan A SD. Hybrid Systems Based on Solid Oxide Fuel Cells: Modelling and Design. Sussex: John Wiley and Sons Ltd; 2017.

[33] Maggio G, Nicita A, Squadrito G. How the hydrogen production from RES could change energy and fuel markets: A review of recent literature. Int J Hydrogen Energy 2019;44:11371–84. https://doi.org/10.1016/j.ijhydene.2019.03.121.

[34] Staffell I, Scamman D, Velazquez Abad A, Balcombe P, Dodds PE, Ekins P, et al. The role of hydrogen and fuel cells in the global energy system. Energy Environ Sci 2019. https://doi.org/10.1039/c8ee01157e.

[35] Holladay JD, Hu J, King DL, Wang Y. An overview of hydrogen production technologies. Catal Today 2009;139:244–60. https://doi.org/10.1016/j.cattod.2008.08.039.

[36] Ogbonnaya C, Abeykoon C, Nasser A, Turan A. Prospects of Integrated Photovoltaic-Fuel Cell Systems in a Hydrogen Economy : A Comprehensive Review 2021:1–33.

[37] Cengel, Yunus; Turner R; CJ. Fundamentals of Thermal-Fluid Sciences. Third Edit. New York: McGraw Hill; 2008.

[38] U.S. Central Intelligence Agency. CIA: The World Factbook: Saudi Arabia. CIA World Fact Book 2014. https://www.cia.gov/library/publications/the-world-factbook/geos/sa.html.

[39] Egeland-Eriksen T, Hajizadeh A, Sartori S. Hydrogen-based systems for integration of renewable energy in power systems: Achievements and perspectives. Int J Hydrogen Energy 2021;46:31963–83. https://doi.org/10.1016/j.ijhydene.2021.06.218.

[40] Dowling JA, Rinaldi KZ, Ruggles TH, Davis SJ, Yuan M, Tong F, et al. Role of Long-Duration Energy Storage in Variable Renewable Electricity Systems. Joule 2020;4:1907–28. https://doi.org/10.1016/j.joule.2020.07.007.

[41] Colbertaldo P, Agustin SB, Campanari S, Brouwer J. Impact of hydrogen energy storage on California electric power system: Towards 100% renewable electricity. Int J Hydrogen Energy 2019;44:9558–76. https://doi.org/10.1016/j.ijhydene.2018.11.062.

[42] de Sisternes FJ, Jenkins JD, Botterud A. The value of energy storage in decarbonizing the electricity sector. Appl Energy 2016;175:368–79. https://doi.org/10.1016/j.apenergy.2016.05.014.

[43] Tlili N, Neily B, Ben Salem F. Modeling and simulation of hybrid system coupling a photovoltaic generator, a PEM fuel cell and an electrolyzer (Part II). 2014 IEEE 11th Int. Multi-Conference Syst. Signals Devices, SSD 2014, 2014. https://doi.org/10.1109/SSD.2014.6808809.

[44] Arshad A, Ali HM, Habib A, Bashir MA, Jabbal M, Yan Y. Energy and exergy analysis of fuel cells: A review. Therm Sci Eng Prog 2019;9:308–21. https://doi.org/10.1016/j.tsep.2018.12.008.

[45] Ogbonnaya C, Turan A, Abeykoon C. Energy and exergy e ffi ciencies enhancement

analysis of integrated photovoltaic-based energy systems. J Energy Storage 2019;26:101029. https://doi.org/10.1016/j.est.2019.101029.

[46] Sharaf OZ, Orhan MF. An overview of fuel cell technology: Fundamentals and applications. Renew Sustain Energy Rev 2014;32:810–53. https://doi.org/10.1016/j.rser.2014.01.012.

[47] Wilberforce T, El-Hassan Z, Khatib FN, Al Makky A, Baroutaji A, Carton JG, et al. Developments of electric cars and fuel cell hydrogen electric cars. Int J Hydrogen Energy 2017. https://doi.org/10.1016/j.ijhydene.2017.07.054.

[48] Das HS, Tan CW, Yatim AHM. Fuel cell hybrid electric vehicles: A review on power conditioning units and topologies. Renew Sustain Energy Rev 2017. https://doi.org/10.1016/j.rser.2017.03.056.

[49] Whiteman ZS, Bubna P, Prasad AK, Ogunnaike BA. Design, operation, control, and economics of a photovoltaic/fuel cell/battery hybrid renewable energy system for automotive applications. Processes 2015. https://doi.org/10.3390/pr3020452.

[50] Kalogirou SA. Solar thermal collectors and applications. Prog Energy Combust Sci 2004. https://doi.org/10.1016/j.pecs.2004.02.001.

[51] Ogbonnaya C, Abeykoon C, Nasser A, Ume CS, Damo UM, Turan A. Engineering risk assessment of photovoltaic-thermal-fuel cell system using classical failure modes , effects and criticality analyses. Clean Environ Syst 2021;2:100021. https://doi.org/10.1016/j.cesys.2021.100021.

[52] Burke KA, Jakupca I. Unitized regenerative fuel cell system gas storage/radiator development. SAE Tech. Pap., 2004. https://doi.org/10.4271/2004-01-3168.

[53] Millet P, Ngameni R, Grigoriev SA, Fateev VN. Scientific and engineering issues related to PEM technology: Water electrolysers, fuel cells and unitized regenerative systems. Int J Hydrogen Energy 2011. https://doi.org/10.1016/j.ijhydene.2010.06.106.

[54] Ogbonnaya C, Abeykoon C, Nasser A, Turan A. Unitized regenerative proton exchange membrane fuel cell system for renewable power and hydrogen generation: Modelling, simulation, and a case study. Clean Eng Technol 2021;4:100241. https://doi.org/10.1016/j.clet.2021.100241.

[55] Kauranen PS, Lund PD, Vanhanen JP. Development of a self-sufficient solar-hydrogen energy system. Int J Hydrogen Energy 1994. https://doi.org/10.1016/0360-3199(94)90181-3.

[56] Grasse W, Oster F, Aba-Oud H. HYSOLAR: The German-Saudi Arabian program on solar hydrogen-5 years of experience. Int J Hydrogen Energy 1992. https://doi.org/10.1016/0360-3199(92)90215-I.

[57] Ulleberg O. Stand-alone power systems for the future: optimal design, operation and control of solar-hydrogen energy systems. Norwegian University of Science and Technology Trondheim, 1998.

[58] Friberg R. A photovoltaic solar-hydrogen power plant for rural electrification in India. Part 1: a general survey of technologies applicable within the solar-hydrogen concept. Int J Hydrogen Energy 1993. https://doi.org/10.1016/0360-3199(93)90140-6.

[59] Goetzberger A, Bopp G, GrieBhaber W, Stahl W. PV/Hydrogen/Oxygen-System of

the self-sufficient solar house Freiburg. Conf. Rec. IEEE Photovolt. Spec. Conf., 1993. https://doi.org/10.1109/pvsc.1993.346960.

[60] Hwang JJ, Lai LK, Wu W, Chang WR. Dynamic modeling of a photovoltaic hydrogen fuel cell hybrid system. Int J Hydrogen Energy 2009. https://doi.org/10.1016/j.ijhydene.2009.09.100.

[61] El-Shatter TF, Eskandar MN, El-Hagry MT. Hybrid PV/fuel cell system design and simulation. Renew Energy 2002;27:479–85. https://doi.org/10.1016/S0960-1481(01)00062-3.

[62] Choi HJ, Park SJ, Choi JS, Cha IS, Yoon JP, Suh JS, et al. An analysis of PEMFC & photovoltaic 500W hybrid system. 7th Internatonal Conf. Power Electron. ICPE'07, 2007. https://doi.org/10.1109/ICPE.2007.4692442.

[63] Abou El-Maaty M. Abd El-Aal. Modelling and Simulation of a Photovoltaic Fuel Cell Hybrid System. University of Kassel, 2005.

[64] Zervas PL, Sarimveis H, Palyvos JA, Markatos NCG. Model-based optimal control of a hybrid power generation system consisting of photovoltaic arrays and fuel cells. J Power Sources 2008. https://doi.org/10.1016/j.jpowsour.2007.11.067.

[65] Thounthong P, Luksanasakul A, Koseeyaporn P, Davat B. Intelligent model-based control of a standalone photovoltaic/fuel cell power plant with supercapacitor energy storage. IEEE Trans Sustain Energy 2013. https://doi.org/10.1109/TSTE.2012.2214794.

[66] Chávez-Ramírez AU, Cruz JC, Espinosa-Lumbreras R, Ledesma-García J, Durón-Torres SM, Arriaga LG. Design and set up of a hybrid power system (PV-WT-URFC) for a stand-alone application in Mexico. Int. J. Hydrogen Energy, 2013. https://doi.org/10.1016/j.ijhydene.2012.11.019.

[67] Ganguly A, Misra D, Ghosh S. Modeling and analysis of solar photovoltaic-electrolyzer-fuel cell hybrid power system integrated with a floriculture greenhouse. Energy Build 2010;42:2036–43. https://doi.org/10.1016/j.enbuild.2010.06.012.

[68] Karami N, Moubayed N, Outbib R. Energy management for a PEMFC-PV hybrid system. Energy Convers Manag 2014. https://doi.org/10.1016/j.enconman.2014.02.070.

[69] Padmanaban S, Priyadarshi N, Bhaskar MS, Holm-Nielsen JB, Hossain E, Azam F. A Hybrid Photovoltaic-Fuel Cell for Grid Integration with Jaya-Based Maximum Power Point Tracking: Experimental Performance Evaluation. IEEE Access 2019. https://doi.org/10.1109/ACCESS.2019.2924264.

[70] Touati S, Belkaid A, Benabid R, Halbaoui K, Chelali M. Pre-feasibility design and simulation of hybrid PV/fuel cell energy system for application to desalination plants loads. Procedia Eng., 2012. https://doi.org/10.1016/j.proeng.2012.01.1216.

[71] Lajnef T, Abid S, Ammous A. Modeling, control, and simulation of a solar hydrogen/fuel cell hybrid energy system for grid-connected applications. Adv Power Electron 2013;2013. https://doi.org/10.1155/2013/352765.

[72] Hajizadeh A, Tesfahunegn SG, Undeland TM. Intelligent control of hybrid photo voltaic/fuel cell/energy storage power generation system. J Renew Sustain Energy 2011. https://doi.org/10.1063/1.3618743.

[73] Dash V, Bajpai P. Power management control strategy for a stand-alone solar

photovoltaic-fuel cell-battery hybrid system. Sustain Energy Technol Assessments 2015;9:68–80. https://doi.org/10.1016/j.seta.2014.10.001.

[74] Majidi M, Nojavan S, Zare K. Optimal stochastic short-term thermal and electrical operation of fuel cell/photovoltaic/battery/grid hybrid energy system in the presence of demand response program. Energy Convers Manag 2017. https://doi.org/10.1016/j.enconman.2017.04.051.

[75] Zhang X, Liu L, Dai Y. Fuzzy state machine energy management strategy for hybrid electric UAVs with PV/Fuel cell/battery power system. Int J Aerosp Eng 2018. https://doi.org/10.1155/2018/2852941.

[76] Ghenai C, Bettayeb M. Grid-Tied Solar PV/Fuel Cell Hybrid Power System for University Building. Energy Procedia, 2019. https://doi.org/10.1016/j.egypro.2018.12.025.

[77] Sharma RK, Mishra S. Dynamic Power Management and Control of a PV PEM Fuel-Cell-Based Standalone ac/dc Microgrid Using Hybrid Energy Storage. IEEE Trans. Ind. Appl., 2018. https://doi.org/10.1109/TIA.2017.2756032.

[78] Lee B, Kwon S, Park P, Kim K. Active power management system for an unmanned aerial vehicle powered by solar cells, a fuel cell, and batteries. IEEE Trans Aerosp Electron Syst 2014. https://doi.org/10.1109/TAES.2014.130468.

[79] Srisiriwat A, Pirom W. Feasibility Study of Seawater Electrolysis for Photovoltaic/Fuel Cell Hybrid Power System for the Coastal Areas in Thailand. IOP Conf. Ser. Mater. Sci. Eng., 2017. https://doi.org/10.1088/1757-899X/241/1/012041.

[80] Castañeda M, Cano A, Jurado F, Sánchez H, Fernández LM. Sizing optimization, dynamic modeling and energy management strategies of a stand-alone PV/hydrogen/battery-based hybrid system. Int J Hydrogen Energy 2013. https://doi.org/10.1016/j.ijhydene.2013.01.080.

[81] Hassani H, Zaouche F, Rekioua D, Belaid S, Rekioua T, Bacha S. Feasibility of a standalone photovoltaic/battery system with hydrogen production. J Energy Storage 2020. https://doi.org/10.1016/j.est.2020.101644.

[82] Temiz M, Javani N. Design and analysis of a combined floating photovoltaic system for electricity and hydrogen production. Int J Hydrogen Energy 2020. https://doi.org/10.1016/j.ijhydene.2018.12.226.

[83] Kafetzis A, Ziogou C, Panopoulos KD, Papadopoulou S, Seferlis P, Voutetakis S. Energy management strategies based on hybrid automata for islanded microgrids with renewable sources, batteries and hydrogen. Renew Sustain Energy Rev 2020;134:110118. https://doi.org/10.1016/j.rser.2020.110118.

[84] Elmouatamid A, Ouladsine R, Bakhouya M, Kamoun N El, Khaidar M, Zine-Dine K. Review of control and energy management approaches in micro-grid systems. Energies 2021;14. https://doi.org/10.3390/en14010168.

[85] González I, Calderón AJ, Portalo JM. Innovative multi-layered architecture for heterogeneous automation and monitoring systems: Application case of a photovoltaic smart microgrid. Sustain 2021;13:1–24. https://doi.org/10.3390/su13042234.

[86] Szyszka A. Ten years of solar hydrogen demonstration project at Neunburg vorm Wald, Germany. Int J Hydrogen Energy 1998. https://doi.org/10.1016/S0360-

3199(97)00172-9.

[87] Ghosh PC, Emonts B, Janßen H, Mergel J, Stolten D. Ten years of operational experience with a hydrogen-based renewable energy supply system. Sol Energy 2003;75:469–78. https://doi.org/10.1016/j.solener.2003.09.006.

[88] Natarajan SK, Kamran F, Ragavan N, Rajesh R, Jena RK, Suraparaju SK. Analysis of PEM hydrogen fuel cell and solar PV cell hybrid model. Mater Today Proc 2019;17:246–53. https://doi.org/10.1016/j.matpr.2019.06.426.

[89] Adi VSK, Chang CT. Development of flexible designs for PVFC hybrid power systems. Renew Energy 2015. https://doi.org/10.1016/j.renene.2014.08.002.

[90] Ahmadi P, Dincer I, Rosen MA. Transient thermal performance assessment of a hybrid solar-fuel cell system in Toronto, Canada. Int J Hydrogen Energy 2015. https://doi.org/10.1016/j.ijhydene.2014.11.047.

[91] Ogbonnaya C, Turan A, Abeykoon C. Numerical integration of solar, electrical and thermal exergies of photovoltaic module: A novel thermophotovoltaic model. Sol Energy 2019;185. https://doi.org/10.1016/j.solener.2019.04.058.

[92] Ünlü H. A thermodynamic model for determining pressure and temperature effects on the bandgap energies and other properties of some semiconductors. Solid State Electron 1992;35:1343–52. https://doi.org/10.1016/0038-1101(92)90170-H.

[93] Bellia H, Youcef R, Fatima M. A detailed modeling of photovoltaic module using MATLAB. NRIAG J Astron Geophys 2014;3:53–61. https://doi.org/10.1016/j.nrjag.2014.04.001.

[94] Muhammad FF, Yahya MY, Hameed SS, Aziz F, Sulaiman K, Rasheed MA, et al. Employment of single-diode model to elucidate the variations in photovoltaic parameters under different electrical and thermal conditions. PLoS One 2017;12:e0182925. https://doi.org/10.1371/journal.pone.0182925.

[95] Zeitouny J, Katz EA, Dollet A, Vossier A. Band gap engineering of multi-junction solar cells: Effects of series resistances and solar concentration. Sci Rep 2017;7. https://doi.org/10.1038/s41598-017-01854-6.

[96] Spiegel C. PEM Fuel Cell Modeling and Simulation Using Matlab. 2008. https://doi.org/10.1016/B978-0-12-374259-9.X5001-0.

[97] Barbir F. PEM fuel cells: theory and practice. 2005. https://doi.org/10.1016/B978-012078142-3/50013-6.

[98] Khemariya M, Mittal A, Baredar P, Singh A. Cost and size optimization of solar photovoltaic and fuel cell based integrated energy system for un-electrified village. J Energy Storage 2017. https://doi.org/10.1016/j.est.2017.09.011.

[99] Moghaddam S, Bigdeli M, Moradlou M, Siano P. Designing of stand-alone hybrid PV/wind/battery system using improved crow search algorithm considering reliability index. Int J Energy Environ Eng 2019. https://doi.org/10.1007/s40095-019-00319-y.

[100] Elgammal AAA, Sharaf AM. Self-regulating particle swarm optimised controller for (photovoltaic-fuel cell) battery charging of hybrid electric vehicles. IET Electr Syst Transp 2012. https://doi.org/10.1049/iet-est.2011.0021.

[101] Kannayeram G, Prakash NB, Muniraj R. Intelligent hybrid controller for power flow

management of PV/battery/FC/SC system in smart grid applications. Int J Hydrogen Energy 2020. https://doi.org/10.1016/j.ijhydene.2020.05.149.

[102] MacKay DJ. Sustainable Energy — without the hot air. UIT Cambridge Ltd 2009:383. https://doi.org/10.1109/PES.2004.1373296.

[103] Glavin ME, Chan PKW, Armstrong S, Hurley WG. A stand-alone photovoltaic supercapacitor battery hybrid energy storage system. 2008 13th Int. Power Electron. Motion Control Conf. EPE-PEMC 2008, 2008. https://doi.org/10.1109/EPEPEMC.2008.4635510.

[104] Hadidian Moghaddam MJ, Kalam A, Nowdeh SA, Ahmadi A, Babanezhad M, Saha S. Optimal sizing and energy management of stand-alone hybrid photovoltaic/wind system based on hydrogen storage considering LOEE and LOLE reliability indices using flower pollination algorithm. Renew Energy 2019. https://doi.org/10.1016/j.renene.2018.09.078.

[105] Dufo-López R, Bernal-Agustín JL, Yusta-Loyo JM, Domínguez-Navarro JA, Ramírez-Rosado IJ, Lujano J, et al. Multi-objective optimization minimizing cost and life cycle emissions of stand-alone PV-wind-diesel systems with batteries storage. Appl Energy 2011. https://doi.org/10.1016/j.apenergy.2011.04.019.

[106] Lu Q, Zhou X, Krysa A, Marshall A, Carrington P, Tan CH, et al. InAs thermophotovoltaic cells with high quantum efficiency for waste heat recovery applications below 1000 °C. Sol Energy Mater Sol Cells 2018. https://doi.org/10.1016/j.solmat.2017.12.031.

[107] Silva SB, De Oliveira MAG, Severino MM. Sizing and optimization of hybrid photovoltaic, fuel cell and battery system. IEEE Lat Am Trans 2011. https://doi.org/10.1109/TLA.2011.5876425.

[108] Cordiner S, Mulone V, Giordani A, Savino M, Tomarchio G, Malkow T, et al. Fuel cell based Hybrid Renewable Energy Systems for off-grid telecom stations: Data analysis from on field demonstration tests. Appl Energy 2017. https://doi.org/10.1016/j.apenergy.2016.08.162.

[109] Patterson M, Macia NF, Kannan AM. Hybrid microgrid model based on solar photovoltaic battery fuel cell system for intermittent load applications. IEEE Trans Energy Convers 2015. https://doi.org/10.1109/TEC.2014.2352554.

[110] Ogbonnaya C. Novel Code-Based Modeling approach for photovoltaic power generation. Proc. 2019 MACE PGR Conf., 2019, p. 24–6.

[111] Kalogirou S. Solar Energy Engineering. 2009. https://doi.org/10.1016/B978-0-12-374501-9.X0001-5.

[112] Özgirgin E, Devrim Y, Albostan A. Modeling and simulation of a hybrid photovoltaic (PV) module-electrolyzer-PEM fuel cell system for micro-cogeneration applications. Int J Hydrogen Energy 2015;40:15336–42. https://doi.org/10.1016/j.ijhydene.2015.06.122.

[113] Nojavan S, Majidi M, Zare K. Performance improvement of a battery/PV/fuel cell/grid hybrid energy system considering load uncertainty modeling using IGDT. Energy Convers Manag 2017. https://doi.org/10.1016/j.enconman.2017.05.039.

[114] Shockley W, Queisser HJ. Detailed balance limit of efficiency of p-n junction solar cells. J Appl Phys 1961;32:510–9. https://doi.org/10.1063/1.1736034.

[115] Prochowicz D, Saski M, Yadav P, Grätzel M, Lewiński J. Mechanoperovskites for Photovoltaic Applications: Preparation, Characterization, and Device Fabrication. Acc Chem Res 2019. https://doi.org/10.1021/acs.accounts.9b00454.

[116] Green MA, Ho-Baillie A, Snaith HJ. The emergence of perovskite solar cells. Nat Photonics 2014. https://doi.org/10.1038/nphoton.2014.134.

[117] Dinçer I, Joshi AS. Solar based hydrogen production systems. Springer Briefs in Energy 2013:141 S. https://doi.org/10.1007/978-1-4614-7431-9.

[118] Ling Z, Zhang Z, Shi G, Fang X, Wang L, Gao X, et al. Review on thermal management systems using phase change materials for electronic components, Li-ion batteries and photovoltaic modules. Renew Sustain Energy Rev 2014. https://doi.org/10.1016/j.rser.2013.12.017.

[119] Walker G. Solid-state hydrogen storage: Materials and chemistry. 2008. https://doi.org/10.1533/9781845694944.

[120] Baughman RH, Zakhidov AA, De Heer WA. Carbon nanotubes - The route toward applications. Science (80-) 2002. https://doi.org/10.1126/science.1060928.

[121] Dillon AC, Jones KM, Bekkedahl TA, Kiang CH, Bethune DS, Heben MJ. Storage of hydrogen in single-walled carbon nanotubes. Nature 1997. https://doi.org/10.1038/386377a0.

[122] Maeland AJ. Approaches to increasing gravimetric hydrogen storage capacities of solid hydrogen storage materials. Int J Hydrogen Energy 2003. https://doi.org/10.1016/S0360-3199(02)00162-3.

[123] Zhigang S, Baolian Y, Ming H. Bifunctional electrodes with a thin catalyst layer for `unitized' proton exchange membrane regenerative fuel cell. J Power Sources 1999. https://doi.org/10.1016/S0378-7753(99)00047-6.

[124] Ledjeff K, Mahlendorf F, Peinecke V, Heinzel A. Development of electrode/membrane units for the reversible solid polymer fuel cell (RSPFC). Electrochim Acta 1995. https://doi.org/10.1016/0013-4686(94)00273-4.

[125] Wang Y, Leung DYC, Xuan J, Wang H. A review on unitized regenerative fuel cell technologies, part-A: Unitized regenerative proton exchange membrane fuel cells. Renew Sustain Energy Rev 2016. https://doi.org/10.1016/j.rser.2016.07.046.

[126] Ogbonnaya C, Turan A, Abeykoon C. Modularization of integrated photovoltaic-fuel cell system for remote distributed power systems. In: da Silva Bartolo PJ, da Silva FM, Jaradat S, Bartolo H, editors. Ind. 4.0 – Shap. Futur. Digit. World, Manchester: CRC Press; 2020, p. 303–8. https://doi.org/10.1201/9780367823085-53.

[127] Lyons B, Batalov M, Mohanty P, Das S. Rapid prototyping of PEM fuel cell bi-polar plates using 3D printing and thermal spray deposition. 16th Solid Free. Fabr. Symp. SFF 2005, 2005.

[128] Ezzat MF, Dincer I. Development, analysis and assessment of a fuel cell and solar photovoltaic system powered vehicle. Energy Convers Manag 2016. https://doi.org/10.1016/j.enconman.2016.10.025.

[129] United Nations. The sustainable development goals report 2019. United Nations Publ Issued by Dep Econ Soc Aff 2019.

[130] Kong L, Yu J, Cai G. Modeling, control and simulation of a photovoltaic /hydrogen/ supercapacitor hybrid power generation system for grid-connected applications. Int J Hydrogen Energy 2019. https://doi.org/10.1016/j.ijhydene.2019.05.097.

[131] Sumathi S, Ashok Kumar L, Surekha P. Solar PV and Wind Energy Conversion Systems. 2015. https://doi.org/10.1007/978-3-319-14941-7.

[132] Ghenai C, Bettayeb M, Brdjanin B, Hamid AK. Hybrid solar PV/PEM fuel Cell/Diesel Generator power system for cruise ship: A case study in Stockholm, Sweden. Case Stud Therm Eng 2019. https://doi.org/10.1016/j.csite.2019.100497.

[133] REN21. Renewables 2018 Global Status Report (Paris: REN21 Secretariat). Paris Renew Energy Policy Netw 21st Century 2018:1–324. https://doi.org/978-3-9818911-3-3.

[134] Spiegel C, Hagar L, Mckenzie J, Hahn L, Mcgee M, Ingle S. Designing and Building Fuel Cells. 2007.

[135] Hatti M, Meharrar A, Tioursi M. Power management strategy in the alternative energy photovoltaic/PEM Fuel Cell hybrid system. Renew Sustain Energy Rev 2011. https://doi.org/10.1016/j.rser.2011.07.046.

[136] Wu W, Christiana VI, Chen SA, Hwang JJ. Design and techno-economic optimization of a stand-alone PV (photovoltaic)/FC (fuel cell)/battery hybrid power system connected toa wastewater-to-hydrogen processor. Energy 2015. https://doi.org/10.1016/j.energy.2015.03.012.

[137] Sica D, Malandrino O, Supino S, Testa M, Lucchetti MC. Management of end-of-life photovoltaic panels as a step towards a circular economy. Renew Sustain Energy Rev 2018;82:2934–45. https://doi.org/10.1016/j.rser.2017.10.039.

[138] Valente A, Iribarren D, Dufour J. End of life of fuel cells and hydrogen products: From technologies to strategies. Int J Hydrogen Energy 2019;44:20965–77. https://doi.org/10.1016/j.ijhydene.2019.01.110.

[139] Mirantes A. Model-based systems engineering. Aerosp. Proj. Manag. Handb., 2017. https://doi.org/10.1201/9781315154886.

[140] Mordecai Y, Dori D. Model-based requirements engineering: Architecting for system requirements with stakeholders in mind. 2017 IEEE Int. Symp. Syst. Eng. ISSE 2017 - Proc., 2017. https://doi.org/10.1109/SysEng.2017.8088273.

[141] White SM. Systems Theory , Systems Thinking. Syst. Conf. (SysCon), 2015 9th Annu. IEEE Int., 2015, p. 420–5.

[142] Rosen MA, Bulucea CA. Using exergy to understand and improve the efficiency of electrical power technologies. Entropy 2009;11:820–35. https://doi.org/10.3390/e11040820.

[143] Szargut J, Morris DR, Steward FR. Exergy Analysis of Thermal, Chemical, and Metallurgical Processes. Metall Process Early Twentyfirst Century Vol I 1988:332.

[144] Sansaniwal SK, Sharma V, Mathur J. Energy and exergy analyses of various typical solar energy applications: A comprehensive review. Renew Sustain Energy Rev 2018;82:1576–601. https://doi.org/10.1016/j.rser.2017.07.003.

[145] Dincer I. The role of exergy in energy policy making. Energy Policy 2002;30:137–49. https://doi.org/10.1016/S0301-4215(01)00079-9.

[146] Winterbone DE, Turan A. Advanced Thermodynamics for Engineers: Second Edition. 2015. https://doi.org/10.1016/C2013-0-13437-X.

[147] de Oliveira S. Exergy: Production, cost and renewability. Green Energy Technol 2013;63. https://doi.org/10.1007/978-1-4471-4165-5.

[148] Szargut J, Morris DR. Cumulative exergy consumption and cumulative degree of perfection of chemical processes. Int J Energy Res 1987;11:245–61. https://doi.org/10.1002/er.4440110207.

[149] Fraunhofer Institute for Solar Energy Systems ISE. New world record for solar cell efficiency at 46%. Fraunhofer Inst Sol Energy Syst ISE 2014:1–4. https://doi.org/10.1177/0018726710367441.

[150] Sudhakar K, Srivastava T. Energy and exergy analysis of 36 W solar photovoltaic module. Int J Ambient Energy 2014;35:51–7. https://doi.org/10.1080/01430750.2013.770799.

[151] Glavin ME, Hurley WG. Optimisation of a photovoltaic battery ultracapacitor hybrid energy storage system. Sol Energy 2012;86:3009–20. https://doi.org/10.1016/j.solener.2012.07.005.

[152] Shapiro D, Duffy J, Kimble M, Pien M. Solar-powered regenerative PEM electrolyzer/fuel cell system. Sol Energy 2005;79:544–50. https://doi.org/10.1016/j.solener.2004.10.013.

[153] Nehrir MH, Wang C, Strunz K, Aki H, Ramakumar R, Bing J, et al. A review of hybrid renewable/alternative energy systems for electric power generation: Configurations, control, and applications. IEEE Trans Sustain Energy 2011;2:392–403. https://doi.org/10.1109/TSTE.2011.2157540.

[154] Calise F, D'Accadia MD, Vanoli L. Design and dynamic simulation of a novel solar trigeneration system based on hybrid photovoltaic/thermal collectors (PVT). Energy Convers Manag 2012;60:214–25. https://doi.org/10.1016/j.enconman.2012.01.025.

[155] D.Levi. Best Research-Cell Efficiencies, (date accessed on 16/11/2017). Natl Renew Energy Lab 2017. https://commons.wikimedia.org/wiki/File:PVeff(rev171030).jpg.

[156] Ramakumar R, Abouzahr I, Krishnan K, Ashenayi K. Design scenarios for integrated renewable energy systems. IEEE Trans Energy Convers 1995;10:736–46. https://doi.org/10.1109/60.475847.

[157] Hulstrom CR and R. What is an Airmass 1.5 spectrum? Sol Energy 1990:1085–8.

[158] Avezov RR, Akhatov JS, Avezova NR. A review on photovoltaic-thermal (PV-T) air and water collectors. Appl Sol Energy 2011;47:169–83. https://doi.org/10.3103/S0003701X11030042.

[159] Joshi AS, Dincer I, Reddy B V. Analysis of energy and exergy efficiencies for hybrid PV/T systems. Int J Low-Carbon Technol 2011;6:64–9. https://doi.org/10.1093/ijlct/ctq045.

[160] Rosen MA. Thermodynamic comparison of hydrogen production processes. Int J Hydrogen Energy 1996;21:349–65. https://doi.org/10.1016/0360-3199(95)00090-9.

[161] Hussain MM, Baschuk JJ, Li X, Dincer I. Thermodynamic analysis of a PEM fuel cell power system. Int J Therm Sci 2005;44:903–11. https://doi.org/10.1016/j.ijthermalsci.2005.02.009.

[162] Kanoglu M, Dincer I, Rosen MA. Understanding energy and exergy efficiencies for improved energy management in power plants. Energy Policy 2007;35:3967–78. https://doi.org/10.1016/j.enpol.2007.01.015.

[163] Park SR, Pandey AK, Tyagi V V., Tyagi SK. Energy and exergy analysis of typical renewable energy systems. Renew Sustain Energy Rev 2014;30:105–23. https://doi.org/10.1016/j.rser.2013.09.011.

[164] Chow TT. A review on photovoltaic/thermal hybrid solar technology. Appl Energy 2010;87:365–79. https://doi.org/10.1016/j.apenergy.2009.06.037.

[165] Tiwari GN. Solar Energy Fundamentals, Design, Modelling and Applications. 2002.

[166] Maric R, Yu H. Proton Exchange Membrane Water Electrolysis as a Promising Technology for Hydrogen Production and Energy Storage. Nanostructures Energy Gener. Transm. Storage [Working Title], 2019. https://doi.org/10.5772/intechopen.78339.

[167] Ay M, Midilli A, Dincer I. Exergetic performance analysis of a PEM fuel cell. Int J Energy Res 2006;30:307–21. https://doi.org/10.1002/er.1150.

[168] Wang L, Husar A, Zhou T, Liu H. A parametric study of PEM fuel cell performances. Int J Hydrogen Energy 2003;28:1263–72. https://doi.org/10.1016/S0360-3199(02)00284-7.

[169] Hoogersmm Gregor. FUEL CELL TECHNOLOGY HANDBOOK. 2003.

[170] Kabza A. Fuel Cell Formulary. Http://WwwPemfcDe 2015:1–84.

[171] May GJ, Davidson A, Monahov B. Lead batteries for utility energy storage: A review. J Energy Storage 2018;15:145–57. https://doi.org/10.1016/j.est.2017.11.008.

[172] Poonam, Sharma K, Arora A, Tripathi SK. Review of supercapacitors: Materials and devices. J Energy Storage 2019;21:801–25. https://doi.org/10.1016/j.est.2019.01.010.

[173] Masters GM. Chapter 3 The Electric Power Industry. 2004. https://doi.org/10.1002/0471668826.ch3.

[174] Petela R. Exergy of undiluted thermal radiation. Sol Energy 2003;74:469–88. https://doi.org/10.1016/S0038-092X(03)00226-3.

[175] Barbir F, Gómez T. Efficiency and economics of proton exchange membrane (PEM) fuels cells. Int J Hydrogen Energy 1996;21:891–901. https://doi.org/10.1016/0360-3199(96)00030-4.

[176] Granovskii M, Dincer I, Rosen MA. Economic and environmental comparison of conventional, hybrid, electric and hydrogen fuel cell vehicles. J Power Sources 2006;159:1186–93. https://doi.org/10.1016/j.jpowsour.2005.11.086.

[177] Dupré O, Vaillon R, Green MA. Physics of the temperature coefficients of solar cells. Sol Energy Mater Sol Cells 2015;140:92–100. https://doi.org/10.1016/j.solmat.2015.03.025.

[178] Bünzli J-CG, Chauvin A-S. Chapter 261 - Lanthanides in Solar Energy Conversion. Incl. Actinides, vol. Volume 44, 2014, p. 169–281. https://doi.org/http://dx.doi.org/10.1016/B978-0-444-62711-7.00261-9.

[179] Jafarkazemi F, Ahmadifard E. Energetic and exergetic evaluation of flat plate solar

collectors. Renew Energy 2013;56:55–63. https://doi.org/10.1016/j.renene.2012.10.031.

[180] Florschuetz LW. Extension of the Hottel-Whillier model to the analysis of combined photovoltaic/thermal flat plate collectors. Sol Energy 1979;22:361–6. https://doi.org/10.1016/0038-092X(79)90190-7.

[181] Nasrin R, Hasanuzzaman M, Rahim NA. Effect of high irradiation and cooling on power, energy and performance of a PVT system. Renew Energy 2018;116:552–69. https://doi.org/10.1016/j.renene.2017.10.004.

[182] Teo HG, Lee PS, Hawlader MNA. An active cooling system for photovoltaic modules. Appl Energy 2012;90:309–15. https://doi.org/10.1016/j.apenergy.2011.01.017.

[183] Odeh S, Behnia M. Improving photovoltaic module efficiency using water cooling. Heat Transf Eng 2009;30:499–505. https://doi.org/10.1080/01457630802529214.

[184] Wenzl H. BATTERIES | Capacity. Encycl. Electrochem. Power Sources, 2009, p. 395–400. https://doi.org/10.1016/b978-044452745-5.00043-5.

[185] Hashemi F, Rowshanzamir S, Rezakazemi M. CFD simulation of PEM fuel cell performance: Effect of straight and serpentine flow fields. Math Comput Model 2012;55:1540–57. https://doi.org/10.1016/j.mcm.2011.10.047.

[186] Wang Y, Chen KS, Mishler J, Cho SC, Adroher XC. A review of polymer electrolyte membrane fuel cells: Technology, applications, and needs on fundamental research. Appl Energy 2011;88:981–1007. https://doi.org/10.1016/j.apenergy.2010.09.030.

[187] Jang M, Agelidis VG. A minimum power-processing-stage fuel-cell energy system based on a boost-inverter with a bidirectional backup battery storage. IEEE Trans Power Electron 2011. https://doi.org/10.1109/TPEL.2010.2086490.

[188] Members REN. GSR2021_Full_Report. 2021.

[189] Lehman PA, Chamberlin CE. Design of a photovoltaic-hydrogen-fuel cell energy system. Int J Hydrogen Energy 1991;16:349–52. https://doi.org/10.1016/0360-3199(91)90172-F.

[190] Villalva M, Gazoli J, Filho E. Comprehensive Approach to Modeling and Simulation of Photovoltaic Arrays. IEEE Trans Power Electron 2009;24:1198–208. https://doi.org/10.1109/tpel.2009.2013862.

[191] Motahhir S, Ghzizal A El, Sebti S, Derouich A. Modeling of Photovoltaic System with modified Incremental Conductance Algorithm for fast changes of irradiance. Int J Photoenergy 2018;2018:13. https://doi.org/10.1155/2018/3286479.

[192] Krismadinata, Rahim NA, Ping HW, Selvaraj J. Photovoltaic Module Modeling using Simulink/Matlab. Procedia Environ Sci 2013;17:537–46. https://doi.org/10.1016/j.proenv.2013.02.069.

[193] Patel J, Sharma G. Modeling and Simulation of Solar Photovoltaic Module Using Matlab/simulink. Int J Res Eng Technol 2013;2:225–8.

[194] Zainal NA, Yusoff AR. Modelling of Photovoltaic Module Using Matlab Simulink. IOP Conf Ser Mater Sci Eng 2016;114:012137. https://doi.org/10.1088/1757-899X/114/1/012137.

[195] El Hassouni B, Haddi A, Amrani AG. Modeling and simulation of an autonomous PV Generator dedicated to supply an agricultural pumping station. Energy Procedia, vol. 139, 2017, p. 153–60. https://doi.org/10.1016/j.egypro.2017.11.189.

[196] Lo Brano V, Orioli A, Ciulla G, Di Gangi A. An improved five-parameter model for photovoltaic modules. Sol Energy Mater Sol Cells 2010;94:1358–70. https://doi.org/10.1016/j.solmat.2010.04.003.

[197] Fernandes CAF, Torres JPN, Gomes J, Branco PJC, Nashih SK. Stationary solar concentrating photovoltaic-thermal collector - Cell string layout. Proc. - 2016 IEEE Int. Power Electron. Motion Control Conf. PEMC 2016, 2016, p. 1275–82. https://doi.org/10.1109/EPEPEMC.2016.7752179.

[198] Leuchter J, Rerucha V, Zobaa AF. Mathematical modeling of photovoltaic systems. Proc. EPE-PEMC 2010 - 14th Int. Power Electron. Motion Control Conf., 2010. https://doi.org/10.1109/EPEPEMC.2010.5606897.

[199] Elkholy A, Fahmy FH, Abu Elela A. A new technique for photovoltaic module performance mathematical model. ICCCE 2010 - 2010 Int. Conf. Chem. Chem. Eng. Proc., 2010, p. 6–10. https://doi.org/10.1109/ICCCENG.2010.5560349.

[200] Ciulla G, Lo Brano V, Di Dio V, Cipriani G. A comparison of different one-diode models for the representation of I-V characteristic of a PV cell. Renew Sustain Energy Rev 2014;32:684–96. https://doi.org/10.1016/j.rser.2014.01.027.

[201] Gupta S, Tiwari H, Fozdar M, Chandna V. Development of a two diode model for photovoltaic modules suitable for use in simulation studies. Asia-Pacific Power Energy Eng. Conf. APPEEC, 2012. https://doi.org/10.1109/APPEEC.2012.6307201.

[202] Gilman P. SAM Photovoltaic Model Technical Reference SAM Photovoltaic Model Technical Reference. Sol Energy 2015;63:323–333. https://doi.org/NREL/TP - 6A20- 64102.

[203] Gilman P, DiOrio NA, Freeman JM, Janzou S, Dobos A, Ryberg D. SAM Photovoltaic Model Technical Reference 2016 Update. 2018. https://doi.org/10.2172/1429291.

[204] Solar Energy Laboratory. User Manual: TRNSYS 17 a TRaNsient SYstem Simulation program - Volume 4 - Mathematical Reference. vol. 4. 2009.

[205] Sprenger W, Wilson HR, Kuhn TE. Electricity yield simulation for the building-integrated photovoltaic system installed in the main building roof of the Fraunhofer Institute for Solar Energy Systems ISE. Sol Energy 2016;135:633–43. https://doi.org/10.1016/j.solener.2016.06.037.

[206] Wu Y-C, Jhan Y-R, Wu Y-C, Jhan Y-R. Introduction of Synopsys Sentaurus TCAD Simulation. 3D TCAD Simul. C. Nanoeletronic Devices, 2017, p. 1–17. https://doi.org/10.1007/978-981-10-3066-6_1.

[207] Shrivastava RL, Kumar V, Untawale SP. Modeling and simulation of solar water heater: A TRNSYS perspective. Renew Sustain Energy Rev 2017;67:126–43. https://doi.org/10.1016/j.rser.2016.09.005.

[208] PVLIGHTHOUSE. Photovoltaic software and calculators 2019. https://www.pvlighthouse.com.au/ (accessed June 21, 2019).

[209] Ogbonnaya C, Turan A, Abeykoon C. Robust code-based modeling approach for advanced photovoltaics of the future. Sol Energy 2020;199:521–9.

https://doi.org/10.1016/j.solener.2020.02.043.

[210] Vinod, Kumar R, Singh SK. Solar photovoltaic modeling and simulation: As a renewable energy solution. Energy Reports 2018;4:701–12. https://doi.org/10.1016/j.egyr.2018.09.008.

[211] Fatehi JH, Sauer KJ. Modeling the incidence angle dependence of photovoltaic modules in PVsyst. 2014 IEEE 40th Photovolt. Spec. Conf. PVSC 2014, 2014, p. 1335–8. https://doi.org/10.1109/PVSC.2014.6925164.

[212] Aryal A, Bhattarai N. Modeling and Simulation of 115.2 kWp Grid-Connected Solar PV System using PVSYST. Kathford J Eng Manag 2018;1:31–4. https://doi.org/10.3126/kjem.v1i1.22020.

[213] Abdulkadir M, Samosir AS, Yatim AHM. Modeling and simulation based approach of photovoltaic system in Simulink model. ARPN J Eng Appl Sci 2012;7:616–23.

[214] Keles C, Alagoz BB, Akcin M, Kaygusuz A, Karabiber A. A photovoltaic system model for Matlab/Simulink simulations. Int. Conf. Power Eng. Energy Electr. Drives, 2013, p. 1643–7. https://doi.org/10.1109/PowerEng.2013.6635863.

[215] Morshed MS, Ankon SM, Chowdhury MTH, Rahman MA. Designing of a 2kW stand-alone PV system in Bangladesh using PVsyst, Homer and SolarMAT. 2015 Int. Conf. Green Energy Technol. ICGET 2015, 2015. https://doi.org/10.1109/ICGET.2015.7315090.

[216] Mohammed MN, Alghoul MA, Abulqasem K, Mustafa A, Glaisa K, Ooshaksaraei P, et al. TRNSYS Simulation of Solar Water Heating System in Iraq. Recent Res Geogr Geol Energy, Environ Biomed Proc 4th WSEAS Int Conf Eng Mech Struct Eng Geol (EMESEG 2011) Proc 2nd Int Conf 2011:153–6.

[217] Tan YT, Kirschen DS, Jenkins N. A model of PV generation suitable for stability analysis. IEEE Trans Energy Convers 2004;19:748–55. https://doi.org/10.1109/TEC.2004.827707.

[218] Pagrut UP, Sindekar AS, Lachure SS, Lachure JS. Performance of 125 watt PV module using MATLAB-simulink. Proc. 3rd IEEE Int. Conf. Adv. Electr. Electron. Information, Commun. Bio-Informatics, AEEICB 2017, 2017, p. 45–9. https://doi.org/10.1109/AEEICB.2017.7972381.

[219] Mahmood JR, Selman NH. Four matlab-simulink models of photovoltaic system. Int J Energy Environ 2016;7:417–26.

[220] Acakpovi A, Ben Hagan E. Novel Photovoltaic Module Modeling using Matlab/Simulink. Int J Comput Appl 2013;83:27–32. https://doi.org/10.5120/14535-2978.

[221] Ogbonnaya C, Abeykoon C, Nasser A, Turan A. A Computational Approach to Solve a System of Transcendental Equations with Multi-Functions and Multi-Variables. Mathematics 2021;9:920. https://doi.org/10.3390/math9090920.

[222] Chenni R, Makhlouf M, Kerbache T, Bouzid A. A detailed modeling method for photovoltaic cells. Energy 2007;32:1724–30. https://doi.org/10.1016/j.energy.2006.12.006.

[223] Shell Solar. Product Information Sheet Shell S25 Typical I / V Characteristics 2003.

[224] Meyer EL. Extraction of Saturation Current and Ideality Factor from Measuring

Vocand Iscof Photovoltaic Modules. Int J Photoenergy 2017;2017. https://doi.org/10.1155/2017/8479487.

[225] Varshni YP. Temperature dependence of the energy gap in semiconductors. Physica 1967;34:149–54. https://doi.org/10.1016/0031-8914(67)90062-6.

[226] Shi G, Kioupakis E. Electronic and optical properties of nanoporous silicon for solar-cell applications. ACS Photonics 2015;2:208–15. https://doi.org/10.1021/ph5002999.

[227] MATLAB. MATLAB. MATLAB 2016. https://doi.org/10.1201/9781420034950.

[228] Nelson J. The Physics of Solar Cells. Prop. Semicond. Mater., 2003, p. 384. https://doi.org/10.1142/9781848161269_0001.

[229] Kiermasch D, Gil-Escrig L, Bolink HJ, Tvingstedt K. Effects of Masking on Open-Circuit Voltage and Fill Factor in Solar Cells. Joule 2019;3:16–26. https://doi.org/10.1016/j.joule.2018.10.016.

[230] Dupré O, Vaillon R, Green MA. Thermal Behavior of Photovoltaic Devices: Physics and Engineering. Springer 2017. https://doi.org/10.1007/978-3-319-49457-9.

[231] Lee Y, Tay AAO. Finite element thermal analysis of a solar photovoltaic module. Energy Procedia 2012;15:413–20. https://doi.org/10.1016/j.egypro.2012.02.050.

[232] Brinkworth BJ, Cross BM, Marshall RH, Yang H. Thermal regulation of photovoltaic cladding. Sol Energy 1997;61:169–78. https://doi.org/10.1016/S0038-092X(97)00044-3.

[233] Ogbonnaya C, Turan A, Abeykoon C. Novel thermodynamic efficiency indices for choosing an optimal location for large-scale photovoltaic power generation. J Clean Prod 2019:119405. https://doi.org/10.1016/j.jclepro.2019.119405.

[234] Gaitho FM, Ndiritu FG, Muriithi PM, Ngumbu RG, Ngareh JK. Effect of thermal conductivity on the efficiency of single crystal silicon solar cell coated with an anti-reflective thin film. Sol Energy 2009;83:1290–3. https://doi.org/10.1016/j.solener.2009.03.003.

[235] Chander S, Purohit A, Sharma A, Arvind, Nehra SP, Dhaka MS. A study on photovoltaic parameters of mono-crystalline silicon solar cell with cell temperature. Energy Reports 2015;1:104–9. https://doi.org/10.1016/j.egyr.2015.03.004.

[236] Zuhur S, Ceylan İ, Ergün A. Energy, exergy and environmental impact analysis of concentrated PV/cooling system in Turkey. Sol Energy 2019;180:567–74. https://doi.org/10.1016/j.solener.2019.01.060.

[237] Parrott JE. Thermodynamics of solar cell efficiency. Sol Energy Mater Sol Cells 1992;25:73–85. https://doi.org/10.1016/0927-0248(92)90017-J.

[238] National Renewable Energy Laboratory. Research Cell Record Efficiency Chart. Best Res Cell Effic 2016:2016. https://doi.org/10.1360/zd-2013-43-6-1064.

[239] Viganó D, Kenny RP, Müllejans H, Alimonti G. Standardization of the energy performance of photovoltaic modules in real operating conditions. EPJ Web Conf 2014;79:03014. https://doi.org/10.1051/epjconf/20137903014.

[240] Dubey S, Tiwari GN. Analysis of PV/T flat plate water collectors connected in series. Sol Energy 2009;83:1485–98. https://doi.org/10.1016/j.solener.2009.04.002.

[241] Baruch P. A two-level system as a model for a photovoltaic solar cell. J Appl Phys 1985;57:1347–55. https://doi.org/10.1063/1.334486.

[242] De Vos A, Pauwels H. On the thermodynamic limit of photovoltaic energy conversion. Appl Phys 1981;25:119–25. https://doi.org/10.1007/BF00901283.

[243] Baruch P, De Vos A, Landsberg PT, Parrott JE. On some thermodynamic aspects of photovoltaic solar energy conversion. Sol Energy Mater Sol Cells 1995;36:201–22. https://doi.org/10.1016/0927-0248(95)80004-2.

[244] Landsberg, P. T and Baruch P. The thermodynamics of the conversion of radiation energy for photovoltaics. J Phys A Math Gen 1989;22:1911.

[245] Roger M, Jerry V. Photovoltaic Systems Engineering. 2005. https://doi.org/10.1002/1521-3773(20010316)40:6<9823::AID-ANIE9823>3.3.CO;2-C.

[246] Charfi W, Chaabane M, Mhiri H, Bournot P. Performance evaluation of a solar photovoltaic system. Energy Reports 2018;4:400–6. https://doi.org/10.1016/j.egyr.2018.06.004.

[247] Mousavi Baygi SR, Sadrameli SM. Thermal Management of Photovoltaic Solar Cells Using Polyethylene Glycol1000 (PEG1000) as a Phase Change Material. Therm Sci Eng Prog 2018;5:405–11. https://doi.org/10.1016/j.tsep.2018.01.012.

[248] Fraisse G, Ménézo C, Johannes K. Energy performance of water hybrid PV/T collectors applied to combisystems of Direct Solar Floor type. Sol Energy 2007;81:1426–38. https://doi.org/10.1016/j.solener.2006.11.017.

[249] Tiwari A, Dubey S, Sandhu GS, Sodha MS, Anwar SI. Exergy analysis of integrated photovoltaic thermal solar water heater under constant flow rate and constant collection temperature modes. Appl Energy 2009;86:2592–7. https://doi.org/10.1016/j.apenergy.2009.04.004.

[250] Zondag HA, De Vries DW, Van Helden WGJ, Van Zolingen RJC, Van Steenhoven AA. The thermal and electrical yield of a PV-thermal collector. Sol Energy 2002;72:113–28. https://doi.org/10.1016/S0038-092X(01)00094-9.

[251] Schwingshackl C, Petitta M, Wagner JE, Belluardo G, Moser D, Castelli M, et al. Wind effect on PV module temperature: Analysis of different techniques for an accurate estimation. Energy Procedia, vol. 40, 2013, p. 77–86. https://doi.org/10.1016/j.egypro.2013.08.010.

[252] Bauer T. Thermophotovoltaics: Basic principles and critical aspects of system design. Green Energy Technol 2011. https://doi.org/10.1007/978-3-642-19965-3.

[253] Coutts TJ. Review of progress in thermophotovoltaic generation of electricity. Renew Sustain Energy Rev 1999. https://doi.org/10.1016/S1364-0321(98)00021-5.

[254] Bauer T. Thermophotovoltaics: Basic principles and critical aspects of system design. Green Energy Technol 2011;7. https://doi.org/10.1007/978-3-642-19965-3.

[255] Hussain CMI, Duffy A, Norton B. Thermophotovoltaic systems for achieving high-solar-fraction hybrid solar-biomass power generation. Appl Energy 2020;259:114181. https://doi.org/10.1016/j.apenergy.2019.114181.

[256] Zhou Z, Sakr E, Sun Y, Bermel P. Solar thermophotovoltaics: Reshaping the solar spectrum. Nanophotonics 2016. https://doi.org/10.1515/nanoph-2016-0011.

[257] Daneshvar H, Prinja R, Kherani NP. Thermophotovoltaics: Fundamentals, challenges and prospects. Appl Energy 2015. https://doi.org/10.1016/j.apenergy.2015.08.064.

[258] Harder NP, Würfel P. Theoretical limits of thermophotovoltaic solar energy conversion. Semicond Sci Technol 2003. https://doi.org/10.1088/0268-1242/18/5/303.

[259] Ferrari C, Melino F, Pinelli M, Spina PR. Thermophotovoltaic energy conversion: Analytical aspects, prototypes and experiences. Appl Energy 2014. https://doi.org/10.1016/j.apenergy.2013.08.064.

[260] Seyf HR, Henry A. Thermophotovoltaics: A potential pathway to high efficiency concentrated solar power. Energy Environ Sci 2016. https://doi.org/10.1039/c6ee01372d.

[261] Butcher TA, Hammonds JS, Horne E, Kamath B, Carpenter J, Woods DR. Heat transfer and thermophotovoltaic power generation in oil-fired heating systems. Appl Energy 2011. https://doi.org/10.1016/j.apenergy.2010.10.033.

[262] Gentillon P, Singh S, Lakshman S, Zhang Z, Paduthol A, Ekins-Daukes NJ, et al. A comprehensive experimental characterisation of a novel porous media combustion-based thermophotovoltaic system with controlled emission. Appl Energy 2019. https://doi.org/10.1016/j.apenergy.2019.113721.

[263] Laroche M, Carminati R, Greffet JJ. Near-field thermophotovoltaic energy conversion. J Appl Phys 2006. https://doi.org/10.1063/1.2234560.

[264] Lau JZJ, Wong BT. Thermal energy conversion using near-field thermophotovoltaic device composed of a thin-film tungsten radiator and a thin-film silicon cell. J Appl Phys 2017. https://doi.org/10.1063/1.4989870.

[265] Bitnar B, Durisch W, Holzner R. Thermophotovoltaics on the move to applications. Appl Energy 2013. https://doi.org/10.1016/j.apenergy.2012.12.067.

[266] Ogbonnaya C, Abeykoon C, Nasser A, Turan A. Radiation - Thermodynamic Modelling and Simulating the Core of a Thermophotovoltaic System 2020. https://doi.org/10.3390/en13226157.

[267] Bunge M. A General Black Box Theory. Philos Sci 1963. https://doi.org/10.1086/287954.

[268] Kreith EF, Boehm RF. CRC Handbook of Thermal Engineering, The. 2000. https://doi.org/10.1201/9781420050424.

[269] Durisch W, Grob B, Mayor J-C, Panitz J-C, Rosselet A. Interfacing a small thermophotovoltaic generator to the grid 2011;403:403–16. https://doi.org/10.1063/1.57822.

[270] Bhatt R, Kravchenko I, Gupta M. High-efficiency solar thermophotovoltaic system using a nanostructure-based selective emitter. Sol Energy 2020;197:538–45. https://doi.org/10.1016/j.solener.2020.01.029.

[271] Datas A, Martí A. Thermophotovoltaic energy in space applications: Review and future potential. Sol Energy Mater Sol Cells 2017. https://doi.org/10.1016/j.solmat.2016.12.007.

[272] Jiang JA, Wang JC, Kuo KC, Su YL, Shieh JC, Chou JJ. Analysis of the junction

temperature and thermal characteristics of photovoltaic modules under various operation conditions. Energy 2012. https://doi.org/10.1016/j.energy.2012.06.029.

[273] Ogbonnaya C, Turan A, Abeykoon C. Numerical integration of solar, electrical and thermal exergies of photovoltaic module: A novel thermophotovoltaic model. Sol Energy 2019;185:298–306. https://doi.org/10.1016/j.solener.2019.04.058.

[274] Paghasian K, TamizhMani G. Photovoltaic module power rating per IEC 61853-1: A study under natural sunlight. Conf. Rec. IEEE Photovolt. Spec. Conf., 2011, p. 002322–7. https://doi.org/10.1109/PVSC.2011.6186418.

[275] Ojosu JO. The iso-radiation map for Nigeria. Sol Wind Technol 1990;7:563–75. https://doi.org/10.1016/0741-983X(90)90065-A.

[276] Fadare DA. Modelling of Solar Energy Potential in Nigeria using an Artificial Neural Network Model. Appl Energy 2009;86:1410–22. https://doi.org/10.1016/j.apenergy.2008.12.005.

[277] Ohunakin OS, Adaramola MS, Oyewola OM, Fagbenle RO. Solar energy applications and development in Nigeria: Drivers and barriers. Renew Sustain Energy Rev 2014;32:294–301. https://doi.org/10.1016/j.rser.2014.01.014.

[278] Akinyele DO, Rayudu RK, Nair NKC. Global progress in photovoltaic technologies and the scenario of development of solar panel plant and module performance estimation - Application in Nigeria. Renew Sustain Energy Rev 2015;48:112–39. https://doi.org/10.1016/j.rser.2015.03.021.

[279] Osinowo AA, Okogbue EC, Ogungbenro SB, Fashanu O. Analysis of Global Solar Irradiance over Climatic Zones in Nigeria for Solar Energy Applications. J Sol Energy 2015;2015:1–9.

[280] Nigeria FM of H. Nigeria. 2013.

[281] Bridge G, Bouzarovski S, Bradshaw M, Eyre N. Geographies of energy transition: Space, place and the low-carbon economy. Energy Policy 2013;53:331–40. https://doi.org/10.1016/j.enpol.2012.10.066.

[282] RECP. Wind resources potential in Nigeria 2018. https://www.africa-eu-renewables.org/market-information/nigeria/renewable-energy-potential/ (accessed December 3, 2018).

[283] Yang D. A guideline to solar forecasting research practice: Reproducible, operational, probabilistic or physically-based, ensemble, and skill (ROPES). J Renew Sustain Energy 2019;11:022701. https://doi.org/10.1063/1.5087462.

[284] Tsoutsos T, Frantzeskaki N, Gekas V. Environmental impacts from the solar energy technologies. Energy Policy 2005;33:289–96. https://doi.org/10.1016/S0301-4215(03)00241-6.

[285] Harjanne A, Korhonen JM. Abandoning the concept of renewable energy. Energy Policy 2019:330–40. https://doi.org/10.1016/j.enpol.2018.12.029.

[286] Aliyu AK, Modu B, Tan CW. A review of renewable energy development in Africa: A focus in South Africa, Egypt and Nigeria. Renew Sustain Energy Rev 2018;81:2502–18. https://doi.org/10.1016/j.rser.2017.06.055.

[287] Mas'ud AA, Vernyuy Wirba A, Muhammad-Sukki F, Mas'ud IA, Munir AB, Md Yunus N. An assessment of renewable energy readiness in Africa: Case study of

Nigeria and Cameroon. Renew Sustain Energy Rev 2015;51:775–84. https://doi.org/10.1016/j.rser.2015.06.045.

[288] Edozien L, Akinsoji O, Yusuf F, Orokpo L, Folashade O, Owolabi S, et al. The Nigerian Power Sector Investment Opportunities and Guideline 2016:9.

[289] Akuru UB, Onukwube IE, Okoro OI, Obe ES. Towards 100% renewable energy in Nigeria. Renew Sustain Energy Rev 2017;71:943–53. https://doi.org/10.1016/j.rser.2016.12.123.

[290] Mohammed YS, Mustafa MW, Bashir N, Mokhtar AS. Renewable energy resources for distributed power generation in Nigeria: A review of the potential. Renew Sustain Energy Rev 2013;22:257–68. https://doi.org/10.1016/j.rser.2013.01.020.

[291] Shiva Kumar B, Sudhakar K. Performance evaluation of 10 MW grid connected solar photovoltaic power plant in India. Energy Reports 2015;1:184–92. https://doi.org/10.1016/j.egyr.2015.10.001.

[292] Sharma R, Goel S. Performance analysis of a 11.2 kWp roof top grid-connected PV system in Eastern India. Energy Reports 2017;3:76–84. https://doi.org/10.1016/j.egyr.2017.05.001.

[293] Attari K, Elyaakoubi A, Asselman A. Performance analysis and investigation of a grid-connected photovoltaic installation in Morocco. Energy Reports 2016;2:261–6. https://doi.org/10.1016/j.egyr.2016.10.004.

[294] Energy Commission N. Nigerian 2050 Calculator Excel version. http://www.energy.gov.ng/index.php?option=com_docman&task=cat_view&gid=39&Itemid=49&limitstart=40. 2018.

[295] Liu J, Fang W, Zhang X, Yang C. An Improved Photovoltaic Power Forecasting Model With the Assistance of Aerosol Index Data. IEEE Trans Sustain Energy 2015;6:434–42. https://doi.org/10.1109/TSTE.2014.2381224.

[296] Raza MQ, Mithulananthan N, Summerfield A. Solar output power forecast using an ensemble framework with neural predictors and Bayesian adaptive combination. Sol Energy 2018;166:226–41. https://doi.org/10.1016/j.solener.2018.03.066.

[297] Almonacid F, Pérez-Higueras PJ, Fernández EF, Hontoria L. A methodology based on dynamic artificial neural network for short-term forecasting of the power output of a PV generator. Energy Convers Manag 2014;85:389–98. https://doi.org/10.1016/j.enconman.2014.05.090.

[298] Sobri S, Koohi-Kamali S, Rahim NA. Solar photovoltaic generation forecasting methods: A review. Energy Convers Manag 2018;156:459–97. https://doi.org/10.1016/j.enconman.2017.11.019.

[299] Dunlop J, Rymesmrymesnrelnrelgov M, Sloansloanveracom M. Newsletter of the Resource Assessment Division and suggested members of the conference technical review. Sol Energy 2003;16.

[300] Santos JD, Alonso-García MC. Projection of the photovoltaic waste in Spain until 2050. J Clean Prod 2018;196:1613–28. https://doi.org/10.1016/j.jclepro.2018.05.252.

[301] Chen W, Hong J, Yuan X, Liu J. Environmental impact assessment of monocrystalline silicon solar photovoltaic cell production: A case study in China. J Clean Prod 2016;112:1025–32. https://doi.org/10.1016/j.jclepro.2015.08.024.

[302] IRENA, IEA-PVPS. End-Of-Life Management: Solar Photovoltaic Panels. IEA Photovolt Power Syst Program 2016:100. http://www.irena.org/publications/2016/Jun/End-of-life-management-Solar-Photovoltaic-Panels%0Ahttp://www.irena.org/DocumentDownloads/Publications/IRENA_IEAPVPS_End-of-Life_Solar_PV_Panels_2016.pdf (accessed October 9, 2019).

[303] Tao J, Yu S. Review on feasible recycling pathways and technologies of solar photovoltaic modules. Sol Energy Mater Sol Cells 2015;141:108–24. https://doi.org/10.1016/j.solmat.2015.05.005.

[304] Deng R, Chang NL, Ouyang Z, Chong CM. A techno-economic review of silicon photovoltaic module recycling. Renew Sustain Energy Rev 2019:532–50. https://doi.org/10.1016/j.rser.2019.04.020.

[305] Rocchetti L, Beolchini F. Recovery of valuable materials from end-of-life thin-film photovoltaic panels: Environmental impact assessment of different management options. J Clean Prod 2015;89:59–64. https://doi.org/10.1016/j.jclepro.2014.11.009.

[306] Peng J, Lu L, Yang H. Review on life cycle assessment of energy payback and greenhouse gas emission of solar photovoltaic systems. Renew Sustain Energy Rev 2013;19:255–74. https://doi.org/10.1016/j.rser.2012.11.035.

[307] Contreras-Lisperguer R, Muñoz-Cerón E, Aguilera J, Casa J de la. Cradle-to-cradle approach in the life cycle of silicon solar photovoltaic panels. J Clean Prod 2017;168:51–9. https://doi.org/10.1016/j.jclepro.2017.08.206.

[308] Prieto-Sandoval V, Jaca C, Ormazabal M. Towards a consensus on the circular economy. J Clean Prod 2018;179:605–15. https://doi.org/10.1016/j.jclepro.2017.12.224.

[309] Zang QP. A general result in almost sure central limit theory for random fields. Statistics (Ber) 2014;48:965–70. https://doi.org/10.1080/02331888.2013.801974.

[310] Muradov NZ, Veziroğlu TN. From hydrocarbon to hydrogen-carbon to hydrogen economy. Int J Hydrogen Energy 2005;30:225–37. https://doi.org/10.1016/j.ijhydene.2004.03.033.

[311] Izquierdo U, Barrio VL, Cambra JF, Requies J, Güemez MB, Arias PL, et al. Hydrogen production from methane and natural gas steam reforming in conventional and microreactor reaction systems. Int. J. Hydrogen Energy, vol. 37, 2012, p. 7026–33. https://doi.org/10.1016/j.ijhydene.2011.11.048.

[312] Gnanapragasam N V., Reddy B V., Rosen MA. Hydrogen production from coal gasification for effective downstream CO2 capture. Int J Hydrogen Energy 2010;35:4933–43. https://doi.org/10.1016/j.ijhydene.2009.07.114.

[313] Mitlitsky F, Myers B, Weisberg AH, Molter TM, Smith WF. Reversible (unitised) PEM fuel cell devices. Fuel Cells Bull 1999. https://doi.org/10.1016/S1464-2859(00)80110-8.

[314] Doddathimmaiah AK, Andrews J. The use of PEM unitised regenerative fuel cells in solar-hydrogen systems for remote area power supply. 16th World Hydrog. Energy Conf. 2006, WHEC 2006, 2006.

[315] Rabih S, Rallieres O, Turpin C, Astier S. Experimental study of a PEM reversible fuel cell. Renew Energy Power Qual J 2008. https://doi.org/10.24084/repqj06.268.

[316] Grigoriev SA, Millet P, Porembsky VI, Fateev VN. Development and preliminary testing of a unitized regenerative fuel cell based on PEM technology. Int J Hydrogen Energy 2011. https://doi.org/10.1016/j.ijhydene.2010.07.011.

[317] Guo Q, Guo H, Ye F, Ma CF, Liao Q, Zhu X. Heat and mass transfer in a unitized regenerative fuel cell during mode switching. Int J Energy Res 2019. https://doi.org/10.1002/er.4319.

[318] Dhar HP. A unitized approach to regenerative solid polymer electrolyte fuel cells. J Appl Electrochem 1993. https://doi.org/10.1007/BF00241572.

[319] Bertotti G, Mayergoyz ID. The Science of Hysteresis. vol. 1–2. 2006.

[320] Visintin A. Mathematical models of hysteresis. Sci. Hysteresis, vol. 1, 2006, p. 1–123. https://doi.org/10.1016/B978-012480874-4/50004-X.

[321] Kozlov VN. Mathematical modeling of electromechanical systems with hysteresis. Elektrichestvo 2002:52–5.

[322] Comission E. European SmartGrids Technology Platform. 2006. https://doi.org/10.2165/00124363-200519030-00003.

[323] Lu Y, Zhu B, Wang J, Zhang Y, Li J. Hybrid power generation system of solar energy and fuel cells. Int J Energy Res 2016;40:717–25. https://doi.org/10.1002/er.3474.

[324] Gahleitner G. Hydrogen from renewable electricity: An international review of power-to-gas pilot plants for stationary applications. Int J Hydrogen Energy 2013;38:2039–61. https://doi.org/10.1016/j.ijhydene.2012.12.010.

[325] Kelly NA. Hydrogen production by water electrolysis. Adv. Hydrog. Prod. Storage Distrib., 2014, p. 159–85. https://doi.org/10.1533/9780857097736.2.159.

[326] Carmo M, Fritz DL, Mergel J, Stolten D. A comprehensive review on PEM water electrolysis. Int J Hydrogen Energy 2013;38:4901–34. https://doi.org/10.1016/j.ijhydene.2013.01.151.

[327] Larminie J, Dicks A. Fuel Cell Systems Explained. 2003. https://doi.org/10.1002/9781118878330.